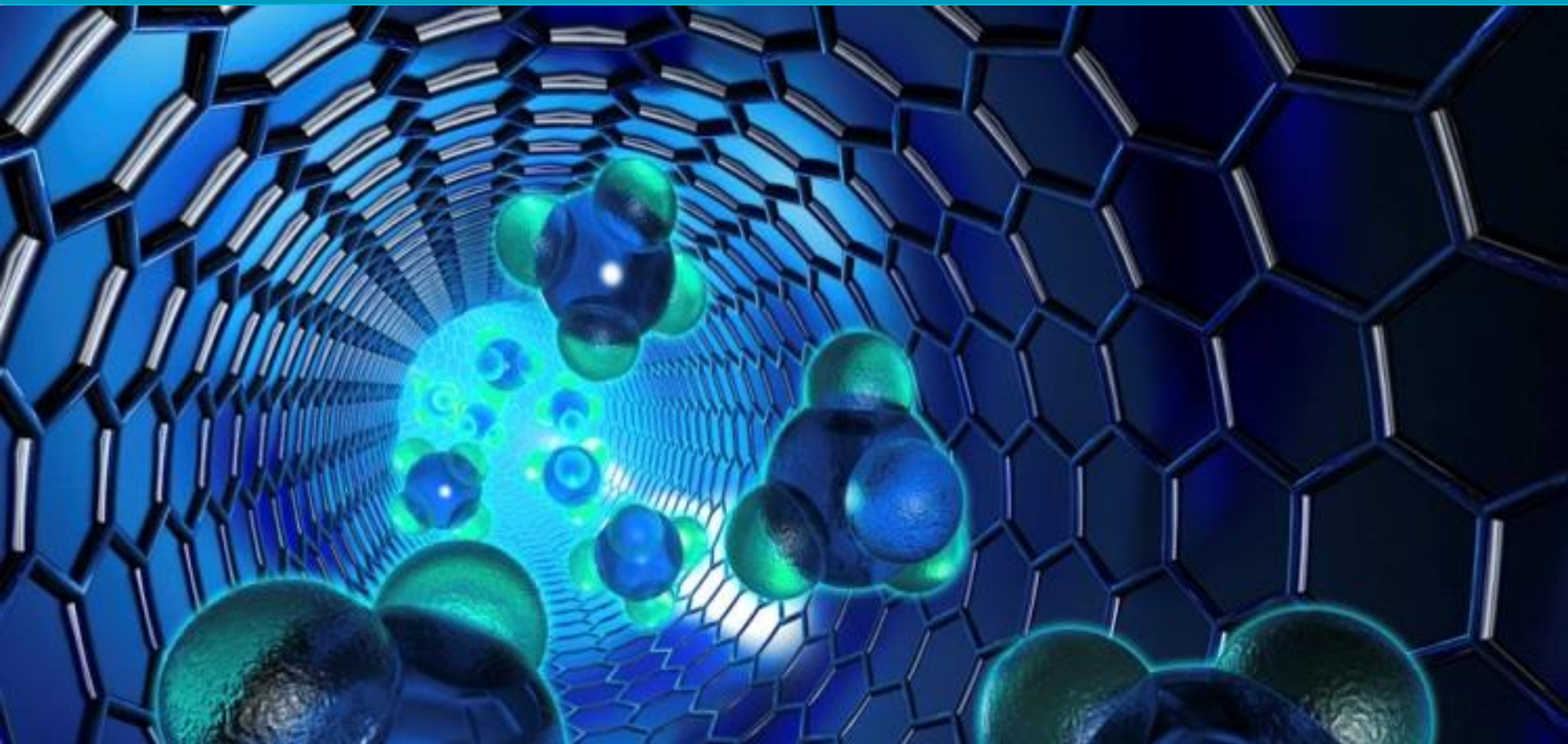


e-ISSN: 2602-277X

International Journal of Chemistry and Technology

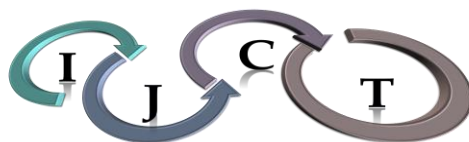


Volume:1, Issue:1

29 December 2017

E - Journal

<http://dergipark.gov.tr/ijct>

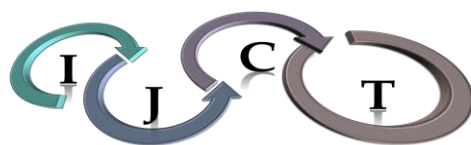


International Journal of Chemistry and Technology

JOURNAL INFO

Journal Name	International Journal of Chemistry and Technology
Journal Initial	IJCT
Journal Abbreviation	Int. J. Chem. Technol.
ISSN (Online)	2602-277X
Year of Launching	2017, August
Editor-in-Chief and Managing Editor	Prof. Dr. Bilal Acemioğlu
Manager of Publication	Assist. Prof. Dr. Mehmet Akyüz
Scope and Focus	Chemistry, Material Science, Technology
Review Type	Peer Review Double-Blinded
Ethical Rules	Plagiarism check, copyright agreement form, conflict of interest, ethics committee report
Access Type	Open Access
Publication Fee	Free
Article Language	English
Frequency of Publication	Biannually
Publication Issue	June, December
Publisher	Prof. Dr. Bilal Acemioğlu
Web Page	http://dergipark.gov.tr/ijct
Contact E-mail address	ijctsubmission@gmail.com, ijctsubmission@yahoo.com
Contact Address and Executive address	Kilis 7 Aralik University, Faculty of Science and Arts, Department of Chemistry, 79000, Kilis
Contact Telephone	90 5535983054 (Editor-in-Chief), 90 530 3645222 (Manager of Publication), 90 532233 17 38 (Secretary)
Publication Date	29/12/2017
Technical Editor	Dr. Evrim Baran
Spelling Editor	Dr. Evrim Baran, Dr. Oğuzhan Koçer, MSc. Rabia Acemioğlu
Language (Grammar) Editor	Doç. Dr. Gülcihan Güzeldağ, Dr. Muhammet Karaman,
Secretary	Dr. Oğuzhan Koçer, English Expert. Abdulkadir Doğan Dr. Oğuzhan Koçer, MSc. Rabia Acemioğlu

All detailed information including instructions for authors, aim and scopes, ethical rules, manuscript evaluation, indexing info, and manuscript template etc. can be found on the main web page of IJCT (<http://dergipark.gov.tr/ijct>).



International Journal of Chemistry and Technology

Volume: 1, Issue: 1 29 December 2017

Founder of IJCT

Prof. Dr. Bilal Acemioğlu

EDITORIAL BOARD

Editor-in-Chief

Prof. Dr. Bilal Acemioğlu

(Kilis 7 Aralik University, Kilis, Turkey)

Associate Editors

Prof. Dr. İbrahim Demirtaş
(Organic Chemistry and Phytochemistry,
Çankırı Karatekin, University, Çankırı, Turkey)

Prof. Dr. M. Hakkı Alma
(Material Science and Technology,
K.Maraş Sütçü İmam/Iğdır University, Turkey)

Prof. Dr. Metin Bülbül
(Biochemistry, Dumlupınar University,
Kütahya, Turkey)

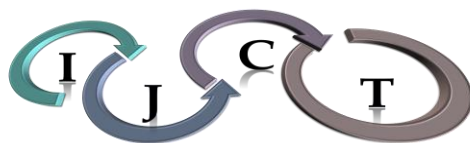
Prof. Dr. Fevzi Kılıçel
(Analytical Chemistry, Karamanoğlu Mehmet
Bey University, Karaman, Turkey)

Prof. Dr. Yuh-Shan Ho
(Chemical and Environmental Engineering,
Asia University, Taichung City, Taiwan)

Prof. Dr. Yahya Güzel
(Theoretical Chemistry and Polymer Chemistry,
Erciyes University, Kayseri, Turkey)

Prof. Dr. Mustafa Arık
(Physical Chemistry, Atatürk University,
Erzurum, Turkey)

Prof. Dr. Mehmet Sönmez
(Inorganic Chemistry, Gaziantep University,
Gaziantep, Turkey)



International Journal of Chemistry and Technology

Advisory Editorial Board

Prof. Dr. Ahmet Çakır
(Kilis 7 Aralık University, Kilis, Turkey)

Prof. Dr. Shaobin Wang
(Curtin University, Perth, Australia)

Prof. Dr. Harun Parlar
(Technical University of Munich, München, Germany)

Prof. Dr. Barbaros Nalbantoğlu,
(Yıldız Technical University, İstanbul, Turkey)

Prof. Dr. Ö. İrfan Küfrevioğlu
(Atatürk University, Erzurum, Turkey)

Prof. Dr. Anatoli Dimoglu
(Düzce University, Düzce, Turkey)

Prof. Dr. Mahfuz Elmastaş
(Health Sciences University, İstanbul, Turkey)

Prof. Dr. Ahmet Tutar
(Sakarya University, Sakarya, Turkey)

Prof. Dr. Birgül Yazıcı
(Cukurova University, Adana, Turkey)

Prof. Dr. İsmet Kaya
(18 Mart University, Çanakklae, Turkey)

Prof. Dr. Nurullah Saraçoğlu
(Atatürk University, Erzurum, Turkey)

Prof. Dr. Giray Topal
(Dicle University, Diyarbakır, Turkey)

Prof. Dr. Salah Akkal,
(University of Mentouri Consatntine, Consatntine, Algeria)

Prof. Dr. Gilbert Kapche Deccaux
(The University of Yaounde I, Yaounde, Cameroon)

Prof. Dr. Mehmet Çiftçi
(Bingöl University, Bingöl, Turkey)

Prof. Dr. M. Salih Ağırtaş
(Yüzüncü Yıl University, Van, Turkey)

Prof. Dr. Özer Çınar
(Yıldız Technical University, İstanbul, Turkey)

Prof. Dr. Rahmi Kasımoğulları
(Dumlupınar University, Kütahya, Turkey)

Prof. Dr. Ahmet Baysar
(Inonu University, Malatya, Turkey)

Prof. Dr. Hamdi Temel
(Dicle University, Diyarbakır, Turkey)

Prof. Dr. Papita Das
(Jadavpur University, Jadavpur, India)

Prof. Dr. Atiqur Rahman
(Islamic University, Kushita, Bangladesh)

Prof. Dr. İlhami Gülçin
(Atatürk University, Erzurum, Turkey)

Prof. Dr. Mehmet Uğurlu
(Sıtkı Kocman university, Muğla, Turkey)

Prof. Dr. Şükrü Beydemir
(Anadolu University, Eskişehir, Turkey)

Prof. Dr. Ramazan Solmaz
(Bingol University, Bingöl, Turkey)

Prof. Dr. Ömer Şahin
(Siirt University, Siirt, Turkey)

Prof. Dr. Mehmet Doğan
(Balıkesir University, Balıkesir, Turkey)



International Journal of Chemistry and Technology

Advisory Editorial Board

Prof. Dr. Jaine H. Hortolan Luiz
(Federal University of Alfenas,
Unifal-MG, Brazil)

Prof. Dr. Vagif Abbasov
(Nef-Kimya Prosesleri Institutu, Baku,
Azerbaijan)

Prof. Dr. Mehmet Muhtar Kocakerim
(Çankırı University, Çankırı, Turkey)

Prof. Dr. Murat Alanyalıoğlu
(Atatürk University, Erzurum, Turkey)

Prof. Dr. İbrahim Işıldak
(Yıldız Technical University, İstanbul, Turkey)

Prof. Dr. T. Abdulkadir Çoban
(Erzincan University, Erzincan, Turkey)

Prof. Dr. Seyithan Taysi
(Gaziantep University, Gaziantep, Turkey)

Prof. Dr. Ömer Işıldak
(Gaziosmanpaşa University, Tokat, Turkey)

Prof. Dr. Jon-Bae Kim
(College of Health Sciences, South Korea)

Prof. Dr. Guang-Jie Zhao
(Beijing Forestry University, Beijing, China)

Prof. Dr. Duygu Ekinci
(Atatürk University, Erzurum, Turkey)

Prof. Dr. Hayrullah Yılmaz
(Dicle University, Diyarbakır, Turkey)

Assoc. Prof. Dr. Metin Açıkyıldız
(Kilis 7 Aralık University, Kilis, Turkey)

Assoc. Prof. Dr. Murat Sadıkoğlu
(Gaziosman Paşa University, Tokat, Turkey)

Assoc. Prof. Dr. Niyaz M. Mahmoodi,
(Institute for Color Science and Technology,
Tehran, Iran)

Assoc. Prof. Dr. Mustafa Özdemir
(Süleyman Demirel University, Isparta, Turkey)

Assoc. Prof. Dr. Ali Kara
(Uludağ University, Bursa, Turkey)

Assoc. Prof. Dr. Mahjoub Jabli
(University of Monastir, Monastir, Tunisia)

Assoc. Prof. Dr. Şenay Şimşek
(North Dakota State University, Fargo, USA)

Assoc. Prof. Dr. Mustafa Karataş
(Aksaray University, Aksaray, Turkey)

Assoc. Prof. Dr. Serhan Uruş
(Sütçü İmam University, K. Maraş, Turkey)

Assoc. Prof. Dr. Murat Saraçoğlu
(Erciyes University, Kayseri, Turkey)

Assoc. Prof. Dr. Murat Ertuş
(Bursa Teknik University, Bursa, Turkey)

Assoc. Prof. Dr. Halim Avcı
(Kilis 7 Aralık University, Kilis, Turkey)

Assoc. Prof. Dr. Muhammet Köse
(Sütçü İmam University, K. Maraş, Turkey)

Assoc. Prof. Dr. Ekrem Köksal
(Erzincan University, Erzincan, Turkey)

Assist. Prof. Dr. Mtasem Z. Bani-Fwaz
(King Khalid University, Asir-Abha, Saudi Arabia)

Assist. Prof. Dr. Bakhtiyor Rasulev
(North Dakota State University, Fargo, USA)



International Journal of Chemistry and Technology

Reviewers for December 2017, Vol: 1, Issue: 1

Prof. Dr. Atiqur Rahman
(Islamic University, Kushita, Bangladesh)

Prof. Dr. Mehmet Hakkı Alma
(Sütçü İmam University, K. Maraş, Turkey)

Prof. Dr. Yahya Güzel
(Erciyes University, Kayseri, Turkey)

Prof. Dr. Mehmet Sönmez
(Gaziantep University, Gaziantep, Turkey)

Prof. Dr. Anatoli Dimoglu
(Düzce University, Düzce, Turkey)

Prof. Dr. Ahmet Çakır
(Kilis 7 Aralık University, Kilis, Turkey)

Prof. Dr. Mehmet Çopur
(Bursa Technical University, Bursa, Turkey)

Prof. Dr. Birgül Yazıcı
(Cukurova University, Adana, Turkey)

Prof. Dr. Murat Alanyalıoğlu
(Atatürk University, Erzurum, Turkey)

Prof. Mustafa Dolaz
(Sütçü İmam University, K. Maraş, Turkey)

Prof. Dr. Abdülmecit Türüt
(Medeniyet University, İstanbul, Turkey)

Prof. Dr. Soner Kuşlu
(Atatürk University, Erzurum, Turkey)

Assoc. Prof. Dr. Mustafa Özdemir
(Süleyman Demirel University, Isparta, Turkey)

Assoc. Prof. Dr. Halim Avcı
(Kilis 7 Aralık University, Kilis, Turkey)

Assoc. Prof. Dr. Murat Sadıkoğlu
(Gaziosman Paşa University, Tokat, Turkey)

Assoc. Prof. Dr. Serhan Uruş
(Sütçü İmam University, K. Maraş, Turkey)

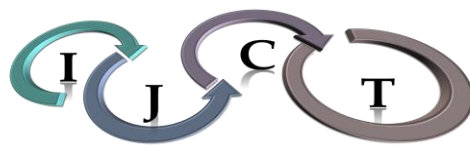
Assoc. Prof. Dr. Mustafa Yazıcı
(Sütçü İmam University, K. Maraş, Turkey)

Assoc. Prof. Dr. Mehmet Gülcan
(Yüzüncü Yıl University, Van, Turkey)

Assoc. Prof. Dr. Murat Saraçoğlu
(Erciyes University, Kayseri, Turkey)

Assoc. Prof. Dr. Muhammet Köse
(Sütçü İmam University, K. Maraş, Turkey)

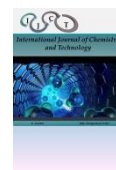
Assist. Prof. Dr. Eyyüp Karaoğul
(Harran University, Şanlıurfa, Turkey)



International Journal of Chemistry and Technology

TABLE OF CONTENTS

Research Articles	Pages
1. Investigating of dielectric anisotropy and birefringence of binary liquid crystal mixtures Şükrü Özğan	1-6
2. Determination of spectrophotometric protonation constant of cholinesterase inhibitors Yaşar Doğan Daldal, Ebru Çubuk Demiralay, Güleren Alsancak	7-13
3. 4D-QSAR study of flavonoid derivatives with MCET method Burçin Türkmenoğlu, Hayriye Yılmaz, Ekrem Mesut Su, Tuğba Alp Tokat, Yahya Güzel	14-23
4. Vibrational spectra of 4-hydroxy-3-cyano-7-chloro-quinoline by Density Functional Theory and ab initio Hartree-Fock calculations Kani Arıcı	24-29
5. Effect of nanoparticles on mechanical and tribological properties of composite friction materials Fikrat Yusubov	30-36
6. Synthesis, characterization and catalytic properties of some transition metal complexes of new phenoxy-imine ligand Ali Çapan, Gökhan Ceyhan, Mehmet Sönmez	37-45
7. Chemical analyzes and antioxidant activities of essential oils of four wild Mentha species growing in the Tokat and its districts Tevfik Ozen, Isa Telci, Fatih Gul, Ibrahim Demirtas	46-57
8. Kinetics, thermodynamics and isotherm studies of malachite green adsorption by modified orange peel Leyla Kule, Bilal Acemioğlu, Evrim Baran	58-66
9. Investigation of leaching conditions of chalcopyrite by chlorine gas in aqueous medium Hakan Temur, Ahmet Yartaşı, Mehmet Muhtar Kocakerim	67-73
10. Electrochemical Pesticide Sensor Based on Anthraquinone Substituted Copper Phthalocyanine Yeliz İpek , M. Kasım Şener, Atıf Koca	74-85



Investigation of dielectric anisotropy and birefringence of binary liquid crystal mixtures

Şükrü ÖZĞAN*

Department of Physics, Faculty of Science and Arts, Kahramanmaraş Sütçü İmam University, 46040, Kahramanmaraş, Turkey

Received: 18 August 2017, Revised: 15 September 2017, Accepted: 25 September 2017

*Corresponding author's e-mail address: ozgans@gmail.com (Ş.Özgan)

ABSTRACT

Absorbance, capacitance, conductance, dielectric anisotropy and birefringence properties and splay elastic coefficient of 4'-Hexyl-4-biphenylcarbonitrile (6CB) and its mixture with 4'-Octyl-4-biphenylcarbonitrile (8CB) were investigated. The absorbance was studied using the UV-visible spectrophotometry. Capacitance, conduction and dielectric measurements for 6CB and its mixture were performed in 0-1000 kHz frequency range at the room temperature. Capacitance-voltage and capacitance-frequency changes were investigated for the mixture. Threshold voltage was determined as 2.1 V. It was seen that the capacitance suddenly damped at this voltage. Capacitance is large at lower frequencies and small at higher frequencies than 100 kHz. The conductance-voltage change was obtained for the mixture. The conduction suddenly rose at the threshold voltage. The conduction is small at lower frequencies and large at higher frequencies. Dielectric, birefringence index and splay elastic constant were investigated for 6CB/8CB mixture. The measured values of the mixture are bigger than 6CB values up to the certain frequency.

Keywords: Electric properties, Elasticity, Optical properties, Liquid crystals

İkili sıvı kristal karışımların dielektrik anizotropi ve çift kırıcılığının araştırılması

ÖZ

4'-Hexyl-4-biphenylcarbonitrile (6CB) ve 4'-Octyl-4-biphenylcarbonitrile (8CB) ile karışımının emilim, sığa, iletkenlik, dielektrik anizotropi ve çift kırınım özellikleri ve splay elektrik katsayısı incelendi. Emilim, görünür bölge ultraviyole spektrofotometre kullanılarak incelendi. 6CB ve karışımı için sığa, iletkenlik ve dielektrik ölçümleri oda sıcaklığında 0-1000 kHz frekans aralığında gerçekleştirildi. Karışım için sığa-voltaj ve sığa-frekans değişimleri araştırıldı. Eşik voltajı 2.10 V olarak belirlendi. Bu eşik voltajında sığanın aniden azaldığı görüldü. Sığa düşük frekanslarda büyük ve 100 kHz'den büyük frekanslarda küçüktür. Karışım için iletkenlik-voltaj değişimi elde edildi. İletkenlik, eşik voltajında aniden yükseldi. İletkenlik düşük frekanslarda küçük daha yüksek frekanslarda büyüktür. 6CB/8CB karışımı için dielektrik, çift kırınım indeksi ve splay elastikiyet katsayısı incelendi. Karışımın ölçülen değerleri belli bir frekansın üzerinde 6CB değerlerinden daha büyüktür.

Anahtar Kelimeler: Elektrik özellikler, elastikiyet, optiksel özellikler, sıvı kristaller

1. INTRODUCTION

The state of matter whose physical properties are between those of a crystalline solid and an isotropic liquid is named liquid crystal (LC). The LC is obtained in two different ways as heat or solvent. According to the used processes, these LCs are called thermotropic or lyotropic LCs. LCs is utilized for the display systems of laptop, television, computers and other devices with display systems increasing in size. Development of LC materials and their physical properties play the most important role for their application in liquid crystal display (LCD) devices. The performance of LC materials in LCDs depends seriously on the temperature dependence of the dielectric, capacitance, conductivity, optical and elastic constants of the materials. There is no known a single mesogen containing all of the properties

needed for displays. Such a material can be obtained only by preparing a mixture of mesogens which collectively have the desired properties.¹⁻⁸ For instance, two eutectic nematic mixture LCs, E7 and E8, of cyanobiphenyls and terphenyls have been developed with positive and high dielectric anisotropy.⁹

The absorption spectra of LCs have been studied by using UV-vis spectrophotometer.^{10,11} The LCs and their composites have paid attention continuously because they have their unique electro-optic and magneto-optic properties and novel display application.^{12,13} 4'-Hexyl-4-biphenylcarbonitrile LC (6CB) is one of the liquid crystalline substances which is known best. This matter has high dipole moment and stability for the application of nematic phase.¹⁴ In the dielectric studies of LCs, it is benefited generally from relationships between their static dielectric permittivity and molecular properties for

a long time.^{15,16} It is known that the static dielectric measurement is a successful technique for characterization of molecular anisotropy and intermolecular ordering in nematic LCs. Nowadays, an LC mixture which has a positive dielectric anisotropy is utilized in most active matrix display. As the physical and optical properties of LCs can be developed by mixing of different organic materials, thus new crystalline materials with high clearing temperature, large dielectric anisotropy and low viscosity can be prepared.¹⁷ Dielectric and optical properties¹⁸⁻²¹, permittivity and conductivity²² and Freedericksz transition²³ of 6CB and 4'-Octyl-4-biphenylcarbonitrile LC (8CB) have been investigated. The 6CB and 8CB nematic LCs are used at display technology. These LCs have low phase transition temperatures and superior physical properties at room temperature. Conductance and dielectric anisotropy properties of 4'-Hexyl-4-biphenylcarbonitrile and 4'-octyloxy-4-biphenylcarbonitrile LCs and their composite have been studied in our previous paper.²⁴

Phase transitions of 6CB and 8CB LC mixtures have been studied by differential scanning calorimeter (DSC). The results of DSC clearly point to the existence of four phase transitions in the 6CB/8CB LC mixtures. The phase diagrams of the mixtures have been obtained from DSC and theoretical calculations. The experimental and theoretical phase diagrams are approximately similar to each other. The phase transition temperatures of the 6CB/8CB LC mixtures rise with the heating rate between 2 and 10°C/min. The activation energies have been determined for the phase transitions of 50% 6CB and 50% 8CB LC mixtures.²⁵

Herein, we aimed to investigate phase transition temperatures for different concentrations of 6CB/8CB LC mixtures, by obtaining their theoretical and experimental phase diagrams. Eutectic concentrations are found as 45% 6CB and 55% 8CB in Ref.25. It is understood from the phase transition diagram that the range of the LC is the greatest value at the eutectic concentration.

In this study, therefore, a LC mixture of 50% 6CB and 50% 8CB was investigated in terms of their absorbance, capacitance, conductance, dielectric, birefringence index and splay elastic constant values. The absorbances of 6CB and 8CB LCs were determined using UV-Vis spectrophotometer. The capacitance-voltage change in different frequencies and the capacitance-frequency change in different voltages were investigated for 6CB/8CB LC mixture at room temperature. The conductance-voltage change in different frequencies was obtained for 6CB/8CB LC mixture. The variation of dielectric, birefringence index and splay elastic constant K_{11} with frequency were investigated for 6CB/8CB LC mixture, and the results were compared with 6CB LC values.

2. EXPERIMENTAL

The 4'-hexyl-4-biphenylcarbonitrile and 4-octyl-4'-cyanobiphenyl LC materials were received from Sigma-Aldrich. The chemical structures and formulas of 6CB and 8CB nematic LCs used are given in Table 1. Because 6CB is a little viscous liquid and 8CB is solid powder at room temperature, the solutions of the mixtures in the concentration range 1.7×10^{-5} and 4.1×10^{-5} M were prepared by dissolving in chloroform after weighed the needed amounts. Uniform samples of 6CB and 8CB LCs were prepared using magnetic stirrer. Absorption measurements were performed in real time between 200 and 350 nm wavelengths using an UV-vis spectrophotometer, Perkin-Elmer Lambda 45. For absorption measurements, the quartz cuvette of 1 cm was used. The capacitance-voltage and conductance-voltage values of both pure 6CB LC and the mixture of 6CB and 8CB LC at the same ratio were measured at room temperature by using a KEITHLEY 4200-SCS (Semiconductor characterization system). Before the construction of the cells, glass substrates coated with indium tin oxide (ITO) were spin coated with a polyimide layer about 100 nm thick. Measurement cell was made of two glass slides separate by Mylar sheets having 14.1 μm thicknesses. The mixture of 6CB and 8CB LCs was mixed in bandeling sonorex and heiddolp type reaxtop for 10 minutes, respectively. The LC cells were filled by insulin hypo with the prepared samples on hot plate at 50°C.

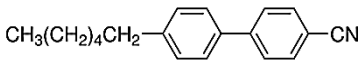
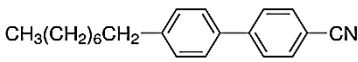
3. RESULTS AND DISCUSSION

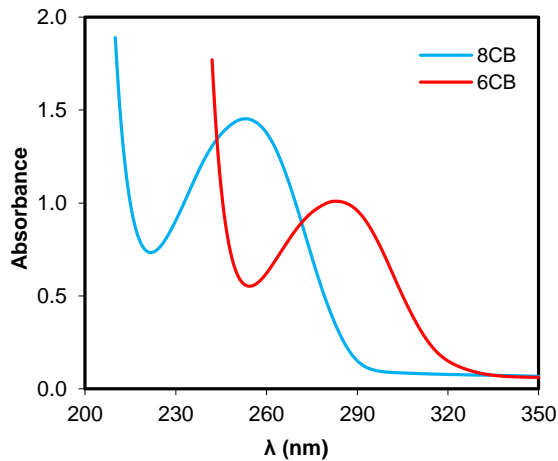
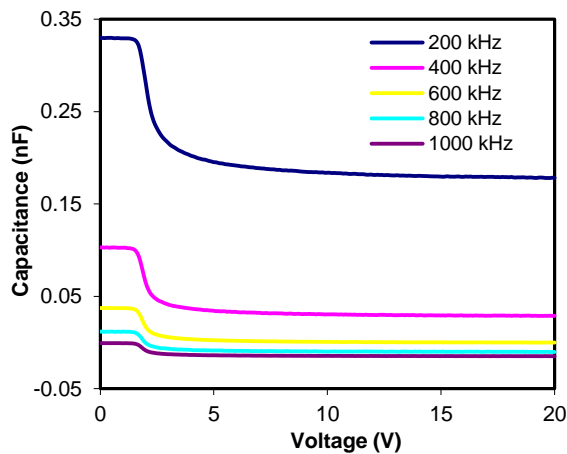
The absorption spectra of 6CB and 8CB LCs in chloroform solutions is shown in Figure 1. The spectra of 8CB and 6CB LC have maximum absorption wavelengths at 253 nm and 283 nm at room temperature, respectively.

Figure 2 shows the change of capacitance depending on voltage for 6CB/8CB LC mixture at different frequencies at room temperature. The capacitance indicates a threshold voltage, and the capacitance values is dropped suddenly and molecular reorientation is occurred above a threshold voltage. The capacitance values are bigger at lower voltages than the threshold voltage, and it is smaller at higher voltages than the threshold voltage. The threshold voltage is about 2.1 V. This voltage is named as Freedericksz threshold voltage. Freedericksz threshold voltage is a key parameter in the electro-optic application of LCs.²⁶

The interaction between a LC and an electric field is dependent on the magnitude of the dielectric permittivity measured parallel ϵ_{\parallel} and perpendicular ϵ_{\perp} to the director and to the difference between them, the dielectric anisotropy $\Delta\epsilon$. When the LC is placed in an electric field, the electric field to LC molecules induces a torque. So, the orientation of the molecules changes and the dielectric anisotropy emerges. The dielectric constants

Table 1. Chemical structures of the 6CB and 8CB LCs

	6CB	8CB
Linear Formula	$\text{CH}_3(\text{CH}_2)_5\text{C}_6\text{H}_4\text{C}_6\text{H}_4\text{CN}$	$\text{CH}_3(\text{CH}_2)_7\text{C}_6\text{H}_4\text{C}_6\text{H}_4\text{CN}$
Chemical Structure		
Molecular Weight (g mol^{-1})	263.39	291.44

**Figure 1.** Absorption spectrum of 6CB and 8CB LCs.**Figure 2.** Plots of capacitance-voltage of the 6CB/8CB LC mixture at the different frequencies.

depend on temperature and frequency of applied electrical field on LC material. Up to nematic-isotropic phase transitions temperature, clearing point temperature, there are two components of dielectric constant as there are two components of dielectric constant as parallel ϵ_{\parallel} and perpendicular ϵ_{\perp} to the director and dielectric anisotropy. Above this temperature, there is only one dielectric constant ($\epsilon_{\parallel} = \epsilon_{\perp}$) and no dielectric anisotropy ($\Delta\epsilon = 0$).

As the capacitance values decrease with increasing frequency, they decrease from the initial value of C_{\parallel} to

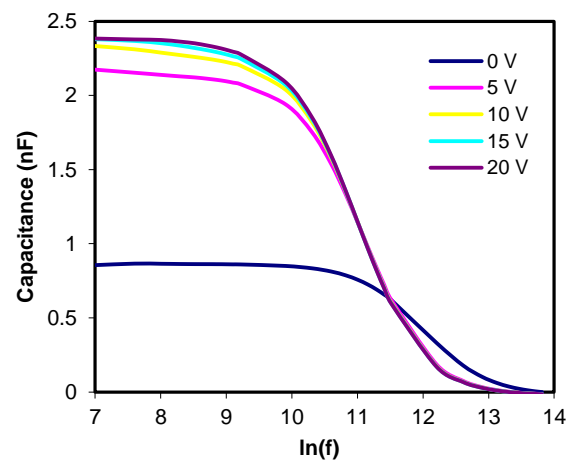
the final value of C_{\perp} . The dielectric constant components, the parallel ϵ_{\parallel} and the perpendicular ϵ_{\perp} to the plane, and the dielectric anisotropy are expressed in Equations (1a-c).

$$\epsilon_{\parallel} = \frac{C_{\parallel}}{C_0} \quad (1a)$$

$$(1a) \quad \epsilon_{\perp} = \frac{C_{\perp}}{C_0} \quad (1b)$$

$$\Delta\epsilon = C_{\parallel} - C_{\perp} \quad (1c)$$

Where, C_0 is the capacitance when the cell is empty. The capacitance-frequency changes of 6CB/8CB LC mixture were obtained for different voltages (see Figure 3). The capacitance is fixed as at low frequency but it decreases with increasing frequency. The capacitance is small at low voltages and is big at high voltages up to a certain frequency, and after 100 kHz this processes is vice versa.

**Figure 3.** Plots of capacitance-frequency of the 6CB/8CB LC mixture at the different voltages.

The electrical conductivity of 6CB/8CB LC mixture is obtained as a function of voltage at different frequencies (see Figure 4). The conductance is small at lower voltages than the threshold voltage, $V_{th} = 2.1$ V, it suddenly rises at the threshold voltage and it is big at higher voltages than the threshold voltage. The conductance is small at lower voltages than the threshold voltage, $V_{th} = 2.1$ V, it suddenly rises at the threshold voltage and it is big at higher voltages than the threshold voltage. What is more, conductance change at the threshold voltage is bigger at the low frequencies than the higher frequencies.

The variations of dielectric constant components and dielectric anisotropy with frequency for 6CB/8CB LC mixture are shown in Figure 5. The parallel and perpendicular components of dielectric constant and dielectric anisotropy have little changes at lower frequencies than 100 kHz, but they decrease with increasing frequency.

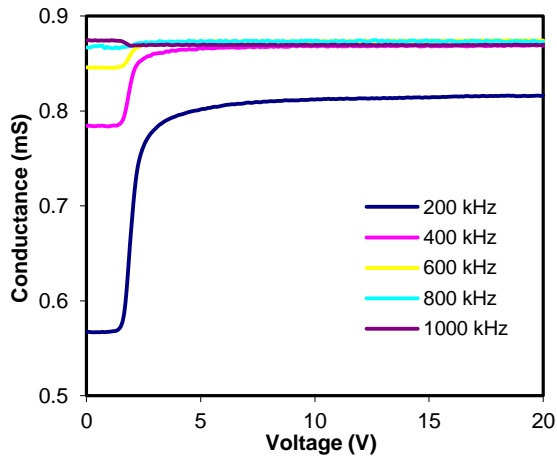


Figure 4. Plots of conductance-voltage of the 6CB/8CB LC mixture at the different frequencies.

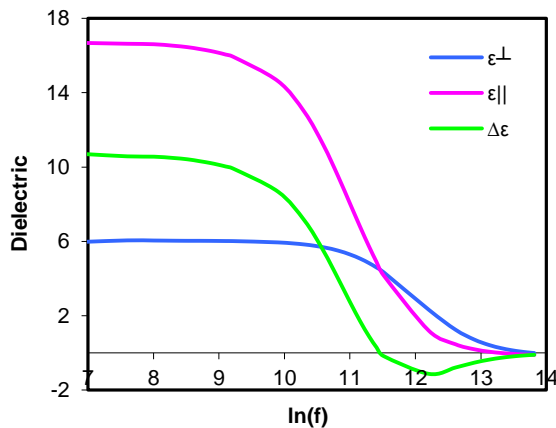


Figure 5. The dielectric anisotropy dependence on frequency for 6CB/8CB LC mixture.

The parallel component of dielectric is bigger than the perpendicular components of dielectric that is, dielectric anisotropy is positive up to a certain frequency (i.e.100 kHz) but after passing 100 kHz, dielectric anisotropy is negative.

The parallel and perpendicular components of birefringence index and birefringence can be written as a function of dielectric constant in Equations (2a-c).⁶

$$n_{\parallel}^2 = \epsilon_{\parallel} \quad (2a)$$

$$n_{\perp}^2 = \epsilon_{\perp} \quad (2b)$$

$$\Delta n = n_{\parallel} - n_{\perp} \quad (2c)$$

The variation of birefringence and parallel and perpendicular components of birefringence index with frequency are given for 6CB/8CB LC mixture (see Figure 6). The birefringence and its components are almost constant toward a frequency of 100 kHz, and then they decrease with increasing frequency.

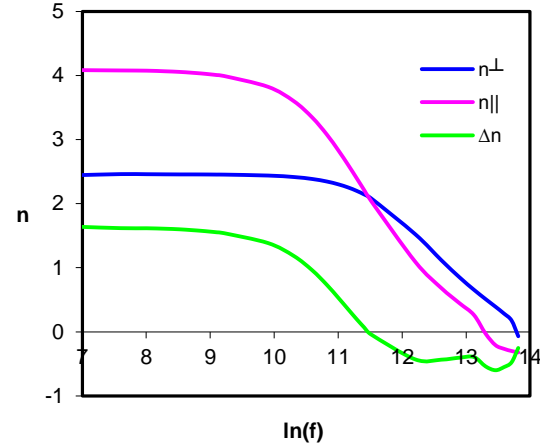


Figure 6. The birefringence index dependence on frequency for 6CB/8CB LC mixture.

The birefringence is negative over the frequency of 100 kHz. Most nematic LC have positive birefringence ($\Delta n > 0$), meaning that the parallel components of birefringence index is bigger than the perpendicular components of birefringence index. After the frequency of 100 kHz, the components of birefringence index are vice versa, and the birefringence index is negative. Birefringence is responsible for the appearance of interference colors in LCDs operating with plane-polarized light. This is meaning of different velocity on every dimensions of light ray which have traveled through the medium. The birefringence depends on light wavelength and temperature. Above the clearing point temperature of nematic LC, nematic-isotropic liquid phase transition temperature, the material is the isotropic liquid, and there is no birefringence ($n_{\parallel} = n_{\perp}$).

Freedericksz threshold voltage for LC samples can be expressed as in Eq. (3).²⁷

$$V_{th} = \pi \left(\frac{K_{11}}{\epsilon_0 \Delta \epsilon} \right)^{1/2} \quad (3)$$

Where, ϵ_0 is dielectric constant of the vacuum, the K_{11} is the splay elastic coefficient, and $\Delta \epsilon$ is the dielectric anisotropy. When a distorting force affects to a LC phase as an electrical force or to an interface with a solid surface, the three elastic constants such as K_{11} , K_{22} , and K_{33} which are called splay, twist, and bend emerge, respectively. The elastic constants are molecular parameters, and they explain the restoring forces on a molecule in a LC phase in response to an external force

that distorts the medium from its lowest energy configuration. At the same time, the elastic constants are reaction to external electrical and magnetic forces applied to the material. Reorientation of LC molecules and LCD devices' response time obviously depend on these elastic constants.

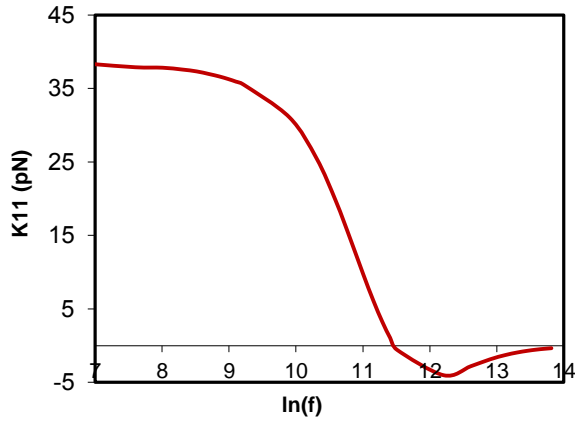


Figure 7. The splay elastic coefficient dependence on frequency for 6CB/8CB LC mixture.

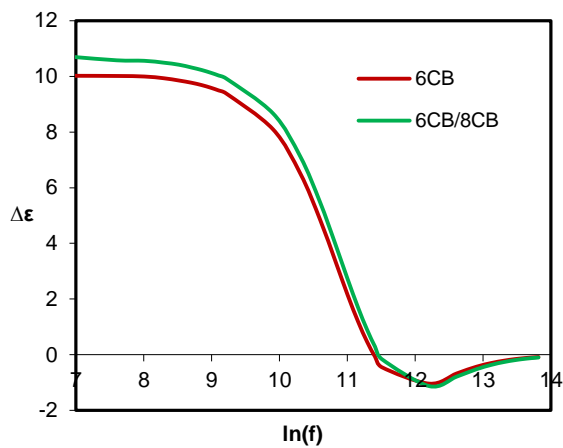


Figure 8. The dielectric anisotropy dependence on frequency for 6CB LC and 6CB/8CB LC mixture.

The splay K_{11} values were estimated by Eq. (3). The K_{11} values obtained for 6CB/8CB LC mixture as a function of frequency are shown in Figure 7. The splay elastic coefficient K_{11} decreases with increasing frequency, and they are negative at bigger frequencies than 100 kHz.

The relationship between dielectric anisotropy and frequency of 6CB LC and 6CB/8CB LC mixture is shown in Figure 8. The dielectric anisotropy of the mixture is bigger than 6CB LCs values up to 100 kHz frequency. The change of birefringence with frequency for 6CB and 6CB/8CB LCs is shown in Figure 9. The birefringence of mixture is bigger than 6CB LC values up to 100 kHz frequency like the dielectric anisotropy. The splay elastic coefficient K_{11} with frequency for 6CB

LC and 6CB/8CB LC mixture is shown in Figure 10. The splay elastic coefficient of mixture is bigger than 6CB LC values up to 100 kHz frequency.

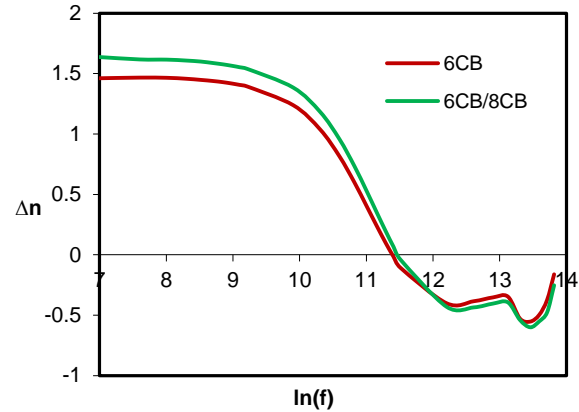


Figure 9. The birefringence index dependence on frequency for 6CB LC and 6CB/8CB LC mixture.

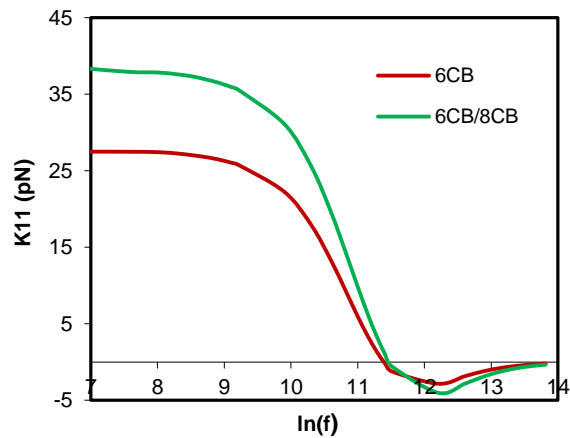


Figure 10. The splay elastic coefficient dependence on frequency for 6CB LC and 6CB/8CB LC mixture.

4. CONCLUSIONS

The absorbencies of 6CB and 8CB LCs were measured using UV-vis spectrophotometer. The mixture of 6CB (50%) and 8CB (50%) LC was prepared, and the capacitance-voltage, capacitance-frequency and conductance-voltage plots for 6CB/8CB LC mixture were investigated at the different frequencies. The dielectric anisotropy, birefringence, parallel and perpendicular components of dielectric and splay elastic coefficient were obtained as a function of frequency. Threshold voltage was found as 2.1 V for 6CB/8CB LC mixture. The dielectric anisotropy of LC mixture is positive at lower frequencies and it is negative at higher frequencies than 100 kHz. The dielectric anisotropy,

birefringence and splay elastic coefficient of 6CB LC and 6CB/8CB LC mixture were compared. The dielectric anisotropy, birefringence and splay elastic coefficient values of 6CB/8CB LC mixture are bigger than those of 6CB LC up to a certain frequency value of 100 kHz. The dielectric anisotropy of 6CB/8CB LC is bigger than that of 6CB LC values up to 100 kHz frequency. The birefringence value of 6CB/8CB LC is bigger than that of 6CB LC up to 100 kHz frequency like the dielectric anisotropy. Similarly, the splay elastic coefficient values of 6CB/8CB LC mixture are bigger than that of 6CB LC.

Conflict of interest

I declare that there is no a conflict of interest with any person, institute or company, etc.

REFERENCES

- de Gennes, P.G.; Prost, J. *The Physics of Liquid Crystals*, Second ed., Oxford, 1995.
- Chandrasekhar, S. *Liquid Crystals*, Second ed. Cambridge, 1993.
- Gray, G.W. (Ed.); *Thermotropic Liquid Crystals*, Wiley, New York, 1979.
- Bahadur, B. (Ed.); *Liquid Crystals: Applications and Uses*, World Scientific, Singapore, 1990.
- Khoo, I. C. (Ed.); *Physics of Liquid Crystalline materials*. First ed., Amsterdam, 1991.
- Kumar, S. (Ed.); *Liquid Crystals: Experimental Study of Physical Properties and Phase Transitions*, First ed., Cambridge, 2001.
- Colling, P. J.; Patel, J. S. (Eds.); *Handbook of Liquid Crystal Research*, Oxford Univ. Press, Oxford, 1997.
- Singh, S. *Phys. Rep.* **2000**, 324, 107-269.
- Malik, M.K.; Bhatia, P.G.; Deshmukh, R.R. *Indian J. Sci. Technol.*, **2012**, 5(10), 3440-3452.
- Grachev, V.T.; Zaitsev, B.E.; Itskovich, E.M.; Pavluchenko, A.I.; Smirnova, N.I.; Titov, V.V.; Dyumaev, K.M. *Mol. Cryst. Liq. Cryst.* **1981**, 65, 133-144.
- David, C.; Baeyens-Volant, D. *Mol. Cryst. Liq. Cryst.* **1984**, 106, 45-65.
- Dalir, N.; Javadian, S.; Gilani, A.G. *J. Mol. Liq.* **2015**, 209, 336-345.
- Yilmaz, S.; Melik, H.; Angay, F.; Emek, M.; Yildirim, A. *J. Mod. Phys.* **2011**, 2, 248-255.
- Smyth, C.P. *Molecular Interactions*, Vol. II, Wiley, New York, 1980.
- Janini, G.M.; Katrib, A.H. *J. Chem. Educ.* **1983**, 60, 1087-1088.
- Maurel, P.; Price, A.H. *J. Chem. Soc. Faraday II*, **1973**, 69, 1486-1490.
- Lagerwall, J.P.F.; Scalia, G. *Curr. Appl. Phys.* **2012**, 12(6), 1387-1412.
- Tripathi, S.; Prakash, J.; Chandran, A.; Joshi, T.; Kumar, A.; Dhar, A.; Biradar, A.M. *Liq. Cryst.* **2013**, 40(9), 1255-1262.
- Goswamia, D.; Debnathb, A.; Mandalb, R.K.; Wegłowski, D.; Dabrowski, R.; Czupryński, K. *Liq. Cryst.* **2016**, 43, 1548-1559.
- Coates, D. *Liq. Cryst.* **2015**, 42(5-6), 653-665.
- Mishra, M.; Dabrowski, R.S.; Vij, J. K.; Mishra, A.; Dhar, R. *Liq. Cryst.* **2015**, 42(11), 1580-1590.
- Singha, U.B.; Dharb, R.; Dabrowski, R.; Pandey, M.B. *Liq. Cryst.* **2013**, 40(6), 774-782.
- Yadav, S.P.; Singh, S. *Prog. Mater. Sci.* **2016**, 80, 38-76.
- Özgan, Ş.; Yazıcı, M.; Ateş, K. *Asian J. Chem.* **2011**, 23, 3247-3451.
- Okumuş, M.; Özgan, Ş. *Asian J. Chem.* **2013**, 25(7), 3879-3883.
- Scheffer, T.; Nehring, J.; Bahadur, B. (Ed.); *Liquid Crystals. Applications and Uses*, Vol.1, World Scientific, Singapore, 1990.
- Demus, D.; Goodby, J.W.; Gray, G.W.; Spiess, H.W.; Vill, V. (Eds.); *Handbook of Liquid Crystals*. 2A, Wiley-VCH, 1998.



0000-0001-9334-327X (Ş. Özgan)



Determination of spectrophotometric protonation constant of cholinesterase inhibitors

Y. Doğan DALDAL, Ebru ÇUBUK DEMİRALAY*, Güleren ALSANCAK

Department of Chemistry, Faculty of Science and Literature, Süleyman Demirel University, 32260, Isparta, Turkey

Received: 24 August 2017, Revised: 03 October 2017, Accepted: 09 October 2017

*Corresponding author's e-mail address: ebrucubuk@sdu.edu.tr (E. Çubuk Demiralay)

ABSTRACT

Spectrophotometric titration for protonation constant (pK_a) determination is one of the popular methods. In the present study pK_a values of rivastigmine, galantamine and donepezil which are cholinesterase inhibitors used in cure of Alzheimer's disease were determined using UV titration in various acetonitrile-water binary mixtures at constant temperature (25 °C) and ionic strength (0.1 mol l⁻¹). Data assessment was carried out with the STAR software program to calculate molar absorbance and stability constants of the compounds studied. Aqueous protonation constants of sparingly soluble drug compounds were calculated from two different extrapolation methods. The extrapolated results are in good agreement with the literature values. Moreover, values of the protonation constant at 37°C, which are scarcely reported, were calculated by using Abraham's solute descriptors.

Keywords: Cholinesterase Inhibitors, Protonation Constant, UV-vis Spectrophotometry, Solute Descriptors

Kolinesteraz İnhibitörlerinin Spektrofotometrik Protonasyon Sabitinin Tayini

ÖZ

Protonasyon sabiti (pK_a) tayini için spektrofotometrik titrasyon popüler metotlardan birisidir. Sunulan çalışmada Alzheimer hastalığının tedavisi için kullanılan kolinesteraz inhibitörleri rivastigmin, galatamin ve donepezilin pK_a değerleri sabit sıcaklık (25 °C) ve iyonik şiddette (0,1 mol l⁻¹) farklı asetonitril-su ikili karışımlarında UV titrasyonla tayin edilmiştir. Veri değerlendirilmesi, çalışılan bileşiklerin kararlılık sabitleri ve molar absorpsanlarının hesaplanması için kullanılan STAR yazılım programı ile yapılmıştır. Suda çözünmeyen ilaç bileşiklerinin sudaki protonasyon sabitleri iki farklı ekstrapolasyon yöntemi ile hesaplanmıştır. Ekstrapolasyon sonuçları literatür değerleri ile uyum içerisindedir. Ayrıca literatürde bulunmayan 37°C' deki protonasyon sabiti değerleri Abraham çözünen parametreleri kullanılarak hesaplanmıştır.

Anahtar Kelimeler: Kolinesteraz inhibitörleri, Protonasyon sabiti, UV-vis spektrofotometri, Çözünen parametreleri

1. INTRODUCTION

Cholinesterase inhibitors are presently the most created cure strategy in Alzheimer's disease. This illness is a neurological disorder in which the death of brain cells causes cognitive decline and memory loss. Existing these inhibitors donepezil, rivastigmine and galantamine are widely recommended for clinical use.¹

Protonation constant (pK_a) value of a molecule is an essential physicochemical parameter using in organic synthesis, medicinal chemistry, and material and food sciences.² The knowledge pK_a value of a molecule having acidic or basic properties help to predict ionization stage of this molecule at a given pH. This constant constitutes important data for agreement of absorption, distribution, metabolism, excretion and toxicology (ADMET).³⁻⁶ Protonation equilibrium are usually determined in constant ionic strength. NaCl and KCl are usually used to maintain ionic strength. These

chemicals are preferentially used in spectrophotometric and potentiometric titrations.

There are many various analytical techniques that allow for accurate investigation of pK_a value. Spectrophotometry is attractive method for pK_a determination because of several advantages such as specificity, rapidity, precision and accuracy. Moreover, this technique is a preferable method for providing foreknowledge to high performance liquid chromatography (HPLC). UV-vis spectrometry ensures the possibility of pK_a determination for compounds with simple equipment, low water solubility and sub-micromolar compound concentration. (about 10⁻⁵ to 10⁻⁶ M).^{7,8} The compounds to be investigate in spectrophotometric pK_a determination should possess to pH-dependant light absorption. Some calculators using spectrophotometric data are often used for the estimation of pK_a .^{9,10}

The effect of temperature on the equilibrium of chemical systems is well known. Calculation of temperature dependent pK_a is very important. The most reliable results come from laboratories where the pK_a is determined under standard conditions, i.e., in thermostated 25°C solutions containing a background electrolyte (e.g., 0.1 M KCl), with special care given to calibrating the pH electrode. Of the published pK_a values of drug molecules, scarcely any are reported at 37°C.¹¹ Data of the protonation constants at biorelevant temperature (37°C), which are barely information, are more significant for biological mechanisms of cellular transfer by ionizable compounds and in mechanistic disintegration works, which are frequently realized at 37°C.

The effect of temperature on pK_a depends on the nature of the functional group. Acidic drugs have nearly the same pK_a at 25 and 37°C, whereas basic drugs usually have a decreased pK_a at the biorelevant temperature ($pK_a/T \approx -0.03 \text{ } ^\circ\text{C}^{-1}$).¹¹ In this work, the prediction of the pK_a value at 37 °C, provided the value at 25°C is known. For this, solute descriptors of Abraham and the pK_a value at 25°C were used in Eq. (1).¹¹

$$\Delta pK_a = k_0 \times pK_a^{25} + c_0 + c_1 \times \sum a_2^H + c_2 \times \sum \beta_2^H + c_3 \times \pi_2 + c_4 \times R_2 + c_5 \times V_x \quad (1)$$

Using calculated differences between the values (ΔpK_a), the pK_a value at 37°C is estimated by Eq. (2).¹¹

$$\Delta pK_a = pK_a^{37} - pK_a^{25} \quad (2)$$

Evaluation of aqueous protonation constants is an inescapable requirement in practice drug development. However, many drugs are sparingly soluble in water and any experimental pK_a determination requires the use of cosolvent. The cosolvent procedure mainly using acetonitrile-water mixtures binary provides a good alternative for sparingly soluble compounds.¹²⁻¹⁴

A common approach for the pK_a measurement of aqueous insoluble compounds involves the use of different percentages of water-organic modifier binary mixtures and extrapolation to 0% water-organic modifier. Usually, at least three and up to six different percentages of water-organic modifier are recommended. There are two approach practised to estimate the aqueous protonation constant from the pK_a values determined in the hydroorganic mixture. In the first attitude, experimental protonation constant is drawn against mole fraction (X) of a hydroorganic mixture. This approach is performed by using Eq. (3).

$$pK_{a,\phi} = aX + b \quad (3)$$

where a indicates the dissociation constant in water, X show the mole fraction of acetonitrile, b is the slope of the linear relationship, and $pK_{a,\phi}$ is the pK_a at the corresponding composition. In second attitude, aqueous

pK_a values are calculated by using Yasuda-Shedlovsky equation (Eq. 4). Based on the Born electrostatic model and Bjerrum's theory of ion association, Yasuda¹⁵ and Shedlovsky¹⁶ independently derived a correlation by means of a plot of $pK_a + \log [H_2O]$ versus $a\epsilon^{-1} + b$, producing a straight line. Where $[H_2O]$ represents the molar water concentration and ϵ^{-1} denotes reverse of the dielectric permittivity of the binary mixture. Terms a and b symbolize the slope and the intercept of the plot, respectively.

$$pK_a + \log [H_2O] = a\epsilon^{-1} + b \quad (4)$$

The results obtained for pK_a in water have been compared with those predicted by the Marvin Sketch program.¹⁷ This program estimates several physico-chemical properties of compounds on the basis of their molecular structure.

In the present work, it was focused to investigate the protonation constants of rivastigmine, galantamine and donepezil. The determination of pK_a values at 25°C were carried out with spectrophotometric method in three different percentage acetonitrile (35%, 40% and 45%, v/v) for donepezil and rivastigmine, 25%, 30% and 35% (v/v) acetonitrile content for galantamine. Aqueous pK_a values of drugs studied were calculated with two different approaches. Moreover, the pK_a values at 37°C were estimated by applying Abraham's solute descriptors.

The main objective of our present work is to study the effect of cosolvents at fixed temperature and ionic strength on rivastigmine, galantamine and donepezil by using spectrophotometric method. Also, the extrapolated protonation constants results are to compare with those determined in aqueous medium or with literature values.

2. MATERIALS AND METHODS

2.1. Materials

Galantamine hydrobromide and donepezil hydrochloride monohydrate were bought from Sigma-Aldrich (St. Louis, USA). Rivastigmine was supplied by Novartis Pharmaceuticals Corporation (Istanbul, Turkey). Potassium hydrogen phthalate (dried at 110 °C), potassium hydroxide using as a Titrisol, potassium chloride using as an ionic strength adjuster, and acetonitrile (HPLC grade) using as a cosolvent were provided by Merck (Darmstadt, Germany). All of the chemicals used in this work were utilized without any further purification. Solutions and solvent mixtures were prepared with distilled water obtained from Millipore, Milli-Q (Bedford, MA, USA) purification system. Chemical structures of donepezil, rivastigmine and galantamine are given in Figure 1.

2.2. Methods

In this study, pH measurements were carried out with a In Lab 412 glass electrode, using a Mettler Toledo MA 235 pH/ion analyser (Schwerzenbach, Switzerland).

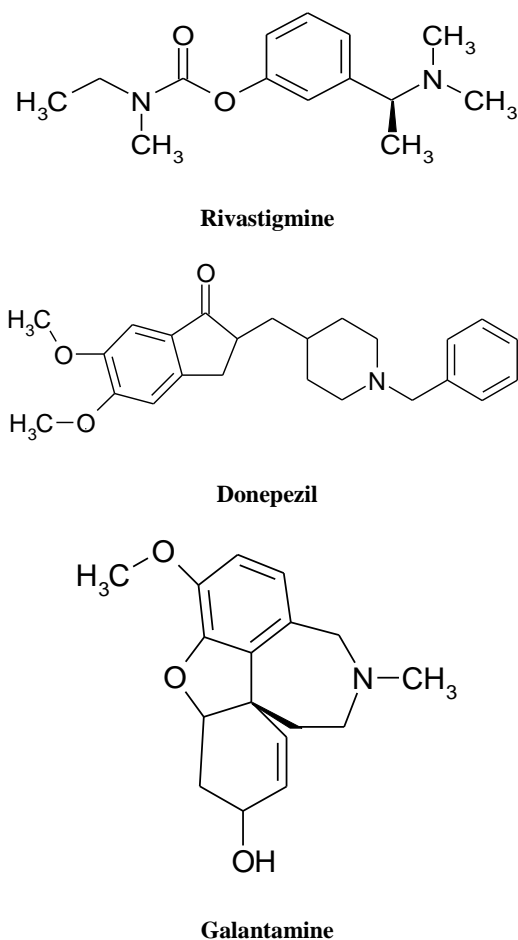


Figure 1. Structure of rivastigmine, donepezil and galantamine.

These measurements were actualized at 25°C. Potassium hydrogen phthalate (0.05 mol kg⁻¹) was used as primary standard buffer reference solution for the standardization of this apparatus in acetonitrile-water mixtures in accordance with IUPAC rules.¹⁸

For the determination of the protonation constants of selected drugs, 35%, 40% and 45% (v/v) water-acetonitrile binary mixtures for donepezil and rivastigmine and 25%, 30% and 35% (v/v) water-acetonitrile binary mixtures for galantamine in 0.1 mol l⁻¹ KCl (ionic strength) adjusted water were prepared and used throughout experimental investigation.

The spectrophotometric pH-titration was performed in hydroorganic mixtures containing 1 x 10⁻⁶ mol l⁻¹ drug and 0.1 mol l⁻¹ KCl solution for adjustment of an ionic strength. In each experiment, drug samples were titrated with 0.05 mol l⁻¹ KOH to an appropriately high pH, usually 11.7. Titrations were performed at 25°C and fixed ionic strength (0.1 mol l⁻¹ KCl).

The attained spectrum was set down using UV-visible spectrophotometry (Lambda 25, Perkin Elmer, USA). All titrations were performed with small volume plus (0.05 ml). Temperature of titration conditions was fixed at 25°C ± 0.1 by way of a cooler system water bath (Heto CBN 8-30). Spectral data were obtained in the pH range

of 5.8-11.7. When the electromotive force (emf) was stable, the spectra of the drugs were recorded with 200 to 400 nm interval for rivastigmine, donepezil and galantamine.

Spectrophotometric protonation constants were calculated using the STAR program (stability constants by absorbance readings).¹⁹ The program refines the absorbance values, until a minimum value in the sum of squared differences between the experimental (A_{exp}) and calculated absorbance (A_{calc}) for each data point. The minimization process is repeated until the relative change of the sum of the squares residual (U) between two iterations is 0.01%.

3. RESULTS AND DISCUSSION

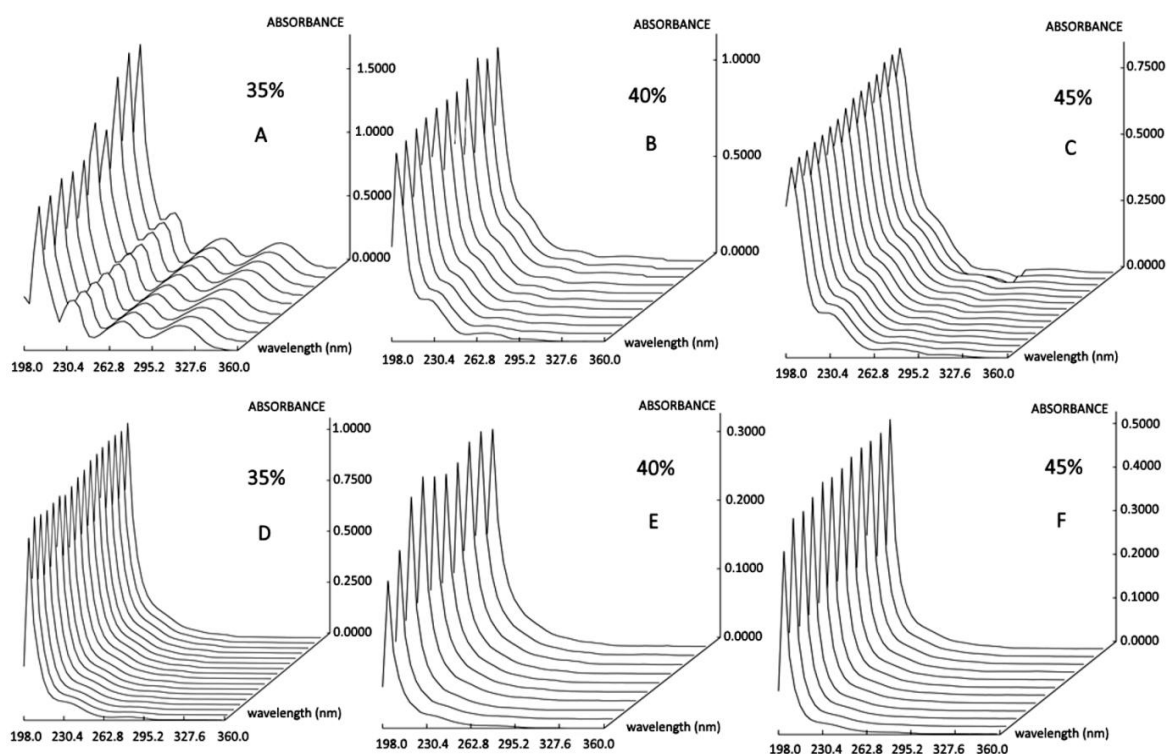
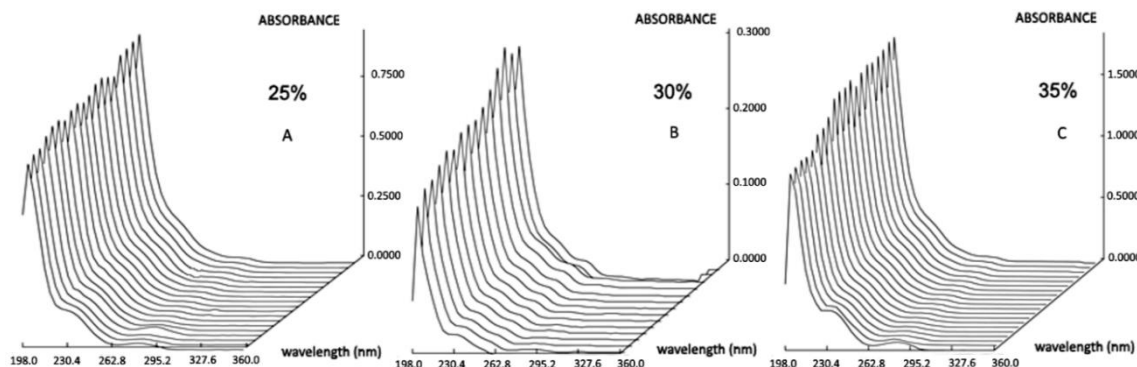
Investigation of pK_a values of the studied basic inhibitors were performed with the UV-spectrophotometric titration measurement in the same acetonitrile-water hydroorganic mixtures to prove the verification of pK_a values obtained in previous work²⁰ (35%, 40% and 45% (v/v) water-acetonitrile binary mixtures for donepezil and rivastigmine; 25%, 30% and 35% (v/v) water-acetonitrile binary mixtures for galantamine). Spectral data of drugs investigated were obtained from absorbance measurements in 200 to 400 nm interval in the pH range of 5.8-11.7, and they were depicted in Figure 2 and 3. The pK_a values evaluated by STAR program using the obtained data for drugs studied at 25°C are given with their standard deviations in Table 1. Typical spectrophotometric titration curves obtained from absorbance measurements at 230 nm for donepezil and galantamine and 225 nm for rivastigmine in acetonitrile-water at 35% volume fraction at 25°C are shown in Figure 4. These sigmoidal curves were obtained from NLREG program.²¹

As a continuation of this determination, the pK_a values at 37°C were predicted using the experimental pK_a values at 25°C. The differences between the values (ΔpK_a) were calculated with Abraham's solute descriptors. According to the values of the Abraham descriptors, small amounts of hydrogen bonding cause pK_a to take on more negative values. The average pK_a in the bases is -0.283; the values range from -0.266 (rivastigmine pK_{a2}) to -0.296 (donepezil and galantamine). Calculated data at 37°C were also compared with experimental data (Table 1).

The studied drugs have one pK_a value corresponding to base functional group. As acetonitrile concentration increases, the dissociate capabilities of basic inhibitors decrease and lead to reduce the value of pK_a. The pK_a values at 37°C of these inhibitors were determined here for the first time. Aqueous pK_a values were calculated for sparingly soluble drug compounds. In the first approach, pK_a values were plotted against to acetonitrile mole fraction. The intercepts of these linear equations obtained from Eq. (3) are the aqueous pK_a values of these compounds.

Table 1. The pK_a values determined by spectrophotometric titration in acetonitrile effect and predicted pK_a values acetonitrile-water binary mixtures

Compounds	Experimental pK _a (25 °C)			ΔpK _a (calculated)			Predicted pK _a (37 °C)		
	35% (v/v)	40% (v/v)	45% (v/v)	35% (v/v)	40% (v/v)	45% (v/v)	35% (v/v)	40% (v/v)	45% (v/v)
Donepezil	8.02±0.03	7.78±0.27	7.54±0.03	-0.296	-0.289	-0.283	7.727	7.492	7.256
Rivastigmine	7.41±0.06	7.17±0.05	6.89±0.09	-0.280	-0.274	-0.266	7.137	6.900	6.626
Galantamine	8.04±0.13	7.68±0.08	7.33±0.03	-0.296	-0.287	-0.278	7.744	7.400	7.052

**Figure 2.** The wavelength (nm)-absorbance graphs for donepezil (1) and rivastigmine (2) in a) 35% (v/v), b) 40% (v/v), c) 45% (v/v) acetonitrile-water binary mixtures.**Figure 3.** The wavelength (nm)-absorbance graphic for galantamine in a) 25% (v/v), b) 30% (v/v), c) 35% (v/v).

Regression analysis results are listed in Table 2. These results indicate that, in general, the assumption of a linear relationship between $pK_{a,\phi}$ and mole fraction of acetonitrile is a good approximation within studied interval (25-45%, v/v).

Table 2. The linear equations data obtained from relationship of acetonitrile mole fraction and $pK_{a,\phi}$ values

Compounds	Equations	r
Donepezil	$pK_{a,\phi} = -8.651(0.045) + 9.311(0.008)$	0.999
Rivastigmine	$pK_{a,\phi} = -9.387(0.213) + 8.819(0.038)$	0.999
Galantamine	$pK_{a,\phi} = -14.379(0.222) + 9.471(0.028)$	0.999

In second approach, Yasuda-Shedlovsky equation (Eq. 4) was used in order to predict aqueous pK_a values using the pK_a values obtained from STAR programme (Table 3). The linearity of the plots is characterized by the regression coefficients (r^2) values which indicate significant linear correlation for the molecules examined drugs. It can be seen from the plots that bases have negative slopes (Figure 5) and produce straight lines with randomly scattered points the total interval (ϵ : 60.109-68.941). As listed in Table 5, the agreement between the pK_a values of the samples obtained from various acetonitrile-water mixtures and literature values is generally good.

Table 3. Data obtained from Yasuda-Shedlovsky extrapolation

Compounds	ACN (v/v%)	ϵ	$pK_a + \log [H_2O] = a\epsilon^{-1} + b$		r	N
			a (slope)	b (intercept)		
Donepezil	35	64.563	-426.0	16.35	1.000	3
	40	62.331				
	45	60.109				
Rivastigmine	35	64.563	-461.9	16.30	0.999	3
	40	62.331				
	45	60.109				
Galantamine	25	68.941	-706.0	20.00	0.999	3
	30	66.770				
	35	64.563				

*a and b are empirical fitting constants, ϵ^{-1} is the reverse of the dielectric permittivity of the binary solvent, r is correlation coefficient, $\log[H_2O] = \log 55.5$ is molar concentration of pure water, N is number of values.

Table 4. Comparison of aqueous pK_a values of cholinesterase inhibitors

	Experimental aqueous pK_a (25°C)		Predicted aqueous pK_a (37 °C)		Our previous work ²⁰ (30 °C)		Our previous work ²² (30 °C)		Literature values	Marvin Sketch ¹⁷
	Yasuda-Shedlovsky	pKa-X	Yasuda-Shedlovsky	pKa-X	Yasuda-Shedlovsky	pKa-X	Yasuda-Shedlovsky	pKa-X		
Donepezil	9.166	9.311	8.835	8.967	8.534	8.555	8.892	8.555	9.10 ²⁶	8.62
Rivastigmine	8.657	8.819	8.347	8.493	9.019	9.035	8.771	9.085	8.90; 8.9 ^{24,25}	8.89
Galantamine	9.239	9.470	8.919	9.138	8.493	8.571	8.269	8.340	8.21 ²³	8.91

20. Reversed phase liquid chromatography determination at 30°C and linear correlation method to obtain the pK_a value

22. Central composite design at 30°C (predicted)

23. Spectrophotometric determination in water at 25°C

24. No estimated uncertainty quoted

25. Radial basis function neural networks and the heuristic method (calculation)

26. Capillary electrophoresis determination at 25°C and ionic strength of 0.05 M

A further comparison between the pK_a values calculated in aqueous medium and those given in the literature and predicted by Marvin Sketch shows that the values corresponding to the pK_a are generally in good agreement. The remarkably good results obtained by this program should be mentioned, because predicted values are within 0.2-0.5 pK_a units from real experimental values.

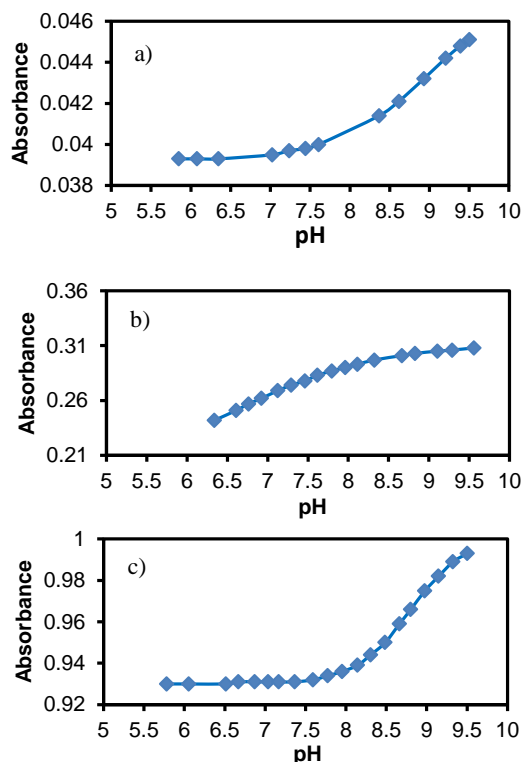


Figure 4. The relationship between A and pH obtained from absorbance measurements in acetonitrile-water at 35% volume fraction at 25°C. a) Donepezil, b) Rivastigmine, c) Galantamine.

Aqueous protonation constant values obtained from two approaches were given in Table 4. Aqueous pK_a values at 37°C were predicted using experimental aqueous pK_a values. These experimental and predicted aqueous pK_a values were compared with pK_a values given from our previous works^{20,22} and the other works reported²³⁻²⁶ (Table 4). In literature reports, different pK_a values for the same compounds are calculated. In the present study, our results^{20,22} are compatible with each other. These calculated values were obtained by using different methods at the same temperature. Investigated compounds were estimated by Demiralay and co-workers²² in the binary mixtures of acetonitrile-water in the same concentrations by the experimental design method. The calculated pK_a values for galantamine are not in full consistency with that reported by Meloun and co-workers.²³ In that study, galantamine was determined in different ionic strengths and temperatures. For rivastigmine, pK_a values were predicted by Hsieh and co-

workers²⁴ and Luan and co-workers.²⁵ In these studies, there are no experimental values. There is only one study for donepezil in the literature.²⁶ This study was carried out by capillary electrophoresis method. Therefore, the calculated pK_a values for donepezil are not in full consistency with that reported by Ishihama and co-workers.²⁶ Table 4 shows that the close values are obtained in determining protonation constants, despite of the use of different equipment by different researchers on different times for different drug concentrations. A comparison with representative pK_a values available in the literature shows that either method gives satisfactory values.

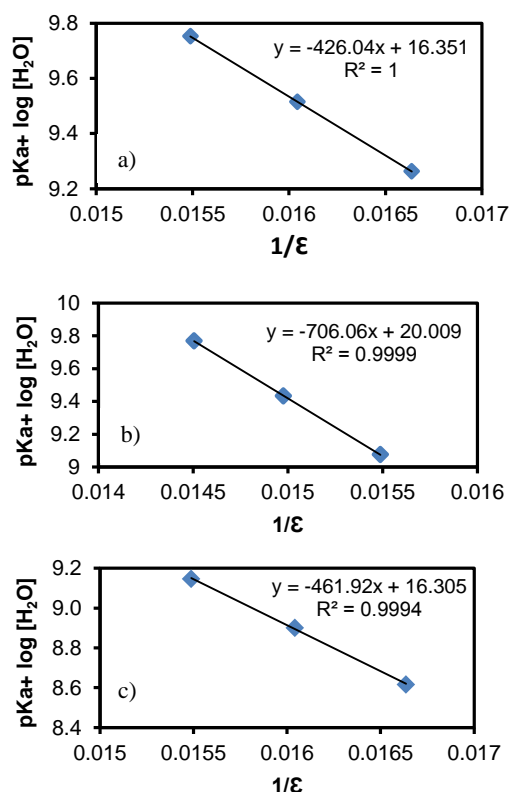


Figure 5. The Yasuda-Shedlovsky plots of a) Donepezil, b) Rivastigmine, c) Galantamine.

4. CONCLUSION

In this study, the pK_a values of galantamine, donepezil and rivastigmine which are used in the cure of Alzheimer's disease were determined by using spectrophotometric titration in acetonitrile-water binary mixtures. pK_a values at 37°C were predicted with Abraham solute descriptors. So, this data is preliminary in the literature. There was of enormous consistence between the aqueous pK_a values of the studied drugs by calculated values and predicted values. The significant data obtained from this study can be used for pharmacological, pharmacokinetic works of cholinesterase inhibitors.

ACKNOWLEDGEMENTS

The authors are thankful to the BAP, Suleyman Demirel University, Turkey (Project 3301-YL2-12) and TÜBİTAK (Project 113Z025) for providing financial assistance for this study. We thank Dr. Jose L. Beltran from Universitat de Barcelona for providing spectral data processing software, STAR.


Conflict of interest


Authors declare that there is no a conflict of interest with any person, institute, company, etc.


REFERENCES

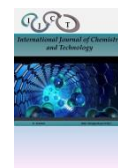
- Nordberg, A.; Svensson, A.L. *Drug Saf.* **1998**, 19(6), 465-480.
- Thompson, P.A.; Wright, D.E.; Counsell, C.E.; Zajicek, J. *Int. Psychogeriatr.* **2012**, 24(5), 689-697.
- Demiralay, E.C.; Alsancak, G.; Ozkan, S.A. *J. Sep. Sci.* **2009**, 32, 2928 - 2936.
- Yılmaz, H.; Demiralay, E.C. *J. Liq. Chromatogr. Relat. Technol.* **2015**, 38(1), 97-103.
- Babič, S.; Horvat, A.J.M.; Pavlović, D.; Kaštelan Macan, M. *Trends Analyt. Chem.* **2007**, 26(11), 1043-1061
- Talay, A.; Demiralay, E.C.; Daldal, Y.D.; Üstün, Z. *J. Mol. Liq.* **2015**, 208, 286-290.
- Tam, K.Y.; Hadley, M.; Patterson, W. *Talanta* **1999**, 49, 539-546.
- Tam, K.Y.; Takács-Novák, K. *Anal. Chim. Acta* **2001**, 434, 157-167.
- Sanli, S.; Altun, Y.; Guven, G. *J. Chem. Eng. Data* **2014**, 59, 4015-4020.
- Daldal, Y.D.; Çakır, C.; Yılmaz, H.; Demiralay, E.C.; Özkan, S.A.; Alsancak, G. *Curr. Drug. Ther.* **2014**, 9, 277-284.
- Sun, N.; Avdeef, A. *J. Pharm. Biomed. Anal.* **2011**, 56, 173-182.
- Narasimham, L.; Dnyandeo Barhate, V. *Eur. J. Chem.* **2011**, 2 (1), 36-46.
- Sanli, N.; Sanli, S.; Sızır, U.; Gumustas, M., Ozkan, S.A. *Chromatographia* **2011**, 73(11-12), 1171-1176.
- Canbay, H.S.; Demiralay, E.C.; Alsancak, G.; Ozkan, S.A. *J. Chem. Eng. Data* **2011**, 56(5), 2071-2076.
- Yasuda, M. *Bull. Chem. Soc. Jpn.* **1959**, 32, 429-432.
- Shedlovsky, T. *Electrolytes*, in: B. Peasce (Ed.), Pergamon Press, New York, 1962.
- Marvin Sketch program, Chemaxon, <http://www.chemaxon.com>, (accessed 2016).
- Rondinini, S.; Mussini, P.R.; Mussini, T. *Pure Appl. Chem.* **1987**, 59, 1549-1560.
- Beltran, J.L.; Codony, R.; Prat, M.D. *Anal. Chim. Acta* **1993**, 276, 441-454.
- Daldal, Y.D.; Demiralay, E.C.; Ozkan, S.A. *J. Braz. Chem. Soc.* **2016**, 27(3), 493-499.
- NLREG Version 4.0. P.H. Sherrod. <http://www.sandh.com/Sherrod>, (accessed 1991).
- Uysal, R.; Daldal, Y.D.; Üstün, Z.; Demiralay, E.C. *Eurasian J. Anal. Chem.* **2017**, 12(1), 23-43.
- Meloun, M.; Bordovská, S.; Galla, L. *SRX Pharmacol.* **2010**, 2010, 1-14.
- Hsieh, Y.H.; Yang, Y.H.; Yeh, H.H.; Lin, P.C.; Chen, S.H. *Electrophoresis* **2009**, 30(4), 644-653.
- Luan, F.; Ma, W.; Zhang, H.; Zhang, X.; Liu, M.; Hu, Z.; Fan, B. *Pharm. Res.* **2005**, 22, 1454-1460.
- Ishihama, Y.; Nakamura, M.; Miwa, T.; Kajima, T.; Asakawa, N. *J. Pharm. Sci.* **2002**, 91(4), 933-942.



 0000-0003-1211-2686 (Y.D. Daldal)

 0000-0002-6270-7509 (E. Çubuk Demiralay)

 0000-0001-5889-1537 (G. Alsancak)



4D-QSAR study of flavonoid derivatives with MCET method

Burçin TÜRKMEMOĞLU*, Hayriye YILMAZ, Ekrem Mesut SU, Tuğba ALP TOKAT, Yahya GÜZEL

Department of Chemistry, Faculty of Science, Erciyes University, 38039, Kayseri, Turkey

Received: 19 September 2017; Revised: 09 October 2017; Accepted: 13 October 2017

*Corresponding author's e-mail address: bkilic@erciyes.edu.tr (B. Türkmenoğlu)

ABSTRACT

The Molecular Conformer Electron Topological (MCET) method was performed for the identification of the pharmacophore (Pha) group and predicting inhibitory activity of 42 flavonoid ligands on gamma-aminobutyric acid/benzodiazepine receptor complex (GABAA/BZR). In this method, Electron Topological Matrix (ETM) was used to visualize 3D structural descriptors. Multiple comparisons of ETM matrices for all flavonoid compounds allow us to define Pha-structure. Genetic algorithm (GA)- Partial Least-Squares (PLS) methods were performed to construct QSAR model and to select most important descriptors of the training set (32 compounds) and test set (10 compounds). The GA-PLS based model showed good results, $q^2 = 0.808$ and $r^2_{\text{test}} = 0.775$ with high internal and external validation. The developed model can help to understand the inhibitory mechanism.

Keywords: Flavonoid derivatives, GABA_A, 4D-QSAR, MCET.

MCET Method ile Flavonoid Türevlerinin 4D-QSAR İncelemesi

ÖZ

Moleküler Konformer Elektron Topolojik (MCET) metodu, gamma-aminobütirik asit/benzodiazepin reseptör kompleksi (GABAA / BZR) üzerindeki 42 flavonoid ligandın farmakofor grubunun tanımlanması ve önleyici aktivitesinin öngörülmesi için gerçekleştirildi. Bu metotta, 3D yapısal tanımlayıcıları görselleştirmek için Elektron Topolojik Matris (ETM) kullanılmıştır. Tüm flavonoid bileşikler için ETM matrislerinin çoklu karşılaştırmaları, Pharmacophore (Pha) yapısını tanımlamamızı sağlar. QSAR modelini oluşturmak ve eğitim setinin (32 bileşik) ve test setinin (10 bileşik) en önemli tanımlayıcılarını seçmek için Genetik Algoritma (GA)-Kısmi En Küçük Kareler (PLS) yöntemleri gerçekleştirildi. GA-PLS'ye dayalı model, yüksek iç ve dış doğrulama ile $q^2 = 0.808$ ve $r^2_{\text{test}} = 0.775$ iyi sonuçlar verdi. Geliştirilen model inhibitör mekanizmasının anlaşılmasına yardımcı olabilir.

Anahtar Kelimeler: Flavonoid türevleri, GABA_A, 4D-QSAR, MCET.

1. INTRODUCTION

Flavonoids are widespread in nature, mainly in green plants¹, and exert a protective effect against both UV light and microbial invasion by pathogens in plants.^{2,3} Flavonoids⁴, which were first isolated from herbal plants and used as tranquilizers in folk medicine, have been shown to possess a selective and relatively mild affinity for the benzodiazepine binding site of γ -amino butyric acid type A receptors (GABA_ARs/BZR).⁵⁻⁷ This new family of natural products, along with various synthetic derivatives⁸, has an extremely potent anxiolytic effect which is not associated with myorelaxant, amnestic, or sedative actions.⁹ Inhibition in the adult mammalian central nervous system (CNS) is mediated by GABA. The fast-inhibitory actions of GABA are mediated by GABA_ARs, which mediate both phasic and tonic inhibition in the brain.¹⁰

QSAR of flavonoids for the inhibition of cAMP phosphodiesterase has been determined¹¹ and new inhibitors of xanthine oxidase have also been developed using a rational design approach.¹² 3-dimensional quantitative structure-activity relationship (3D-QSAR) has been applied to explore the structural requisites of flavone derivatives.^{13,14} The methods and software used for 4D-QSAR model establishment and analysis (including descriptor calculation and selection, partial least-squares-PLS- analysis, and related software) have been described in our previous publication with MCET.^{15,16} Multiple complementary applications of 4D-QSAR paradigm¹⁷ may be a good way to extend our knowledge and understanding of the SARs of flavonoids using this 'quality for quantity' argument. The fourth 'dimension' of the 4D-QSAR paradigm is ensemble sampling of the spatial features of the members of the training set.¹⁷ This sampling process in turn enables the construction of optimized dynamic spatial 4D-QSAR

models, in the form of 3D bioactive structure dependent on the structure and descriptors of the Pha.¹⁸

Complementary to building 4D-QSAR models that embed 3D bioactive structure is the construction of high-throughput 4D fingerprint models for virtual screening. The 4D-QSAR paradigm has been successfully applied to a variety of chemical classes and biological interaction points.¹⁹ Our study was focused on finding a 4D-QSAR model that able to predict the anti-benzodiazepine receptor activity of 42 flavonoid derivatives and even provides clues for mechanism of drug receptor interaction.

2. EXPERIMENTAL

2.1. Data Set

A series of flavonoids derivatives (42 compounds) with experimental biological activities was taken from the literature.²⁰ The sum of set molecules was randomly divided a training set (32 compounds) and test set (10 compounds) for confirming 4D-QSAR model. The activities of studied compounds are shown in Table 1.

2.2. Quantum Chemical Calculations

The first step in developing a QSAR model is a numerical representation of the molecular descriptors for molecules. The minimum energy conformations of the molecular geometries of fullerenes were optimized with 3-21 G* Hartree-Fock method by SPARTAN '08 (Wavefunction Inc., Irvine, CA, 2000).^{21,22} The ETM was constructed using the electronic and geometric features obtained from quantum-chemical calculations which information related to both the topological environment and the electronic character of each atom in a molecule.²³ The quantum chemical calculations were completed in water; conformers with less than 2 kcal mol⁻¹ of relative energy were selected and saved as MolFiles. The MolFiles databases were transformed to Electron Topological Matrix (ETM) format using ETM Programmer (ETMP).¹⁶

2.3. ETM and Conformer Selection

The molecular structures under investigation were represented with many conformers. The number of all total calculated conformers for each molecule was reduced to one hundred. The most active conformers were selected, and the remaining conformers and the duplicate conformers were eliminated. If each corresponding distance between the atoms in the two conformers was less than the threshold (0.4 Å), then the higher energy conformation was rejected.²³ In most populated conformers those which provided an almost perfect fit were selected. The idea underlying 4D-QSAR analysis was related to differences in the Boltzmann

average spatial distribution of conformers with respect to 3D pharmacophores.²⁴ The resulting activity is averaged over all the selected conformers of the molecule. Considering the Boltzmann population of each conformer, we obtained a mean value which contains the total of terms for all selected conformations as follows:

$$P^i \left[\% \right] = \left[\exp \left(- \frac{\Delta H^i}{RT} \right) \right] * 100 \quad (1)$$

Where P^i is the probability of a conformer, ΔH^i is the relative heat of the formation of the i^{th} conformer with respect to the lowest energy conformer (J mol⁻¹), R is the gas constant (8.314 J mol⁻¹ K⁻¹), T is the temperature in Kelvin, and N is the total number of the selected conformers. ETM is 3D structural descriptors derived from 3D structure of the molecule and are electronic in nature.²³ A detailed description of ETM has been reported in previous publications.²⁵⁻³⁰ This contains all the information about the possible action of the molecule. Theoretically, nothing is better than a full electronic structure and topology, which represent molecular ability to interact with other systems.³¹

2.4. Identification of Pha and QSAR Model Generation

In the software, firstly, the Pha structure was extracted by comparing the ETMs of all the conformers with the template conformer, and then the descriptor set in the detailed positions was automatically created and visualized. It is possible to distinguish between the repulsive and attractive effects of the descriptors such as auxiliary groups (AG) and anti-pharmacophore shielding groups (APS). The Pha structure, and subsequently the AG and APS groups should be used for QSAR modeling. The lowest energy conformer of the lead molecule was selected as the template conformer, the starting-structure for the generation of bioactive structures. The MCET method was applied for the detection and interpretation of crucial interaction patterns. The advanced bioactive structure, consisting of the Pha, AG and APS, was defined from the generated models. A bioactive structure is a 3D description developed by specifying the distance (or bond length) and amount of electronic values in the ETM. It may be generated from the superposition of the active molecules by means of their common features. Given a set of active molecules, the 3D approximate model generation of the bioactive structure involves three steps: (1) comparing and matching the molecules to identify the key pharmacophore, (2) aligning three-ordered atoms (based on Pha structure) to superimpose the remaining atoms, and (3) analyzing the various positions to define an AG and APS set, the independent variables.

In specific cases, the analysis of the group of active molecules shows that the Pha does not influence the activity quantity, and is a constant (A_0). The atoms

forming the Pha are defined as a basic skeleton. In the presence of the Pha the activity of the molecule may be diminished (partially or completely) by APS which hinders its proper docking with the receptor, or it may be enhanced by AG which provides for other properties (e.g. hydrophobicity or electrostatic attraction between L-R). To determine the AG and APS descriptors, we had to examine the structures (conformations) of the superimposed molecules. Their influence could be used to parameterize the receptor points. This parameterization at the receptor was based on AG and APS described by the electronic and geometric values known from the ETM. We suggested a general scheme for quantitative evaluation to estimate their approximate role in the activity. The main idea (somewhat similar to that involved in Pha identification) was to describe each of them by means of structural and electronic parameters and to reveal their role using a minimization procedure, as is usually done in QSAR problems. Then by processing these descriptors for the training set in comparison with the activities and performing PLS, we obtained the adjustable constants that represent each of these parameters in the activity.

In general, there is not a priority division of the AG and APS in “shielding” and “enhancing” L-R binding, and only the final optimization of the parameter values shows the different kinds of AG and APS contribution. First, we took into account that their contribution reduced or enhanced L-R binding by an amount E which reduced (or increased) the activity by a factor of $\exp(-E/kT)$. We denoted $S_{ni} = E_{ni}/kT$ and introduced the function S in a general way as follows:

$$S_{ni} = \sum_{j=1}^N \kappa_j \cdot a_{ni}^j \quad (2)$$

Where a_{ni}^j are the independent variables that describe the j^{th} kind of AG or APS in the i^{th} conformation of n^{th} molecule, N is the number of expected interactions in spite of the different position of scaffold, and κ_j indicates variational parameters (adjustable constant) relative to the interaction point of the receptor. The interaction points were selected from positions of the lowest energy conformers of the most and least active molecule. L-R cross-term descriptors in the positions were also considered, which could be helpful in the identification of AG and APS interactions in determining variation of activity. The interaction between L-R was defined by multiplying the descriptors capturing the properties of the ligand with the descriptors of the receptor and was given by Eq. (2). The magnitude of the individual weighting coefficients within the parameters indicates the relative importance of AG and APS in each position when determining activity. Thus, specific regions in the three-dimensional space, where AG and APS interactions were important, could be identified by superposition, and plotted to derive the pharmacophoric receptor maps. Using this function and taking into account the Boltzmann population of each conformation as a function of its energy and temperature T , we obtained the following general formula of activity: A_0 was a constant

(see below), and for the n^{th} molecule, m_n and m_n^{Pha} were the numbers of the selected conformations and the conformations possessing a Pha (Table 1), respectively.

$$A_n = A_0 \frac{\sum_{i=1}^{m_n^{\text{Pha}}} e^{-S_{ni}} e^{-E_{ni}/kT}}{\sum_{i=1}^{m_n} e^{-E_{ni}/kT}} \quad (3)$$

In this formula, the S_{ni} value for conformations that have a Pha contributed to the activity, and these contributions were weighted in accordance with the relative numbers of conformations in the active molecules. These numbers decreased rapidly with the energy of the conformation E_{ni} (at $E_{ni} \sim 2 \text{ kcal mol}^{-1}$ the number of conformations became lower than a 0.02 part of those in the lowest conformation at $E_{n0} = 0$). In the next section we describe how we handled the multi-conformation problem. To determine the A_0 constant, we chose a reference molecule (1) from the training set for which the activity was known and calculated A_1 after Eq. (3) by determining A_0 from this equation and substituting it in Eq. (3), we obtained:

$$A_\ell = A_0 \frac{\sum_{i=1}^{m_\ell^{\text{Pha}}} e^{-S_{\ell i}} e^{-E_{\ell i}/kT}}{\sum_{i=1}^{m_\ell} e^{-E_{\ell i}/kT}} \quad (4)$$

$$A_n = A_\ell \frac{\sum_{i=1}^{m_n} e^{-E_{ni}/kT} \sum_{i=1}^{m_n^{\text{Pha}}} e^{-S_{ni}} e^{-E_{ni}/kT}}{\sum_{i=1}^{m_n} e^{-E_{ni}/kT} \sum_{i=1}^{m_\ell^{\text{Pha}}} e^{-S_{\ell i}} e^{-E_{\ell i}/kT}} \quad (5)$$

Using the experimental data for the activities of the molecules in the training set, we estimated the adjustable constants κ_j in Eq. (2) by performing a least-squares minimization operation on the function $|A_n^{\text{pred}} - A_n^{\text{exp}}|^2$. With the constants κ_j determined in this way, we could evaluate the expected activity of any molecular system using Eq. (5). In this formula, only the choice of the $a_{ni}^{(i)}$ independent variable remained uncertain. It required some experience and skill. Bersuker and co-workers have shown how to handle the multiconformation problem successfully by using electron-conformational (EC) method.³²⁻³⁴ In comparison with the EC method, the MCET method automatically took into account a set of 3D structural descriptors for all compounds in the training set. This had a significant role for a method that considers the L-R binding, consisting of a large number of positions of the different conformers. By

simultaneously solving the rather complex problem of NLME, we demonstrated that the κ_j constant parameters for all the compounds in the training set could be defined. To do this we have presented an improved MCET method and shown its application to the problem of the binding affinities of flavonoids. As we have previously how to employ the MCET method in an earlier paper, we have not repeated it again here.¹⁶

We applied the variable selection method based on multi-objective GA to the flavonoids data and constructed the nonlinear QSAR model using Eq. (5) of NLME. The best QSAR model was selected according to the correlation coefficient R^2 and the Leave-One-Out Cross Validation (LOO-CV) correlation coefficient Q^2 . The obtained results were accurate and interpretable.

3. RESULTS AND DISCUSSION

The chemical structures of 42 flavonoids given in Table 1 were chosen from the literature.²⁰ In the MCET method, all the conformers' ETMs were compared with that of the template conformer to define Pha structure firstly, then the molecular activities were computed through 3D structural descriptors, which were analyzed using PLS regression in combination with GA. Both ETMP for transforming the data and MCET for computing the activity were written by us in C#. Electron

Topological Sub-Matrix (ETSM) representing the Pha structure were given in bold letters in Figure 1.

Using cluster analysis, the molecules were first divided into two subsets: one training set composed of 32 molecules, and one external test set (marked as *) composed of 10 molecules (N05, 06, 07, 10, 20, 22, 32, 34, 36, 38). The test set molecules were not included in 4D-QSAR model development but rather employed to analyze predictive performance. The size of the test set comprised about 22% of the whole set, ensuring that the test set contained representative samples of the training group.

Pha structures were created by combining four to six atoms in the template conformer, which was the lowest energy conformer of the N01 reference molecule. In the Pha hypotheses scoring process, each Pha and its associated bioactive structure were treated temporarily as a reference in order to assign a score, and the hypotheses were ranked according to the following scores: 1) the alignment score of Pha atoms, 2) the superimposed score of oriented atoms related to Pha 3) a superposition score consisting of Pha, AG and APS. After analysis of the alignment Pha structure in the training set, the hypothesis was generated, and then the best hypothesis consisting of 3D structural descriptors determined by the relative arrangement according to Pha structure was selected for further research.

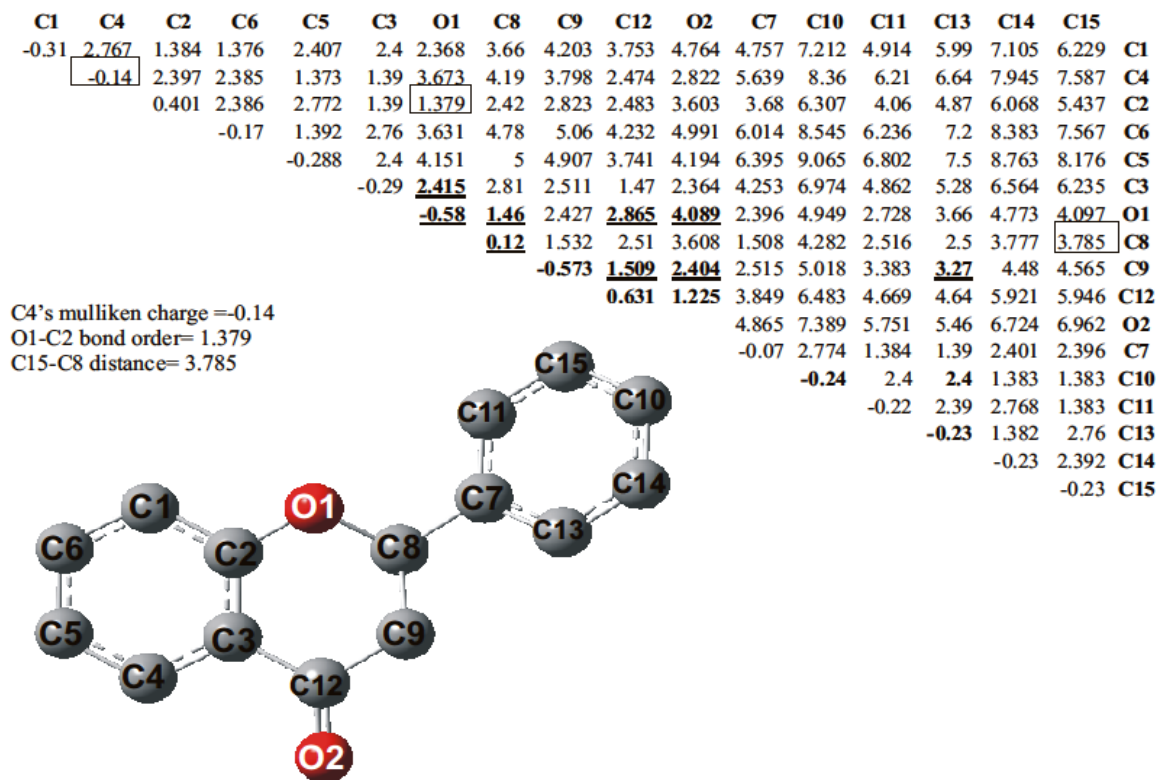


Figure 1. Reference molecule's (N01) ETM and Pha's ETSM.

Table 1. Chemical structures and observed and predicted $-\log K_i$ values by MCET method

No	Compounds							$-\log K_i$		
	R5	R6	R7	R8	R2'	R3'	R4'	Obsd.	Pred.	Residual
1	H	H	H	H	H	H	H	6.00	6.00	0
2	H	F	H	H	H	OH	H	5.60	5.90	-0.30
3	H	Cl	H	H	H	OH	H	6.07	6.29	-0.22
4	H	Br	H	H	H	OH	H	6.22	6.29	-0.70
5	H	F	H	H	H	NO ₂	H	6.74	6.61	0.13
6	H	Cl	H	H	H	NO ₂	H	8.10	7.10	1.00
7	H	Cl	H	H	H	H	OCH ₃	5.90	5.80	0.10
8	H	Br	H	H	H	H	OCH ₃	5.68	5.76	-0.08
9	H	Br	H	H	NO ₂	H	H	6.68	6.51	0.17
10	H	NO ₂	H	H	H	H	Br	7.60	6.80	0.80
11	H	Cl	H	H	F	H	H	6.38	5.82	0.56
12	H	Br	H	H	F	H	H	6.42	5.82	0.60
13	H	H	H	H	F	H	H	5.45	6.17	-0.72
14	H	F	H	H	H	F	H	6.04	6.18	-0.14
15	H	Cl	H	H	H	F	H	6.93	6.50	0.43
16	H	Br	H	H	H	F	H	7.38	6.50	0.88
17	H	H	H	H	H	H	F	5.44	5.70	-0.26
18	H	F	H	H	H	H	F	5.60	5.70	-0.10
19	H	Cl	H	H	H	H	F	6.74	6.45	0.29
20	H	Br	H	H	H	H	F	6.94	6.45	0.49
21	H	H	H	H	H	Cl	H	6.21	6.30	-0.09
22	H	F	H	H	H	Cl	H	6.70	6.31	0.39
23	H	Cl	H	H	H	Cl	H	7.64	6.73	0.91
24	H	Br	H	H	H	Cl	H	7.77	7.73	0.04
25	H	H	H	H	H	Br	H	6.38	6.31	0.07
26	H	F	H	H	H	Br	H	6.63	6.32	0.31
27	H	Cl	H	H	H	Br	H	7.64	6.73	0.91
28	H	Br	H	H	H	Br	H	7.72	6.73	0.99
29	H	Br	H	H	H	F	H	7.72	6.73	0.99
30	H	Br	H	H	H	H	NO ₂	7.15	6.73	0.42
31	H	NO ₂	H	H	H	NO ₂	H	6.70	6.70	0.00
32	H	Br	H	H	H	NO ₂	H	7.92	7.08	0.84
33	OH	Br	OH	Br	H	H	H	9.00	9.10	0.10
34	OH	H	OH	H	H	H	H	6.15	6.19	-0.04
35	OH	H	OH	H	H	H	OH	5.52	5.98	-0.46
36	OH	H	OH	H	Cl	H	H	5.52	5.58	-0.06
37	OH	H	OH	H	F	H	H	5.10	5.80	-0.70
38	OH	OCH ₃	OH	H	H	H	OH	5.10	5.80	-0.70
39	OH	OH	C ₆ H ₅ O ₇	H	H	H	H	6.00	5.50	-0.50
40	OH	OH	OH	H	H	H	H	4.11	4.98	-0.87
41	OH	OH	OH	H	H	H	OH	5.25	6.01	-0.76
42	OH	H	OH	OCH ₃	H	H	H	4.92	5.62	-0.70

The active molecules were employed to generate regression models utilizing the GA. According to the GA, all Pha hypotheses produced in the previous step were used to build the 4D-QSAR models. The 4D-QSAR model for binding affinity in the training set was constructed with the LOO-CV technique from the superposition, and then the predictive power of this model was validated by the test set molecules. For the interpretation of the results, only the relative magnitudes and signs of 3D structural descriptors at the ligand are important, not their absolute values. The degree of increase or decrease in binding affinity is strongly dependent on the values of descriptors. We studied the global structure (backbone-traces) as well as the local structure (binding sites) by comparing pair-wise the related atoms. Potentials created by atoms of the receptor and the ligand were computed on each point of the interaction interface. The number of interaction points in the ligand and receptor were considered as measures of the complexity of the system. The adjustable constants with related points in the binding site were calculated by Eq. (5) using values of the ligand atoms. For a molecule, a set of descriptors was obtained by computing the interaction energy between each surface point from the virtual receptor and the atoms in the molecule.

A Pha structure consisting of four atoms stabilized the L-R complex. In the Pha structure which was depicted in Figure 2, O1 and O2 atoms made hydrogen bonds with the receptor and the other two carbon atoms made hydrophobic bonds. The two O atoms were essential for BzR site binding affinities together with other two C atoms on Pha structure.

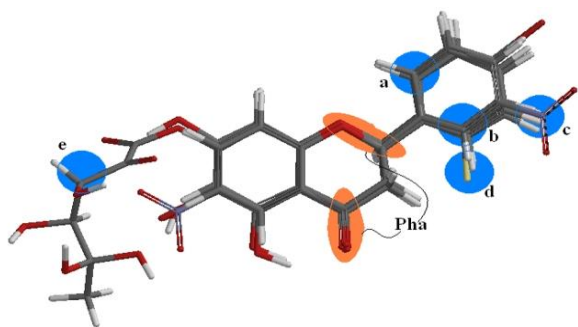


Figure 2. Common Pha structure and descriptors (AG and APS) with letters a, b, c etc. were circled.

The five descriptors shown in Figure 2 were based on simple statistics. We marked these positions with letters (a, b, c, etc.) as given in Table 2. 4D-QSAR visualization was indicated by regions of Pha structure and favorable and unfavorable descriptors of AG and APS for binding affinity, respectively.

The values of κ_j , the receptor binding parameters, were the adjustable constants corresponding to the j^{th} positions given in Table 2. The positions were properly determined by the dihedral angle, angle and distance according to the first 3 atoms (O1, C8 and C12) of the Pha. One can describe the distance between 2 atoms, the

angle among 3 atoms and the dihedral angle among 4 atoms. As could be seen in Table 2, for instance, the distance between the C13 atom and O1 in N32 molecule was 2.71 Å; in the same orientation in atomic order the angle among C13-O1-C8 was about 66.72 degrees and the dihedral angle among C13-O1-C8-C12 was 42.61 degrees, where the Pha atoms were shown as underlined.

The quantitative explanation of the binding affinity is impossible due to the cooperative effects of the interacting points. It is appropriate to explain each interaction by discarding the relationships among different types of interaction. Since quantitative explanation required all the interactions of the model in Eq. (5), qualitative analysis was done for each interaction. The qualitative analysis occurred when the simple treatment effect in at least one position had a different sign or magnitude from that in other positions: this interaction was important. Only qualitative interpretation of the data obtained from the lowest energy conformers seemed to be easy because their effect on activity was greater. Therefore, the use of descriptors for only these conformers might be appropriate.

In this study, the atomic charge was used as a descriptor. Systematic studies on the influence of descriptors in various positions in Table 3 revealed the introduction of their sign and magnitude change activity. Discussing the magnitude and sign of the different charge at each position, we could qualitatively interpret the effect of a-, b-, c- descriptors on the predicted binding affinities in the following text.

To show the effect of charge exchange in the a- and b-positions of the interaction points, the instances of the molecules N01, N10, N29, N30 and N40 in Table 3, in which the first of the two conformers included a- and b-positions, were taken. Although atomic charge values in b-position were almost constant, the difference of those in a-position helped us to interpret its effect on the activity. A smaller negative value of the charges in a-position correlated with a lower activity value for the molecules. The correlation between the charge values in a-position and activities is due to the negative interaction between L-R. The higher magnitude of negative charge in N01 and N40 (-0.573 and -0.568 au, respectively) dramatically decreased the activity more than in N10, N29 and N30 (-0.204, -0.218 and -0.230 au). This result indicates that the negative charge in the a-position of the ligands interacts with the negative charge on the corresponding receptor site. Hence, an atom of negative charge in a-position for any ligand would act as APS with this point of receptor, and leads to the negative interaction.

With regards to b-position, there is no a clear clue in Table 3 since there was no ligand possessing only b-position, and since the charge value in the b-position for the aforementioned molecules was not changed. However, we could interpret the effect of b-position by comparing the values of κ_j in Table 2. The negative charges of conformers in a-position had a negative interaction with the negative value (-0.354) of κ_j , and

Table 2. The positions defined from the proper places of the atoms within 3 molecules (N32, N37 and N39), among the most and least active molecules

Mol. No	Conf. No	Atom No	j-nth Position	Dihedral Angle	Angle	Distance	κ_j
N32_01		C13	a	42.61	66.72	2.71	-0.354
N32_01		C11	b	16.78	29.98	3.65	0.116
N32_01		N1	c	16.70	35.71	6.03	-0.156
N37_01		F1	d	356.11	11.08	4.14	-0.256
N39_01		C18	e	347.64	138.44	7.81	-17.622

Table 3. Exp. and pred. binding affinities, relative energy and structural properties of molecules N01, N10, N29, N30 and N40, which had two conformers of a- and b-position

Mol.	Exp.	Pred.	Position	Atomic charge (au)	Conformer-1	Conformer-2	$\Delta E_{(\text{conf2-conf1})}$
					Heat of form. (kJ mol ⁻¹)	Heat of form. (kJ mol ⁻¹)	
N01	6.0	6.0	a	-0.573	-1892260.32	-1892254.34	5.98
			b	-0.232			
N10	7.6	6.8	a	-0.204	-9143856.68	-9143852.22	4.46
			b	-0.217			
N29	7.15	6.73	a	-0.218	-8612723.14	-8612717.8	5.34
			b	-0.231			
N30	6.70	6.70	a	-0.230	-9143853.63	-9143846.65	6.98
			b	-0.243			
N40	5.25	6.01	a	-0.568	-2478674.71	-2478668.64	6.07
			b	-0.231			

worked as an APS group. In the same way, the negative charge in b-position acts as an AG group with the positive value (0.116) of κ_j . In this case, the higher negative charge in b-position had more effect for AG group.

As for N17-N20, they also had substituents in c-position together with a- and b- positions at their lowest energy conformer. Likewise, their second conformers did not contain an atom in any positions like N01, N10, N29, N30 and N40. Furthermore, the addition of negative charge in c-position of ligands N17 and N18 reduced activity; on the other hand, the addition of positive charge in ligands N19 and N20 enhanced activity. The activity of ligands N19 and N20 was the much more potent than that of ligands N17 and N18 due to the change in charge from negative to positive in c-position. The negative charge in c-position may have been responsible for their lower binding affinities.

To explain of charge effect in d-position there was no restricted molecule. We could interpret it as for the b-position by looking at the value of κ_j . The interaction of the negative value (-0.256) of κ_d with positive charges of conformers in d-position enhanced activity, and acted as an AG group.

For the e-position in which only ligand N39 had a substituent, the activity was decreased dramatically to 4.98 with a κ_e value of -17.622. The big change in interaction shows that there might be steric hindrance between the large size of groups within receptor and groups crowded around the C18-atom at N39. The repulsion in e-position between the receptor and ligand may occur.

This method also aided in understanding the structure–activity relationship revealed by 4D-QSAR. After a series of hierarchical filters in the MCET was systematically used to search for possible locations of the ligand in the active-site region, the study was applied to show the functional group effects. The molecules were analyzed with the binding sites to study the possible binding mode. The resultant activity revealed that a total of five functional groups were formed together with a Pha structure. The negative charges in a-, c- and d-positions of the ligand destabilized the L-R complex due to the negative interaction; on the other hand, the positive interaction in the b-position stabilized it. In addition, the active site of the receptor may be surrounded by some groups of carbon atoms in the e-position.

The statistical parameters associated in the generated QSAR model are as follows: leave-one-out $q^2 = 0.808$ (for internal validation), and predictive $r^2 = 0.775$ (for external validation). These values indicated a high degree of confidence. The regression scheme of the observed and predicted activities was shown in Figure 3. The predicted activities of the training and test set molecules were also listed in Table 4. The MCET method has been shown to be both useful and reliable for the construction of 4D QSAR models with a 3D bioactive structure.

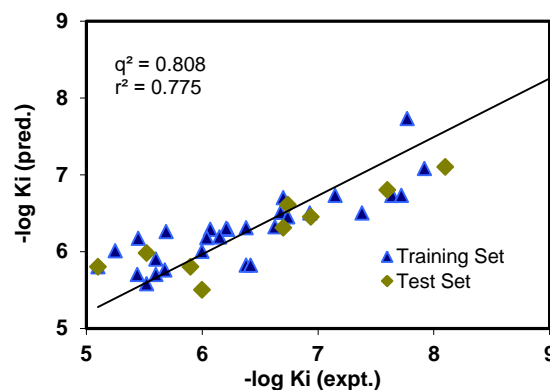


Figure 3. Fitness graph between observed and predicted binding affinity for training and test set molecules.

Table 4. Experimental and predicted activities of molecules, relative energy of the conformers and each atomic position showed by a letter a, b, c etc. in conformers

Mol	Exp.	Pred.	The heat of formation (kJ mol ⁻¹) and positions of conformers*					
N01	6.00	6.00	-1892260.3ab	-1892254.3	-	-	-	-
N02	5.60	5.90	-2345858.9ab	-2345857.9abc	-2345857.6ab	-2345856.4abc	-	-
N03	6.07	6.29	-3287100.8ab	-3287099.9abc	-3287099.5ab	-3287098.2abc	-	-
N04	6.22	6.29	-8808180.4ab	-8808179.4abc	-8808178.9ab	-8808177.8abc	-	-
N05*	6.74	6.61	-2681531.3ab	-2681531.3abc	-	-	-	-
N06*	8.10	7.10	-3622773.4abc	-3622773.2ab	-	-	-	-
N07*	5.90	5.80	-3388991.9abc	-3388991.6ab	-3388988.3	-	-	-
N08	5.68	5.76	-8910071.6abc	-8910071.1ab	-8910067.8	-	-	-
N09	6.68	6.51	-9143844.9abd	-9143832.3	-9143821.5a	-9143820.0ab	-9143817.4a	-
N10*	7.60	6.80	-9143856.7ab	-9143852.2	-	-	-	-
N11	6.38	5.82	-3349802.2abd	-3349795.5	-3349790.7ab	-3349787.4a	-	-
N12	6.42	5.82	-8870881.78abd	-8870875.1	-8870870.3ab	-8870866.9a	-	-
N13	5.45	6.17	-2150410.1ab	-2150409.4abc	-2150403.9	-2150403.2	-	-
N14	6.04	6.18	-2408551.0ab	-2408550.2abc	-2408545.3	-2408544.4	-	-
N15	6.93	6.50	-3349792.9ab	-3349792.2abc	-3349787.3	-3349786.5	-	-
N16	7.38	6.50	-8870872.5ab	-8870871.7abc	-8870866.8	-8870865.9	-	-
N17	5.44	5.70	-2150409.3abc	-2150403.6	-	-	-	-
N18	5.60	5.70	-2408550.2abc	-2408544.9	-	-	-	-
N19	6.74	6.45	-3349792.2abc	-3349787.1	-	-	-	-
N20*	6.94	6.45	-8870871.8abc	-8870866.6	-	-	-	-
N21	6.21	6.30	-3091649.1ab	-3091648.4ab	-3091642.6	-3091641.9	-	-
N22*	6.70	6.31	-3349790.1ab	-3349789.3ab	-3349784.0	-3349783.2	-	-
N23	7.64	6.73	-4291032.1ab	-4291031.4ab	-4291026.2	-4291025.5	-	-
N24	7.77	7.73	-9812111.6ab	-9812110.9ab	-9812105.6	-9812104.9	-	-
N25	6.38	6.31	-8612727.9ab	-8612727.4ab	-8612721.6	-8612720.7	-	-
N26	6.63	6.32	-8870868.9ab	-8870868.3ab	-8870863.1	-8870862.0	-	-
N27	7.64	6.73	-9812110.9ab	-9812110.3ab	-9812105.2	-9812104.2	-	-
N28	7.72	6.73	-15333190.4ab	-15333189.9ab	-15333184.7	-15333183.7	-	-
N29	7.15	6.73	-8612723.1ab	-8612717.8	-	-	-	-
N30	6.70	6.70	-9143853.6ab	-9143846.7	-	-	-	-
N31	7.92	7.08	-2954518.4ab	-2954518.3abc	-2954513.1	-2954512.8	-	-
N32*	9.00	9.10	-9143852.9abc	-9143852.8ab	-9143846.8	-9143846.8	-	-
N33	6.15	6.19	-15724126.4ab	-15724124.2	-15724123.4ab	-	-	-
N34*	5.52	5.98	-2283217.7ab	-2283215.4ab	-2283211.6	-	-	-
N35	5.52	5.58	-2478673.9abc	-2478671.4abc	-2478670.9ab	-2478668.8 [§]	-2478668.2	-
N36*	5.10	5.80	-3482602.9ab	-3482591.3	-3482588.8	-3482586.2 [§]	-348258.9ab	-
N37	5.10	5.80	-2541376.7abd	-2541370.2	-2541363.0ab	-2541360.2 [§]	-	-
N38*	6.00	5.50	-2776015.1abc	-2776010.1	-2775985.7abc	-	-	-
N40	5.25	6.01	-2478674.7ab	-2478668.6	-2478646.0ab	-	-	-
N41	4.92	5.62	-2674131.0abc	-2674130.2ab	-2674125.6	-2674102.1abc	-	-
N42	5.69	6.26	-2580553.6ab	-2580551.5	-2580545.4a	-2580531.8ab	-2580531.4	-

*More than 5 conformers were not shown

[§]Conformers, which not possessing Pha structure, were not affecting the binding affinity

*Test set compounds

4. CONCLUSIONS

The MCET method used in this work is related to the class of ligand-based approaches in drug design. Considering the properties of a ligand rather than its biological target (biological receptor), such methods are especially useful for the prediction of activity when the structure of the receptor is unknown. As the main part of this work, we have constructed a model showing the interaction between the receptor and the Pha, AG and APS groups in the multiple conformers of the ligand.

In summary, for a series of flavonoids, a significant 4D-QSAR model was applied to 32 ligands in the training set and validated with satisfactory predictions with 10 ligands in the test set. The results of the model suggest that a Pha structure consisting of four atoms is required for the activity, depending on the interactions of the 3D structural identifiers. In addition, the model shows the contribution of the different AG and APS values of each ligand conformer to activity. Furthermore, it is explained how the AG and APS atoms have influence in which positions due to the alignment of the Pha structure in the model. It has been shown how the activity of flavone derivatives can be influenced by positive (AG) or negative (APS) interactions in the defined positions. The present study provided useful guidelines through 3D structural identifiers to develop flavone derivatives as potent active molecules in ligand-based drug design approaches.

Conflict of interest






Authors declare that there is no a conflict of interest with any person, institute, company, etc.

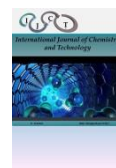
REFERENCES

- Martens, S.; Mithöfer A. *Phytochem.* **2005**, 66, 2399-2407.
- Harborne, J.B.; Williams C.A. *Phytochem.* **2000**, 55, 481-504.
- Treutter, D. *Environ. Chem. Lett.* **2006**, 4: 147-157.
- Medina, J.H.; Viola, H.; Wolfman, C.; Marder, M.; Wasowski, C.; Calvo, D. Paladini AC. *Neurochem. Res.* **1997**, 22, 419-425.
- Marder, M.; Viola, H.; Wasowski, C.; Wolfman, C.; Waterman, P.G.; Cassels, B.K.; Medina, J.H.; Paladini, A.C. *Biochem. Biophys. Res. Commun.* **1996**, 223, 384-389.
- Marder, M.; Zinczuk, J.; Colombo, M.I.; Wasowski, C.; Viola, H.; Wolfman, C.; Medina, J.H.; Ruveda, E.A.; Paladini, A.C. *Bioorg. Med. Chem. Lett.* **1997**, 7, 2003-2008.
- Marder, M.; Viola, H.; Bacigaluppo, J.A.; Colombo, M.I.; Wasowski, C.; Wolfman, C.; Medina, J.H.; Ruveda, E.A.; Paladini, A.C. *Biochem. Biophys. Res. Commun.* **1998**, 249, 481-485.
- Teuber, L.; Watjen, F.; Jensen, L.H. *Curr. Pharm. Des.* **1999**, 5, 317- 343.
- Argyropoulos, S.V.; Nutt, D. *Eur. Neuropsychopharmacol.* **1999**, 6, 407-412.
- Tija, C.J.; Stephen, J.M.; Rachel, J. *Nat. Rev. Neurosci.* **2008**, 9, 331-343.
- Amić, D.; Davidović-Amić, D.; Jurić, A.; Lučić, B.; Trinajstić, N. *J. Chem. Inf. Comput. Sci.* **1995**, 35, 1034-1038.
- Costantino, L.; Rastelli, G.; Albasini, A. *Eur. J. Med. Chem.* **1996**, 31, 693-699.
- Li, G.; Mian, Z.; Song, W.; Ai-Lin, L.; Guan-Hua, D. *Bioorg. Med. Chem. Lett.* **2011**, 21, 5964-5970.
- Duchowicz, P.R.; Vitale, M.G.; Castro, E.A.; Autino, J.C.; Romanelli, G.P.; Bennardi, D.O. *Eur. J. Med. Chem.* **2008**, 43, 1593-1602.
- Yilmaz, H.; Güzel, Y.; Önal, Z.; Altiparmak, G.; Özhan-Kocakaya, Ş. *Bull. Korean Chem. Soc.* **2012**, 32, 4352-4360.
- Yilmaz, H.; Güzel, Y.; Boz, M.; Türkmenoğlu, B. *Trop. J. Pharm. Res.* **2014**, 13,117-129.
- Hopfinger, A.J.; Wang, S.; Tokarski, J.S.; Jin, B.; Albuquerque, M.; Madhav, P.J.; Duraiswami, C. *J Am Chem Soc.* **1997**, 119, 10509-10524.
- Hopfinger, A.J.; Reaka, A.; Venkatarangan, P.; Duca, J.S.; Wang, S. *J. Chem Inf Comput Sci.* **1999**, 39: 1151-1160.
- Senese, C.L.; Duca, J.; Pan, D.; Hopfinger, A.J.; Tseng, Y.J. *J. Chem. Inf. Comput. Sci.* **2004**, 44: 1526-1539.
- Huang, X.; Liu, T.; Gu, J.; Luo, X.; Ji, R.; Cao, Y.; Xue, H.; Wong, J.T.; Wong, B.L.; Pei, G.; Jiang, H.; Chen, K. *J. Med. Chem.* **2001**, 44, 1883-1891.
- Bernardino, A.M.R.; Castro, H.C.; Frugulhetti, L.C. P.P.; Loureiro, N.I.V.; Azevedo, A.R.; Pinheiro, L.C.S.; Souza, T.M.L.; Giongo, V.; Passamani, F.; Magalhaes, U.O.; Albuquerque, M.G.; Cabral, L.M.; Rodrigues, C.R. *Bioorg. Med. Chem.* **2008**, 16, 8670-8675.

22. Bernardino, A.M.R.; Pinheiro, L.C.S.; Rodrigues, C.R.; Loureiro, N.I.V.; Castro, H.C.; Lanfredi-Rangel, A.; Sabatini-Lopes, J.; Borges, J.C.; Carvalho, J.M.; Romeiro, G.A.; Ferreira, V.F.; Frugulhetti, I.C.P.P.; Vannier-Santos, M.A. *Bioorg. Med. Chem.* **2006**, *14*, 5765-5770.
23. Bharatam, P.V. Modeling and Informatics in Drug Design. *Precilinal Development Handbook.* **2008**, 1-47.
24. Hopfinger, A.J.; Wang, S.; Tokarski, J.S.; Jin, B.; Albuquerque, M.; Madhav, P.J.; Duraiswami, C. *J. Am. Chem. Soc.* **1997**, *119*, 10509-10524.
25. Karelson, M.; Lobanov, V.S.; Katritzky, A.R. *Chem Rev.* **1996**, *96*, 1027-1044.
26. Bersuker, I.B.; Dimoglo, A.S. In *Reviews in Computational Chemistry*, Lipkowitz, K. B., Boyd, D.B., Eds.; VCH: New York, NY, U.S.A., 1991; Vol 2, pp 423-460.
27. Bersuker, I.B.; Dimoglo, A.S.; Yu, M.; Gorbachov, P.; Vlad, F.; Pesaro, M. *New J. Chem.* **1991**, *15*, 307-320.
28. Dimoglo, A.S.; Beda, A.A.; Shvets, N.M.; Gorbachov, M.Y.; Kheifits, L.A.; Aulchenko, I.S. *New J. Chem.* **1995**, *19*, 149-154.
29. Guzel, Y.; Saripinar, E.; Yildirim, I. *J. Mol. Struct.* **1997**, *418*, 83-91.
30. Guzel, Y.; Ozturk, E. *Bioorg. Med. Chem.* **2003**, *11*, 4383-4388.
31. Bersuker, I.B. *J Comput. Aided Mol. Des.* **2008**, *22*, 423-430.
32. Bersuker, I.B.; Bahceci, S.; Boggs, E.J. *The Electron Conformational Method of Identification of Pharmacophore and Anti-Pharmacophore Shielding*. In *Pharmacophore Perception. Development, and Use in Drug Design*. Guner OF., Ed.; International University Line: La Jolla, 2000, 457-474.
33. Bersuker, I.B.; Bahceci, S.; Boggs, E.J.; Pearlman, R.S. *J. Comput. Aided Mol. Des.* **1999**, *13*, 419-434.
34. Bersuker, I.B.; Bahceci, S.; Boggs, E.J.; Pearlman, R.S. *Environ. Res.* **1999**, *10*, 157-173.

ORCID

-  0000-0002-5770-0847 (B. Türkmenoğlu)
-  0000-0001-9305-8364 (H. Yılmaz)
-  0000-0002-4519-914 3 (E.M. Su)
-  0000-0003-2713-7093 (T. Alp Tokat)
-  0000-0002-4698-1866 (Y. Güzel)



Vibrational Spectra of 4-hydroxy-3-cyano-7-chloro-quinoline by Density Functional Theory and ab initio Hartree-Fock Calculations

Kani ARICI*

Department of Physics, Faculty of Sciences and Arts, 7 Aralık University, 79000, Kilis, Turkey

Received: 19 September 2017, Revised: 23 October 2017, Accepted: 24 October 2017

*Corresponding author's e-mail address: arici@kilis.edu.tr (K. Arıcı)

ABSTRACT

The infrared vibrational spectra of 4-hydroxy-3-cyano-7-chloro-quinoline (4H3CN7CLQ) molecule in the solid phase were download from the NIST Chemistry WebBook. In order to calculate the frequency of molecular vibrations the 4H3CN7CLQ molecule was optimized in the HF and DFT theories in the basic case. All frequencies calculated with HF/6-311G(dp) and DFT/B3LYP/6-311G(dp) were scaled to 0.9085 and 0.9669, respectively. All calculations were not limited and performed on a personal computer using GaussView visualization and GAUSSIAN09 program package. The frequencies values obtained by scaling were compared with the experimental values one by one. Correlation graphs were drawn between experimental and theoretical values. However, some modes of vibration frequencies are also provided. The frequency values obtained from the HF and DFT methods are seen in good agreement with the experimental data.

Keywords: 4-hydroxy-3-cyano-7-chloro-quinoline, IR, HF, DFT

4-hidroksi-3-siyano-7-kloro-kinolin'in Yoğunluk Fonksiyon Teorisi ve Hartre Fock ile titreşim spektrumunun hesaplanması

ÖZ

4 - hidroksi - 3 - siyano - 7 - kloro - kinolin (4H3CN7CLQ) molekülünün katı fazdaki kızılötesi titreşim spektrumu, NIST Chemistry Web sayfasından alındı. Moleküler titreşimlerin frekansını hesaplamak için, temel durumda HF ve DFT teorilerinde 4H3CN7CLQ molekülünün optimize edilmesi yapıldı. HF / 6-311G (dp) ve DFT / B3LYP / 6-311G (dp) ile hesaplanan tüm frekanslar sırasıyla 0.9085 ve 0.9669 ile ölçeklendirildi. Tüm hesaplamalar sınırlandırılmadan GaussView ve GAUSSIAN09 paket programı kullanılarak kişisel bilgisayarda yapıldı. Ölçekleme ile elde edilen frekans değerleri, deneysel değerlerle bire bir karşılaştırıldı. Deneysel ve teorik veriler arasında korelasyon grafikleri çizildi. Bununla birlikte bazı titreşim frekanslarının şekilleri verilmiştir. HF ve DFT yöntemlerinden elde edilen frekans değerlerinin deney verileri ile iyi uyum içinde olduğu görülmektedir.

Anahtar Kelimeler: 4-hidroksi-3-siyano-7-kloro-kinolin, IR, HF, DFT

1. INTRODUCTION

8-Hydroxyquinoline and its derivatives are well known with their antibacterial, antifungal and antiamoebic activities.¹ Quinoline derivatives have attracted a special interest due to their therapeutic properties.² Quinoline sulphonamides have been used in the treatment of tuberculosis, malaria, diabetes and cancer.³⁻⁶ Recently, Arjunan and co-workers⁷ have calculated the infrared vibrations of the 7-bromo-5-chloro-8-hydroxyquinoline molecule by the HF and DFT methods. Arıcı and Yılmaz⁸ have studied infrared spectrum of 2-Methyl-8-quinolinol using DFT and HF theoretical calculations. At present, there is no theoretical infrared vibrational work on the 4-hydroxy-3-cyano-7-chloro-quinoline molecule in the literature. In this study,

vibrational frequency results of 4-hydroxy-3-cyano-7-chloro-quinoline molecule are obtained by ab initio HF and DFT calculations. Optimal vibrational wavenumbers and modes of 4-hydroxy-3-cyano-7-chloro-quinoline molecule are also given.

2. EXPERIMENTAL

In this study, 4-hydroxy-3-cyano-7-chloro-quinoline molecule is named as 4H3CN7CLQ. Infrared spectra of 4H3CN7CLQ recorded between 4000-600 cm⁻¹ using solid KBR pellet of 1.0% were download from the NIST Chemistry WebBook.⁹ Infrared spectra of 4H3CN7CLQ recorded between 4000-600 cm⁻¹ using solid KBR pellet of 1.0%.

2.1. Computational details

The 4H3CN7CLQ was optimized in the base case using the 6-311G(dp) baseline set in HF and DFT/B3LYP method. The optimized parameters were used in the vibrational frequency calculations at HF and DFT levels. DFT for all studies reported in this paper was calculated from Eq. (1)

$$E_{xc} = (1 - a_0) E_x^{LSDA} + a_0 E_x^{HF} + a_x \Delta E_x^{B88} + a_c E_c^{LYP} + (1 - a_c) E_c^{VWN} \quad (1)$$

Where, the energy terms are the Slater exchange, the Hartree-Fock exchange, Becke's exchange functional correlation, the gradient correlated functional correlation of Lee, Yang and Parr and the local correlation functional of Vosko, Wilk and Nusair¹⁰, respectively.

HF/6-311G(dp) and DFT/B3LYP/6-311G(dp) levels of theory with the optimized geometries were used to calculate infrared vibrations of the 4H3CN7CLQ molecule. All the calculated vibrational frequencies was scaled by 0.9085 for HF/6-311G(dp) and 0.9669 for BLYP/6-311G(dp).¹¹ All calculations were made on a computer using GaussView¹² visualization and GAUSSIAN09¹³ package programs without limitation of the molecular structure.

3. RESULTS AND DISCUSSION

The 4H3CN7CLQ molecule includes 19 atoms. The 51 normal vibrational modes are distributed in the a' and a'' symmetry species at the Cs point group. The normal vibrations of a' and a'' can be attributed to the plane-in and plane-out modes, respectively. All vibrations are both infrared and Raman active. The molecular structure of the 4H3CN7CLQ and numbering of atoms in the molecule are shown in Figure 1.

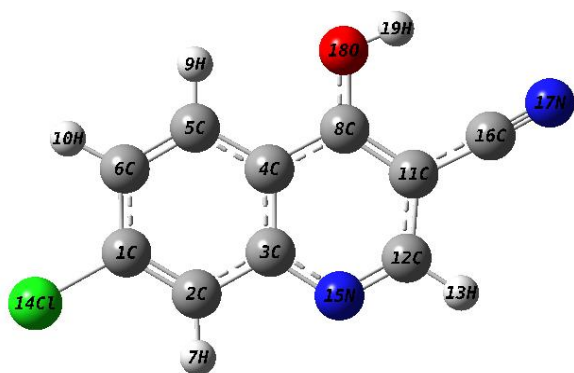


Figure 1. The molecular structure of 4H₃CN₇CLQ.

3.1. Vibrational Assignments

The observed infrared spectra of the 4H3CN7CLQ molecule are given in Figure 2. The frequencies calculated with HF/6-311G(dp) and DFT/B3LYP/6-

311G(dp) are given in Table 1 with their relative intensities, probable assignments. The observed frequencies are usually lower than the corresponding calculated frequencies which are unscaled. It is well known that HF method tends to overestimate vibrational frequencies.

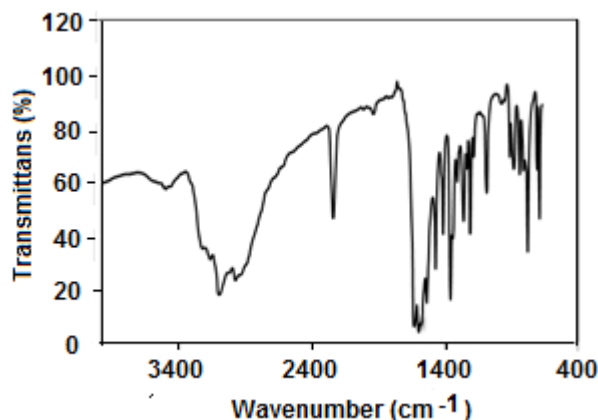


Figure 1. Infrared spectra of 4H₃CN₇CLQ molecule.

3.1.1. O-H vibrations

O-H vibrations are sensitive in hydrogen-bonded molecules, so marking them is difficult. The non-hydrogen bonded or free hydroxyl group give a strong absorption peak in 3700-3500 cm⁻¹.¹⁴ For solids, liquids and concentrated solutions, a broad band of less intensity is observed normally. If Inter-molecular hydrogen bonding is present, the O-H stretching band would reduce to 3550-3200 cm⁻¹ region.¹⁵ The computed wave number for the O-H stretching is observed at 3737.950 cm⁻¹ by HF/6-311G(d,p) and at 3738.723 cm⁻¹ by B3LYP/6-311G(d,p), while the O-H stretching in the experimental FT-IR spectrum are observed at 3500 cm⁻¹. The O-H in-plane bending vibrations are mixed with C-H stretching vibrations. In-plane O-H vibrations were observed between 1440- 1260 cm⁻¹.¹⁶ The experimentally observed strong band at 1216 cm⁻¹ can be assigned to O-H in-plane bending vibration. This band is calculated at 1229.872 cm⁻¹ by HF/6-311G(d,p) and at 1259.441 cm⁻¹ by B3LYP/6-311G(d,p) method. The O-H out-of-plane bending vibrations are appeared as broad region around 700-600 cm⁻¹. The strong band observed at 696 cm⁻¹ at the spectrum is assigned to O-H out-of-plane bending vibration, which shows good correlation with computed wave number at 689.094 cm⁻¹ by HF/6-311G(d,p) and at 682 cm⁻¹ by B3LYP/6-311G(d,p) methods. The weak band observed at 1187 cm⁻¹ indicates C-(OH) stretching band, whereas this band have been calculated at 1176.953 cm⁻¹ by the HF/6-311G(d,p) and at 1204,272 cm⁻¹ by the B3LYP/6-311G(d,p), respectively. Some researchers have assigned C-(OH) stretching band around 1200 cm⁻¹ in substituted benzenes and pyridine molecule.^{17,18}

Table 1. The observed infrared wavenumbers and calculated frequencies using HF/6-311G(dp) and DFT/B3LYP/6-311G(dp) with scaled frequencies, their intensities and probable assignments of 4H3CN7CLQ

N.	S.	Calculation HF/6-311G(dp)			Calculation BLYP/6-311G(dp)			Exp. (cm ⁻¹) ¹	Approximate description
		Unscaled (cm ⁻¹)	Scaled ^a (cm ⁻¹)	Infrared int.	Unscaled (cm ⁻¹)	Scaled ^b (cm ⁻¹)	Infrared int.		
1	A''	63.002	57.237	1.3831	57.683	57.504	1.130	-----	Butterfly
2	A''	127.209	115.569	0.3266	115.038	114.682	0.222	-----	Torsion Molecule
3	A'	130.715	118.754	7.314	115.685	115.326	6.397	-----	δ (C≡N)
4	A''	184.443	167.567	4.981	168.317	167.796	4.225	-----	δ Molecule
5	A'	223.296	202.865	2.761	204.513	203.879	2.170	-----	δ (C-Cl) + δ (C-OH)
6	A''	286.651	260.422	0.141	260.572	259.764	0.420	-----	γ (CCC)
7	A''	311.493	282.991	6.602	285.172	284.288	4.966	-----	Fluctation
8	A'	312.847	284.221	2.609	291.1792	290.276	2.415	-----	γ (CCC)
9	A'	391.502	355.679	6.158	364.865	363.734	6.243	-----	γ (CCC)
10	A''	468.565	425.692	98.163	437.168	435.813	26.070	-----	δ (C-OH)
11	A''	493.862	448.674	32.485	468.122	466.671	4.460	-----	δ (CCC)+δ (CCN)
12	A'	504.858	458.663	8.093	474.876	473.404	5.130	-----	γ (CCC)
13	A'	512.480	465.588	1.901	491.4503	489.926	50.563	-----	γ (CCC)
14	A''	540.161	490.736	1.301	492.732	491.205	32.424	-----	δ (CCC)
15	A'	577.716	524.854	2.620	537.518	535.851	3.538	-----	γ (CCC)
16	A'	613.981	557.802	3.273	571.347	569.575	0.499	-----	δ (CCC)
17	A''	629.762	572.138	0.353	571.886	570.113	3.311	-----	δ (CCC)
18	A'	684.579	621.940	0.039	638.569	636.590	0.319	-----	δ (CCN)
19	A''	709.142	644.255	7.207	645.7285	643.726	5.735	-----	γ (CCC) + γ (CNC)
20	A'	758.497	689.094	0.992	699.731	697.562	14.253	696 s.	δ (CCC)
21	A''	773.134	702.392	19.713	706.668	704.477	2.1463	712 m.	γ (O-H)
22	A'	847.389	769.853	26.409	790.111	787.662	30.424	784 s.	ν(C-Cl)
23	A''	882.412	801.671	36.475	798.921	796.444	18.614	814 m.	γ(C-H)
24	A''	932.683	847.342	7.628	846.018	843.395	12.495	841 m.	γ(C-H)
25	A'	988.191	897.771	61.037	913.982	911.149	11.541	888 m.	δ (CCC)
26	A''	1009.357	917.000	21.848	915.393	912.555	54.068	918 w.	γ(C-H)
27	A'	1011.930	919.338	75.725	950.847	947.899	71.132	-----	δ (CCC)
28	A''	1086.895	987.444	4.181	960.247	957.270	8.192	979 w.	γ(C-H)
29	A''	1107.031	1005.737	0.751	988.649	985.585	0.887	-----	γ(C-H)
30	A'	1152.299	1046.864	38.854	1083.254	1079.896	40.163	1089 m.	Ring Breathing
31	A'	1186.092	1077.564	30.358	1137.942	1134.414	14.115	-----	δ(C-H)
32	A'	1232.556	1119.777	42.117	1195.758	1192.051	46.715	1187 w.	ν(C-OH)
33	A'	1295.490	1176.953	6.560	1208.019	1204.274	5.290	-----	δ(C-H)
34	A'	1353.739	1229.872	65.053	1263.357	1259.441	70.196	1216 s.	δ(O-H)
35	A'	1378.370	1252.249	3.727	1280.163	1276.195	8.644	1265 s.	δ(C-H)
36	A'	1399.001	1270.992	29.103	1292.227	1288.221	31.244	1312 m.	δ(C-H)
37	A'	1433.059	1301.934	54.790	1358.340	1354.129	38.757	1345 s.	Ring ν(C-C)
38	A'	1483.143	134.435	45.820	1385.083	1380.790	49.139	1364 v.s.	Ring ν(C-C)
39	A'	1533.148	1392.865	65.705	1421.695	1417.287	44.677	1420 s.	Ring ν(C-C)
40	A'	1578.032	1433.642	80.289	1466.028	1461.483	54.311	1447 s.	Ring ν(C-C)
41	A'	1600.953	1454.466	2.264	1476.435	1471.858	1.2246	-----	Ring ν(C-C)
42	A'	1638.573	1488.644	102.302	1516.220	1511.520	86.740	1541 v.s.	Ring ν(C-C)
43	A'	1757.813	1596.973	202.014	1592.599	1587.662	133.577	1585 v.s.	Ring ν(C-C) + ν(C-N)
44	A'	1796.870	1632.457	24.111	1634.487	1629.420	9.1501	1602 v.s.	Ring ν(C=C)
45	A'	1823.409	1656.567	388.168	1651.032	1645.914	235.855	1636 v.s.	Ring ν(C=C)+ ν(C=N)
46	A'	2569.205	2334.122	105.272	2318.738	2311.549	78.652	2243 s.	ν(C≡N)
47	A'	3328.739	3024.159	10.885	3154.583	3144.804	7.607	2979 s. br	ν(C-H)
48	A'	3364.817	3056.936	0.239	3199.817	3189.898	0.080	3102 s. br	ν(C-H)
49	A'	3382.392	3072.903	1.568	3213.726	3203.763	1.022	3168 s.br.	ν(C-H)
50	A'	3385.895	3076.085	0.928	3219.655	3209.674	0.846	3225 s.br.	ν(C-H)
51	A'	4114.420	3737.950	166.759	3750.349	3738.723	112.306	3500 br.	ν(O-H)

^aScaling factor (s.f.): 0.9085, ^b(s.f.): 0.9669, def.: deformation, int.: intensity, br.: broad, m.: medium, s.: strong, w.: weak, v.: very, ν: stretching, δ: in-plane bending, γ: out of plane bending, Exp.: Experimental, N.: number, S.: species, W.num.: wavenumber.

3.1.2. C-H vibrations

Usually, CH stretching vibrations in aromatic structures have observed in the region $3000\text{--}3250\text{ cm}^{-1}$ ¹⁹ and they are pure vibrations. In the present study, the bands at 3225 , 3168 , 3102 and 2979 cm^{-1} in infrared spectrum are assigned to C-H stretching vibration (see Table 1). These bands were calculated to be at 3076.085 , 3072.903 , 3056.936 and 3024.159 cm^{-1} by HF/6-31G(d,p) and at 3209.674 , 3203.763 , 3189.898 and 3144.804 cm^{-1} by DFT/B3LYP/6-31G(d,p), respectively. The calculated frequencies in the HF/6-31G(d,p) are shifted down too much, while the frequencies calculated in the DFT/B3LYP/6-31G(d,p) are shifting down less. These assigned frequencies are affected much by the substitutions. The C-H in-plane and out-of-plane bending vibrations generally lies in the ranges $1000\text{--}1300\text{ cm}^{-1}$ and $950\text{--}800\text{ cm}^{-1}$ ²⁰⁻²², respectively. The bands at 1312 , 1265 and 1187 cm^{-1} in infrared spectrum are assigned to C-H in-plane bending vibration, which are calculated at 1270.992 , 1252.249 and 1119 cm^{-1} by HF/6-31G(d,p) and at 1288.221 , 1276.195 and 1192.051 cm^{-1} by DFT/B3LYP/6-31G(d,p), respectively. Three C-H out-of-plane bending vibrations are observed at 1089 , 979 and 918 cm^{-1} . These bands have been calculated to be at 1046.864 , 987.44 and 917.000 cm^{-1} by HF/6-31G(d,p) and 1079.896 , 957.270 and 912.555 cm^{-1} by DFT/B3LYP/6-31G(d,p), respectively. According to the literature, the in-plane and out-of-plane bending vibrational frequencies are found to be within their characteristic regions.

3.1.3. C-Cl vibrations

The C-Cl stretching vibrations give generally a broad band at region $800\text{--}600\text{ cm}^{-1}$ depending on the configuration, conformation and substitutions of compound.²³ A strong infrared spectra band at 784 cm^{-1} is assigned to C-Cl stretching vibration, which is calculated at 796.853 cm^{-1} by HF/6-31G(d,p) and 787.662 cm^{-1} by DFT/B3LYP/6-31G(d,p), respectively. The computed values are well correlated with the experimental observations.

3.1.4. C≡N vibrations

Nitriles are characterized by the C≡N stretching vibrations which occur at $2260\text{--}2240\text{ cm}^{-1}$ in aliphatic nitriles. Conjugation lowers the nitrile frequency, due to resonance, to $2235\text{--}2215\text{ cm}^{-1}$ in most cases.²⁴ The experimentally observed strong band at 2243 cm^{-1} is assigned to C≡N stretching vibration. This band is calculated at 2334.122 cm^{-1} by HF/6-311G(d,p) and at 2311.549 cm^{-1} by B3LYP/6-311G(d,p), respectively. It can be said that the experimentally observed band is greater than calculated theoretically. The reason for this may be attributed to the calculations done in the gas phase.

3.1.5. Skeletal vibrations

The identification of C-N stretching band is a very difficult, since this band is always mixed with other bands. This band is generally observed in the region $1645\text{--}1575\text{ cm}^{-1}$ ²⁵ at pyridine derivatives. C-N stretching vibrations bands in combination with C-C are observed in strong intensity at 1636 and 1585 cm^{-1} . This bands are calculated at 1656.567 and 1659.4973 cm^{-1} by HF/6-31G(d,p) and at 1645.914 and 1587.662 cm^{-1} by DFT/B3LYP/6-31G(d,p), respectively.

In general, the bands which appear between 1430 and 1650 cm^{-1} are C-C stretching vibrations.^{16,18} The C=C stretching vibrations are observed in very strong intensity at 1636 and 1602 cm^{-1} . This bands are calculated at 1657.567 and 1632.457 cm^{-1} by HF/6-31G(d,p) and 1645.914 and 1629.420 cm^{-1} by DFT/B3LYP/6-31G(d,p), respectively. The stretching vibrations bands for C-C bond are obtained in strong intensity at 1585 , 1541 , 1447 , 1420 , 1364 and 1345 cm^{-1} . The experimentally observed these strong bands are found to be in agreement with the theoretically calculated both the intensity and the spectrum bands. The peaks are observed at 888 and 696 cm^{-1} due to C-C-C in-plane bending vibrations.

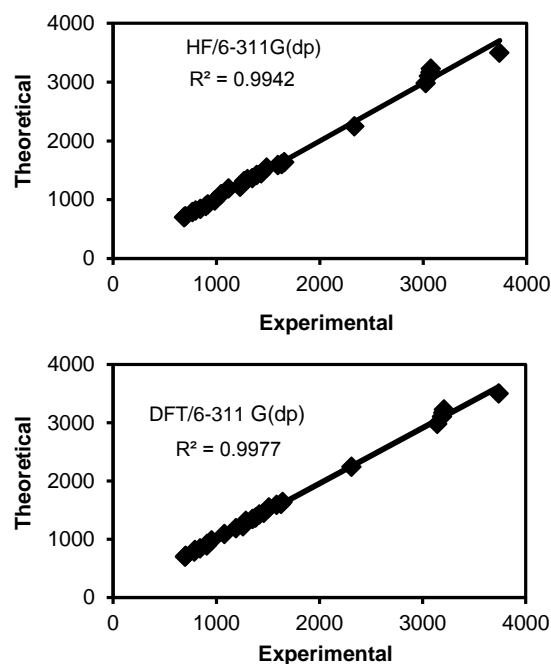


Figure 3. Correlations graphics of frequencies for of 4H3CN7CLQ molecule.

For the 4H3CN7CLQ molecule, the correlation graphs obtained by comparing the frequencies experimentally and theoretically are shown in Figure 3. As can be seen from Figure 3, the experimental fundamentals are in better agreement with the scaled fundamentals and are found to have a good correlation for DFT/B3LYP than HF for the 4H3CN7CLQ molecule. The some sensitive modes characterized at DFT/B3LYP/6-311G(dp) level in the 4H3CN7CLQ molecule are illustrated in Figure 4.

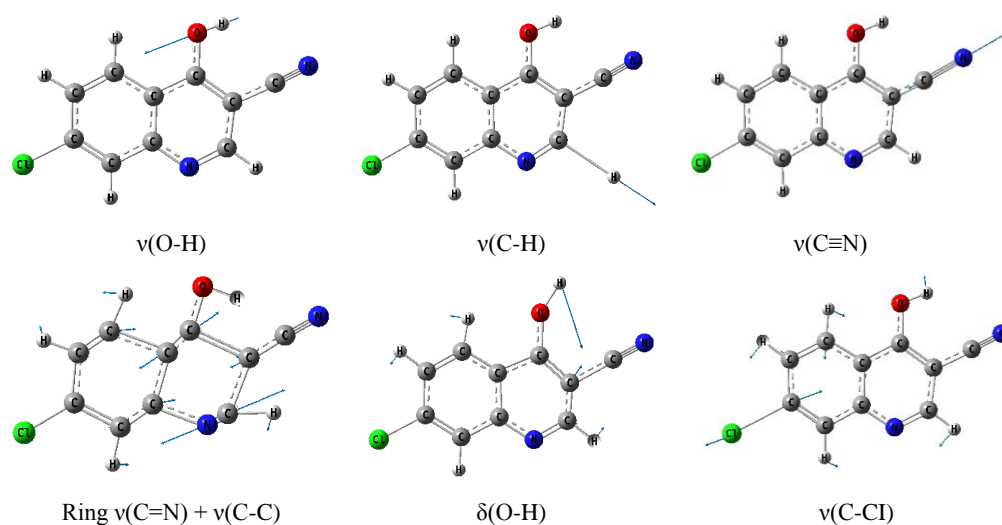


Figure 4. The some sensitive modes characterized at DFT/B3LYP/6-311G(dp) level in 4H3CN7CLQ molecule.

4. CONCLUSION

For the first time, the infrared spectrum of the 4-hydroxy-3-cyano-7-chloro-quinoline molecule was studied theoretically and experimentally. The title compound was theoretically optimized using HF and B3LYP/DFT methods with 6-311G(dp) basis set and calculated the vibrational frequencies. The computed vibrational wavenumbers were assigned and compared with experimental infrared spectra. The infrared absorption and intensities computed by HF and B3LYP methods with 6-311G(dp) basis set were in reasonable agreement with the experimental data. Comparison of the observed fundamental vibrational frequencies and calculated results for this molecule indicates that is superior to scaled HF and B3LYP approach for molecular vibrational problems.

ACKNOWLEDGEMENT

The Gaussian 09 program used in this study was provided by The Scientific Research Projects Council of Kilis 7 Aralık University, project number: 2010/02/08.


Conflict of interest

I declare that there is no a conflict of interest with any person, institute, company, etc.

REFERENCES

- Bambury, R.E. In *Burger's Medicinal Chemistry*, Part II, Wolff, M.E (Ed.), John Wiley, New York, 1979, pp. 41–81.
- Martell, A.E.; Calvin, M., *Chemistry of the Metal Chelate Compounds*, Chapter 10, Prentice Hall, Englewood Cliffs, 1959.
- Vaichulis, J. A., U.S. Patent 3272, 352, 1966.
- Schmidt, L.H. *Annu. Rev. Microbiol.* **1969**, 23, 427-454.
- Dietrich, H. Swiss Patent 454874, 1968.
- Hoffman La Roche Co., Swiss Patent 416648, 1967.
- Arjunan, V.; Mohanb, S.; Ravindranc, P.; Mythilid, C.V. *Spectrochim. Acta A.* **2009**, 72, 783-788.
- Arıcı, K.; Yılmaz, R. *Asian J. Chem.* **2013**, 25, 13, 7106-7114.
- NIST Chemistry WebBook. <http://webbook.nist.gov/chemistry> (accessed July 7, 2017).
- Vosko, S. H.; Wilk, L.; Nusair, M. *Can. J. Phys.* **1980**, 58, 1200-1211.

11. Kral Irikura, K.; Russel Johnson III, D.; Raghu Kacker, N. *J. Phys. Chem. A*, **2005**, 109, 8426-8435.
12. Frisch, A.; Nielsen, A. B.; Holder, A. J. *Gaussview Users Manuel*, (Gaussian inc., Pittsburg, 2009).
13. Frisch, M.J.; Trucks, G.W.; Schlegel, H.B.; Scuseria, G.E.; Robb, M.A.; Cheeseman, J.R.; Scalmani, G.; Barone, V.; Mennucci, B.; Petersson, G.A.; Nakatsuji, H.; Caricato, M.; Li, X.; Hratchian, H.P.; Bloino, A.F. J.; Zheng, G.; Sonnenberg, J.L.; Hada, M.; Ehara, M.; Toyota, K.; Fukuda, R.; Hasegawa, J.; Ishida, M.; Nakajima, T.; Honda, Y.; Kitao, O.; Nakai, H.; Vreven, T.; Montgomery, J.; Jr.A.; Peralta, J.E.; Ogliaro, F.; Bearpark, M.; Heyd, J.J.; Brothers, E.; Kudin, K.N.; Staroverov, V.N.; Kobayashi, R.; Normand, J.; Rendell, K. A.; Burant, J.C.; Iyengar, S.S.; Tomasi, J.; Cossi, M.; Rega, N.; Millam, J.M.; Klene, M.; Knox, J.E.; Knox, J.B.; Bakken, V.; Adamo, C.; Jaramillo, J.; Gomperts, R.; Stratmann, R.E.; Yazyev, O.; Austin, A.J.; Cammi, R.; Pomelli, C.; Ochterski, J.W.; Martin, R.L.; Morokuma, K.; Zakrzewski, V.G.; Voth, G.A.; Salvador, P.; Dannenberg, J.J.; Dapprich, S.; Daniels, A.D.; Farkas, O.; Foresman, J.B.; Ortiz, J.V.; Cioslowski, J.; Fox, D.J. *Gaussian 09, Revision A.02*, Gaussian Inc., Wallingford CT, 2009.
14. Michalska, D.; Bienko, D.C.; Bienko, A.J.A.; Latajaka, Z. *J. Phys. Chem.* **1996**, 100, 17786-17790.
15. Krishnakumar, V.; Muthunatesan, S. *Spectrochim. Acta A*. **2006**, 65, 815-825.
16. Sathyanarayana, D.N. *Vibrational Spectroscopy-Theory and Applications*, ed. 2, New Age International (P) Limited Publishers, New Delhi, 2004.
17. Singh, D.N.; Singh, I.D.; Yadav, R.A. *Indian J. Phys.* **2002**, 76B, 307-318.
18. Krishnakumar, V. R.; John X. *Indian J. Pure Appl. Phys.* **2003**, 41, 597-601.
19. Sharma, A.; Gupta, V.P.; Viridi, A. *Indian J. Pure Appl. Phys.* **2004**, 42, 251-257.
20. Krishnakumar, V.; Prabavathi, N. *Spectrochim Acta A*. **2008**, 71, 449-457.
21. Altun, A.; Golcuk, K.; Kumru, M. *J. Mol. Struct. (THEOCHEM)* **2003**, 637, 155-169.
22. Singh, S.J.; Pandey, S.M. *Indian J. Pure Appl. Phys.* **1974**, 12, 300-305.
23. Ramana Rao, B. G. *J. Raman Spect.* **1989**, 20, 439-448.
24. Kitson, R. E.; Griffith, N. E. *Anal. Chem.* **1952**, 24, 334-341.
25. Gunasekaran, S.; Natarajan, R.K.; Syamala, D.; Rathika, R. *Indian J. Pure Appl. Phys.* **2006**, 44, 315-319.

 0000-0001-7947-0766 (K. Arıcı)



Effect of nanoparticles on mechanical and tribological properties of composite friction materials

Fikrat YUSUBOV*

Department of Mechanical Engineering, Azerbaijan State Oil and Industrial University, 16/21 Azadliq Avenue, Baku, Azerbaijan

Received: 11 October 2017, Revised: 19 October 2017, Accepted 26 October 2017

*Corresponding author's e-mail address: fikratyusub@gmail.com (F. Yusubov)

ABSTRACT

Wear mechanism of newly developed asbestos-free frictional materials (i.e. brake pads material) was investigated by physical-mechanical experiments. The suitability of the developed these new composite materials were investigated by friction tests at the different temperatures. Thermal investigation was performed by a differential scanning calorimetry (DSC) and thermogravimetric analysis (TGA). Stability and mechanical properties at different temperatures of the brake pad materials were comparatively evaluated. Testing results showed that under the given conditions, new developed frictional material has the advantages of the good tribological properties over the widely used commercial asbestos enhanced material as a FK-24A (Retinax, mark B). The research of the thermal and wear behaviour of materials indicates that brake pair has better frictional characteristics and wear resistance performance at high temperature. With use of new friction brake pads materials will be improved the safety of braking processes, and the quality in drilling will be increased. There is also an environmental and economic advantages in using the new asbestos-free materials in the brake pads.

Keywords: Composite material, Brake pads, Friction, Thermal analysis

Nanoparçacıkların kompozit sürtünme malzemelerinin mekanik ve tribolojik özelliklerine etkisi

ÖZ

Yeni geliştirilen asbest içermeyen sürtünme malzemesinin (yani fren balataları malzemesi) aşınma mekanizması, fiziksel mekanik deneylerle incelendi. Geliştirilen bu yeni kompozit malzemesinin uygunluğu farklı sıcaklıklarda sürtünme deneyleri ile araştırıldı. Isı analizleri, diferansiyel tarama kalorimetresi (DTK) ve termogravimetrik analiz (TGA) ile yapıldı. Fren balata malzemelerinin dayanıklılığı ve mekanik özellikleri farklı sıcaklıklarda karşılaştırmalı olarak değerlendirildi. Test sonuçları, verilen şartlar altında, yeni geliştirilen sürtünme materyalinin, FK-24A (Retinax, mark B) gibi yaygın olarak kullanılan ticari asbest katkılı materyalden daha iyi tribolojik özellik avantajlarına sahip olduğunu gösterdi. Malzemelerin ısı ve aşınma davranışlarının araştırılması, fren çiftinin yüksek sıcaklıkta daha iyi sürtünme özelliğine ve aşınma direnci performansına sahip olduğunu göstermektedir. Yeni sürtünme fren balatası malzemelerinin kullanımı ile frenleme işlemlerinin güvenliği iyileştirilecek ve tüm sondajlamada kalite arttırılacaktır. Fren balatalarında yeni asbest içermeyen malzemelerin kullanılmasında çevresel ve ekonomik avantajlar da vardır.

Anahtar Kelimeler: Kompozit malzeme, Fren balataları, Sürtünme, Isı analizi

1. INTRODUCTION

Modern drilling equipments and parts are characterized by problems such as heat and wear due to friction. While lifting and lowering operations, the working surface parts of disc-brake system generates intensively heat due to the increase of the temperature of the sliding bodies and therefore causes the rise of the surface temperature, even its temperature can reach above 1000°C. Temperature flash originating temperature gradient and the result of this disorder occurs a thermal stress. The temperature gradient rise at the contact between sliding bodies can have an important influence

on the tribological behaviour of the contacting components such as friction and also mechanical properties of brake block material.¹

Heavily loaded friction contacts with high temperature gradient makes growth of physical-chemical-mechanical formations, and pair materials and structure changes causes abrasion and decomposition of contacting materials.^{2,3} These temperature increases can often cause to oxidation and even possibly the melting of the contacting solids or friction burn. Also, this increase in temperature causes enlargement of microcracks which leads directly decomposition⁴, as illustrated in Figure 1. This figure shows thermal worn of

front and back surfaces of the asbestos-containing friction material (FK-24A (Retinax, mark B)).



a) front



b) back

Figure 1. Thermal worn surfaces of the asbestos-containing friction materials FK-24A (Retinax, mark B).

Progress of stress related microcracks strongly arises as a result of thermal-physical properties of material.⁵ Wear rate of brake pair materials increases with friction temperature rising, and tribological-mechanical performance becomes poorer. As damaged brake pads are changed with new pads after worn every time, driving efficiency and productivity decrease. The brake block material must have some properties such as higher thermal conductivity, wear resistant, stable friction coefficient and better mechanical properties. Resistance to humidity, good heat and electrical conductivity, low noise, stable friction, reliable mechanical performance and the absence of harmful environmental impact are important requirements for friction materials. Because of thermal, electrical resistance and tensile strength characteristics, asbestos are used widely in industry, especially in brake pads development. But due to its association with lung diseases, like mesothelioma and different disorders in human body, new uses of asbestos have been banned in many countries. However, the use of asbestos material was inevitable for a long time as new materials were either economically not profitable, or could not exceed the quality of the asbestos based materials. But rapidly progress of nanotechnology also influences the development of composite materials. Composite materials are used in braking systems due to

several reasons such as heat resistance, high endurance, good resistance to wear.⁶ Recently, the use of nanoscale particles in composition materials has caused to arise of new development approaches and methods which is providing new materials with different properties and better quality indicators. In obtaining of the brake pads material with desirable tribomechanical properties, polymer based composite materials included different fillers, modifiers can be used. For this reason, we are offering new durable materials filled with nanoparticles and suggesting the help of various modifiers to get suitable and more stable composition for the purpose of obtaining economically and environmentally friendly materials. Removal of the asbestos from composition and replacing it with new materials will ensure a continuous and at the same time safe working regime in the driving process. Also, due to excellent heat conductivity and adhesive performance, the use of phenolic resin are the reason for preference as a binder or matrix in the development of friction brake composites.^{7,8} Therefore, in this study, we aimed development new friction brake block material for oil drilling rigs brake system (friction pair materials for disc brake of drilling rig). For this purpose, we have developed two new friction materials.

The first is phenolic resin-containing material without asbestos. The second is inorganic nanoparticles-containing material besides phenolic resin without asbestos. At the same time, thermal and mechanical properties of these new composite materials are compared with that of widely used friction material Retinax (FK-24A - Retinax, mark B).

2. MATERIALS AND METHODS

2.1. Materials

FK-24A (Retinax, mark B) was received from Suraxani Oil Company. This material is widely used as friction material in post Soviet countries. FK-24A (Retinax, mark B) contains 40% asbestos, 35% barite, and 15% phenol-formaldehyde. Herein, this material was named as sample A, and used as reference.

Chemicals and materials required for the production of sample B are graphite, silica, phenol-formaldehyde, and barite. These materials were received from Department of "Organic substances and technology of high molecules compounds" (Azerbaijan State Oil and Industry University). The material produced was named as sample B.

Chemical and materials required for the production of sample C are inorganic fibre (Ceramic fiber), silicon dioxide, heat resistant adhesives (epoxy), zinc oxide, short glass fibers, modified phenol-formaldehyde, phenolic resin (Phenol formaldehyde resin), and Cu-graphite nanoparticles. The materials were received from Department of "Organic substances and technology of high molecules compounds" (Azerbaijan State Oil and

Industry University) and Institute of Polymer Materials (Azerbaijan National Academy of Sciences).

Size of Cu-graphite nanoparticles produced with mechanical-chemical methods in Department of Machine-building and Materials Science, Azerbaijan State Oil and Industrial University is 70 μm . The material produced was named as sample C.

The production of samples B and C are given in methods section of the article.

Devices used for the measurements are as follows: A thermogravimetric analyzer (TGA Q50,TA Instrument) was used for thermal analysis. A differential scanning calorimetry (DSC) (Mettler Toledo DSC 823e) was used for specific heat capacities of sample materials. A band-block machine (developed in base M/II-I) was used for the determination of friction coefficients. Brinell hardness 20 device was used for hardness measurements. A pycnometer was used for the estimation of the densities of sample materials.

2.2. Methods

In the laboratory, two new materials (samples B and C) have been developed. These samples were obtained using hot press method.

First material was named as sample B. This material was produced using certain amounts of graphite and silica, and also modified phenol-formaldehyde oligomer without asbestos. In order to obtain sample B, the used solid materials was firstly powdered and then all materials was mixed well. The resulted mixture was kept under 25 kpa press at 100-120°C temperature for 3,5 h.

In the production of sample B, barit still remained in the composition of sample B. On the other hand, modified phenol-formaldehyde was used instead of raw phenol-formaldehyde included in the sample A .

Second material was named as sample C. This material was developed without reference material A. Sample C is a completely new material produced by using reinforcing inorganic fibre (Ceramic fiber), silicon dioxide, heat resistant adhesives (epoxy), zinc oxide, short glass fibers, modified phenolic resin (Phenol formaldehyde resin) and small amount of Cu-graphite nanoparticles. The used solid materials was firstly powdered and then all materials was mixed well. The resulted mixture was kept under 30-35 kpa press at 135-175°C temperature for 4 h, and at the final stage sample was subjected to vulcanization (dry insulation) for 25 min.

So, these two new materials (Samples B and C) produced have become ready for all analyses.

On the other hand, the percent proportions the materials used in the production of the samples A, B, and C are given in Table 1.

2.2.1. Thermogravimetric analysis (TGA)

When the temperature increases the weights of samples changes due to decomposition.⁹ For example, At

very high temperatures, the covalent bonds between the atoms in the linear chain may be destroyed, and the material pair may burn or char.¹⁰

Therefore, thermal experiments has been done to determine the decomposition mechanism of materials and to estimate their thermal stability at the temperatures up to 1000°C.

Table 1. The portions of different categories of polymerbased composition materials used in experiments

Proportions (wt%)	Sample (A)	Sample (B)	Sample (C)
Matrix	40 (asbestos)	15	23
Modifiers	-	25	15
Filler	35	35	25
Binders	25	25	35
Friction modifiers	-	-	2

TG analyses of sample A, B, and C was conducted using a thermogravimetric analyzer (TGA Q50,TA Instrument). For accurate measurements, all test runs were performed under the same experimental conditions. As a specimen holders platinum crucible was used and re-zeroed after each run. During experiments, high purity nitrogen (the flow rate 60 ml min⁻¹) was used as the inert gas. Each of the three sample materials are powdered (weight: 25 mg) and were heated at 10°C/min, from 45 to 1000°C and hold for 49 min. The decomposition and weight loss by temperatures of the three samples is shown in Figure 2.

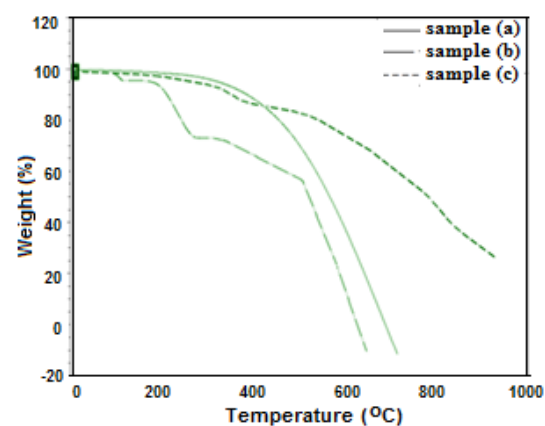


Figure 2. Thermogravimetric analysis (TGA) curves for sample materials.

2.2.2. Determination of weight loss

Weight losses of Sample A, B, and C were calculated according to ISO 7111 standards of 1987 (Plastics Thermogravimetry of Polymers - Temperature Scanning Method). After decomposition with the effect of the temperature, the mass losses and the remnant masses of

the materials were determined using Equations (1) and (2), respectively.

$$m_1 = \frac{m_B - m_A}{m_0} \cdot 100 \quad (1)$$

$$R = \frac{m_A}{m_0} \cdot 100 \quad (2)$$

where, m_1 is mass loss percentage, m_B is sample mass before loss, m_A is sample mass after loss, m_0 is beginning mass of sample, R is remnant mass percentage.

2.2.3. Differential scanning calorimetry (DSC) analysis

One of the most important demand while developing friction material is transforming energy to the heat at the short time period without any damage to material.¹¹ Herein, DSC analyses to determine the heat capacities of sample materials were performed by differential scanning calorimetry (DSC) analysis (a Mettler Toledo DSC823e brand) which is calibrated with indium as a standard. To calculate the heat capacities of the samples, calorimetric measurements were performed in the dynamic mode. The experiments were conducted in dynamic nitrogen atmosphere environmental a flow rate of 40 ml min⁻¹ with a heating rate of 10°C/min and heated up to 500°C. All powdered samples (weight 8.1 mg) were loaded into alumina crucible. With the aim to measure the heat flow difference, first pan was filled with the sample material and second pan kept empty.

Specific heat capacities of sample materials in the temperature range 250 to 500°C were determined from this equation using DSC method:¹²

$$C_s = \frac{q}{m \cdot \Delta T} \quad (3)$$

where, q is units of heat, m is mass of the sample, ΔT is change in the temperature. DSC curves for the sample materials shown in Figure 3.

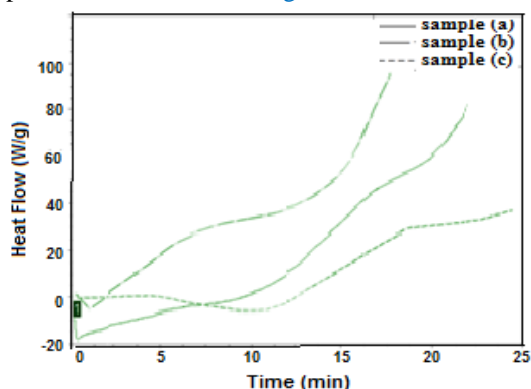


Figure 3. Differential scanning calorimetric (DSC) curves for the sample materials.

2.2.4. Determination of friction coefficients

Determination of friction coefficients of sample A, B, and C were explained in the following.

Tribological test devices such as pin-on-disk can give useful information about friction and wear behavior of materials.¹³ All materials were tested in pairs under nominally non-abrasive conditions. Tests was conducted with laboratory procedure by using a band-block machine (developed in base МДП-I)¹⁴ (Figure 4).

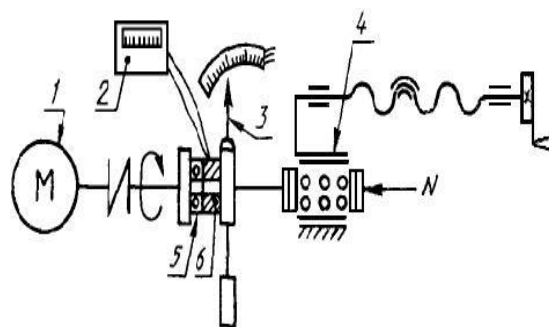


Figure 4. Device for measuring the friction under laboratory conditions.

where, 1- engine, 2- potentiometer, 3- force meter, 4- loader, 5- friction material sample, 6- metallic material sample.

The tribological tests for all specimens was conducted with same experimental parameters: under loads of 30 N and a sliding velocity of 4 m s⁻¹. The pin dimensions was 40 mm in length and 10 mm in diameter.^{15,16} Friction measurements were conducted at the temperatures up to 700°C. During experiment, friction coefficients were recorded with sliding distance. The obtained results is shown in Figure 5.

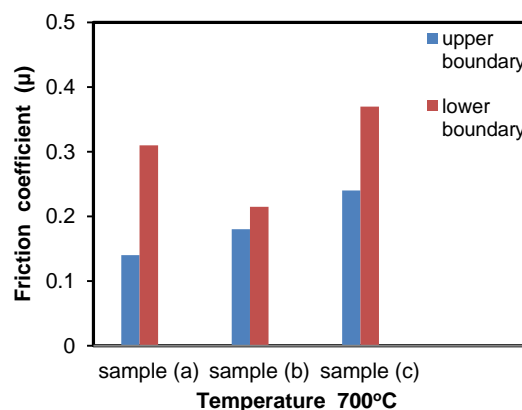


Figure 5. Friction coefficients for upper and lower boundary of the reference area by pin-on-disc wear up to 700°C.

2.2.5. Hardness measurements

For the hardness measurements of all samples, Brinell hardness tester was used.¹⁷ Brinell hardness process was conducted in a period of 25 seconds using a 10 mm diameter-steel ball by applying a 500 kg-load.

2.2.6. Density measurements

In order to determine densities of sample materials, pycnometer method was used.¹⁸ Materials were divided to small parts and measured by pycnometer using water.

3. RESULTS AND DISCUSSION

Results show that the sample A undergoes thermal degradation beginning at 310°C with a mass loss of 19.6%, when the temperature is >310 °C do its weight-loss rates increase slightly (to 0.3 wt %/°C). Sample B loses about 1,7% of its mass about 114°C.

This effect occurs mainly because silica desorbs into the gas phase during the initial stages of passive oxidation.¹⁹ As can be seen from Figure 2, TGA curve shows that there are two mass losses at 114 °C and 326 °C and starting from 326°C to 520°C the sample decomposes completely. Measurements showed that the sample C was more thermally stable than other materials. The weight loss at 374°C represents the decomposition of the sample C when the material have absorbed certain amounts of heat energy. No drastic change in the sample mass was observed for temperatures up to 400°C.

The statements about friction are evidenced in Figure 4, where it can be observed that the temperature increases determined both the sliding speed and nominal contact pressure increase. According to the analyses, the surface friction temperature of the brake pair at beginning of the wear is low and with temperature rising surface layer begins to soften. After temperature rises much higher micro crack enlargements leads decomposition of material. Common method to improve the mechanical properties or performance at wide temperature range is to include a glass fiber as filler or binder in the polymer. Reinforcement material shall have characteristics which improve the stiffness and well relation tie to the matrix.

Glass fiber also has advantages from an economic point of view.²⁰ Compared to the Retinax material, the sample C showed an important improvement of the overall thermal stability profile. The increasing in thermal stability was found in all decomposition stages. The results indicates that the decomposition of the sample C occurs at a higher temperature than that for other compositions, showing greater degree of thermodynamic stability. Also the results reveal that sample C has higher friction coefficient than other sample materials.

The coefficient of friction between two surfaces is influenced by the mechanical properties of material, the surface structure, temperature and other parameters.

Braking materials must ensure a stable friction with a high friction coefficient.^{21,22} The coefficient of friction increases as disc temperature is increased from 29°C to 200°C and phenolic resin does not affect disc temperature sensitivity of coefficient of friction. During the study of tribological behaviors, it became clear that glass fibers increased hardness and thermal conductivity depending on load percentage. On the average, the friction coefficient in the 5-10% glass fiber material has decreased due to the increase in load. The friction coefficient of 0.1 kg under normal load rises at the initial stage, then gradually rises to 0.50. In the later stages, the slowly begins to decrease. When we look at the overall frictional activity of the material, we have the same mechanism as the smallest difference for all cases. However, the effect of load percentage on friction behavior cannot be overlooked. The friction coefficient in the material consisting of glass fiber particles under all loads are the lowest.

Phenolic resin do not affect the trend of increasing of coefficient of friction toward disc.²³ For retinax material (sample A), when the temperature increases from 100°C to 700°C, friction coefficient changes from 0,270-0,605 to 0,200-0,387. It is observed that friction coefficient decreases with the increase of temperature from starting point. After 380-440°C phase, no changes has been dedected, and thus the friction coefficient becomes constant. Friction coefficient starts to increase significantly after 480°C, but it never reaches to higher numbers. Same temperature effect to the friction has also been observed for other materials, but the obtained results indicates that the sample B has lowest (0,115-0,237) and the sample C has highest friction coefficient (0,264-0,400) at the highest temperatures. During the measurement of the friction coefficient of Cu-graphite in dynamic conditions, the values varying under different loads have reached the highest value of 0.4. Since graphite has good antifriction properties, the high friction coefficient of the sample C can be explained by the role of Cu-graphite particles with increasing the heat conductivity of the material. Also, one of the reasons why the sample C shows good mechanical performance is the use of modified phenol-formaldehyde. Overall physical-mechanical measurement results and other parameters are summarized in Table 2.

Table 2. Physical-mechanical properties of materials

Properties	Sample (A)	Sample (B)	Sample (C)
Thermal decompost. (°C)	>310	114- >336	>374
Density (kg m ⁻³)	2134	2112	2238
Hardness (HB20/500/25)	32	29	38
Specific heat cap.(kJ/kg°C)	0.96	0.77	1.32
Mass loss (1000°C)	82%	97%	43%

Figure 6 shows scanning electron microscopy (SEM) surface images of the sample C. It can be clearly observed structural formation of cu-graphite and modified phenol-formaldehyde which is played significant role on mechanical properties.

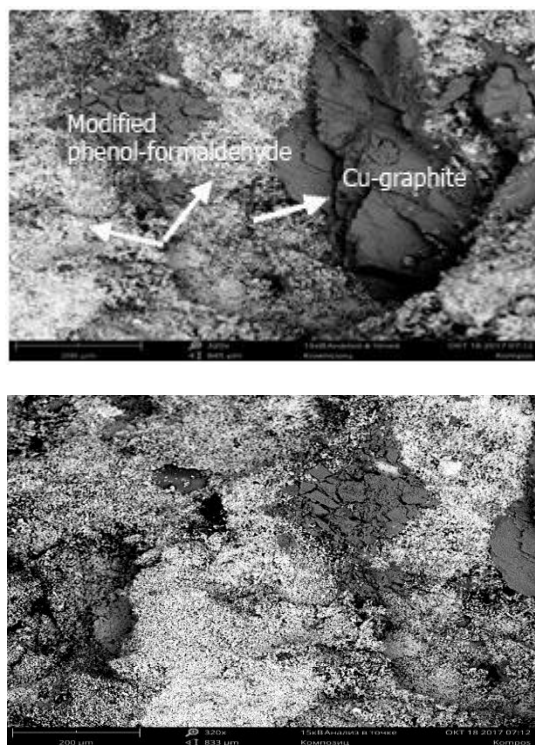


Figure 6. SEM images of the sample material C.

In addition, a large amount of frictional dance was observed in the sample material B with a barite mass percentage, and some signs of damage on the friction surface of contact appeared. Rising temperature also affected frictional stability in sample materials where barite mass percentage is high. From the results, it can be seen that the density of silica dioxide leads a high density of materials. Besides, it should be noted the effect of silica dioxide on mechanical properties. One of the reasons why the hardness of the sample material C is not too low is due of silica dioxide.

4. CONCLUSIONS

Based on the experimental investigation and analysis, conclusions are drawn that the sample C has better tribological performance compared to the samples A (FK-24A, Retinax material) and B materials. Friction and wear performance of the sample materials has improved with addition of nanoparticles to material content. From experiments, it is found that sample C has highest friction coefficient. Both sample materials which are reinforced with inorganic fibres, heat resistant adhesives

and different nanoparticles has higher mechanical characteristics. The effect of modified phenol-formaldehyde on mechanical performance of the sample materials are considerably high. But due to poor heat conductivity, the sample B showed 97% mass loss at 1000°C. Thanks to Cu-graphite particles and fillers, the mass loss of the sample material C was only 43% at 1000 °C following the decomposition starting at 374°C. Results indicates that polymer based composite material C can be used as brake block material instead of asbestos. By providing reliability and stability of the braking process with newly developed composite friction materials, high efficiency and economic advantage in driving process can be achieved.

ACKNOWLEDGEMENTS

The author is thankful to his advisor, Associate Professor Guliyev Agali, Department of Machine-building and Materials Science, Azerbaijan State Oil and Industrial University for his valuable comments and encouragement during the investigation.

Conflict of interest

I declare that there is no a conflict of interest with any person, institute, company, etc.

REFERENCES

1. Kragelsky, I. V. ; Alisin, V.V. *Tribology: Lubrication, Friction and Wear, Tribology in practice series*, Wiley, 2001.
2. Bos, J.; Moes, H. *ASME J. Tribol.* **1995**, 117, 4-12.
3. Shpenkov, G.P. *Tribology Series*, Elsevier Science, 1995; Vol. 29, pp 291-296.
4. Kennedy, F.E. *Frictional Heating and Contact Temperatures*, In: *Modern Tribology Handbook*, Bhushan, B. Ed.; *CRC press*, Boca Raton, FL, 2001.
5. Dzhanakmedov, A.; Gurbanov, R.E.; Aliyev, A.M. *Fundamentals of Tribology*, Baku, Chashioglu, 2001.
6. Peter, J. B.; *Compositions, Functions, and Testing of Friction Brake Materials and Their Additives*, Oak Ridge National Laboratory, 2001.
7. Jamasri, S.E.; Malau, V.; Iلمان, M.N. *ARPN J. Eng. Appl. Sci.* **2014**, 9(11), 2234-2240.
8. Ho, S.C.; Chern Lin, J.H.; Ju, C.P. *Wear*, **2005**, 258, 861-869.

9. Galwey, A.K.; Brown, M.E. *Thermal Decomposition of Ionic Solids*. 1st Ed.; Elsevier Science, 1999, Vol. 86, pp. 62-63.
10. Askeland, D.R.; Fulay, P.; Wright, W.J. *The Science and Engineering of Materials*, 6th Ed.; Cengage Learning, 2010.
11. Stachowiak, G.W. *Wear: Materials, Mechanisms and Practice (Tribology in Practice Series, Book 8)*, 1st Ed.; Wiley, 2005, pp 223-225.
12. O'Neil, M.J. *Anal. Chem.* **1966**, 38 (10), 1331-1336.
13. Deleanu, L.; Georgescu, C.; Gheorghies, C. *The Annals of "Dunarea de Jos Galati. Fascicle IX. Metall. Mater. Sci.* **2011**, 29 (4), 5-15.
14. Friction articles of retinax. Specifications. <http://docs.cntd.ru/document/gost-10851-94>, 1996.
15. Peter, J. B. *Tribol. Int.*, 39 (9), **2001**, 585-591.
16. Bayer, R.G. *Mechanical Wear Fundamentals and Testing*, 2nd Ed.; Revised and Expanded, Marcel Dekker Inc., New York, 2004.
17. Suryanarayana, C. *Experimental Techniques in Materials and Mechanics*, CRC Press, 2011.
18. Hidnert, P.; Peffer E.L. *Density of solids and liquids*, U.S. Government Printing Office: Washington, DC, 1950.
19. Starodub, D.; Gusev, E.P.; Garfunkel, E.; Gustafsson, T.; *Surf. Rev. Lett.* **1999**, 6 (1), 45-52.
20. Eriksson, M.; Lord, J.; Jacobson, S.; *Wear*, **2001**, 249 (3-4), 272-278.
21. Djafri, M.; Bouchetara, M.; Busch, C.; Weber, S. *Mechanika* **2014**, 20 (4), 420-425.
22. Larsen-Basse, J. Basic theory of solid friction, In: Henry, S.D (Ed.), *ASM. Handbook: Friction Lubrication, and Wear Technology*, ASM International, Metals Park, OH. 1992. Voll. 18, p.17.
23. Sundén, B.; Brebbia, C. *AWIT Transactions on Engineering Sciences*, WIT Press, 2014; Vol. 83, pp 203-260.

Note: This work has been presented in 3rd International Turkic World Conference on Chemical Sciences & Technologies (ITWCCST-2017).

 ORCID

 0000-0002-2095-2469 (F. Yusubov)



Synthesis, characterization and catalytic properties of some transition metal complexes of new phenoxy-imine ligand

Ali ÇAPAN¹, Gökhan CEYHAN², Mehmet SÖNMEZ^{3,*}

¹Vocational School of Higher Education in Nizip, Department of Food Technology, Gaziantep University, Turkey

²Technical Sciences Vocational School, Food Technology, Kahramanmaraş, Turkey

³Department of Chemistry, Faculty of Science and Arts, Gaziantep University, 27310, Gaziantep, Turkey

Received: 20 October 2017, Revised: 10 November 2017; Accepted: 11 November 2017

*Corresponding author's e-mail address: msonmez@gantep.edu.tr (M. Sönmez)

ABSTRACT

In this study a new Schiff base ligand was synthesized by the reaction of salicylaldehyde, 1,2-bis(bromomethyl)benzene and 4-nitrobenzenamine. $[\text{Cr}(\text{L})\text{Cl}_2]\text{Cl}\cdot\text{H}_2\text{O}$, $[\text{Fe}(\text{L})\text{Cl}_2]\text{Cl}\cdot 2\text{H}_2\text{O}$ and $[\text{Ru}(\text{L})\text{Cl}_2]\text{Cl}$ complexes were synthesized with this ligand and Cr(III), Fe(III) and Ru(III) chloride salts. The structures of the ligand and the obtained complexes were characterized using Elemental Analysis, FT-IR, ¹H-NMR, ¹³C-NMR, UV-Vis, Magnetic Susceptibility and thermogravimetric analysis. The synthesized phenoxy-imine ligand is a ligand of the O₂N₂ type. The resulting metal complexes are mononuclear and have octahedral geometry. Preliminary studies have also been carried out on the catalytic effects of complexes in cycloalkane oxidation and in cycloalkene epoxidation. In the general sense, the catalyst that triggers the highest product formation in the synthesized catalysts are the Ru(III) complex. It is suggested that Ru(III) complexes can be used in such catalysis reactions since they exhibit a high catalytic effect on cyclohexane oxidation.

Keywords: Phenoxy-imine ligand, metal complexes, catalyst

Yeni fenoksi-imin ligandının bazı geçiş metal komplekslerinin sentezi, karakterizasyonu ve katalitik özellikleri

ÖZ

Bu çalışmada, yeni bir Schiff baz ligandı, salisilaldehit, 1,2-bis (bromometil) benzen ve 4-nitrobenzenamin reaksiyonu ile sentezlenmiştir. $[\text{Cr}(\text{L})\text{Cl}_2]\text{Cl}\cdot\text{H}_2\text{O}$, $[\text{Fe}(\text{L})\text{Cl}_2]\text{Cl}\cdot 2\text{H}_2\text{O}$ ve $[\text{Ru}(\text{L})\text{Cl}_2]\text{Cl}$ kompleksleri, ligand ve Cr(III), Fe(III) ve Ru(III) klorür tuzları ile sentezlenmiştir. Ligand ve elde edilen komplekslerin yapıları Elemental Analiz, FT-IR, ¹H-NMR, ¹³C-NMR, UV-Vis, Manyetik Duyarlılık ve Termogravimetrik Analiz kullanılarak karakterize edildi. Sentezlenmiş fenoksi-imin ligandı O₂N₂ tip bir ligandır. Elde edilen metal kompleksleri mononükleer ve oktahedral geometriye sahiptir. Komplekslerin sikloalkan oksidasyonundaki ve sikloalken epoksidasyonundaki katalitik etkileri üzerine de ön çalışmalar yapılmıştır. Genel anlamda, sentezlenmiş katalizörler içerisinde en yüksek ürün oluşumunu tetikleyen katalizör L-Ru(III) kompleksidir. Ru(III) komplekslerinin, sikloheksan oksidasyonu üzerinde yüksek bir katalitik etki sergilediğinden, bu tür kataliz reaksiyonlarında kullanılabileceği önerilmektedir.

Anahtar Kelimeler: Fenoksi-imin ligand, metal kompleksleri, katalizör

1. INTRODUCTION

Phenoxy-imine compounds with ethereal oxygen in their structure are obtained from the condensation of dialdehyde-structured compounds resulting from the reaction of aromatic/aliphatic halide with salicylaldehyde and its derivatives with primary amines. In recent years, the planning and synthesis of phenoxy Schiff bases and metal complexes has been an important research area because of its importance in basic and applied sciences. Schiff bases containing phenoxy groups have been widely used in coordination chemistry due to their ability

to form stable complexes with transition metals and high catalytic effects.¹⁻⁴ These ligands and metal complexes are of interest because of their important contributions in material science and the use of these compounds as antibacterial, antifungal, anticancer and herbicide agents has led to the intensification of scientific studies in this area.⁵⁻⁷ These compounds have been used as catalysts to convert simple organic compounds found in synthetic and marketable functional derivatives. The Schiff base metal complexes containing the phenoxy group are exciting in their catalytic effects during reactions such as oxidation, epoxidation and hydrolysis, and they are the

most commonly used catalysts in the reaction of asymmetric cyclopropane and Henry (nitroaldol).⁸⁻¹⁰

In this study, the synthesis and characterization of Schiff base compound (L) and their metal complexes are discussed with various spectroscopic methods. Metal complexes have been tested as a catalyst for the oxidation of cyclohexane and cyclohexene with hydrogen peroxide as oxidant at room temperature.

2. MATERIALS AND METHODS

2.1. Materials

Acetonitrile, n-butanol, diethylether, toluene, THF, EtOH, MeOH, DMF, RuCl₃ were obtained from Aldrich and Merck. All the solvents were dried and purified before use. Elemental analyses were performed on a Thermo Scientific Flash 2000 elemental analyzer. Molar conductance of the Schiff base ligands and their transition metal complexes were determined in DMF at room temperature by using Thermo Scientific electron corporation model conductivity meter. Electronic absorption spectra were recorded on a PG Instruments T80+UV/Vis spectrometer. Infrared spectra were measured in the range of 4000-400 cm⁻¹ on a Perkin-Elmer Spectrum 100 FTIR (ATR sampling accessory) spectrophotometer. The samples were dissolved in DMF and the absorption spectra were recorded in the range of 190-1100 nm. The magnetic moments of the complexes were measured by the Gouy method on a type Sherwood Scientific model Instrument. ¹H and ¹³C NMR spectra were recorded on a Bruker High Performance Digital FT-NMR (400 MHz) spectrometer with the samples dissolved in d₆-DMSO using TMS as an internal standard. Mass spectrum, EU Sciex QTRAP 3200 LC/MS/MS in the spectrophotometer were taken using electro-spray method. Thermal behaviors were examined with a SetaramLabsys TGA/DTA model thermal analyzer heated from 20-900°C under air.

2.2. Methods

Preparation of 2-((4-nitrophenylimino)methyl)phenol has been designed in keeping with the references.¹¹

2.2.1. 2(2((2((4-nitrophenylimino)methyl)phenoxy)methyl)benzyloxy)benzylidene)-4-nitrobenzenamine (L)

The synthetic route for the ligand L is shown in Scheme 1. 2-((4-nitrophenylimino)methyl)phenol (10 mmol), potassium carbonate (10 mmol) in MeCN (50 cm³) were stirred and refluxed for two hours and then 1,2-bis(bromomethyl)benzene (5 mmol) was added. The reaction mixture was stirred and refluxed for 24 h. After cooling down, the mixture was poured into water (100 cm³) and then 0.1 N 100 cm³ NaOH solution was added and extracted by CHCl₃. The CHCl₃ layer was

evaporated to dryness to give the crude product, which was recrystallized in MeCN to afford pure ligand L. Yield 80 %; color: yellow; m.p. 188°C. Mw: 586.19 g mol⁻¹. Elemental Anal. Calc. (%): C, 72.21; H, 4.63; N, 4.95. Found: C, 71.92; H, 4.46; N, 5.12% for C₃₄H₂₆N₄O₆. IR (cm⁻¹): 3072 (Ar-CH); 1615 (C=N); 1220 (C-O-C). ¹H NMR (400 MHz, CDCl₃): δ, ppm 5.31 (s, 4H, -OCH₂), 7.0-8.23 (m, 20H, aryl-H), 8.78 (d, 2H, N=C-H). ¹³C NMR (400 MHz, CDCl₃): δ, ppm 68.82, 121.32, 121.61, 124.26, 124.93, 128.20, 120.04, 129.55, 133.80, 134.53, 145.28, 158.07, 158.35, 158.85. UV-Vis: λ_{max} (nm) in DMF: 270 (0.923), 340 (1.848). LC/MS/MS, m/z: 587.1 [L+H]⁺.

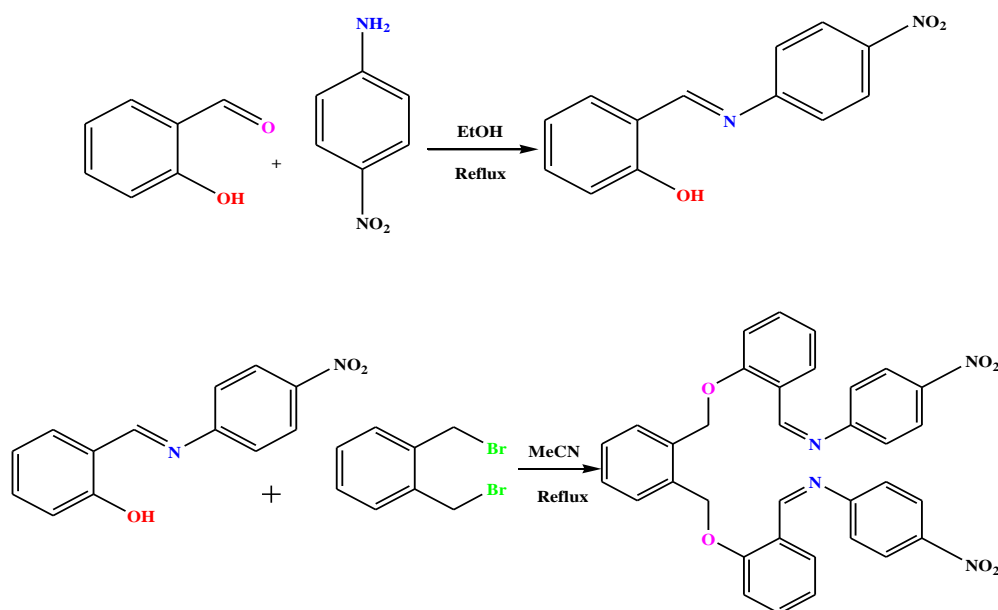
2.2.2. Synthesis of Cr(III), Fe(III) and Ru(III) complexes

Metal (III) complexes of the Schiff bases were synthesized with the addition of MCl₃.nH₂O (0.25 mmol) solutions in 10 ml ethanol (40°C) to the solutions of the Schiff base ligand (L) (0.25 mmol) in 30 ml CHCl₃ (40°C). The mixtures were refluxed for 6 h. After the reactions were completed, the mixtures were evaporated to dryness and obtained the crude product, which was filtered off and washed several times with petroleum ether.

[Cr(L)Cl₂]Cl·H₂O: Dark yellow solid, yield 26%, mp. 115-118°C. C₃₄H₂₈Cl₃CrN₄O₇ (762.96 g mol⁻¹) Elemental Anal. Calc.: C, 53.52; H, 3.70; N, 7.34. Found: C, 54.79; H, 4.27; N, 6.38 %. IR (cm⁻¹): 3073 (Ar CH); 1644 (C=N); 1240 (C-O-C), 2988 (Aliphatic CH), 532 (Cr-O); 495 (Cr-N). Meff, BM: 2.92. UV-Vis (DMF) λ_{max} (log ε): 270 (0.339), 375 (0.892), 420 (0.198) nm. Mol. Cond (S cm² mol⁻¹): 28.57. LC/MS/MS, m/z: 762.8 [[Cr(L)Cl₂]Cl·H₂O]⁺.

[Fe(L)Cl₂]Cl·2H₂O: Dark yellow solid, yield 56%, mp. 157-159°C. C₃₄H₃₀Cl₃FeN₄O₈ (784.83 g mol⁻¹) Elemental Anal. Calc. (%): C, 52.03; H, 3.85; N, 7.14. Found: C, 52.42; H, 3.61; N, 6.74%. IR (cm⁻¹): 3083 (Ar CH); 1645 (C=N); 1243 (C-O-C), 2988 (Aliphatic CH), 502 (Fe-O); 458 (Fe-N). Meff, BM: 7.51. UV-Vis (DMF) λ_{max} (log ε): 275 (0.559), 355 (1.182), 425 (0.113) nm. Mol. Cond (S cm² mol⁻¹): 19.36. LC/MS/MS, m/z: 784.7 [[Fe(L)Cl₂]Cl·2H₂O]⁺.

[Ru(L)Cl₂]Cl: Brown solid, yield 71%, mp. 112-116°C. C₃₄H₂₆Cl₃N₄O₆Ru (794.02 g mol⁻¹) Elemental Anal. Calc. (%): C, 52.43; H, 3.30; N, 7.06. Found: C, 53.54; H, 3.98; N, 7.12%. IR (cm⁻¹): 3073 (Ar CH); 1646 (C=N); 1227 (C-O-C), 2988 (Aliphatic CH), 530 (Ru-O); 493 (Ru-N). Meff, BM: 1.51. UV-Vis (DMF) λ_{max} (log ε): 270 (0.681), 375 (1.463), 550 (0.123) nm. Mol. Cond (S cm² mol⁻¹): 15.26. LC/MS/MS, m/z: 794.9 [[Ru(L)Cl₂]Cl]⁺.



Scheme 1. The possible reaction mechanism of the ligand.

2.2.3. General procedure for oxidation under microwave irradiation

The optimum conditions were obtained as catalyst: substrate: oxidant ratio of 1:100:250 in acetonitrile under max 300 W microwave power for 30 min. The temperature and pressure were controlled at about 100°C and max 25 bar by the instrument. A blank has been run under the similarly conditions without any catalyst.¹² The metal complexes have the octahedral geometry. The products formed by the effect of metal complexes in the catalytic oxidation of cyclohexane and cyclohexene under microwave irradiation are shown in Figures 1 and 2. The method of catalytic oxidation of cyclohexane and cyclohexene; 0.02 mmol catalyst: 2 mmol cyclohexane: 4 mmol hydrogen peroxide (1:100:250) and 5 ml acetonitrile were used for each reaction. The reaction temperature and pressure were held at around 100°C and 25 bar in closed DAP60 vessels.

3. RESULTS AND DISCUSSION

3.1. Synthesis

The Schiff base used as an intermediate (2-((4-nitrophenylimino)methyl)phenol) was synthesized from the reaction of 2-hydroxybenzaldehyde with 4-nitroaniline as described in the literature.¹¹ The new phenoxy-imine compound was synthesized from the condensation of 1,2-bis(bromomethyl)benzene and 2-((4-nitrophenylimino)methyl)phenol. Metal complexes of these ligands with metal(III) chlorine salts were obtained. The structure of ligand was characterized by using

elemental analysis, ¹H and ¹³C NMR, FT IR. The possible reaction is shown in Scheme 1. In the proposed structure, the ligand has a O₂N₂ core to form mononuclear metal(III) complexes. The stoichiometries of the complexes determined by mass and elemental analysis correspond to the general formula [MLCl₂]Cl.nH₂O (where M are Cr(III), Fe(III) and Ru(III)). These propositions are also in accord with IR, UV-Vis data, TGA, magnetic and molar conductivity measurements. The proposed structures of the reported complexes are shown in Figure 3. The white-colored ligand and its complexes are insoluble in water and common organic solvents, but soluble in DMSO and DMF.

3.2. FT-IR analysis

The FT-IR spectra show marked changes of the ligand L. The characteristic bands of Schiff base ligand and its metal(III) complexes are given in Table 1. The IR spectra of Schiff base L showed a weak broad absorption band at 3072 cm⁻¹ assigned to the aromatic rings a stretching vibration respectively^{13,14}, absorption bands at 1615 cm⁻¹ assigned to the imine C=N stretching vibration, absorption band at 1220 cm⁻¹ assigned to the etheric oxygen C-O-C a stretching vibration, respectively. The FT-IR spectrum of the isolated L ligand shows sharp absorption band characteristic of ν(C=N) stretching at 1615 cm⁻¹. In the complexes, these bands are shifted to higher about 29-31 cm⁻¹ wavenumbers indicating the participation of azomethine nitrogen in the coordination to metal ion.¹⁵⁻¹⁷ Aromatic C-H bands in ligands are shifted to upper about 4 cm⁻¹ in complexes respectively.

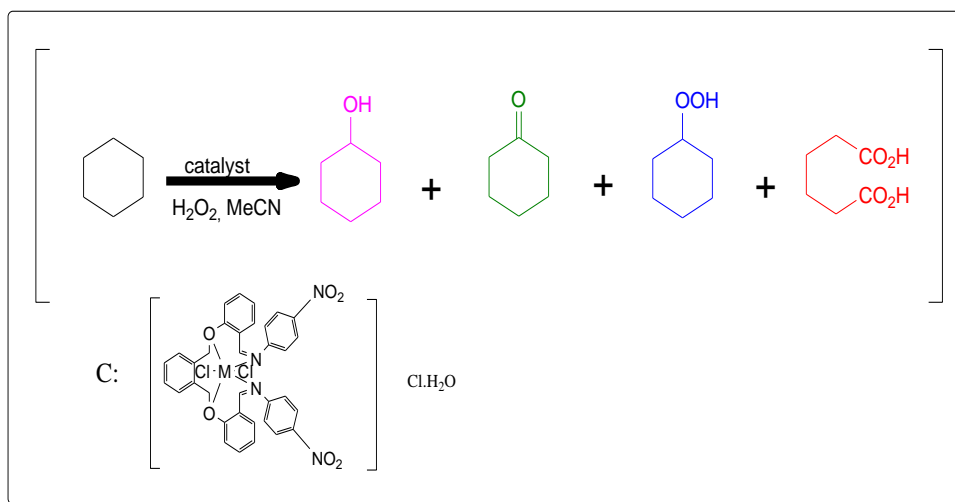


Figure 1. Catalytic oxidation of cyclohexane under microwave irradiation.

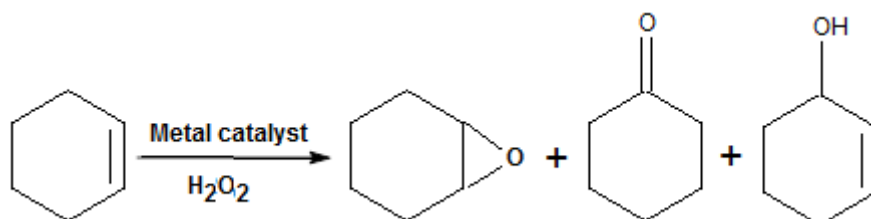


Figure 2. Catalytic oxidation of cyclohexene under microwave irradiation.

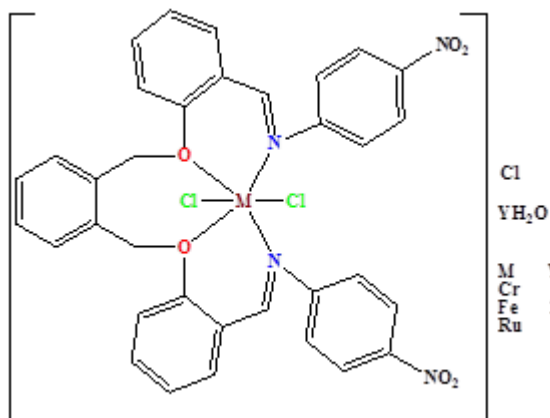


Figure 3. Suggested structures of Schiff base metal complexes.

A weak intensity absorption bands at 1220 cm^{-1} up to 1240 cm^{-1} in L-Cr, 1243 cm^{-1} in L-Fe and 1227 cm^{-1} in L-Ru are related to $\nu(\text{C-O-C})$ etheric oxygen stretching vibration in complexes. New bands in the complexes at $532\text{-}495\text{ cm}^{-1}$ in L-Cr(III), $502\text{-}458\text{ cm}^{-1}$ in L-Fe(III) and $530\text{-}493\text{ cm}^{-1}$ in L-Ru(III) are attributed to the $\nu(\text{Ru-O})$ and $\nu(\text{Ru-N})$ vibrations.^{18,19} The IR spectra of the Schiff base ligand and a representative example of metal complexes are given in Figure 4.

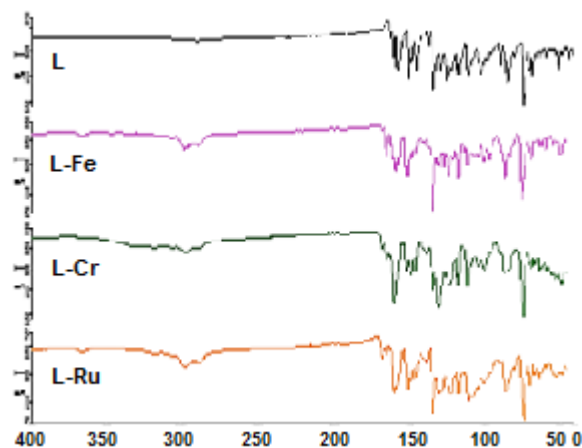


Figure 4. FT-IR Spectra of L and metal complex.

3.3. NMR spectra

^1H and ^{13}C NMR spectra of Schiff base ligand (L) were recorded in CDCl_3 solution. The ^1H NMR and ^{13}C NMR spectrum was recorded and presented in Figure 5 and 6 for L. The ^1H NMR spectra of L showed the singlets (2H) at 8.78 ppm.²⁰⁻²² The signals of Aryl-H were assigned at δ : 7.0-8.23 (m, 20H) ppm for L,

respectively. The signals of -Ph-O-C were observed at 5.31 (s, 4H) ppm for L, respectively.^{2,23,24} More detailed information about the structure of Schiff base L is provided by its ¹³C NMR spectrum in the spectrum of Schiff base was observed a new signal at 158.85 ppm for L due to imine carbon (C=N). The signal for the C_{Ar}-O carbons of the ligand was observed at 158.07 ppm, and

the peak observed at 145.28 ppm is belong to the C_{Ar}-N carbon. Etheral oxygen of the C is considerable to correspond to δ 68.82 ppm for L. The peaks of the other aromatic ring carbons were observed at 112.62-134.53 ppm, respectively. All these observations is an evidence of formation of Schiff base.²⁵⁻²⁷

Table 1. Characteristic IR bands of the Schiff base and their metal complexes (in cm⁻¹)

Compounds	$\nu(\text{Ar C-H})$	$\nu(\text{C=N})$	$\nu(\text{C-O-C})$	$\nu(\text{Ru-O})$	$\nu(\text{Ru-N})$	$\nu(\text{H}_2\text{O})$
L (C ₃₄ H ₂₆ N ₄ O ₆)	3072	1615	1220	-	-	-
[Cr(L)Cl ₂]Cl.H ₂ O	3073	1644	1240	532	495	3348
[Fe(L)Cl ₂]Cl·2H ₂ O	3083	1645	1243	502	458	3379
[Ru(L)Cl ₂]Cl	3073	1646	1227	530	493	3355

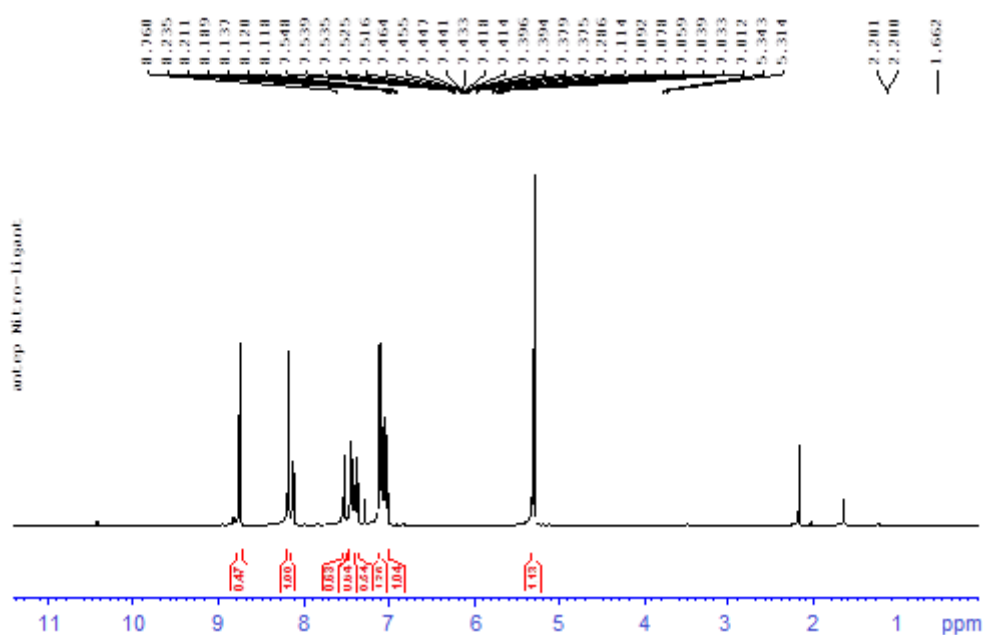


Figure 5. ¹H NMR spectra of the ligand L.

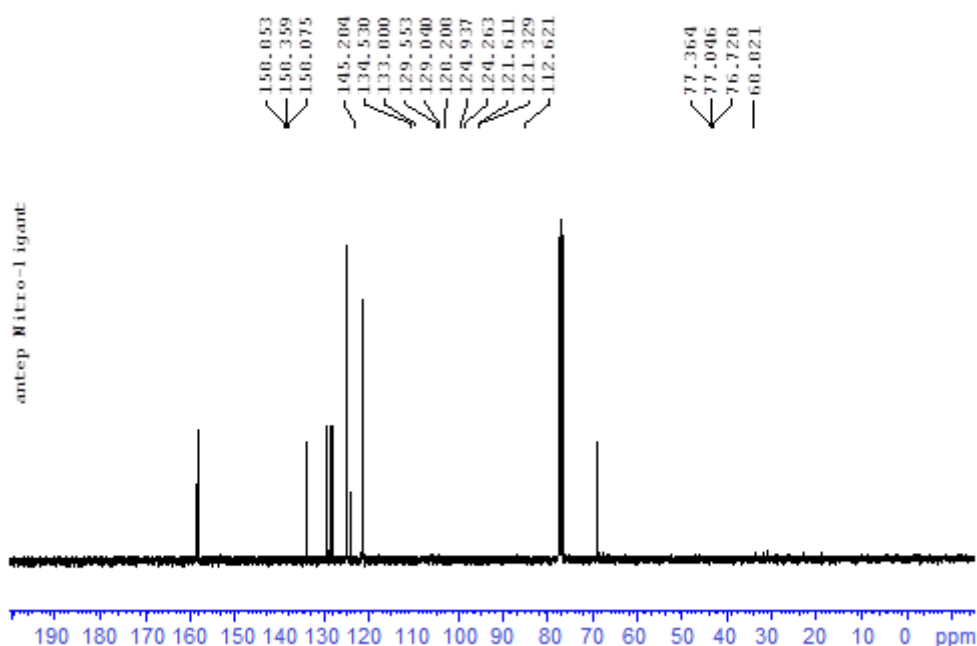


Figure 6. ^{13}C NMR spectra of the ligand L.

3.4. UV-Vis absorbance and emission studies

Ultraviolet visible spectra of phenoxy-imine ligand and metal complexes in the DMF solvent was recorded experimentally at 190-1100 nm, and the obtained spectra are shown in Figure 7.

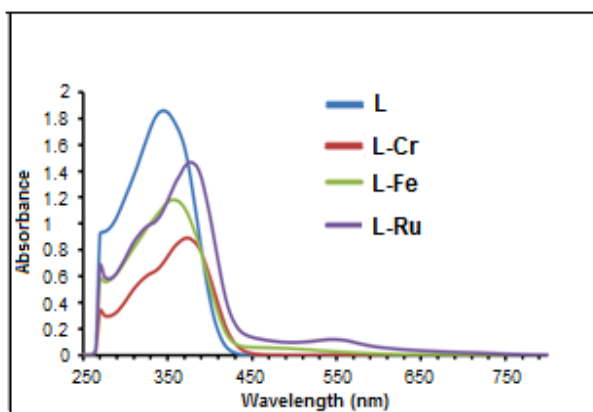


Figure 7. UV-Vis spectra of ligand and its metal(III) complexes.

The C=N system is a weak chromophor, which absorbs ultraviolet light. Conjugation with phenyl groups shifts the absorbance to the visible region. Schiff base was observed approximately when the UV-Vis spectra gave two peaks between 210-400 nm. Transitions observed in the UV-Vis spectrum between 200 and 275 nm wavelengths are transitions originating from the

aromatic rings and unshared electrons of the ligand.²⁸ The maximums are observed at 275-345 nm in L_1 related to $n-\pi^*$ transitions of the imine groups. Approximately 345-275 nm in L is related to $n-\pi^*$ and $\pi-\pi^*$ transitions of the imine and etheric oxygen groups in complexes of ligand.^{29,30} The bands at 420-700 nm in L_1 show weak and intermediate transitions of d-d. Shifts of these bands to the lower and higher wavelengths indicate the complex forms of the nitrogen atoms of the imine groups and of the oxygen atoms of the phenoxy groups in coordination with the metal ion.³¹

3.5. Magnetic Moment and Molar Conductivity

The magnetic susceptibility values of the complexes obtained indicate that all the complexes are paramagnetic. The magnetic moment values of the Cr(III) complex is 2.91 B.M. which is in good agreement with the presence of three unpaired electrons.

The measured μ_{eff} value for the Fe(III) complex is 6.51 B.M. which is monomeric and high-spin at room temperature for the octahedral geometry. Magnetic moment value for the Ru(III) complex was determined to be 1.51 B.M.^{31,32} which is in good agreement with the presence of one unpaired electron. From the magnetic studies, it is evident that all the metal complexes possess octahedral configuration in accordance with literature data.^{33,34}

The electrolytic conductivities of ligand Cr(III), Fe(III), and Ru(III) complexes were taken at room temperature and 10^{-3} molar concentration in DMF

solvent. The compounds have an electrolytic conductivity of 15.26-28.57 $\mu\text{S}/\text{cm}$ indicating their slightly polar nature due to the electrolytic behavior of chlorine. L-Cr(III), L-Fe(III), L-Ru(III) metal complexes exhibit electrolytic behavior.³⁵ The molar conductance values indicate all the complexes have 1:1 stoichiometry.

3.6. TGA

The thermal stabilities of ligand and Cr(III), Fe(III), Ru(III) complexes, thermal degradation steps of complex compounds and TGA/DTA spectra were used to determine the hydrate water in the structure. The thermal properties of the metal complexes were investigated by measuring the TGA/DTA by increasing the temperature by 10°C per minute with a continuous 2 bar nitrogen gas at 25-1000°C temperature under N₂ atmosphere. The TGA/DTA curves of the complexes are given in Figure 8.

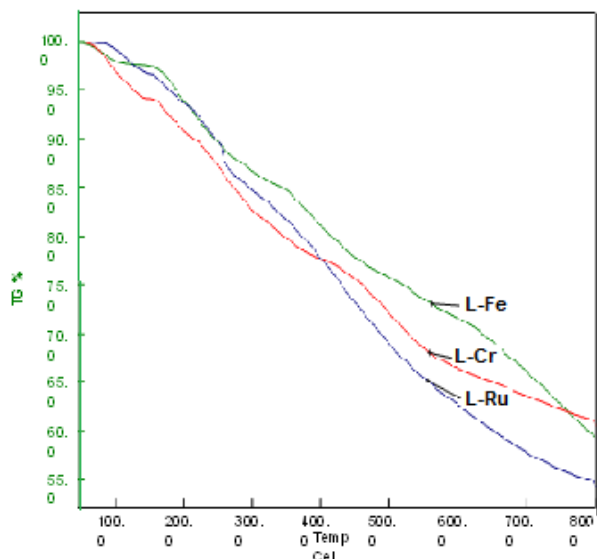


Figure 8. The TGA/DTA/DTG curves of Ligand and its metal complexes.

As a result of this data, it is considered that the crystal water, HCl acid and phenyl group dissociate during the thermal decomposition of the complexes. When the mass losses of the complexes are considered, the TGA values and the calculated values of organic groups and crystal water which are degraded are in accordance with the literature.³⁶ The thermal stability of all the complexes increases in the order: Fe(III) < Cr(III) < Ru(III).

3.7. Cyclohexane oxidation under microwave irradiation

The reaction medium for alkane oxidation and alkene epoxidation was carried out using a Berghof MWS3+

microwave device. After the calibration procedure was completed, 1 μl samples were prepared from the catalyzed sample using an electronic pipette and GC-MS spectra were taken. In the alkane oxidation process, conversion %, yield % and selectivity % formation of the catalysts used (Cr(III), Fe(III) and Ru(III) complexes) and conversion percentages of cyclohexane in different catalysts are reported under microwave irradiation with cyclohexane hydrogen peroxide.³⁷ The possible reaction products are shown in Figure 9.

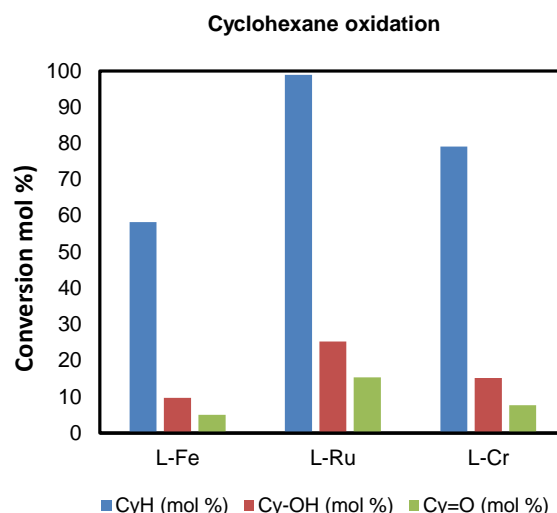


Figure 9. Influence of the complexes in cyclohexane oxidation under microwave irradiation.

According to the cyclohexane transformations and product formations in which the metal complexes are used as catalysts, the CyH conversion% is the highest 99.92% L-Ru(III), while the lowest is 58.28% L-Fe(III) complexes. Cyclohexanol (CyOH) formation is the most observed catalyst with 25.27% L-Ru(III) and the least observed is 9.75% L-Fe(III) complex. In the cyclohexanone formation, the catalyst effect was at most 15.37% L-Ru, but at least 5.09% L-Fe(III) complex is observed. In this sense, the catalyst with the most by-product formation is L-Ru(II). Generally catalysts synthesized are the catalyst L-Ru(III) complex which triggers the highest product formation in the catalyst. The catalytic performance of mononuclear Ru(III) complexes can be compared to the catalytic activity exhibited by the different complexes reported in the literature.^{38,39}

3.8. Cyclohexene oxidation under microwave irradiation

Epoxidation reactions of cyclohexene substrates were carried out using synthesized Schiff base metal complexes. For the epoxidation, H₂O₂ was used as the initiator in the reaction medium and the reaction was carried out in microwave. As a result of the epoxidation

reaction of cyclohexene, the catalytic effects of all metal complexes appear to be high in the reaction of substrate conversion (Figure 10).

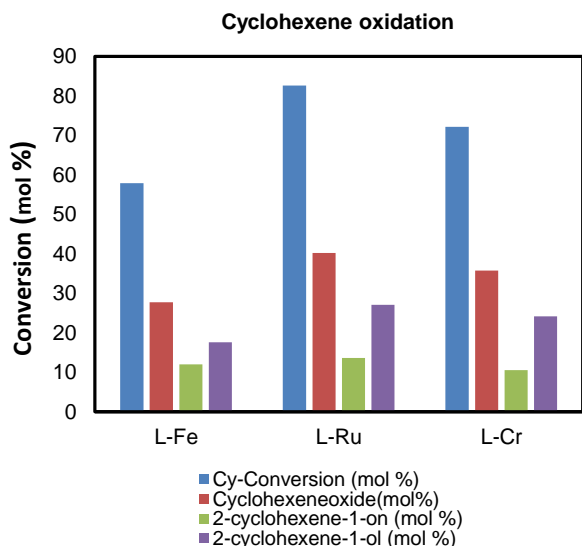


Figure 10. Influence of the complexes in cyclohexene oxidation under microwave irradiation.

However the cyclohexene conversion rates are lower. According to the instructions obtained in the epoxidation reactions, 2-cyclohexen-1-one and 2-cyclohexen-1-ol are formed. The highest cyclohexane conversion rate is epoxidation reactions using L-Ru(III) (82.64%) and L-Cr(III) (72.15%) metal complexes. The catalytic effects of iron and chrome complexes are lower. It is thought that one of the reasons for the low yield is due to the fact that the amount of H_2O_2 used as an oxidant in the reactions is lower than that in the literature.

4. CONCLUSIONS

The new Schiff base ligand containing the phenoxy group and their metal(III) complexes were synthesized and characterized by analytical and spectroscopic methods. All of the obtained results can be attributed to the fact that the Schiff base ligand functions as ONNO tetradentate chelate in mononuclear complexes. The synthesized complexes were assayed as oxidative catalysts for cyclohexane and cyclohexene oxidation products under microwave irradiation. The catalytic effect of L-Ru(III) complexes appears to be high as shown in the substrate conversion reaction. For the further work in this direction, this study indicates that the use of these kinds of complexes for catalytic purposes will be possible.

ACKNOWLEDGEMENTS

The authors are grateful to Presidency of Scientific Research Projects of University Gaziantep (FEF.10.08) for financial supports.

Conflict of interest

Authors declare that there is no a conflict of interest with any person, institute, company, etc.

REFERENCES


- Karaoglu, K.; Baran, T.; Serbest, K.; Er, M.; Degirmencioglu, I. *J. Mol. Struct.* **2009**, 922, 39-45.
- Ekmekcioglu, P.; Karabocek, N.; Karabocek, S.; Emirik, M. *J. Mol. Struct.* **2015**, 1099, 189-196.
- Er, M.; Sancak, K.; Degirmencioglu, I., Serbest, K. *J. Mol. Struct.* **2008**, 882, 35-46.
- Azadbakht, R.; Khanabadi, J. *Inorg. Chem. Commun.* **2013**, 30, 21-25.
- Abbo, H. S.; Titinchi, S. J. J.; Prasad, R.; Chand, S. *J. Mol. Catal. A: Chem.* **2005**, 225, 225-232.
- Wang, Y.; Fu, Z.; Wen, X.; Rong, C.; Wu, W.; Zhang, Chao.; Deng, J.; Dai, B.; Kirk S.R.; Yin, D. *J. Mol. Catal. A: Chem.* **2014**, 384, 46-52.
- Zoubi, W.A.L.; Kandil, F.; Chebani, M.K. *Spectrochim. Acta Part A: Mol. Biomol. Spectrosc.* **2011**, 79(5), 1909-1914.
- Çolak, M.; Demirel, N. *Tetrahedron: Asymmetry* **2008**, 19(5), 635-639.
- Temel, H.; Çakır, Ü.; Uğraş, H.İ.; Şekerçi, M. *J. Coord. Chem.* **2003**, 56, 943-951.
- Sönmez, M.; Çelebi, M.; Berber, İ. *Eur. J. Med. Chem.* **2010**, 45, 1935-1940.
- Sivakumar, R.; Reena, V.; Ananthi N.; Babu, M.; Anandan, S.; Velmathi, S. *Spectrochim. Acta Part A: Mol. Biomol. Spectrosc.* **2010**, 75(3), 1146-1151.
- Ceyhan, G.; Çelik, C.; Uruş, S.; Demirtaş, İ.; Elmastaş, M.; Tümer, M. *Spectrochim. Acta Part A: Mol. Biomol. Spectrosc.* **2011**, 81(1), 184-198.
- Masih, I.; Fahmi, N. *Spectrochim. Acta Part A: Mol. Biomol. Spectrosc.* **2011**, 79(5), 940-947.

14. Rajsekhar, G.; Rao, C.P.; Saarenketo, P.; Nattinenb, K.; Rissanen, K. *New J. Chem.* **2004**, 28, 75-84.
15. Hailu, S. L.; Nair, B.U.; Redi-Abshiro, M.; Diaz, I.; Aravindhnan, R.; Tessema, M. *Chinese J. Catal.* **2016**, 37(1), 135-145.
16. Zhao, Y.; Tang, Y.; Liu, W.S.; Tang, Ning.; Tan, M.Y. *Spectrochim. Acta Part A: Mol. Biomol. Spectrosc.* **2006**, 65(2), 372-377.
17. Shoair, A.F.; El-Shobaky, A.R., Azab, E.A. *Spectrochim. Acta Part A: Mol. Biomol. Spectrosc.* **2015**, 151, 322-334.
18. Baran, T.; Karaoglu, K.; Serbest, K.; Ağır, H.; Sandallı, C.; Değirmencioglu, İ. *Monatshefte für Chemie.* **2013**, 144, 1107-1115.
19. El-Shobaky, A. R. *Met-Org. Nano-Met. Chem.* **2015**, 45, 1481-1488.
20. Yilmaz Obali, .A.; Ucan, H.I. *J. Mol. Struct.* **2015**, 1081, 74-78.
21. Karahan, A.; Yardan, A.; Yahsi, Y.; Kara, H.; Kurtaran, R. *SDU J. Sci. (e-Journal).* **2013**, 8(2), 163-174.
22. Naeimi, H.; Tarazian, R. *J. Heterocyclic Chem.* **2014**, 51, 566.
23. Kaya, İ.; Çulhaoğlu, S. *Chinese J. Polym. Sci.* **2012**, 5, 682-693.
24. Taşkın, O.K.; Öztürk, Ö.F.; Canpolat, E.. *BEÜ Fen Bilimleri Dergisi.* **2012**, 1, 34-39 (in Turkish).
25. Canpolat, E.; Ağlamış, A., Şahal, H.; Kaya, M. *Fen Bilimleri Dergisi (CFD)*, **2016**, 37(1), 65-73.
26. Serbest, K.; Karaoğlu, K.; Erman, M.; Er, M.; Değirmencioglu, İ. *Spectrochim. Acta Part A: Mol. Biomol. Spectrosc.* **2010**, 77(3), 643-651.
27. Rajakumar, P.; Murali, V. *Tetrahedron* **2004**, 60, 2351-2360.
28. Rsmussen, J.C.; Toftlund, H.; Nivorzhkin, A.N.; Bourasse, J.; Ford, P.C. *Inorg. Chim. Acta* **1996**, 251, 291-298.
29. Islam, Sk.M.; Paul, S.; Roy A.S.; Banerjee, S.; Ghosh, K.; Dey, R.C.; Santra, S.C. *Trans. Metal. Chem.* **2013**, 38(6), 675-682.
30. Wang, Y.; Wen, X.; Rong, C.; Tang, S.; Wu, W.; Zhang, C.; Liu, Y.; Fu, Z. *J. Mol. Catal. A: Chem.* **2016**, 411, 103-109.
31. Pramanik, A.K.; Mondal, T.K. *Inorg. Chim. Acta* **2014**, 411, 106-112.
32. Dhara, P. K.; Drew, M. G. B.; Chattopadhyay P. *Polyhedron* **2006**, 25, 1939-1945.
33. Anastasiadis, N.; Bilis, G.; Plakatouras, J.C.; Raptopoulou, C.P.; Psycharis, V.; Beavers, C.; Teat, S.J.; Louloudi, M., Perlepes, S.P. *Polyhedron* **2013**, 64, 189-202.
34. Geary, W J. *Coord. Chem. Rev.* **1971**, 7(1), 81-122.
35. Manonmani, J.; Kandaswamy, M.; Narayanan, V.; Thirumurugan, R.; Shanmuga Sundura Raj, S.; Shanmugam, G., Ponnuswamy, M.N.; Fun, H.K. *Polyhedron* **2001**, 20, 3039-3048.
36. Abdel-Latif, S. A.; Hassib, H. B.; Issa, Y. M. *Spectrochim Acta Part A: Mol. Biomol. Spectrosc.* **2007**, 67(3-4), 950-957.
37. Urus, S.; Keles M.; Serindag, O. *J. Inorg. Organometal Polym.* **2010**, 20, 152-160.
38. Retcher, B.; Costa, J.S.; Tang, J.; Hage, R.; Gamez, P.; Reedijk, J. *J. Mol. Catal. A: Chem.* **2008**, 286, 1-5.
39. Luque R.; Badamali, S.K.; Clark, J.H.; Fleming, M.; Macquarrie, D.J. *Appl. Catal. A: Gen.* **2008**, 341, 154-159.

ORCID

 0000-0002-6477-6604 (A. Çapan)

 0000-0002-9127-2348 (G. Ceyhan)

 0000-0003-3127-666X (M. Sönmez)



Chemical analyzes and antioxidant activities of essential oils of four wild *Mentha* species growing in the Tokat and its districts

Tevfik OZEN^{1,*}, Isa TELCI², Fatih GUL³, Ibrahim DEMIRTAS³

¹Department of Chemistry, Faculty of Arts and Sciences, Ondokuz Mayıs University, Samsun, 55139, Türkiye

²Department of Field Crops, Faculty of Agriculture, Süleyman Demirel University, Isparta, 32260, Türkiye

³Department of Chemistry, Faculty of Science, Çankırı Karatekin University, Çankırı, 18100, Türkiye

Received: 13 October 2017, Revised: 19 November 2017; Accepted: 22 November 2017

*Corresponding author's e-mail address: tevfikoz@omu.edu.tr (T. Ozen)

ABSTRACT

The current work evaluated the chemical compositions of the essential oils (EOs) extracted from *Mentha longifolia* subsp. *typhoides* (Briq.) Harley var. *typhoides* PH. Davis, *Mentha spicata* L. subsp. *spicata*, *Mentha longifolia* (L.) Hudson subsp. *longifolia* and *Mentha villosa nervata* Opiz from gowning in the different locations of Tokat. The antioxidant activities of EOs were tested using total antioxidant activity, reducing power, inhibition of lipid peroxidation, metal chelating, H₂O₂, DPPH[•] and O₂^{•-} scavenging activities. The chemical compositions of EOs were determined by GC and GC-MS. Significant differences were recorded between the percentages of many constituents depending on the geographical. The most important components were identified consecutively: linalool (nd-62.80%), menthone (0.31-60.81%), pulegone (nd-21.52%), isomenthone (nd-30.15%) and piperitoneoxide (nd-68.92%). The inhibition of lipid peroxidation, O₂^{•-} and H₂O₂ scavenging activities of the EOs were very effective but their reduction power values were low. The results obtained validate that EOs of four *Mentha* species possess a source of antioxidant potential for medicinal and foods.

Keywords: *Mentha* species, essential oils, chemical contents, antioxidant activity

Tokat ve ilçelerinde yetişen dört yabancı nane (*Mentha*) türünün uçucu yağlarının kimyasal analizleri ve antioksidan aktiviteleri

ÖZ

Bu çalışma Tokat'ın farklı yerlerinde yetişen *Mentha longifolia* subsp. *typhoides* (Briq.) Harley var. *typhoides* PH. Davis, *Mentha spicata* L. subsp. *spicata*, *Mentha longifolia* (L.) Hudson subsp. *longifolia* ve *Mentha villosa nervata* Opiz' den ekstrakte edilen uçucu yağların kimyasal bileşimleri belirlendi. Uçucu yağların antioksidan aktiviteleri toplam antioksidan aktivite, indirgeyici güç, lipid peroksidasyonunun inhibisyonu, metal şelat, H₂O₂, DPPH[•] ve O₂^{•-} giderme aktiviteleri uygulanarak test edildi. Herbir uçucu yağın kimyasal bileşimleri GC ve GC-MS ile belirlendi. Coğrafyaya bağlı olarak birçok bileşenin yüzdesi arasında önemli farklılıklar kaydedildi. En önemli bileşenleri sırayla linalool (nd-% 62.80), menthone (% 0.31-60.81), pulegone (nd-% 21.52), isomenthone (nd-% 30.15) ve piperitoneoxide (nd-% 68.92) tespit edildi. Uçucu yağların lipid peroksidasyon inhibisyonu, O₂^{•-} ve H₂O₂ giderme aktiviteleri çok etkiliydi, fakat indirgeme gücü değerleri düşüktü. Elde edilen sonuçlar, dört nane (*Mentha*) türünün uçucu yağlarının tıbbi ve gıdalarda bir antioksidan potansiyel kaynak olduğunu doğrulamaktadır.

Anahtar Kelimeler: Nane (*Mentha*) türleri, uçucu yağlar, kimyasal bileşenler, antioksidan aktivite

1. INTRODUCTION

Mentha species are members of the Lamiaceae, which almost show a cosmopolitan distribution of moderate to the tropical regions.¹ They have been used for different purposes throughout the history with aim of usages of their various features. For example, *Mentha* oil is the world's oldest known herbal remedy.² Essential oils (EOs) are a mixture of complex, naturally occurring volatile compounds synthesized by plants as secondary

metabolites in *Mentha* species.³ EOs are abundant in flowers, leaves and seeds in plants. It is usually isolated by hydro-distillation methods.⁴ Nowadays, about 3000 EOs are known, among which particularly 300 are commercial of vital importance for food, pharmaceutical, cosmetic, agronomic, sanitary and perfume industries. For example, D-carvone, D-limonene and geranyl acetate are used as perfumes, creams, soaps, as flavor agents for food product and as industrial solvents in household cleaners.⁵ EOs in combination with vegetable oils are

also used in massages. Some of EOs appear to have medical features and are reported to have treated one or more diseases, and also are used in paramedical applications. Terpenoids and aromatic in the EOs components can also be used to enhance the efficacy of existing treatments. Hundreds of studies performed *in vitro* and *in vivo* in animals demonstrate their efficacy when used alone, without conventional chemotherapy or radiotherapy treatments.⁶⁻⁷ Numerous experimental data indicate that toxicity focuses primarily on cancer cells without affecting healthy cells and it is important to investigate new effective natural products.⁸

In the present study, the EOs of four widely consumed wild Turkish mints, namely *M. longifolia* subsp. *typhoides* (Briq.) Harley var. *typhoides* PH. Davis, *M. longifolia* (L.) Hudson subsp. *Longifolia*, *M. spicata* L. subsp. *spicata* and *M. villosa nervata* Opiz collected from different locations of Tokat, Turkey were investigated in September 2014 for their chemical composition and their *in vitro* antioxidant properties. The antioxidant activities of EOs were evaluated by total antioxidant activity, reducing power, inhibition of lipid peroxidation, metal chelating, H₂O₂, DPPH· and O₂^{·-} scavenging assays for the first time for this region. And, there are no records of correlations between chemical compositions of the EOs and their antioxidant activities of the taxon from Tokat, Turkey. In addition to being used as spices, these *Mentha* samples are also used as foodstuffs and beverages. Moreover, it is known that they are also used as traditional medicines in the treatment of different diseases or conditions.⁹ The main purpose of this study is to further explore the potential benefits of these *Mentha* species as a naturally occurring source of bioactive substances.

2. MATERIALS AND METHODS

2.1. Materials

2.1.1. Chemicals

Folin–Ciocalteu reagent (FCR), nicotine adenine dinucleotide (NADH), trichloroacetic acid (TCA), butylated hydroxyanisole (BHA), α -tocopherol, butylated hydroxytoluene (BHT), pyrocatechol, quercetin, phenazine methosulphate (PMS), 1,1-diphenyl-2-picryl-hydrazyl (DPPH[·]), ferrous chloride, ammonium molybdate, K₃[Fe(CN)₆], trolox, sodium acetate (CH₃COONa), sodium carbonate, thiobarbituric acid (TBA), nitrobluetetrazolium (NBT) and ascorbic acid were provided from Sigma. The organic solvents used in analyses were of HPLC grade and purchased from Merck. All the other chemicals were supplied from other commercial sources.

2.1.2. Plant material

The fresh plant materials of *M. longifolia* subsp. *typhoides* (Briq.) Harley var. *typhoides* PH. Davis (K4;

40° 24 235, Y1; 40° 02 275, Y3; 40° 08 325, Y10; 40° 06 909, Z2; 40° 16 092, Z7; 40° 16 228, K2; 40° 23 744, R2; 40° 27 156, R7; 40° 30 794, Y12; 40° 03 187, Y13; 40° 03 954, Y15; 40° 03 958, Z4; 40° 16 202, R1; 40° 25 894, R4; 40° 34 000, Y4; 40° 03 187, Y7; 40° 14 823, Y11; 40° 04 975, Y14; 40° 00 251, Z1; 40° 16 206, Z10; 40° 18 144, Z11; 40° 19 272), *M. longifolia* (L.) Hudson subsp. *longifolia* (R5; 40° 31 737 616, R6 40° 30 739 596), *M. spicata* subsp. *spicata* (Z5; 40° 16 024 540, Y9; 39° 59 151 1030) and *M. villosa nervata* Opiz (K3; 40° 24 235 647, R9; 40° 32 068 1434) were collected in the different locations of Tokat city of Turkey in September 2014 (Figure 1). The samples were verified by Prof. Dr. Isa Telci and prepared in the Herbarium of Agriculture Faculty, Gaziosmanpasa University, Tokat-Turkey. The collected samples were air-dried and kept for analysis.

2.2. Methods

2.2.1. Analysis of EOs

2.2.1.1. GC-MS Analysis

The EOs were determined using Agilent Technologies GC 7890A with a built-in 5975 Triple Axis Detector MS system, equipped ionization system, HP5-ms (30 m x 250 mm x 0.25 mm) column and ionization energy for GC-MS detection (70 eV). The helium was used as carrier gas at a flow rate (1 mL min⁻¹). The same column temperature was achieved with GC analysis given above in our laboratory, by comparison of their mass spectral fragmentation patterns (WILEY and NIST database/Chem Station data system), and then their retention indices were determined with reference to homologue series of *n*-alkanes (C6-C26).¹⁰

2.2.1.2. Separations of EO components

A sample of the EO was separated using a method described by Amzazi¹¹ using silica-gel column chromatography (*n*-pentane and *n*-pentane: diethyl ether (5:95, v/v)). The 600 fractions were eluted with a gradient of increasing solvent polarity (*n*-pentane: diethyl ether 100:0-90:10). All fractions were submitted to GC-MS analysis. The combined fractions were evaporated under air flow and determined by GC-MS.¹¹

2.2.2. Antioxidant activity

2.2.2.1. Assay of total antioxidant activity by phosphomolybdate method

The total antioxidant activities of the EOs were evaluated to the method described in literature.¹² The assay was based on the reduction of Mo (VI) to Mo (V) by the EOs. The subsequent formation of green phosph-

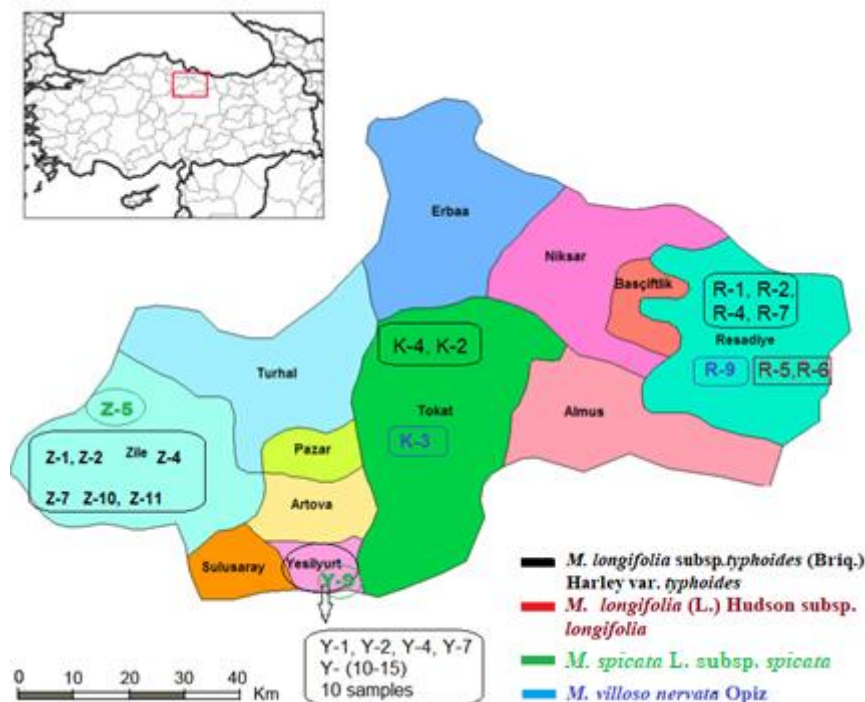


Figure 1. Distribution map of four *Mentha* species (*Mentha longifolia* subsp. *typhoides* (Briq.) Harley var. *typhoides* PH. Davis, *Mentha longifolia* (L.) Hudson subsp. *Longifolia*, *Mentha spicata* L. subsp. *spicata* and *Mentha villosa nervata* Opiz in Tokat and its Districts.

hate/Mo(V) compounds monitored at acidic pH. A 0.3 ml EO was added to 4 mM ammonium molybdate, 0.6 M sulfuric acid and 28 mM sodium phosphate, respectively. The mixture of the reaction was incubated at 95°C and measured absorbance at 695 nm. The total antioxidant activities of the EOs were calculated as an equivalent of α -tocopherol according to the extinction coefficient of $4 \times 10^3 \text{ M}^{-1} \text{ cm}^{-1}$ and expressed as $\mu\text{mol } \alpha\text{-tocopherol/g}$ sample.

2.2.2.2. Assay of reducing power

The reducing powers of the EOs were determined using Oyaizu Method with slight modification.¹³ The EO samples ($100 \mu\text{g ml}^{-1}$) were added to phosphate buffer (0.2 M, pH 6.6) and $\text{K}_3\text{Fe}(\text{CN})_6$ (10 g l^{-1}), respectively. After incubation for 25 min at 50 °C, TCA (2.5 ml; 10%) was added to the mixture and centrifuged at $3.000 \times \text{g}$ for 20 min. Finally, 2.5 ml of supernatant was combined with water and FeCl_3 solution (0.5 ml; 0.1%). The absorbance of the mixture was read at 700 nm. It is indicated that the high absorbance of the sample has effective reducing power in the reaction condition that the reducing capacity had increased.

2.2.2.3. Assay of DPPH' scavenging activity

DPPH' (free radical) scavenging activities of the EOs were assayed according to the reference.¹⁴ The DPPH' solution (2.7 ml; 1 mM) was mixed with the sample (100

$\mu\text{g ml}^{-1}$) in the test tubes. After incubating at room temperature in the dark for 30 min, the absorbance of the mixture was monitored at 517 nm. The reduction of sample absorbance indicated higher DPPH' scavenging activity. The activities were calculated as a percentage of DPPH' discoloration, using the following equation. For the free radical scavenging activity, the equation is

$$\% = [(A_{517}(\text{control}) - A_{517}(\text{sample})) / A_{517}(\text{control})] \times 100$$

where $A_{532}(\text{control})$ is the absorbance of control and $A_{532}(\text{sample})$ is the absorbance of the sample.

2.2.2.4. Assay of H₂O₂ scavenging activity

H₂O₂ scavenging activity of the sample was evaluated according to the reference.¹⁵ A 1 ml extract solution was added in a flask to 0.1 mM H₂O₂ in phosphate buffer (pH 7.4), ammonium molybdate, 10 ml of 2 M H₂SO₄ and 7 ml of 1.8 M KI. The mixture was titrated with 5 mM Na₂S₂O₃ until the disappearance of yellow color. The activity was calculated as the percentage of H₂O₂ scavenging, using the following equation. For the H₂O₂ scavenging activity, the equation is

$$\% = [(V_{\text{control}} - V_{\text{sample}}) / V_{\text{control}}] \times 100$$

where $V_{(\text{control})}$ is the volume of control and $V_{(\text{sample})}$ is the volume of the sample.

2.2.2.5. Assay of superoxide scavenging activity

Superoxide scavenging activities of the EOs (100 $\mu\text{g ml}^{-1}$) were estimated according to a minor modification.¹⁶ Superoxide anion radicals were generated in a PMS-NADH system by oxidation of NADH and assayed by reduction of NBT. Briefly, an EO sample was mixed with NBT (156 μM : 1 ml) and NADH (468 μM : 1 ml), respectively. Then, the reaction was started by adding PMS (60 μM : 0.1 ml). After incubating at room temperature, the absorbance of the mixture was monitored at 532 nm. A decrease in absorbance of the mixture indicates an increase in superoxide anion-scavenging activity.¹⁷ The activities were calculated as inhibition of superoxide anion generation by the following equation. For the superoxide anion scavenging activity, the equation is

$$\% = [(A_{532(\text{control})} - A_{532(\text{sample})}) / A_{532(\text{control})}] \times 100$$

where $A_{532(\text{control})}$ is the absorbance of control and $A_{532(\text{sample})}$ is the absorbance of the sample.

2.2.2.6. Assay of metal chelating (Fe^{2+}) activity

The metal chelating activities of the EOs (100 $\mu\text{g ml}^{-1}$) were measured according to the method in the literature with modifications.¹⁸ In this method, ferrozine can form complex with Fe^{2+} (ferrozine- Fe^{2+}), effectively. In the presence of other chelating compounds, this complex is disrupted with chelator compounds. Briefly, EOs was mixed with of FeCl_2 (2 mM, 0.05 ml) solution. After 30 min incubation at 25°C, the reaction was initiated with the addition of 5 mM ferrozine. Each mixture was shaken vigorously and then left to stand at 25°C. The absorbance of the mixture was read at 562 nm. The activities were calculated as a percentage of inhibition of Fe^{2+} -ferrozine complex formation according to the following equation. For, the metal chelating activity, the equation is

$$\% = [(A_{562(\text{control})} - \text{Abs}_{562(\text{sample})}) / \text{Abs}_{562(\text{control})}] \times 100$$

where $A_{562(\text{control})}$ is the absorbance of control and $A_{562(\text{sample})}$ is the absorbance of the sample.

2.2.2.7. Inhibition of lipid peroxidation

The inhibition of lipid peroxidation assay for EOs (100 $\mu\text{g ml}^{-1}$) was carried out using TBA method based on inhibition of linoleic acid peroxidation according to the literature.¹⁹ Briefly, the EO sample was mixed with 500 μl of 20 mM linoleic acid, 50 μl of 100 μM phosphate buffer (pH 7.4), 150 μl of 20 μM ascorbic acid. The reaction of peroxidation was initiated by adding of 10 μM FeSO_4 (0.1 ml) and incubated at room temperature for 60 min. The mixture was added to 10%

TCA solution and kept in a water bath (95 °C). After cooling at room temperature, butanol was added to the mixture and centrifuged at 4000 \times g. After removing the supernatant, the formation of TBA reactive substance was monitored at 532 nm. The inhibition ration was calculated by the following formula. For the inhibition of lipid peroxidation, the equation is

$$\% = [(A_{532(\text{control})} - A_{532(\text{sample})}) / A_{532(\text{control})}] \times 100$$

where $A_{532(\text{control})}$ is the absorbance of control and $A_{532(\text{sample})}$ is the absorbance of the sample.

2.2.3. Statistical Analysis

The data were presented as the mean \pm standard deviation (S.D.). The results were analyzed by one-way ANOVA analysis of variance followed by Duncan's test and considered to be significant with $p < 0.05$ and $p < 0.01$ confidence level, statistically.

3. RESULTS AND DISCUSSION

3.1. Quantitative analysis

The retention indexes (RI) and retention time (RT) of EOs of leaves and flowers of wild *Mentha* species were determined as quantitative compositions. The major variations were determined among the parts of *Mentha* species and extraction applications. The chemical composition of essential oils of *Mentha* species was shown in Table 1-4. 30 compounds were identified in the EOs and the percentage of identified compounds ranged from nd to 68.92%. Compounds that were the most abundant in the EOs of *M. longifolia* subsp. *typhoides* (Briq.) Harley var. *typhoides* PH. Davis were linalool [Z-2L (45.68%), Z-2F (62.88%), Z-4L 52.32)], menthone [K-4L (60.81%), K-4F (50.15%), Y-10L (34.89%), Y-10F (27.54%), Y-13L (26.70%), Z-1F (35.25%)], isomenthone [Y-10L (16.85%), Y-10F (13.28%), Z-2L (30.15%), Z-2F (14.09%)], piperitoneoxide [K-4L (15.46%), K-4F (18.13), Y-1L (35.69%), Y-2L (28.62%), Y-2F (23.74%), Y-3L (63.15%), Y-3F (25.99%), Y-10L (24.00%), Y-10F (31.06%), Z-7L (69.43%), K-2L (47.57%), R-2L (20.74%), Y-15L (63.81%), R-4F (25.34%), Y-4F (35.39%), Y-11F (46.78%), Y-14F (41.83%), Z-1F (13.93%), Z-10F (26.90%), Z-11F (49.22%)], thymol [Y-1L (14.07%), Y-12L (57.13%)], 1-acetoxy-p-menth-3-one (Y-1F 22.09%) and anhydroserricornin [K-2L (16.51%), Y-3F (14.82%), Z-10F (20.62%), R-2L (24.04%)] (Table 1-4). The menthone [K-3L (19.41%)] in *M. villosa nervata* Opiz and menthone [Y-9L (10.60%)], pulegone [Z-5L (21.52%)] in *M. spicata* L. subsp. *spicata* were the highest content because of growing at high altitude. The piperitone oxide is major component in *M. villosa nervata* Opiz [K-3L (56.19%); R-9F (68.92%)], *M.*

spicata [Y-9L (46.82%)] and *M. longifolia* (L.) [R-5F (47.60%)] (Table 1-4). The EO components of *M. longifolia* subsp., *M. longifolia* (L.), *M. spicata* and *M. villosa nervata* Opiz show different compositions. When the EOs of *M. longifolia* subsp., *M. longifolia* (L.), *M. spicata* and *M. villosa nervata* Opiz are compared with the same species grown in different counties, the found results are the same major constituents with slightly different levels.^{20,21} Also, many compounds in the EOs

such as sabinene hydrate, linalool oxide, 3-octyl acetate, methylvaleric acid, 2-propylmalonic acid, 5-caranol, 4-terpineol, levomenthol, citronellol, carvone, linalyl acetate, dihydroedulan, isopulegol acetate, thymol acetate, dihydrocarvyl acetate, ascaridole, ethyl hydroden pimelate, formic acid, cubedol, α -humulene, jasmine lactone, hexanoic acid, cinerolone, dodecanoic acid and aromadendrene oxide were determined as trace amounts.

Table 1. Identified chemical components in EOs of wild *M. longifolia* subsp. *Typhoides* (Brig) Harley var. *typhoides* PH. Davis samples from Reşadiye (R) and center of Tokat (K)

Components	RT (min)	RI	K-2	K-4		R-1	R-2	R-4	R-7
			L	L	F	F	L	F	L
3-octanol	13.531	965	nd	0.43	nd	nd	nd	0.33	0.45
o-cymene	14.699	999	0.36	0.65	0.45	nd	nd	0.13	0.23
Eucalyptol	14.991	1009	0.26	0.24	0.23	nd	nd	0.10	0.13
Linalool oxide	17.105	1071	nd	0.30	nd	0.48	nd	0.14	0.23
Linalool	17.127	1072	nd	nd	nd	nd	nd	nd	nd
β -linalool	19.233	1132	0.48	60.81	50.15	1.26	0.69	0.65	0.38
Menthone	20.053	1156	nd	nd	nd	nd	nd	nd	0.07
α -terpineol	19.634	1144	0.48	5.85	5.35	0.50	0.48	0.42	0.31
Isomenthone	19.833	1150	nd	3.14	nd	nd	nd	nd	nd
Menthol	20.734	1175	0.43	0.22	0.36	68.30	0.30	0.33	0.18
Dihydrocarvone	22.212	1217	nd	3.34	5.68	nd	2.74	0.72	0.75
Pulegone	22.416	1224	nd	nd	nd	nd	nd	nd	nd
Linalyl acetate	22.797	1235	47.57	15.46	18.13	2.56	20.74	25.34	0.36
Piperitone oxide	23.700	1262	nd	nd	nd	nd	nd	1.10	1.13
Thymol	24.234	1277	0.77	nd	nd	nd	1.34	nd	0.56
Diosphenol	24.802	1293	nd	nd	0.46	nd	0.97	nd	nd
3-methylidenedecan-4-ol	26.431	1344	nd	nd	nd	nd	8.05	21.95	7.37
Humulene epoxide 2	26.865	1357	7.05	0.44	nd	nd	8.48	12.96	1.70
1-[tert-butyl(dimethyl)silyl]-4-(2,2-dimethyl-6-methylidencyclohexyl)butan-1-ol	27.125	1365	nd	0.28	nd	0.26	nd	nd	nd
β -bourbonene	27.145	1366	0.79	nd	nd	nd	nd	nd	nd
7-(2-acetylcyclopropyl)-6,6-dimethylheptane-2,5-dione	27.826	1391	1.19	nd	nd	nd	2.42	nd	0.77
5-(tetrahydro-2-furanyl)-2-heptanol	28.272	1399	nd	0.27	nd	1.31	nd	nd	1.45
\square -caryophyllene	28.973	1422	2.08	0.22	nd	nd	0.48	nd	nd
1-acetoxy-p-menth-3-one	29.341	1434	7.44	nd	nd	nd	12.47	2.56	1.41
Anhydroserricornin	29.798	1449	16.51	0.41	0.56	0.12	24.04	8.70	8.02
2-tridecyn-1-yl hexanoate	31.306	1497	1.01	nd	nd	nd	1.15	1.43	0.20
3-(hydroxymethyl)-5-methoxyphenol	32.002	1521	nd	nd	nd	nd	0.35	nd	nd
Cinerolone	33.069	1558	0.51	nd	nd	0.21	0.22	nd	0.38
Spathulenol	33.296	1565	1.99	2.56	4.22	1.63	0.58	1.33	1.73
Caryophyllene oxide	40.067	1810	nd	0.61	nd	nd	0.52	nd	0.44

nd: not detected

Table 2. Identified chemical components in EOs of wild *M. longifolia* subsp. *typhoides* (Briq.) Harley var. *typhoides* PH. Davis samples from Yeşilyurt (Y)

Components	RT (min)	RI	Y-1		Y-2		Y-3		Y-4	Y-7	Y-10		Y-11	Y-12	Y-13	Y-14	Y-15
			L	F	L	F	L	F	F	F	L	F	F	L	L	F	L
3-octanol	13.531	965	nd	nd	0.20	nd	nd	nd	nd	0.15	nd	nd	nd	0.46	nd	nd	0.27
o-cymene	14.699	999	nd	nd	0.24	nd	nd	nd	nd	0.36	0.59	nd	nd	0.61	nd	nd	0.52
Eucalyptol	14.991	1009	nd	nd	nd	nd	nd	nd	nd	0.20	nd	nd	nd	7.13	nd	nd	0.35
Linalool oxide	17.105	1071	2.90	2.80	6.01	9.07	0.64	0.29	0.33	0.17	nd	nd	0.27	0.72	0.78	0.32	0.36
Linalool	17.127	1072	nd	nd	nd	nd	nd	nd	nd	nd	nd	nd	nd	nd	nd	nd	nd
β -linalool	19.233	1132	1.36	1.02	0.84	0.95	0.68	1.17	1.03	0.80	34.89	27.54	1.26	2.84	26.70	0.60	0.89
Menthone	20.053	1156	0.14	nd	nd	0.15	nd	nd	nd	nd	nd	nd	nd	1.21	0.87	nd	nd
α -terpineol	19.634	1144	0.79	0.63	0.54	0.48	0.87	0.64	0.60	0.36	16.85	13.28	0.54	2.22	9.23	0.26	0.48
Isomenthone	19.833	1150	nd	nd	nd	nd	nd	nd	nd	nd	4.49	nd	nd	nd	1.82	nd	nd
Menthol	20.734	1175	1.12	0.55	0.73	0.53	nd	0.58	0.64	24.23	0.49	nd	0.45	0.72	0.69	0.41	nd
Dihydrocarvone	22.212	1217	0.29	1.00	0.94	nd	nd	2.35	nd	0.31	2.11	5.63	nd	0.75	2.37	nd	nd
Pulegone	22.416	1224	0.68	0.71	0.98	0.87	nd	nd	nd	nd	nd	nd	nd	nd	nd	nd	nd
Linalyl acetate	22.797	1235	35.69	2.51	28.62	23.74	63.15	25.99	35.39	5.13	24.0	31.06	46.78	2.30	nd	41.83	63.81
Piperitone oxide	23.700	1262	14.07	8.97	0.48	0.46	1.57	1.33	0.95	nd	nd	nd	nd	57.13	35.61	nd	0.58
Thymol	24.234	1277	nd	nd	0.52	nd	nd	nd	0.72	24.23	nd	nd	nd	nd	nd	1.68	nd
Diosphenol	24.802	1293	0.70	0.72	nd	nd	nd	nd	nd	nd	nd	nd	nd	nd	nd	nd	nd
3-methylidenedecan-4-ol	26.431	1344	nd	nd	5.55	nd	nd	11.03	nd	nd	nd	nd	nd	nd	nd	nd	nd
Humulene epoxide	26.865	1357	0.27	4.01	8.58	0.75	nd	11.98	8.72	0.34	1.46	2.20	5.23	nd	nd	4.10	2.91
1-[tert-butyl(dimethyl)silyl]-4-(2,2-dimethyl-6-methylidencyclohexyl)butan-1-ol	27.125	1365	nd	nd	nd	nd	nd	nd	nd	nd	nd	nd	nd	nd	0.64	2.30	nd
β -bourbonene	27.145	1366	0.79	1.20	0.62	nd	nd	nd	nd	nd	nd	nd	nd	nd	nd	nd	0.42
7-(2-acetylcyclopropyl)-6,6-dimethylheptane-2,5-dione	27.826	1391	nd	nd	0.37	nd	nd	1.10	nd	nd	nd	nd	nd	nd	nd	nd	nd
5-(tetrahydro-2-furanyl)methyl-2-heptanol	28.272	1399	3.80	2.63	1.05	1.03	nd	nd	nd	nd	nd	nd	nd	2.66	3.36	nd	nd
\square -caryophyllene	28.973	1422	nd	nd	0.59	nd	0.86	nd	0.63	nd	nd	nd	nd	nd	nd	nd	0.99
1-acetoxy-p-menth-3-one	29.341	1434	7.74	22.09	12.59	0.38	nd	3.56	nd	3.29	nd	nd	0.76	nd	nd	25.34	3.37
Anhydrosericorinin	29.798	1449	0.94	4.22	7.94	0.37	nd	14.82	6.04	0.95	1.70	1.89	8.63	nd	nd	7.98	3.50
2-tridecyn-1-yl hexanoate	31.306	1497	nd	0.59	1.10	nd	nd	1.32	0.87	nd	nd	nd	0.69	nd	nd	0.50	0.34
3-(hydroxymethyl)-5-methoxyphenol	32.002	1521	nd	0.85	nd	nd	nd	2.70	1.34	nd	0.30	0.46	0.85	nd	nd	1.03	0.48
Cinrolone	33.069	1558	1.20	0.78	0.49	0.30	nd	nd	0.36	3.01	0.68	nd	nd	1.26	0.85	nd	0.99
Spathulenol	33.296	1565	0.85	0.53	1.46	2.04	3.22	0.76	1.39	nd	2.30	1.59	2.72	1.82	1.17	1.27	3.05
Caryophyllene oxide	40.067	1810	nd	nd	0.60	0.27	nd	nd	nd	0.63	0.57	nd	nd	nd	nd	nd	0.30

nd: not detected

3.2.1. Antioxidant activities

The antioxidant compounds affect different mechanisms such as retention of transition metal ions, inhibition of hydrogen abstraction, the breakdown of peroxides and radical clearing. One of the most important factors affecting antioxidant capacity is the ability of antioxidants to donate electrons. Because of the harmful effects of BHA and BHT on synthetic antioxidants, the antioxidant capacities of plant-derived natural polyphenols and EOs continue to be investigated and studied extensively.^{22,23} Many methods have been developed to evaluate the antioxidant activities of naturally occurring compounds, crude extracts and EOs. Among these methods, the most commonly used assays are total antioxidant activity, inhibition of lipid

peroxidation, reducing power, metal chelating, DPPH[•] and O₂^{•-} scavenging activities.²⁴ The evaluation of the antioxidant activity of the EOs of the *Mentha* species is shown in Table 5. Statistical analysis of EOs activities showed a similarity between each other ($p < 0.01$). Since leaf and flower parts of *Mentha* species have different chemical contents of EOs, the effects of applied antioxidant activities have been affected.

3.2.1.1. Total antioxidant activity by phosphomolybdenum method

The phosphomolybdenum method has been widely used to evaluate the antioxidant activity of secondary metabolites, food and medicinal bioactive molecules.²⁵

The antioxidants are able to prevent oxidation of a substrate exposed to the oxidation process and scavenge free radicals via deoxygenating processes.²⁶ The antioxidant capacities of EOs were tested for the formation of a green phosphomolybdenum (phosphate/Mo(V)) and compared with standard antioxidants and exhibited in Table 5. The experimental data indicated that EOs were likely to have the potential for reducing Mo(V) into Mo(IV) and to show statistically significant differences, ($p < 0.01$). The total antioxidant activities of EOs were lower than those of standards in terms of phosphomolybdenum reduction potential. The activities of K-4L, K-4F, K-1L, R-2L, Z-1F, Z-10F, Z-11F, R-9F and R-5F had the higher activity than among EOs due to containing a high amount of β -linalool (60.81%)-linalyl acetate (15.46%), β -linalool (50.15%)-linalyl acetate (18.13%), linalyl acetate (47.57%), linalyl acetate (20.74%), linalyl acetate

(13.93%), linalyl acetate (26.90%), linalyl acetate (49.22%), piperitone oxide, (68.92%) and piperitone oxide (47.60%), respectively (Table 1-4).

3.2.1.2. Reducing power ($\text{Fe}^{3+} \rightarrow \text{Fe}^{2+}$ reduction)

The reduction power of EOs of *Mentha* species was determined by measuring the reduction of $\text{Fe}^{3+} \rightarrow \text{Fe}^{2+}$. The reducing power of the EOs detects the complex compound in purple blue color by the addition of FeCl_3 at 700 nm.²⁷ Another different defense mechanism to protect the cell against the hazardous effects of free radicals is the reduction ability of these molecules by the natural antioxidants. The EOs of *Mentha* species demonstrated reducing ability at $100 \mu\text{g ml}^{-1}$ (Table 5). As can be seen from Table 2 and 3, linalyl acetate is the major component of the Y-1F, Y-2L, Y-3F, Z-10F, Y-12L and Y-11F EOs studied here.

Table 3. Identified chemical components in EOs of wild *M. longifolia* subsp. *typhoides* (Briq.) Harley var. *typhoides* PH. Davis leaf (L) and flower (F) samples from Zile (Z)

Components	RT (min)	RI	Z-2		Z-7		Z-4	Z-1	Z-10	Z-11
			L	F	L	F	L	F	F	F
3-octanol	13.531	965	0.43	0.42	0.48	nd	0.32	nd	nd	nd
o-cymene	14.699	999	0.31	0.40	0.38	nd	0.30	0.32	nd	0.46
Eucalyptol	14.991	1009	0.19	0.30	0.83	nd	0.28	0.27	nd	nd
Linalool oxide	17.105	1071	45.68	62.88	0.41	0.33	52.32	nd	0.39	nd
Linalool	17.127	1072	nd	nd	nd	nd	nd	nd	nd	nd
β -linalool	19.233	1132	1.27	0.55	0.50	1.34	0.64	35.25	0.74	0.52
Menthone	20.053	1156	0.61	0.37	0.11	nd	0.14	nd	nd	nd
α -terpineol	19.634	1144	30.15	14.09	nd	0.85	0.42	6.03	0.45	0.34
Isomenthone	19.833	1150	nd	nd	nd	nd	nd	nd	nd	nd
Menthol	20.734	1175	0.24	0.10	0.21	0.77	0.20	0.62	0.47	nd
Dihydrocarvone	22.212	1217	8.63	9.13	0.34	0.38	nd	4.51	2.59	1.60
Pulegone	22.416	1224	4.19	3.50	nd	nd	6.23	nd	nd	nd
Linalyl acetate	22.797	1235	2.08	1.05	69.43	nd	nd	13.93	26.90	49.22
Piperitone oxide	23.700	1262	nd	nd	1.26	nd	0.21	nd	0.66	nd
Thymol	24.234	1277	nd	nd	nd	nd	0.28	0.56	1.54	1.05
Diosphenol	24.802	1293	nd	nd	0.52	nd	nd	nd	0.50	1.32
3-methylidenedecan-4-ol	26.431	1344	nd	0.15	nd	13.21	nd	nd	10.74	13.15
Humulene epoxide	26.865	1357	0.49	nd	0.56	7.80	0.53	0.88	9.02	0.41
1-[tert-butyl(dimethyl)silyl]-4-(2,2-dimethyl-6-methylidencyclohexyl)butan-1-ol	27.125	1365	nd	0.76	nd	nd	nd	nd	nd	8.23
β -bourbonene	27.145	1366	nd	nd	nd	nd	0.43	nd	0.19	nd
7-(2-acetylcyclopropyl)-6,6-dimethylheptane-2,5-dione	27.826	1391	nd	nd	0.27	0.62	nd	nd	nd	0.83
5-(tetrahydro-2-furanyl)methyl-2-heptanol	28.272	1399	0.93	0.36	3.32	nd	2.79	nd	0.73	nd
β -caryophyllene	28.973	1422	nd	nd	0.91	nd	0.20	nd	2.63	nd
1-acetoxy-p-menth-3-one	29.341	1434	nd	nd	nd	0.90	1.59	6.64	8.47	2.53
Anhydrosericornin	29.798	1449	nd	0.05	1.09	5.49	nd	1.38	20.62	5.12
2-tridecyn-1-yl hexanoate	31.306	1497	nd	nd	nd	0.97	nd	0.50	0.93	0.85
3-(hydroxymethyl)-5-methoxyphenol	32.002	1521	nd	nd	nd	nd	nd	nd	nd	1.35
Cinerolone	33.069	1558	nd	nd	0.82	0.86	nd	nd	nd	nd
Spathulenol	33.296	1565	0.92	0.58	3.69	3.81	0.56	2.69	1.42	0.88
Caryophyllene oxide	40.067	1810	nd	nd	0.71	nd	nd	nd	0.69	nd

nd: not detected

They were exhibited better reducing power potential than α -tocopherol with high absorbance values. But the other EOs had low reduction powers compared to the standards.

The difference observed in the results is due to the component difference of EOs. The same taxons that grow in different areas often have different chemical components. Therefore, the increase in Fe^{3+} reducing activity over developmental period matched well with the increase in chemical contents.

3.2.1.3. Free radical scavenging activity on DPPH'

The EOs of *Mentha* species were effective in reducing pink DPPH' to colorless 2,2-diphenyl-1-picryl hydrazine (DPPH₂) due to the presence of antioxidants in the medium.²⁸ The DPPH', initially purple in color, takes up hydrogen from the antioxidant substance, and then the yellow colored hydrazine compound is formed. It is observed that absorbance values decrease as color (purple to yellow). The DPPH' scavenging activities of the EOs were tested at 517 nm and compared with the standards used as a reference (Table 5).

Table 4. Identified chemical components EOs of wild *M. longifolia* (L.) Hudson subsp. *longifolia*, *M. spicata* L. subsp. *spicata* and *M. villosa nervata* Opiz in leaf (L) and flower (F) samples from the center of Tokat (K), Zile (Z), Yeşilyurt (Y) and Reşadiye (R)

Components	RT (min)	RI	<i>M. villosa nervata</i>		<i>M. spicata</i>		<i>M. longifolia</i> (L.)	
			K-3L	R-9F	Y-9L	Z-5L	R-5F	R-6L
3-octanol	13.531	965	nd	nd	nd	0.92	0.34	0.44
o-cymene	14.699	999	nd	nd	nd	0.33	0.51	0.32
Eucalyptol	14.991	1009	nd	nd	nd	0.23	0.23	0.19
Linalool oxide	16.293	1048	nd	nd	nd	nd	nd	nd
Linalool	17.105	1071	nd	nd	nd	0.81	nd	nd
β -linalool	17.127	1072	0.55	0.77	nd	nd	nd	0.24
Menthone	19.233	1132	19.41	2.58	10.60	1.00	0.31	0.40
α -terpineol	20.477	1168	nd	nd	0.21	0.52	nd	0.23
Isomenthone	19.634	1144	1.67	0.67	2.65	1.63	nd	nd
Menthol	19.833	1150	0.59	nd	1.12	nd	nd	nd
Dihydrocarvone	20.734	1175	0.50	0.70	0.74	1.20	nd	0.22
Pulegone	22.212	1217	6.18	1.97	1.87	21.52	nd	nd
Linalyl acetate	22.416	1224	nd	nd	nd	nd	nd	nd
Piperitone oxide	22.797	1235	56.19	68.92	46.82	2.08	47.60	nd
Thymol	23.700	1262	nd	1.95	nd	nd	0.92	1.04
Diosphenol	24.234	1277	nd	nd	0.60	nd	nd	1.06
3-methylidenedecan-4-ol	24.802	1293	0.88	nd	1.35	nd	nd	nd
Humulene epoxide	26.431	1344	nd	8.60	8.17	nd	11.68	nd
1-[tert-butyl(dimethyl)silyl]-4-(2,2-dimethyl-6-methylidene-cyclohexyl)butan-1-ol	26.865	1357	nd	2.08	3.50	nd	9.70	3.75
β -bourbonene	27.125	1365	nd	nd	nd	nd	nd	0.31
7-(2-acetylcyclopropyl)-6,6-dimethylheptane-2,5-dione	27.145	1366	nd	nd	nd	0.64	nd	nd
5-(Tetrahydro-2-furanyl-methyl)-2-heptanol	27.984	1391	nd	0.48	0.58	nd	0.70	0.95
β -caryophyllene	28.272	1399	nd	0.42	0.31	nd	nd	nd
1-acetoxy-p-menth-3-one	28.973	1422	nd	0.62	1.19	nd	nd	nd
Anhydroserricornin	29.341	1434	2.84	4.55	7.73	nd	6.67	9.30
2-tridecyn-1-yl hexanoate	30.575	1474	nd	1.40	1.83	nd	5.24	1.71
3-(hydroxymethyl)-5-methoxyphenol	31.306	1497	nd	nd	0.25	nd	1.18	0.37
Cinrolone	32.002	1521	nd	nd	nd	nd	nd	nd
Spathulenol	33.069	1558	nd	nd	0.38	1.19	0.51	0.61
Caryophyllene oxide	33.296	1565	3.83	1.73	1.44	8.32	2.05	1.89
Dihydro- β -agarofuran	32.015	1521	nd	0.39	0.53	nd	1.88	0.40

nd; not detected

Table 5. Comparisons of total antioxidant activity (A), reducing power (B), free radical scavenging activity (C), H₂O₂ scavenging activity (D), O₂^{-•} scavenging activity (E) metal-chelating activity (F) and inhibition of lipid peroxidation (G) of EOs at 100 µg ml⁻¹

No	Sample		Result of antioxidant assay						
			A, µmol α-toc/g	B, 700 nm	C, %	D, %	E, %	F, %	G, %
<i>M. longifolia</i> subsp. <i>typhoides</i> (Briq.) Harley var. <i>typhoides</i> PH. Davis									
1	K-2	L	17867±1178 ^{bcd}	0.109±0.003 ^{h-k}	26.92±0.00 ^{cd}	55.03±9.00 ^{abc}	31.84±11.71 ^{b-g}	36.40±9.58 ^{bcd}	74.25±3.89 ^{abc}
2	K-4	L	16303±361 ^{bcd}	0.117±0.016 ^{h-k}	16.43±1.78 ^{fg}	50.00±1.57 ^{a-f}	33.16±1.94 ^{b-g}	22.65±13.77 ^{cde}	53.75±22.27 ^{b-e}
3	K-4	F	12257±505 ^{ef}	0.125±0.001 ^{d-i}	23.08±1.09 ^{ef}	51.11±6.29 ^{a-f}	36.42±2.01 ^{a-e}	11.11±2.24 ^g	77.75±6.01 ^{ab}
4	R-1	F	12308±914 ^{ef}	0.088±0.003 ^{klm}	20.00±1.09 ^{fg}	23.33±4.71 ^{ghi}	39.83±1.07 ^{a-b}	21.27±15.56 ^{def}	80.75±3.89 ^{bc}
5	R-2	L	15759±1274 ^{cd}	0.098±0.001 ^{klm}	29.62±0.54 ^{cd}	36.67±1.57 ^{c-i}	40.54±0.07 ^{a-b}	43.44±15.34 ^{bc}	81.75±6.72 ^{ab}
6	R-4	F	12257±505 ^{ef}	0.110±0.001 ^{h-k}	36.54±7.07 ^{bc}	40.00±6.29 ^{b-h}	43.38±1.40 ^a	29.47±5.70 ^{c-d}	90.75±4.60 ^a
7	R-7	L	17901±457 ^{bcd}	0.113±0.084 ^{h-k}	nd	46.67±9.43 ^{b-f}	30.65±3.88 ^{b-g}	23.70±12.57 ^{cde}	77.75±0.35 ^{ab}
8	Y-1	L	6069±710 ^{hk}	0.154±0.006 ^{bc}	21.54±0.01 ^{ef}	53.33±6.29 ^{a-e}	37.32±0.20 ^{a-e}	12.96±9.20 ^{fg}	nd
9	Y-1	F	11390±144 ^{ef}	0.174±0.007 ^a	25.01±7.07 ^{ef}	23.33±1.57 ^{ghi}	40.44±5.82 ^{a-b}	57.62±0.97 ^{ab}	5.25±3.18 ^h
10	Y-2	L	7378±192 ^{ghij}	0.199±0.004 ^a	21.54±4.35 ^{ef}	23.33±1.57 ^{ghi}	37.32±1.14 ^{a-e}	17.35±13.02 ^{def}	16.75±19.45 ^{gh}
11	Y-2	F	24038±481 ^a	0.122±0.003 ^{d-i}	66.15±1.09 ^a	34.44±7.86 ^{d-i}	28.76±0.27 ^{c-g}	13.76±7.63 ^{fg}	92.75±8.84 ^a
12	Y-4	F	11050±240 ^{ef}	0.128±0.002 ^{d-i}	46.15±0.01 ^b	3.33±1.57 ^j	31.22±1.07 ^{b-g}	20.95±3.29 ^{def}	72.50±7.07 ^{bcd}
13	Y-10	L	11934±433 ^{ef}	0.148±0.001 ^{bcd}	14.62±1.09 ^{ef}	7.78±1.57 ^j	31.41±1.87 ^{b-g}	10.95±14.44 ^{gh}	69.25±11.67 ^{abc}
14	Y-10	F	7582±192 ^{ghij}	0.135±0.006 ^{c-g}	13.85±5.44 ^{ef}	22.22±9.43 ^{ghi}	28.71±0.07 ^{c-g}	15.56±1.95 ^{d-g}	87.50±4.95 ^a
15	Y-7	F	11526±481 ^{ef}	0.130±0.003 ^{d-h}	38.46±5.44 ^{bc}	32.22±1.57 ^{e-i}	32.73±2.41 ^{b-g}	10.88±0.41 ^{fg}	44.00±0.71 ^{def}
16	Y-11	F	5542±192 ^{hk}	0.153±0.001 ^{bc}	4.23±27.74 ⁱ	25.56±4.71 ^{f-i}	31.65±4.08 ^{b-g}	29.50±5.95 ^{cd}	nd
17	Y-12	L	4960±420 ^{klm}	0.165±0.051 ^{ab}	39.23±8.70 ^{bc}	37.78±9.43 ^{c-i}	32.36±1.74 ^{b-g}	9.37±6.81 ^{gh}	nd
18	Y-13	L	5831±120 ^{kl}	0.143±0.013 ^{cde}	14.23±5.98 ^{fg}	57.78±6.29 ^{ab}	35.24±4.75 ^{a-f}	9.58±5.76 ^{gh}	nd
19	Y-14	F	3995±720 ^a	0.115±0.011 ^{h-k}	nd	54.94±1.57 ^{a-d}	36.80±4.95 ^{a-f}	12.22±3.97 ^{dg}	nd
20	Y-15	L	8432±481 ^{gh}	0.136±0.001 ^{c-f}	nd	50.00±7.86 ^{a-f}	35.43±1.40 ^{a-f}	29.74±7.78 ^{cd}	nd
21	Z-1	F	18938±577 ^b	0.151±0.006 ^{bc}	nd	40.00±9.43 ^{b-h}	35.86±4.01 ^{a-f}	29.50±13.36 ^{cd}	94.25±5.30 ^a
22	Z-2	L	8670±240 ^{gh}	0.129±0.004 ^{d-i}	nd	44.44±9.43 ^{b-g}	26.40±1.87 ^{e-g}	13.23±10.63 ^{d-g}	91.00±3.54 ^a
23	Z-2	F	8840±962 ^{gh}	0.139±0.001 ^{c-f}	nd	43.33±1.57 ^{b-g}	26.96±1.61 ^{e-g}	nd	73.25±3.89 ^{abc}
24	Z-4	L	10506±274 ^{efg}	0.138±0.010 ^{c-f}	nd	51.11±9.43 ^{a-f}	27.72±0.54 ^{d-g}	18.68±3.22 ^{efg}	97.50±2.12 ^a
25	Z-7	L	19703±2284 ^b	0.105±0.001 ^{kl}	13.46±4.90 ^{fg}	53.33±3.14 ^{a-e}	36.94±1.54 ^{a-f}	58.47±0.22 ^{bc}	82.75±1.06 ^a
26	Z-7	F	10387±601 ^{efg}	0.084±0.001 ^m	9.23±1.09 ^{gh}	37.78±6.29 ^{c-i}	35.10±3.61 ^{a-f}	5.82±7.93 ^h	77.50±16.26 ^{ab}
27	Z-10	F	18564±240 ^{bc}	0.181±0.005 ^a	12.69±0.54 ^{fg}	38.89±1.57 ^{b-h}	35.34±0.74 ^{a-f}	12.75±6.51 ^{fg}	87.00±6.36 ^{ab}
28	Z-11	F	14178±1346 ^{de}	0.142±0.011 ^{c-f}	10.00±2.18 ^{fg}	18.89±4.71 ^{hi}	38.84±3.14 ^{abc}	58.99±0.67 ^{bc}	nd
<i>M. longifolia</i> (L.) Hudson subsp. <i>longifolia</i>									
29	R-5	F	30073±890 ^a	0.078±0.005 ^m	4.23±0.54 ⁱ	nd	42.38±0.27 ^c	23.33±0.97 ^{def}	83.04±7.07 ^{abc}
30	R-6	L	15861±938 ^{cd}	0.137±0.008 ^{c-f}	nd	54.04±4.71 ^{a-d}	22.33±3.75 ^g	1.69±0.6 ^h	69.25±2.47 ^{bcd}
<i>M. spicata</i> L. subsp. <i>spicata</i>									
31	Z-5	L	17153±890 ^{bcd}	0.177±0.002 ^a	14.62±7.61 ^{fg}	51.11±3.14 ^{a-f}	44.04±1.27 ^c	14.34±2.92 ^{fg}	82.5±7.78 ^{ab}
32	Y-9	L	12546±240 ^{ef}	0.123±0.003 ^{d-i}	nd	33.33±6.29 ^{d-i}	29.66±2.34 ^{b-g}	nd	78.5±4.24 ^{cd}
<i>M. villosa</i> <i>nervata</i> Opiz									
33	K-3	L	7939±216 ^{ghi}	0.095±0.006 ^{klm}	19.23±2.18 ^{ef}	56.67±4.71 ^{a-e}	33.11±2.68 ^{b-f}	26.35±4.04 ^{cde}	59.25±5.3 ^d
34	R-9	F	16303±1370 ^{bcd}	0.112±0.006 ^{e-k}	nd	38.89±7.86 ^{b-h}	25.54±2.14 ^{efg}	26.51±37.64 ^{cde}	87.75±1.77 ^{ab}
Standards									
35	α-tocopherol		-	0.179±0.011 ^h	56.15±15.23 ^d	53.33±3.14 ^b	29.23±3.08 ^{cd}	49.21±1.20 ^{bc}	88.00±0.00 ^{abc}
36	BHA		158100±1252 ^{cd}	0.636±0.003 ^b	70.00±4.71 ^a	33.11±7.28 ^c	83.60±2.00 ^{abc}	91.92±4.90 ^a	80.00±2.83 ^{bcd}
37	BHT		89930±5049 ^{de}	0.872±0.012 ^a	44.44±15.71 ^{bc}	33.21±7.22 ^c	55.56±0.90 ^{bc}	97.31±1.63 ^a	78.75±0.35 ^{cd}
38	Trolox		81260±8174 ^{de}	0.414±0.006 ^d	72.22±1.57 ^a	41.11±1.81 ^c	80.11±2.54 ^{ab}	94.23±1.63 ^a	82.00±2.12 ^{bcd}
39	TBHQ		166600±1097 ^{cd}	0.539±0.004 ^c	32.22±1.57 ^d	40.30±0.80 ^c	56.77±2.02 ^{bc}	81.15±1.65 ^{abc}	42.25±3.89 ^g
**			<i>p</i> < 0.01	**	**	**	**	**	**

TOC: α-tocopherol, BHA: butylated hydroxyanisole, BHT: butylated hydroxytoluene, TBHQ: tert-Butylhydroquinone, nd: not detected

The EOs showed lower performance than the standards. With the exception of the Z-2L, Z-2F, R-7L, Y-14F, Z-1F, Y-15L and Z-4L, all EOs exhibited a good inhibitory performance of the DPPH[•] (Table 5). Especially, Y-2F had significantly ($p < 0.01$) better activity than α -tocopherol due to containing high rate menthone, piperitone oxide, linalool and caryophyllene oxide. The results indicated that some EOs are a free radical scavenger, and also phenolic composition capacity to scavenge the free radical may contribute to its antioxidant activity.^{2,29} Furthermore, the EOs have previously been reported to have high free radical scavenging of *Mentha* species.³⁰

3.2.1.4. H₂O₂ Scavenging activity

H₂O₂ is naturally formed and the most important source of $\cdot\text{OH}$ as a by-product of oxygen related metabolism in organisms. In the presence of Fe²⁺ and other transition elements, Fenton and Haber-Weiss reactions cause the formation of the $\cdot\text{OH}$, which is the most active and harmful.³¹ In this sense, removal of H₂O₂ is very important. Therefore, we evaluated EOs on reactive oxygen species using H₂O₂ scavenging test, $p < 0.01$. In Table 5, the EOs of K-2L, Y-13L, Y-14F, K-3L and R-6L exhibited higher H₂O₂ scavenging activity than α -tocopherol, BHT and TBHQ due to the high content of linalyl acetate, β -linalool, menthone and piperitone oxide molecules (Table 1-4).

3.2.1.5. Superoxide anion scavenging activity

The superoxide anion radical (O₂^{•-}) is formed during the process of normal metabolism in all aerobic organisms and causes the formation of H₂O₂. H₂O₂ affects cells and their components due to strong oxidizing. The O₂^{•-} can damage proteins, lipids and nucleic acids. In this assay, O₂^{•-} is produced by the reduction of NBT and by the oxidation of NADH with the PMS-NADH system.³² The conversion of yellow color to the formazan blue was determined with the reaction of NBT at 560 nm. The results showed that the EOs showed remarkable superoxide anion scavenging capacity ($p < 0.01$) and found to be comparable to the standards (Table 5). In this study, superoxide anion scavenging assay is successfully used to determine the antioxidant behavior of the EOs of the *Mentha* species, reaching the standard value of 41% (trolox). The EOs of R-4F, R-5F and Z-5L have higher superoxide anion scavenging activity than compared with α -tocopherol, BHA, BHT, trolox and TBHQ at 100 $\mu\text{g ml}^{-1}$. The high secondary content of the EOs may contribute to strong superoxide radical scavenging activities.²

3.2.1.6. Metal chelating activity

The transition metal ions are powerful oxidative catalysts that form free radicals in the living system. The free forms of iron, which display an important role in oxygen transport, ATP production and DNA synthesis in biological systems, are toxic in living cells. The reactive oxygen species (ROS) formed as a result of this toxicity can promote lipid oxidation or attack DNA molecules. The Fe²⁺ may facilitate ROS production in live systems. The removal of free-Fe²⁺ with a good chelating effect may be useful in the prevention of oxidative stress-related diseases since the Fe²⁺ is derived from effective prooxidants in food systems.³³ Hence, the Fe²⁺ chelating ability is important for antioxidant properties of natural materials. For this reason, metal chelating activities of the EOs were examined. The metal chelating activities were determined by measuring the absorbance of Fe²⁺-ferrozine complex. The absorbance of a decrease in the assay indicates that the Fe²⁺ chelate without binding to the ferrous. The EOs interfered with the formation of ferrous (Table 5). The EOs of Z-11F, Y-1F and Z-7L exhibited significantly ($p < 0.01$) higher activity than TBHQ, α -tocopherol and BHT.

3.2.1.7. Inhibition of lipid peroxidation

Lipids are biomolecules that are most sensitive to the effects of free radicals. Oxidative degradation of polyunsaturated fatty acids is known as a lipid peroxidation. Lipid peroxidation is quite harmful and proceeds as a self-sustaining chain-reaction. The formations of lipid-free radicals (L[•]) and lipid peroxide radicals (LOO[•]) on cell membranes are considered to be an important feature of cell damage caused by reactive oxygen species. ROS disrupts the structure of polyunsaturated lipids, lead to the formation of malondialdehyde (MDA) and cause toxic stresses in the cells.³⁴ The formation of MDA is used as a biomarker to read the level of lipid peroxidation in the organism and the TBA-MDA complex. The low intensity of the absorbance indicates less lipid peroxidation. For this reason, the decrease in reaction color intensity of the EOs exhibits that it is effective in lipid peroxidation (Table 5). The inhibition levels of Y-2F, Y-1F, R-4F, Z-1F and Z-10F (*M. longifolia* subsp. *typhoides*) EOs were 92, 87, 90, 94 and 87%, respectively due to containing high levels of linalyl acetate, and they may contribute to antioxidant potential. The results are consistent with previous work.³⁵ Since piperitone oxide is major compound of *M. villosa nervata* Opiz, *M. longifolia* (L.) Hudson subsp. *longifolia*, *M. spicata* L. subsp. *spicata* leaf and flower EOs, it exhibits a high inhibition of lipid peroxidation compared to the standards.

4. CONCLUSIONS

The results of the study were summarized as follows:

- i. The current study exhibited that the EOs of *Mentha* species (*M. longifolia* subsp. *typhoides* (Briq.) Harley var. *typhoides* PH. Davis; *M. villosa nervata* Opiz; *M. longifolia* (L.) Hudson subsp. *longifolia*; *M. spicata* subsp. *spicata*) contain high-value chemical composition such as linalool, menthone, isomenthone, pulegone, piperitoneoxide, 1-[tert-butyl(dimethyl)silyl]-4-(2,2-dimethyl-6-methylidencyclohexyl) butan-1-ol, anhydroserricornin and caryophylleneoxide.
- ii. Almost all the EO samples exhibited antioxidant activity (total antioxidant, reducing power, inhibition of lipid peroxidation, metal chelating, H₂O₂, DPPH[•] and O₂^{•-} scavenging assays) compared with standards.
- iii. The study of the relation between the chemical composition of the EOs and the antioxidant activities revealed the presence of different strong correlations with some major identified compounds in each case of study.
- iv. It could be concluded that EOs of *Mentha* species were effective as antioxidant activity due to the presence of several compounds in their chemical compositions. They could be used as flavoring agents and sources of antioxidants to make healthy food and healthy sensory acceptability. Further studies are required to research about the in vivo antioxidant activity of these EOs.

Acknowledgements: The authors are grateful to the Scientific Research Projects (PYO.FEN.1904.13.003; PYO.FEN.1904.13.006), Ondokuz Mayıs University for their financial support.

Conflict of interest

All authors declare that there is no a conflict of interest with any person, institute, company, etc.





REFERENCES

1. Lawrence, B. M. (Ed.); *Mint: The genus Mentha*. CRC Press, 2007.
2. Brahmi, F.; Khodir, M.; Mohamed, C.; Pierre, D. (Eds.); *Aromatic and Medicinal Plants-Back to Nature*, Intech, 2017.
3. del Rosario Cappellari, L.; Chiappero, J.; Santoro, M. V.; Giordano, W.; Banchio, E. *Sci. Horticulture-Amsterdam*. **2017**, 220, 193-198.

4. Katiyar, R. *Int. Res. J. Engin. Technol.* **2017**, 4(6), 2793-2798.
5. Ayaz, M.; Sadiq, A.; Junaid, M.; Ullah, F.; Subhan, F.; Ahmed, J. *Front. Aging Neurosci.* **2017**, 1-9.
6. Lesgards, J. F.; Baldovini, N.; Vidal, N.; Pietri, S. *Phytother. Res.* **2014**, 28(10), 1423-1446.
7. Mogosan, C.; Vostinaru, O.; Oprean, R.; Heghes, C.; Filip, L.; Balica, G.; Moldovan, R.I. *Molecules* **2017**, 22(2), 263, 1-11.
8. Cseke, L. J.; Kirakosyan, A.; Kaufman, P. B.; Warber, S.; Duke, J. A.; Brielmann, H. L. (Eds.); *Natural products from plants*. CRC press, 2016.
9. Aksit, H.; Demirtas, I.; Telci, I.; Tarimcilar, G. *J. Essent. Oil Res.* **2013**, 25(5), 430-437.
10. Geçibesler, I. H.; Demirtas, I.; Koçak, A. *J. Essent. Oil Bear. Pl.* **2015**, 18(4), 840-843.
11. Amzazi, S.; Ghoulami, S.; Bakri, Y.; Idrissi, A. I.; Fkih-Tétouani, S.; Benjouad, A. *Therapie* **2003**, 58(6), 531-534.
12. Prieto, P.; Pineda, M.; Aguilar, M. *Anal. Biochem.* **1999**, 269(2), 337-341.
13. Duh, P.D.; Tu, Y.Y.; Yen, G.C. *LWT-Food Sci. Technol.* **1999**, 32(5), 269-277.
14. Blois, M. S., *Nature* **1958**, 181, 1199-1200.
15. Zhao, G.R.; Xiang, Z.J.; Ye, T.X.; Yuan, Y.J.; Guo, Z.X. *Food Chem.* **2006**, 99(4), 767-774.
16. Nishikimi, M.; Rao, N. A.; Yagi, K. *Biochem. Bioph. Res. Co.* **1972**, 46(2), 849-854.
17. Ozen, T. *Grasas Y Aceites* **2010**, 61(1), 86-94.
18. Dinis, T. C.; Madeira, V. M.; Almeida, L. M. *Arch. Biochem. Biophys.* **1994**, 315(1), 161-169.
19. Choi, C. W.; Kim, S. C.; Hwang, S. S.; Choi, B. K.; Ahn, H. J.; Lee, M. Y.; Park, S. H.; Kim, S. K. *Plant Sci.* **2002**, 163(6), 1161-1168.
20. de Sousa Barros, A.; de Moraes, S.M.; Ferreira, P.A.T.; Vieira, Í.G.P.; Craveiro, A.A.; de Santos Fontenelle, R.O.; de Menezes, J.E.S.A.; da Silva, F.W.F.; de Sousa H.A. *Ind. Crops Prod.* **2015**, 76, 557-564.
21. Okut, N.; Yagmur, M.; Selcuk, N.; Yildirim, B. *Pak. J. Bot.* **2017**, 49(2), 525-529.

22. Saad, B.; Zaid, H.; Shanak, S.; Kadan, S. (Eds.); *Introduction to Medicinal Plant Safety and Efficacy*. Springer, 2017.
23. Ozkan, G.; Ozcan, M.M. *J. Food Meas. Charact.* **2017**, 11(2), 812-817.
24. Ozen, T.; Yenigun, S.; Altun, M.; Demirtas, I. *Comb. Chem. High T. Scr.* **2017**, 20, 558-577.
25. Martins, N.; Barros, L.; Ferreira, I. C. *Trends Food Sci. Technol.* **2016**, 48, 1-12.
26. Rene, A.; Abasq, M.-L.; Hauchard, D.; Hapiot, P., *Anal. Chem.* **2010**, 82(20), 8703-8710.
27. Gülcin, I. *Adv. Protocols in Oxidative Stress. III*. Springer, New York, 2015, pp. 233-246.
28. Li, X.J.; Wang, W.; Luo, M.; Li, C.Y.; Zu, Y.G.; Mu, P.S.; Fu, Y.J. *Food Chem.* **2012**, 133(2), 437-444.
29. Iqbal, T.; Hussain, A. I.; Chatha, S. A. S.; Naqvi, S. A. R.; Bokhari, T. H. *J. Anal. Methods Chem.* **2013**, 1-6.
30. Cherrat, L.; Espina, L.; Bakkali, M.; Pagán, R.; Laglaoui, A. *Innov. Food Sci. Emerg. Technol.* **2014**, 22, 221-229.
31. Treml, J.; Šmejkal, K. *Compr. Rev. Food Sci. F.* **2016**, 15(4), 720-738.
32. Niranjana, A.; Prakash, D. *J. Food Sci. Technol. Mys.* **2008**, 45(2), 109-116.
33. Santos, J. S.; Brizola, V. R. A.; Granato, D. *Food Chem.* **2017**, 214, 515-522.
34. Prisacaru, A. E. *Acta Sci. Pol. Technol. Aliment.* **2016**, 15(2), 121-129.
35. Mimica-Dukic, N.; B. Bozin. *Current Pharm. Design* **2008**, 14, 3141-3150.

ORCID

-  0000-0003-0133-5630 (T. Ozen)
-  0000-0002-3651-1641 (I. Telci)
-  0000-0002-4297-786X (F. Gul)
-  0000-0001-8946-647X (I. Demirtaş)



Kinetics, thermodynamics and isotherm studies of malachite green adsorption by modified orange peel

Leyla KULE, Bilal ACEMIOĞLU*, Evrim BARAN

Department of Chemistry, Faculty of Science and Arts, Kilis 7 Aralık University, 79000, Kilis, Turkey,

Received: 17 October 2017, Revised: 24 November 2017; Accepted: 25 November 2017

*Corresponding author's e-mail address: acemioglu@kilis.edu.tr (B. Acemioglu)

ABSTRACT

Kinetics, thermodynamics and isotherm studies of malachite green (MG) adsorption by orange peel (OP) modified with ethanol, calcium chloride and sodium hydroxide were performed. Adsorption kinetics was best fit the pseudo-second order model with correlation coefficients of 0.99 and 1 for the concentrations studied. Thermodynamic results indicated a spontaneous adsorption. Adsorption isotherm obeyed the Langmuir model. The Langmuir adsorption capacity was determined as 14.55 mg g⁻¹. Moreover, effects of initial dye concentration, temperature and pH on the adsorption were studied at the different contact times. The amounts of MG adsorbed onto OP increased with increasing contact time, initial dye concentration, solution temperature, and pH. Maximum dye adsorption was about 92.90% under all the experimental conditions. Percent desorption of MG from the surface of OP was lower in the alkali and HCl solutions and higher in an acetone-water mixture of 50%. FT-IR and SEM analyses were also recorded before and after the adsorption.

Keywords: Adsorption kinetics, thermodynamics, malachite green, orange peel

Modifiye portakal kabuğu tarafından malaşit yeşili adsorpsiyonunun kinetik, termodinamik ve izoterm incelemeleri

ÖZ

Etanol, kalsiyum klorür ve sodyum hidroksit ile modifiye edilen portakal kabukları (PK) tarafından malaşit yeşili (MY) adsorpsiyonunun kinetik, termodinamik ve izoterm incelemeleri gerçekleştirildi. Adsorpsiyon kinetiği incelenen konsantrasyonlar için 0.99 ve 1' lik korelasyon katsayıları ile yalnızca ikinci dereceden modele en iyi uyum gösterdi. Termodinamik sonuçlar, adsorpsiyonun kendiliğinden olma eğiliminde olduğuna işaret etti. Adsorpsiyon izotermi ise Langmuir modeline uyum gösterdi. Langmuir adsorpsiyon kapasitesi 14.55 mg g⁻¹ olarak belirlendi. Ayrıca, adsorpsiyon üzerine başlangıç boyar madde konsantrasyonu, sıcaklık ve pH'nın etkileri farklı temas sürelerinde incelendi. PK üzerine adsorplanan MY'nin miktarları, artan temas süresi, başlangıç boyar madde konsantrasyonu, çözelti sıcaklığı ve pH ile arttı. Maksimum boyar madde adsorpsiyonu tüm deneysel şartlar altında yaklaşık % 92 idi. PK yüzeyinden MY'nin yüzde desorpsiyonu alkali ve HCl çözeltilerinde daha düşük ve % 50' lik aseton-su karışımında daha yüksekti. Adsorpsiyondan önce ve sonra FT-IR ve SEM analizleri de kaydedildi.

Anahtar Kelimeler: Adsorpsiyon kinetiği, termodinamik, malaşit yeşili, portakal kabuğu,

1. INTRODUCTION

Many synthetic dyes have been used in various industries such as paper, textile, plastics, rubber, leather, cosmetics, pharmaceutical, and food industries.¹ The fact that these synthetic dyes mixture into water resources give greatly harm human's health and animals. Because, in the contact with organic body, these kinds of colored dyes cause harmful effects such as carcinogenic, mutagenic, allergic dermatitis, and skin irritation.² Therefore, it is highly important to remove these kinds of the dyes from wastewaters. For this aim, a lot of methods such as activated carbon adsorption,

coagulation, flocculation, membrane flotation, ion exchange, biosorption, etc. have been developed in treating the wastewaters which has various dyes.^{3,4} Of these, activated carbon adsorption is an effective method to remove undesired dye or metal pollutants. However, its use is expensive and not suitable for developing countries. For this reason, the use of the cheapest adsorbents such as clay^{5,6}, fly ash^{2,7}, peat^{8,9}, perlite^{4,10}, fungi¹¹⁻¹³, yeast^{14,15}, alge¹⁶ has been preferred by the researchers, recently. On the other hand, some researchers have extensively investigated the removal of dyes using as adsorbent the lignocellulose based materials such as rice husk¹⁷, banana peel and orange

peel¹⁸, apple shell¹⁹, lemon peel²⁰, jackfruit peel²¹, pumpkin seed hull²², olive pomace^{23,24}, walnut and poplar woods²⁵, recently. Of these low-cost adsorbents, orange peel (OP) is an agricultural waste and highly plenty. In orange production in the world, Brazil, America, Mexico, India, China, Spain, Indonesia come ahead, respectively.²⁶ Following these countries, the production of orange in Turkey is too much. Its amount is approximately 1 million 730 thousand tons according to the reports of year 2011.²⁶ OP is a lingo-cellulosic waste material which consists of cellulose, pectin, hemicellulose and lignin.²⁷ According to the literature investigation, the adsorption of some dyes using OP has been studied. For example, Annadurai and co-workers¹⁸ have used orange peel for the adsorption of amido black 10B, congo red, methylene blue, rhodamine B, methyl violet and methyl orange. Arami and co-workers²⁸ have utilized orange peel as an adsorbent in removing the Direct red 80 and Direct red 23 from colored textile wastewater. In another study, Kumar and Porkodi²⁹ have studied only batch adsorber design and isotherm for malachite green adsorption onto orange peel.

However, any work with regard to kinetic and thermodynamics of the adsorption of malachite green (MG) onto OP has been not reported so far. In this study, orange peel was considered to be used as an alternative and inexpensive adsorbent to the active carbon. Therefore, the kinetic and thermodynamics of the adsorption of MG onto OP was investigated by using batch adsorption technique. Moreover, the effects of contact time, initial concentration of MG, temperature, and pH on the adsorption were studied. Furthermore, desorption studies were also studied.

2. MATERIALS AND METHOTDS

2. 1. Materials

Firstly, orange was provided from orange fruit sold commercially from market. Then, peel of orange was stripped. Orange peel (OP) was washed for the removal of soil and dusts, and dried in an oven. The dried OP was crushed into powder. Then the powdered peels were sieved using a molecular sieve of 100-mesh. The component of OP is given in Table 1.

Table 1. The component of OP

Component	Percentage
Fleshy part of peel (crude fiber)	17.60
Extract without nitrogen	71.40
Protein	6.08
Oil	2.24
Ash	2.68

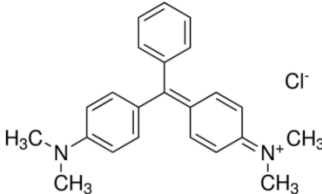
2. 1. 1. Modification of OP

OP was modified because it was determined that the adsorption capacity of OP was too low. Modification process was conducted as described in the literature.³⁰ Firstly, 10 g of OP was washed, dried and powdered. Then the powdered OP was treated with 50 ml of ethanol, 25 ml of 0.8 M NaOH solution and 25 ml of 0.8 M CaCl₂ solution for 20 h. After treatment for 20 h, the mixture obtained was filtered and washed well to pH 7. Then, it was dried to a constant weight at 60°C for 24 h.

2. 1. 2. Dye molecule as an adsorbate

Malachite green (MG), a cationic dye was provided by Merck. MG was utilized as received without any purification in adsorption process. Some physical properties and the molecular structure of MG are given in Table 2.^{24,31}

Table 2. Some physical properties of MG

Common name	Malachite green
Other name	Aniline green; Basic green 4; Diamond green B; Victoria green B
IUPAC name	4-[(4-dimethylaminofenil)fenil-metil]-N,N dimetilanolin
Chemical formula	C ₂₃ H ₂₅ ClN ₂
Class	Basic
Color index (C.I.)	42,000
Molecular weight (g mol ⁻¹)	364.91
Solubility in water (g l ⁻¹) in 298 K	40
Solubility in ethanol	Good
Colors at different pH (indicator property)	Green-blue in water Yellow < pH 2 Green between pH 2-11.8 Colorless > pH 13.8
λ _{max} (nm)	617
pKa	pKa ₁ = 6.90, pKa ₂ = 10.3
Molecular structure	

2. 2. Methods

2. 2. 1. Experiments for the adsorption of MG

Firstly, the 500 mg l⁻¹ stock solutions of MG were prepared with pure water. Then the desired concentrations were prepared by diluting from these stock solutions. The pH values of dye solutions were adjusted by dropping diluted solutions of NaOH and HCl using a pH meter. The experiments were performed by shaking 0.20 g of OP with 100 ml-aqueous solutions of MG in 250 ml-Erlenmeyers. In the experiments, a temperature-controlled shaking water bath was used. Adsorption process was performed at different concentrations, pHs and temperatures as for various contact times. After these contact times, the samples were taken from shaking bath and the centrifuged for 10 min at 4200 rpm. The supernatants were then analyzed to calculate the final concentration of MG at $\lambda_{\max} = 617$ nm by an UV-Vis spectrophotometer. The adsorbed amounts of MG onto OP were calculated using Eq. (1).

$$q_t = \frac{(C_0 - C_t)V}{m} \quad (1)$$

where, q_t represents the adsorbed amount of MG at time t (mg g⁻¹). C_0 indicates the initial MG concentration. C_t is concentrations of MG remained in solution at any time t (mg l⁻¹). V point to the dye solution volume used (l), and m indicates the adsorbent mass used (g). At the equilibrium time, q_t and C_t are expressed as q_e and C_e , respectively.

3. RESULTS AND DISCUSSION

3. 1. Determination of the equilibrium time

In order to determine the adsorption equilibrium time of MG onto OP, the experiments were conducted at various contact times, concentrations, pHs and temperatures. It was determined that a high adsorption taken place within the first 10 min. After this time, a gradual rise in the adsorption continued until 90 min. The maximum adsorption was reached at 90 min. Thus, the period of 90 min was adopted as an equilibrium time under all conditions studied.

3.2. Concentration effect on adsorption

The dye concentration effect on the adsorption of MG by OP was investigated for the concentrations between 20 and 100 mg l⁻¹. The results obtained are demonstrated in Figure 1.

From Figure 1a, it is clear that a rapid adsorption

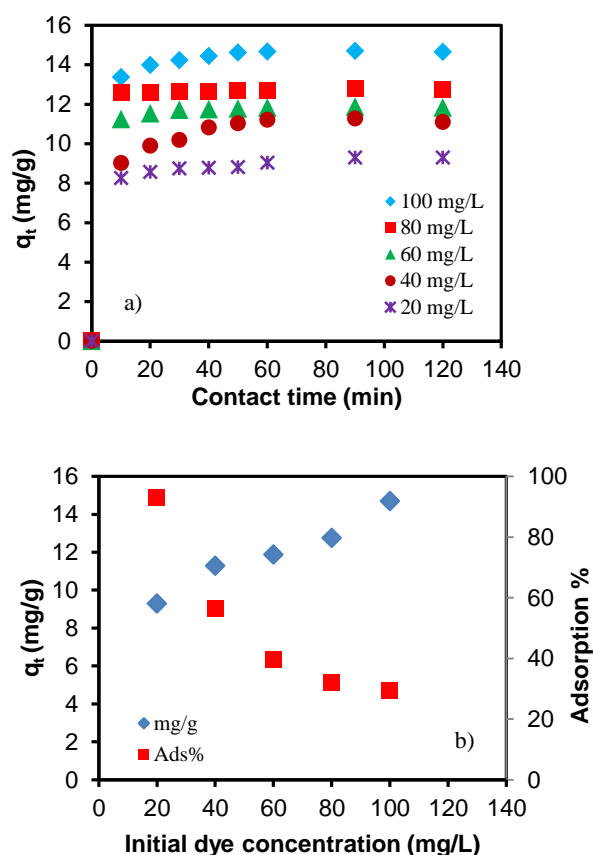


Figure 1. a) Effect of initial dye concentration on the adsorption of MG by OP as a function of contact time, b) The maximum adsorption and percent adsorption for individual concentration at the equilibrium time.

occurs within 10 min for all concentrations. After this time, a gradual increase in the adsorption continued to the equilibrium time of 90 min. The adsorption increased from 9.20 to 14.69 mg g⁻¹ when the initial dye concentration increased from 20 to 100 mg l⁻¹. Percent adsorption was higher at the lower concentrations, lower at the higher concentrations (see Figure 1b). For example, the adsorption percent decreased from 92.90% to 29.39% when initial dye concentration increased from 20 to 100 mg l⁻¹. The fact that the adsorption percent decreases with a rise in the initial concentration indicates the saturation of adsorbent's surface. A similar trend has also been reported for MG biosorption by pineapple leaf powder.³²

3. 3. pH effect on adsorption

The initial pH effect on MG adsorption by OP was investigated at pH values of 3, 5, 7 and 9. The results are demonstrated in Figure 2. It was seen that a high adsorption taken place 10 min for all the values, and

thereafter a gradual rise in the adsorption of dye continued to 90 min. The adsorption was seen to be increased with an increase in pH from 3 to 9 (see Figure 2a). This situation can be explained as follows. Excess hydroxyl ions release into medium at the higher pH values, and the adsorbent surface becomes more negative. Therefore, more electrostatic interaction occurs between positively charged MG molecules and negatively charged OP. The adsorption percent also increased from 48.83% to 89.05% with a rise in pH from 3 to 9 (Figure 2b). A similar result has been found for MG adsorption by neem sawdust.³³

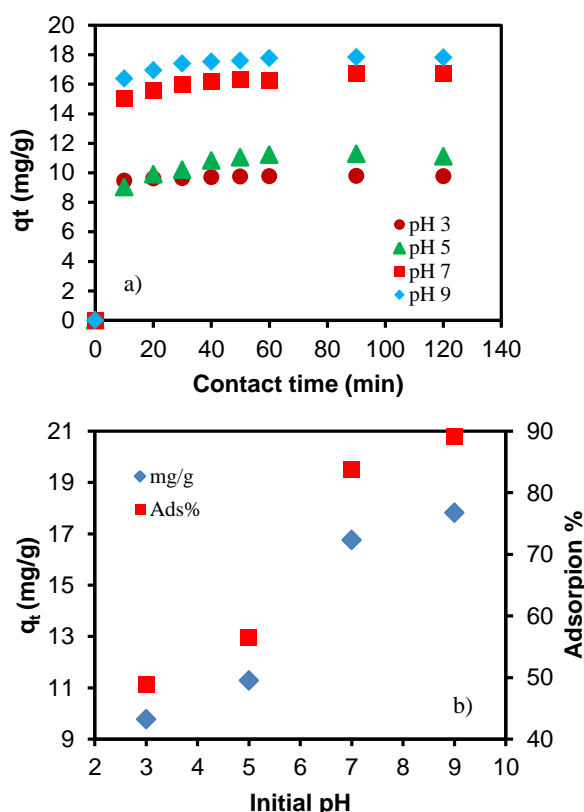


Figure 2. a) Effect of initial pH on the adsorption of MG by OP as a function of contact time, b) The maximum adsorption and percent adsorption for each pH at the equilibrium time.

3. 4. Temperature effect on adsorption

The temperature effect on MG adsorption by OP was studied at the temperatures of 293, 303, 313 and 323 K. The results are demonstrated in Figure 3. A high adsorption of MG was observed within 10 minutes for all temperatures as seen in concentration and pH effects, then small increments of adsorption continued to 90 min. The maximum adsorption of MG was determined as 11.28 and 12.50 mg g⁻¹ at 293 K and 323 K, respectively (Figure 3a). As seen in pH effect, when the dye solution temperature increased up from 293 to 323

K, the adsorption percent also increased from 56.40% to 62.50% (Figure 3b). As seen from these data, the temperature effect on the adsorption is less. A similar result has been obtained for MG adsorption onto olive pomace.²⁴

3. 5. Isotherm study

The equilibrium data obtained for MG adsorption by OP were fitted according to the Langmuir and the Freundlich isotherm models used commonly.

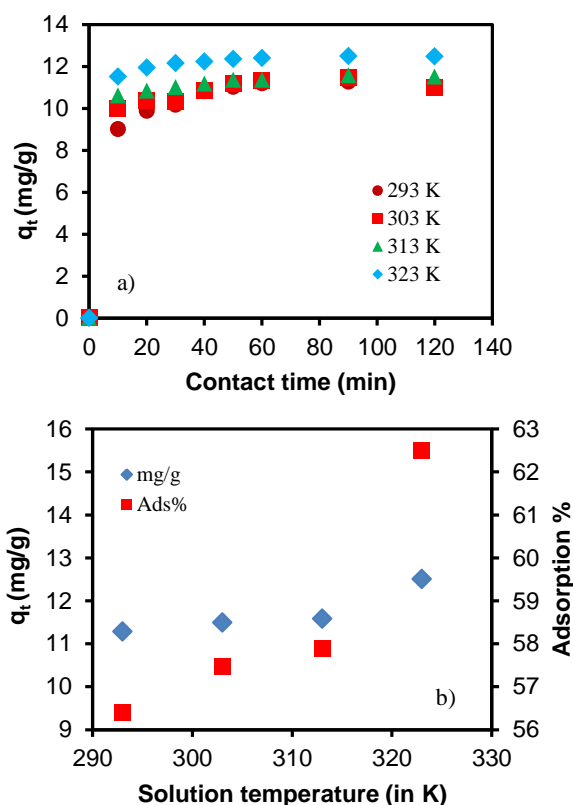


Figure 3. a) Effect of solution temperature on the adsorption of MG by OP as a function of contact time, b) The maximum adsorption and percent adsorption for each temperature at the equilibrium time.

The linearized equations of these models are given in Equations (2) and (3).

$$C_e/q_e = 1/Q_o b + C_e/Q_o \quad \text{The Langmuir equation (2)}$$

$$\ln q_e = \ln k + 1/n \ln C_e \quad \text{The Freundlich equation (3)}$$

where, q_e indicates the adsorbed MG amount at equilibrium time (mg/g), C_e points to the MG concentration remained in solution at equilibrium time

(mg l^{-1}). Q_0 is Langmuir adsorption capacity, and the b is the Langmuir constant indicating the adsorption energy. k and n are Freundlich isotherm constants, indicating the capacity and intensity of the adsorption, respectively. Isotherm studies were conducted for the initial concentrations of 20, 40, 60, 80, and 100 mg l^{-1} .

The Q_0 and b values were estimated from the slope and intercept of the plot of C_e/q_e versus C_e , respectively. Q_0 and b were estimated as 14.55 mg g^{-1} and 0.237 l mg^{-1} under concentration conditions studied, respectively. The value of the r^2 for the Langmuir isotherm was determined to be 0.98.

The k and n values were found from the intercept and slope of the plot of $\ln q_e$ against $\ln C_e$, respectively. k and n were estimated as 5.71 mg g^{-1} and 5.19 g l^{-1} , respectively. The value of r^2 for the Freundlich isotherm was obtained as 0.88. From these results, the adsorption can be said to follow best the Langmuir model. The compatibility to the Langmuir isotherm points to monolayer coverage of MG on OP surface. A similar result has been found for MG adsorption by neem sawdust.³³

3. 6. Desorption study

The experiments for desorption of MG from OP surface were conducted in 50% acetone-water mixture, 0.1 N HCl solution, and various alkali waters with various pH values. For this aim, 0.125 g dye-adsorbed OP was stirred well with each of 100 mL solutions for 120 min. After this time, samples withdrawn from the mixture were analyzed as described before. The results obtained are shown in Figure 4.

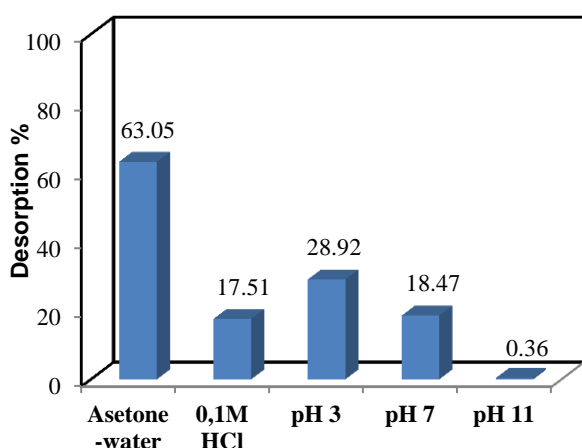


Figure 4. Desorption of MG from the surface of OP.

It was determined that percent desorption was lower in alkali and HCl solutions, and higher in 50% acetone-water mixture. For example, desorption percent was found to be 28.92, 18.47 and 0.36 in pH values of 3, 7 and 11, respectively. Percent desorption was 17.51 in 0.1

N HCl solution. Percent desorption was determined as 63.05 in 50% acetone-water mixture. The fact that desorption is low in alkali and HCl medium and higher in 50% acetone-water mixture indicates probably a chemical activation between OP and MG molecules. A similar result has been obtained for MG adsorption by olive pomace (pirina).²⁴ This situation has also been confirmed by kinetic study.

3. 7. Kinetics study

Kinetics of MG adsorption by OP was investigated according to three models used commonly. These kinetic models are given in linearized forms in Equations (4-6), respectively.

(a) The pseudo-first order kinetic model proposed by Lagergren³⁴ is given in Eq. (4)

$$\log(q_e - q_1) = \log q_1 - \frac{k_1}{2.303} t \quad (4)$$

(b) The pseudo-second order kinetic model proposed by Ho and McKay³⁵ can be expressed as in Eq. (5)

$$\frac{t}{q_t} = \frac{1}{h} + \frac{1}{q_2} t \quad (5)$$

(c) The intra-particle diffusion model proposed by Weber and Morris³⁶ is expressed in Eq. (6).

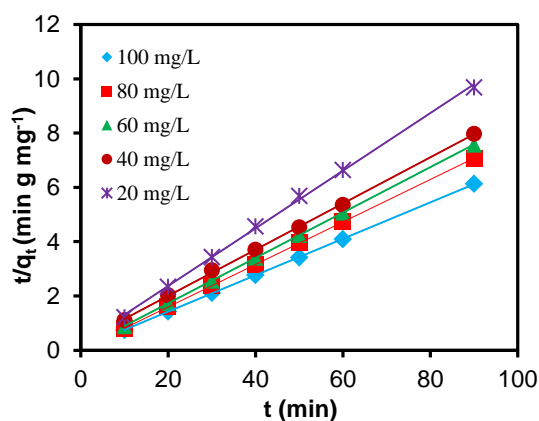
$$q_t = k_i t^{1/2} + C \quad (6)$$

where, k_1 indicates the rate constant for the pseudo-first order model, k_2 shows the rate constant for the pseudo-second order model, and k_i indicates the intra-particle diffusion rate constant. q_e indicates the adsorbed MG amounts per unit mass of OP at equilibrium. q_t is the adsorbed MG amounts as mg g^{-1} at any time. In Eq. (5), the initial adsorption rate (h) is equal to $k_2 q_2^2$. Kinetic studies were performed for the initial concentrations of 20, 40, 60, 80, and 100 mg l^{-1} . All of the kinetic data obtained are presented in Table 3.

Firstly, the plots of $\log(q_e - q_1)$ versus t for the pseudo-first order model were drawn for all the initial concentrations at 293 K and natural pH. Correlation coefficients of the plots (i.e. r^2 values) obtained by means of linear regression analysis were between 0.896 and 0.987 for all concentrations between 20 and 100 mg l^{-1} . The values of q_e from the pseudo-first order kinetics model are not in agreement with experimental q_e values ($q_{e(\text{exp})}$). This situation indicates that the adsorption does not follow this model. Therefore, these plots are not given.

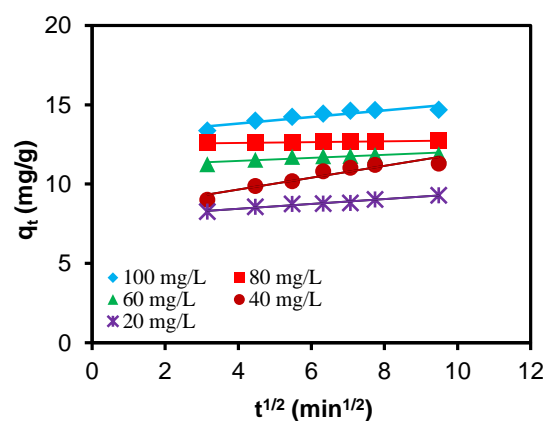
Table 3. Kinetic parameters of adsorption of MG onto OP at different concentrations

C_0 (mg l ⁻¹)	$q_{e(\text{exp})}$	Pseudo-first order model			Pseudo-second order model			Intra-particle diffusion		
		k_1 (min ⁻¹)	q_e (mg l ⁻¹)	r^2	k_2 (g mg ⁻¹ min ⁻¹)	q_e (mg l ⁻¹)	r^2	k_1 (mg/g.min ⁻²)	r^2	C
20	9.29	0.023	1.236	0.896	0.0459	9.425	0.999	0.1525	0.961	7.826
40	11.28	0.065	5.494	0.958	0.0236	11.765	0.999	0.3730	0.892	8.157
60	11.88	0.046	1.150	0.964	0.1197	11.961	1	0.0944	0.828	11.08
80	12.76	0.016	4.822	0.987	0.2550	12.771	1	0.0258	0.952	12.49
100	14.69	0.076	3.602	0.964	0.0538	14.925	1	0.2091	0.842	12.97

**Figure 5.** Pseudo-second order plots of the adsorption of MG by OP.

Secondly, the linear plots of t/q_t versus t for the pseudo-second order model were drawn for all concentrations at 293 K and natural pH. The plots obtained are shown in Figure 5. The r^2 values were between 0.994 and 1 for all concentrations studied. The r^2 from these plots have high values. The values of q_e from these model were in consistent with experimental q_e values ($q_{e(\text{exp})}$), and thus the adsorption obeys the pseudo-second order kinetics. This situation may probably indicate a chemical activation of MG molecules with the functional groups on OP surface. Similar results have been reported for the adsorption of MG by clinoptilolite³¹ and biosorption of MG by pineapple leaf powder.³²

Finally, due to mass transfer effect, the plots of q_t against $t^{1/2}$ for the intra-particle diffusion model were drawn for all the concentrations at 293 K and natural pH. The obtained plots are illustrated in Figure 6. For these plots, the r^2 values were determined as 0.842 and

**Figure 6.** Intra-particle diffusion plots of the adsorption of MG by OP.

0.961 for all concentrations studied. It may be said that the adsorption obeys the intra-particle diffusion for only a low concentration of 20 mg l⁻¹ with a high correlation coefficient of 0.961. Also, the C values increased with a rise in initial dye concentration, representing boundary layer thickness between adsorbent and adsorbate.

3. 8. Thermodynamic study

The thermodynamic parameters of MG adsorption by OP were investigated using Equations (7-9) below.²⁴

$$\Delta G^\circ = -RT \ln K_c \quad (7)$$

$$K_c = C_{Ae}/C_{As} \quad (8)$$

$$\ln K_c = -\Delta H^\circ/RT + \Delta S^\circ/R \quad (9)$$

where, C_{Ae} denote the concentrations of MG adsorbed onto OP at the equilibrium time (mg l^{-1}). C_{Se} represents MG concentration unadsorbed in solution at the equilibrium (mg l^{-1}). K_c indicates the adsorption equilibrium constant. ΔG° shows standard Gibbs free energy change. ΔH° and ΔS° indicate standard enthalpy and entropy changes, respectively. R points to the ideal gas constant. The values of ΔG° and K_c were estimated using Equations (7) and (8), respectively. Eq. (9) indicates Van't Hoff equation. The ΔH° and ΔS° values were estimated from the slope and intercept of the plot of $\ln K_c$ against $1/T$ according to Van't Hoff equation, respectively. All thermodynamic parameters determined are given in Table 4. The ΔG° values were found as negative. These negative values indicate a spontaneous nature of the adsorption. The ΔH° and ΔS° values were determined as 6.04 kJ mol^{-1} and $22.52 \text{ J mol}^{-1} \text{ K}^{-1}$, respectively. The ΔH° value indicates an endothermic adsorption process. The positive ΔS° indicates a randomness adsorption of MG molecules onto OP. A similar result has been determined for MG adsorption onto olive pomace.²⁴

Table 4. Thermodynamic parameters of the adsorption of MG onto OP

Temperature (in K)	K_c	ΔG° (kJ/mol)	ΔH° (kJ/mol)	ΔS° (J/mol K)
293	1.29	-6.27		
303	1.35	-7.56		
313	1.37	-8.26	6.04	22.52
323	1.66	-1.37		

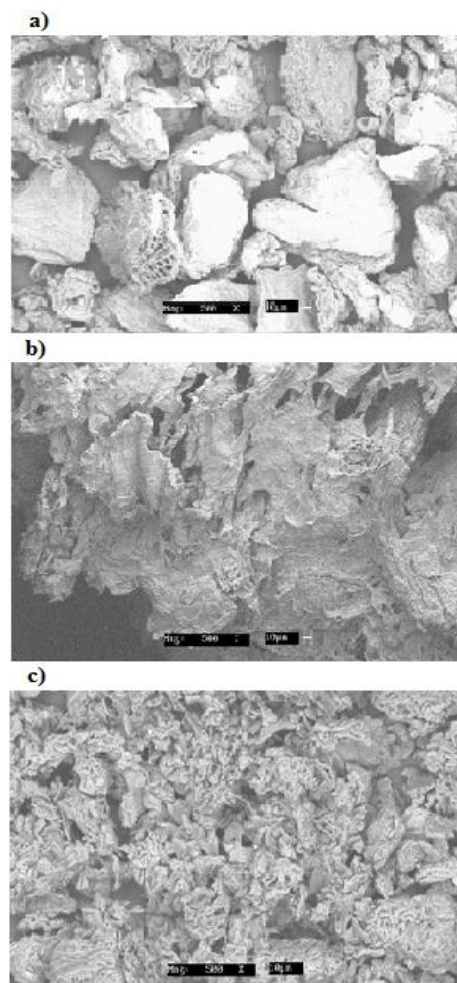


Figure 7. SEM image of orange peel: a) before adsorption, b) modified orange peel, c) after adsorption.

3. 9. SEM analysis

The SEM analyses of raw OP, modified OP and the dye-adsorbed modified OP were recorded. The images obtained are shown in Figure 7. The SEM images in Figure 7a and b show the surface structures of OP and modified OP, respectively. After modification, as can be seen from Figure 7b, the surface of OP has become some homogeneous. After adsorption, OP surface is significantly coated with MG molecules, denoting a surface adsorption (Figure 7c).

3. 10. FT-IR analysis

In order to determine the functional groups on OP surface caused to the adsorption, FT-IR analyses were conducted. Before and after the adsorption, FT-IR spectra are illustrated in Figure 8. As seen in Figure 8a, the broad and strong band at $3,304 \text{ cm}^{-1}$ indicates OH groups of cellulose and the stretching vibration of NH

and NH_2 groups. After modification, this band shifted to $3,270 \text{ cm}^{-1}$. After adsorption, this band shifted to $3,294 \text{ cm}^{-1}$. The band at $2,902 \text{ cm}^{-1}$ can be attributed to CH stretching vibration of CH, CH_2 and CH_3 groups.³⁷ After modification, this band shifted to $2,987 \text{ cm}^{-1}$. After adsorption, this band shifted to $2,918 \text{ cm}^{-1}$. The band at $1,606 \text{ cm}^{-1}$ indicates the stretching of COO^- group.²⁴ After modification the intensity of this band increased slightly. After adsorption this band shifted to $1,599 \text{ cm}^{-1}$. The peak at 1408 cm^{-1} indicates the stretching of $\text{C}=\text{C}$ groups in aromatic ring.³⁷ After modification, the intensity of this band increased slightly. After adsorption, the intensity of the band decreased markedly and shifted to $1,414 \text{ cm}^{-1}$. The band at $1,049 \text{ cm}^{-1}$ may be assigned to stretching vibration of CO groups of carboxylic and alcohols.³⁰ After modification and adsorption, this band did not change. All these findings indicate that phenolic and carboxylic groups, characteristic bonds of proteins, and polymeric compounds in the structure of OP have an important role to adsorb MG molecules.

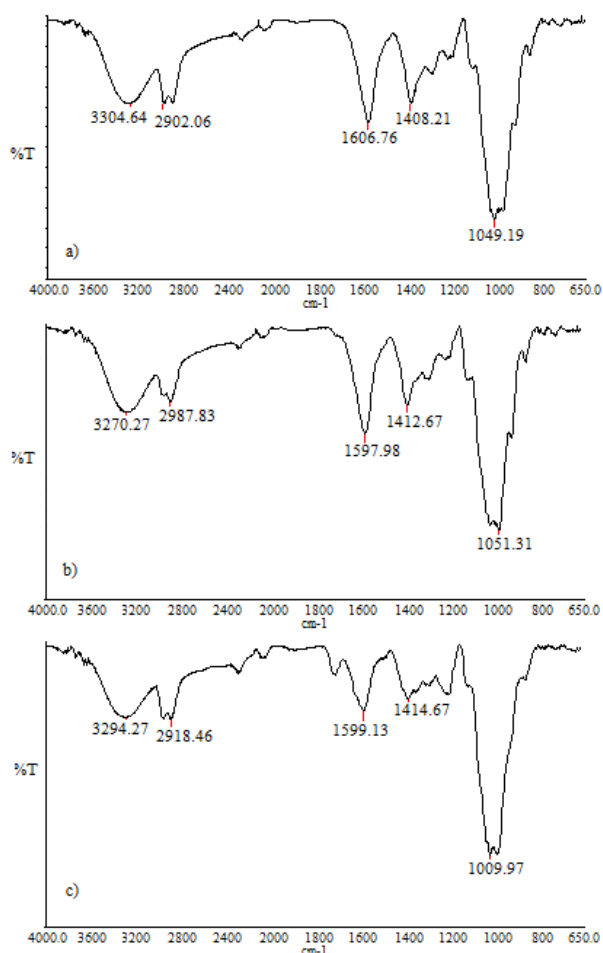


Figure 8. FT-IR spectra of orange peel: a) before adsorption, b) modified orange peel, c) after adsorption.

4. CONCLUSIONS

As an alternative to activated carbon, OP was utilized as an adsorbent for MG adsorption from solution by batch adsorption technique. The kinetics, thermodynamics, and isotherm studies of the adsorption process were performed. Adsorption kinetics was in the best consistent with the pseudo-second order model. Thermodynamic results indicated a spontaneous and endothermic adsorption. Adsorption isotherm obeyed best the Langmuir model. Moreover, the adsorption of MG onto OP was studied at various initial dye concentrations, pHs, and temperatures. The amounts of the dye adsorbed by OP increased with increasing contact time, initial dye concentration, solution temperature, and pH. The maximum dye adsorption was determined about 92.90% under all the experimental conditions studied. Desorption results showed that a chemical activation may be between OP particles and MG molecules. Consequently, it was concluded that OP would be also utilized as a potential, cheap and effective adsorbent for the removal of some other dyes as well as MG.

ACKNOWLEDGEMENTS

This study was supported financially by The Scientific and Research Projects Council of Kilis 7 Aralik University, project number: 2012/1/LT-P01.

Conflict of interest


We declare that there is no a conflict of interest with any person, institute, and company, etc.


REFERENCES


- Ergene, A.; Ada, K.; Tan, S.; Katurcioğlu, H. *Desalination* **2009**, 249, 1308-1314.
- Acemioğlu, B. *J. Colloid Interf. Sci.* **2004**, 274, 371-379.
- Nigam, P.; Armour, G.; Banat, I.M.; Singh, D.; Marchant, R. *Bioresour Technol.* **2000**, 72, 219-226.
- Dogan, M.; Alkan, M. *Chemosphere* **2003**, 50, 517-528.
- Errais, E.; Duplay, J.; Darragi, F. *Environ. Technol.* **2010**, 31 (4), 373-380.
- Vanaamudan, A.; Pathan, N.; Pamidimukkala, P. *Desalin. Water Treat.* **2014**, 52 (7-9), 1589-1599.
- Dizge, N.; Aydiner, C.; Demirbas, E.; Kobya, Kara, S. *J. Hazard. Mater.* **2008**, 150, 737-746.
- Gundogan, R.; Acemioğlu, B.; Alma, M.H. *J. Colloid Interf. Sci.* **2004**, 269, 303-309.
- Ho, Y.S.; McKay, G. *Chem. Engin. J.* 1998, 70, 115-124.
- Acemioğlu, B. *Chem. Eng. J.* **2005**, 106, 73-81.
- Bayramoğlu, G.; Çelik, G.; Arica, M.Y. *J. Hazard. Mater.* **2006**, B137, 1689-1697.
- Mukhopadhyay, M.; Noronha, S.B. Suraishkumar, G.K. *Bioresour. Technol.* **2007**, 98, 1781-1787.
- Acemioğlu, B.; Kertmen, M.; Digrak, M.; Alma, M.H.; Temiz, F. *Asian J. Chem.* **2010**, 22(2), 1394-1402.
- Bingol, A.; Uzun, H.; Bayhan, Y.K.; Karagunduz, A.; Cakici, A.; Keskiner, B. *Bioresour. Technol.* **2003**, 94, 245-249.

15. Farah, J.Y.; El-Guendy, N.; Farahat, L.A. *J. Hazard. Mater.* **2007**, *148*, 402-408.
16. Errgene, A.; Ada, K.; Tan, S.; Katircioğlu, H. *Desalination* **2009**, *249*, 1308-1314.
17. Kumar, K.V.; Sivanesen, S. *Process Biochem.* **2006**, *41*, 1198-1202.
18. Annadurai, G.; Juang, R.S.; Lee, D.J. *J. Hazard. Mater.* **2002**, *92* (3), 263-274.
19. Jain, S.; Jayaram, R.V. *Desalination* **2010**, *250*(3), 921-927.
20. Kumar, K.V. *Dyes Pigm.* **2007**, *74*, 595-597.
21. Hameed, B.H. *J. Hazard. Mater.* **2009**, *162*, 344-350.
22. Hameed, B.H.; El-Khaiary. *J. Hazard. Mater.* **2008**, *155*, 601-609.
23. Akar, T.; Tosun, I.; Kaynak, Z.; Ozkara, E.; Yeni, O. *J. Hazard. Mater.* **2009**, *166*, 1217-1225.
24. Koçer, O.; Acemioğlu, B. *Des. Water Treat.* **2016**, *57* (35), 16653-16669.
25. Heibati, B.; Rodriguez-Couto, S.; Al-Ghouti, M.A.; Asif, M.; Tyagi, I.; Agarwal, S.; Gupta, V.K. *J. Mol. Liq.* **2015**, *208*, 99-105.
26. Web-1: [http:// www.batem.gov.tr](http://www.batem.gov.tr)
27. Lugo-Lugo, V.; Barrea, C.; Urena-Nunez, F.; Bilyeu, B.; Lineras, I. *J. Environ. Manag.* **2012**, *112*, 120-127.
28. Arami, M.; Limaee, N.Y.; Mahmoodi, N.M.; Tabrizi, N.S. *J. Colloid Interf. Sci.* **2005**, *288*, 371-376.
29. Kumar, K.V.; Porkodi, K. *Dyes Pigm.* **2007**, *74*, 590-594.
30. Feng, N.; Guo, X. *Trans Nonferrous Met. Soc. China*, **2012**, *22*, 1224-1231.
31. Baran, E.; Acemioğlu, B. *Clays Clay Min.* **2016**, *64* (3), 299-313.
32. Chowdhury, S.; Chakraborty, S.; Saha, P. *Colloid Surf. B: Biointerfaces.* **2011**, *84*, 520, 527.
33. Khattri, S.D.; Singh, M.K. *J. Hazard. Mater.* **2009**, *167*, 1089-1094.
34. Lagergren, S. *Kung. Sven. Vet. Hand.* **1898**, *24* (4), 1-39.
35. Ho, Y.S.; Mackay, G. *Process Biochem.* **1998**, *34*, 451-465.
36. Weber, W.J.; Morris, J.C. *J. Sanit. Engin. Div.* **1963**, *ASCE 89* (SA2), 31-39.
37. Kamsonlian, S.; Suresh, S.; Majumder, C.B.; Chand, S. *Int. J. Sci. Technol. Manag.* **2011**, *2* (4), 1-7.

ORCID

 0000-0002-2222-9186 (L. Kule)

 0000-0002-0728-2747 (B. Acemioğlu)

 0000-0003-3551-8451 (E. Baran)



Investigation of leaching conditions of chalcopyrite by chlorine gas in aqueous medium

Hakan TEMUR¹, Ahmet YARTAŞI², Mehmet Muhtar KOCAKERİM^{2,*}

¹Department of Chemical Engineering, Engineering Faculty, Atatürk University, 25240, Erzurum, Turkey

²Department of Chemical Engineering, Engineering Faculty, Çankırı Karatekin University, 18100, Çankırı, Turkey

Received: 14 November 2017, Revised: 07 December 2017; Accepted: 11 December 2017

*Corresponding author's e-mail address: mkocakerim@yahoo.com (M. M. Kocakerim)

ABSTRACT

Generally, copper is obtained by pyrometallurgical methods from sulphide ores and SO₂, a dangerous gas is emitted to environment. Hydrometallurgical processes is preferred over pyrometallurgical processes in recent years. The present work aims to optimize leaching of chalcopyrite with chlorine gas in aqueous medium by an experimental design using Taguchi method. Thus, both Cl₂, a by-product of chlor-alkali industry, is removed using as a reagent, and emission of SO₂ from copper sulphide prometallurgy is prevented. In this study, experimental parameters and their values were 16-45°C for reaction temperature, 0.05-0.20 g ml⁻¹ for solid-to-liquid ratio, 30-120 min for reaction time, 0.027-0.4 mol l⁻¹ for [Fe³⁺] and 0.025-0.4 mol l⁻¹ for [Cu²⁺]. The optimum conditions were 45°C for reaction temperature, 0.05 g ml⁻¹ for solid-to-liquid ratio, 0.2 mol l⁻¹ for [Fe³⁺], 0.025 mol l⁻¹ for [Cu²⁺] and 120 min for reaction time. Under these conditions, 68.44% of copper in chalcopyrite dissolved.

Keywords: Chalcopyrite, optimization, Taguchi method, chlorine

Sulu Ortamda Klor Gazıyla Kalkopirit Liçinginin İncelenmesi

ÖZ

Genellikle bakır, sülfürlü cevherlerden pirometallurjik yöntemlerle elde edilmekte ve çevreye tehlikeli bir gaz olan SO₂ salınmaktadır. Son yıllarda pirometallurjik prosesler yerine hidrometallurjik prosesler tercih edilmektedir. Mevcut çalışmada, Taguchi metodunu temel alan bir deneysel tasarımla sulu ortamda klor gazı ile kalkopirit çözünmesinin optimize edilmesi amaçlanmıştır. Böylece, hem klor-alkali sanayiinin yan ürünü olarak elde edilen Cl₂ bir reaktif olarak kullanılmak suretiyle bertaraf edilmekte ve hem de bakır sülfüre uygulanan pirometallurjik işlemlerden çıkan SO₂'nin çevreye yayılması önlenmektedir. Bu çalışmada kullanılan deneysel parametrelerin aralıkları, reaksiyon sıcaklığı için 16-45°C, katı-sıvı oranı için 0,05-0,20 g.ml⁻¹, reaksiyon süresi için 30-120 dk. [Fe³⁺] için 0,027-0,4 mol l⁻¹ ve [Cu²⁺] için 0,025-0,4 mol l⁻¹ dir. Optimum şartlar, reaksiyon sıcaklığı için 45°C, katı-sıvı oranı için; 0,05 g.ml⁻¹, [Fe³⁺] için; 0,2 mol l⁻¹, [Cu²⁺] için; 0,025 mol.L⁻¹ ve reaksiyon süresi için; 120 dk. olarak bulundu. Bu şartlar altında, kalkopirit içindeki bakırın % 68,44'ü çözüldü.

Anahtar Kelimeler: Kalkopirit, optimizasyon, Taguchi metodu, klor

1. INTRODUCTION

Recently, in production of copper and its compounds hydrometallurgical processes have taken the place of classical metallurgical processes.¹ In pyrometallurgical methods, chalcopyrite and other sulphides contained in complex ore form sulphur dioxide during roasting process and thus flue gases released to atmosphere pollute the environment. Because of this, new processes which are friendly to the environment must be developed.

Chlorine gas is effect on metal sulphides and it is candidate to be an important reagent for leaching in this area.² Chlorine gas, a by-product of chlor-alkali industry

which sodium hydroxide is produced is very toxic for being human, animals and plants. To preclude this damage, new use areas must be research to dispose of chlorine.

In recent years, the kinetics of the reaction of pyrite and chalcopyrite with chlorine gas in aqueous media have been investigated. In result, kinetic parameters and speed control mechanisms have been determined.^{1,3} Groves and Smith⁴ studied the reaction of copper sulfur minerals with chlorine gas in an aqueous medium and revealed reaction products.

FeCl₃, CuCl₂ or mixtures thereof have been used as leaching reagents in the leaching of copper sulphide ores.⁵ Lu and co-workers⁶ investigated the effect of

chloride ions on the dissolution of chalcopyrite in solutions acidified with H_2SO_4 and found that excellent dissolution kinetics existed for solutions containing chloride, while for solutions without chloride, the leaching was very slow. It was believed that the role of chloride was to promote the formation of a more porous sulphur product, thus permitting the dissolution reaction to proceed at a reasonable rate.

Bonan co-workers⁷ studied chalcopyrite leaching by $CuCl_2$ in NaCl solutions. They stated that increasing in Cu^{2+}/Cu^+ ratio and chloride concentration increased copper leaching. Wilson and Fisher⁸, contrary to this result, claimed that Cu^{2+} and Cl^- concentrations did not influence the rate of chalcopyrite dissolution in chloride solutions.

Scrobian co-workers⁹ studied the effect of NaCl concentration and particle size on chalcopyrite leaching in solutions acidified with HCl and found that while NaCl concentration had a definitely positive effect on the leaching rate, the effect of particle size was almost negligible.

Lunström co-workers¹⁰ made an electrochemical study of the dissolution behavior of chalcopyrite in a concentrated sodium chloride solution (250 g l^{-1}) with cupric ion concentrations varied in the range $0.09\text{--}26.6\text{ g l}^{-1}$. They found that increase in dissolution rate was observed to be proportional to the increase in the temperature and to bigger cupric ion concentration than 9 g l^{-1} . Also, the results suggested that iron oxides, hydroxides and chlorides gathered on the chalcopyrite surface at higher pHs, chalcopyrite passivated and a sulphur-rich layer was detected on the surface.

Havlik co-workers¹¹ examined leaching of chalcopyrite with ferric chloride. Authors found that leaching rate increased with concentration of Fe^{3+} up to 0.5M and does not depend on acidity of the solution within the range of $0.25\text{--}1.0\text{ M}$ concentration of HCl.

Dutrizac¹² elucidated the formation of elemental sulphur during the $FeCl_3$ leaching of chalcopyrite and found that more than 95% of sulphur converted to S^0 and less than 5% of sulphur to SO_4^{2-} under studied conditions. Chalcopyrite has been leached with various leaching reagents such as HCl¹³, Cl^-/OCl^- media¹⁴, $FeCl_3$ ^{12,15}, acidic Cl^- solutions⁶, CCl_4 saturated with Cl_2 ¹⁶ and $H_2SO_4\text{--}NaCl\text{--}O_2$ ¹⁷, by a lot of authors, too.

Determination of conditions of recovering metallic values from the ores by hydrometallurgical methods in industrial processes is important and many researches have been realized by various authors.¹⁸⁻³⁰

In this study, the optimum conditions of chalcopyrite leaching by chlorine gas in aqueous media were investigated by using Taguchi method. Experimental parameters have been chosen as reaction temperature, solid-to-liquid ratio, reaction time, $[Fe^{3+}]$, $[Cu^{2+}]$ and $[H^+]$.

2. MATERIALS AND METHOTDS

$75\text{ }\mu\text{m}$ -chalcopyrite sample used in this study was prepared by sieving chalcopyrite concentrate ore from Çayeli-Rize, Turkey. The chemical analysis of ore gave a composition of 24.02% Cu, 29.36% Fe, 36.55% S, 2.19% Zn, 0.19% Pb, 0.1% Al_2O_3 , 0.9% moisture and 6.69% other components. X-ray diffractogram of chalcopyrite concentrate is seen in Figure 1.

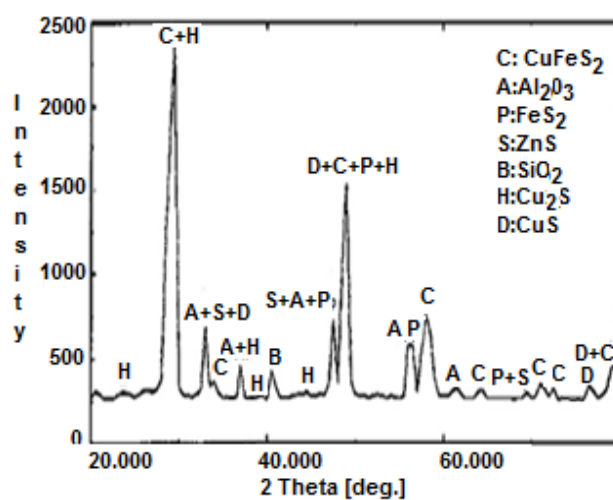


Figure 1. X-Ray diffractogram of the chalcopyrite concentrate.

As seen, the chalcopyrite concentrate contains $CuFeS_2$, FeS_2 , ZnS , Cu_2S , CuS and very small amount of Al_2O_3 and SiO_2 . Also, SEM photogram of the concentrate is shown in Figure 2.



Figure 2. SEM photogram of the chalcopyrite concentrate.

In the experiments, temperature, solid-to-liquid ratio, $[Fe^{3+}]$, $[Cu^{2+}]$ and reaction time were parameters. Levels of parameters of the experiments designated according to Taguchi method are given in Table 1.

Table 1. Parameters and their values corresponding to their levels studied in experiments

Parameters	Levels			
	1	2	3	4
A Reaction temperature (°C)	16	25	35	45
B Solid-to-liquid ratio (g ml ⁻¹)	0.05	0.1	0.15	0.2
C [Fe ³⁺] (mol l ⁻¹)	0.027	0.1	0.2	0.4
D [Cu ²⁺] (mol l ⁻¹)	0.025	0.1	0.2	0.4
E Reaction time (min)	30	60	90	120

In the first stage of dissolution experiments carried out in two stages, 7.0 g chalcopyrite was added to 200 ml of distilled water saturated with chlorine gas and the mixture was stirred at ambient temperature for two hours. In the second stage, 3.5 g chalcopyrite was added to 100 ml of the first stage filtrate, saturated with chlorine gas and the mixture was stirred under the same conditions of the first stage.

Leaching experiments were carried out in 250 mL a jacketed glass reactor equipped with a mechanical stirrer with tachometer, a constant temperature circulator and a condenser to prevent the volume reduction of the solution by the evaporation.

In the experiments, 100 ml-distilled water was saturated previously with Cl₂ at the desired experimental temperature. After the sample was added to the reactor, Cl₂ was passed through the reaction mixture during the desired experiment time while the mixture was stirring at a fixed speed. At the end of dissolution period, the amounts of Cu²⁺ passing to the solution during the reaction were determined with the volumetric method.³¹

In this study, L₁₆ (5⁴) design, with five parameters each four values given in Table 2 was chosen as the most suitable experimental design.²³ Each experiment was repeated twice under the same conditions at different times, to determine the effects of noise sources on results.

In Taguchi method, performance characteristics chosen as the optimization criteria are divided by three categories, the larger-the-better, the smaller-the-better and the nominal-the-best. The first two of them were calculated by using Equations (1) and (2).

$$\text{Larger-the-better } S_{NL} = -10 \text{Log}_{10} \left(\frac{1}{n} \sum_{i=1}^n \frac{1}{Y_i^2} \right) \quad (1)$$

$$\text{Smaller-the-better } S_{NS} = -10 \text{Log}_{10} \left(\frac{1}{n} \sum_{i=1}^n Y_i^2 \right) \quad (2)$$

where S_{NL} and S_{NS} are performance characteristics, n number of repetition done for an experimental combination, and Y_i performance value of i^{th} experiment.²³

In Taguchi method, the experiment corresponding to optimum working conditions might not be found in randomized experimental plan table. In such cases; the performance value for optimum conditions can be predicted by using the balanced characteristic of orthogonal array. For this purpose, an additive model can be used as follows.²³

$$Y_i = \mu + X_i + e_i \quad (3)$$

Where, μ is the overall mean of performance value, X_i the fixed effect of the parameter level combination used in i^{th} experiment, and e_i the random error in i^{th} experiment.

If experimental results are in percentage (%), before evaluating Eq. (3) Ω transformations of percentage values should be applied first using the Eq. (4) by which values of interest are also later determined by carrying out reverse transformation by using the same equation:²³

$$\Omega(db) = -10 \text{Log} \left(\frac{1}{P} - 1 \right) \quad (4)$$

where $\Omega(db)$ is the decibel value of percentage value subject to Ω transformation and P the percentage of the product obtained experimentally.

Because Eq. (3) is a point estimation, which is calculated by using experimental data in order to determine whether the additive model is adequate or not, the confidence limits for the predictive error must be evaluated.²¹ The predictive error is the difference between the observed Y_i and the predicted \hat{Y}_i . The confidence limits for the predictive error, S_e , is

$$S_e = \pm 2 \sqrt{\left[\frac{1}{n_0} \right] \sigma_e^2 + \left[\frac{1}{n_r} \right] \sigma_e^2} \quad (5)$$

$$\sigma_e^2 = \frac{\text{sum of squares due to error}}{\text{degrees of freedom for error}} \quad (6)$$

$$\frac{1}{n_o} = \frac{1}{n} + \left[\frac{1}{n_{A_i}} - \frac{1}{n} \right] + \left[\frac{1}{n_{B_i}} - \frac{1}{n} \right] + \left[\frac{1}{n_{C_i}} - \frac{1}{n} \right] \dots \quad (7)$$

where s_e is the two-standard-deviation confidence limit, n is the number of rows in the matrix experiment, n_r is the number of repetition in confirmation experiment

Table 2. L₁₆(4⁵) experimental plan table and results of experiments

Experiment No	Quantities and their levels					Conversion fraction of copper		
	A	B	C	D	E	Experiment (I)	Experiment (II)	Average
						Cu %	Cu %	Cu %
1	1	1	1	1	1	34.65	39.88	37.27
2	1	2	2	2	2	31.75	23.01	27.38
3	1	3	3	3	3	30.45	25.73	28.09
4	1	4	4	4	4	16.22	20.17	18.20
5	2	1	2	3	4	48.11	41.70	44.91
6	2	2	1	4	3	33.65	36.33	34.99
7	2	3	4	1	2	25.73	22.12	23.93
8	2	4	3	2	1	18.61	23.33	20.97
9	3	1	3	4	2	56.62	54.23	55.43
10	3	2	4	3	1	18.78	20.18	19.48
11	3	3	1	2	4	38.63	37.09	37.86
12	3	4	2	1	3	30.85	34.65	32.75
13	4	1	4	2	3	47.79	43.14	45.47
14	4	2	3	1	4	56.75	49.62	53.19
15	4	3	2	4	1	24.68	29.38	27.03
16	4	4	1	3	2	29.54	26.52	28.03

and $n_{A_i}, n_{B_i}, n_{C_i}, \dots$ are the replication number for parameter level A_i, B_i, C_i, \dots . If the predictive error is inside these limits, it can be accepted that the additive model is adequate. Otherwise, it cannot be accepted that the additive model to be adequate.

A verification experiment is a powerful tool for detecting the presence of interactions among the control parameters. If the predicted response matches the observed response, then it implies that the interactions are probably not important and that the additive model is a good approximation.³²

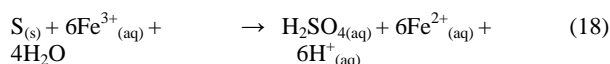
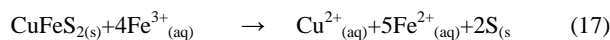
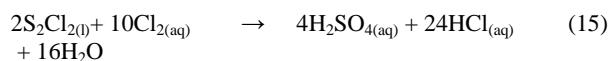
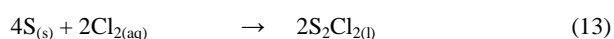
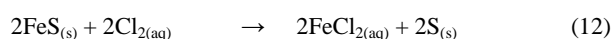
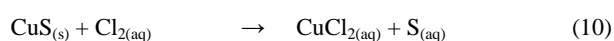
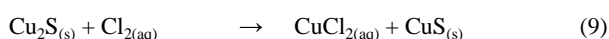
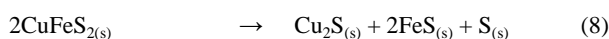
3. RESULTS AND DISCUSSION

3.1. Dissolution

Dissolution carried out at two stages: At the end of the first stage experiment, it was seen that 17.99% of Fe and 13.66% of Cu in the ore passed to the filtrate. At the end of second stage, it was determined that 65% of Fe and 60% of Cu in the ore passed to the filtrate. This means that Cu²⁺ and/or Fe³⁺ are effective parameters in this dissolution system.

3.2. Dissolution reactions

The reactions between chalcopyrite and chlorine gas in aqueous medium can be stated as follows



3.3. Statistical analysis

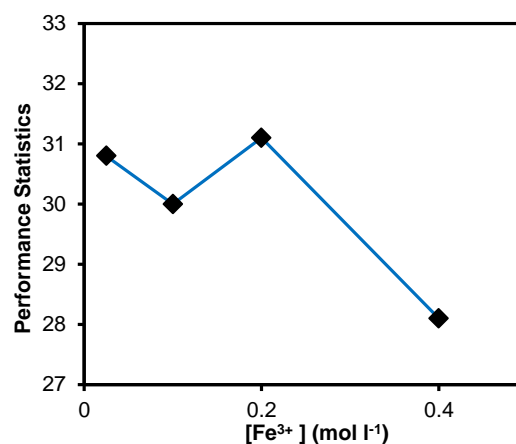
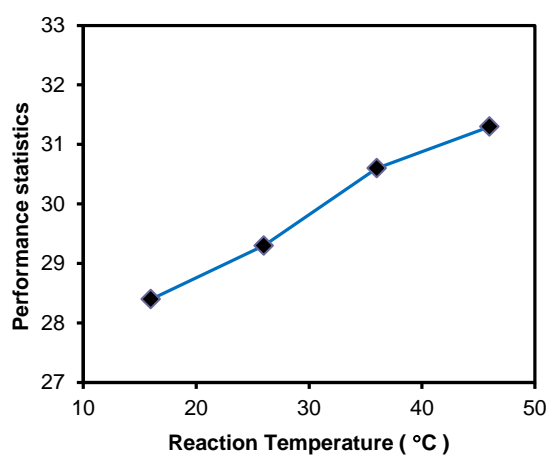
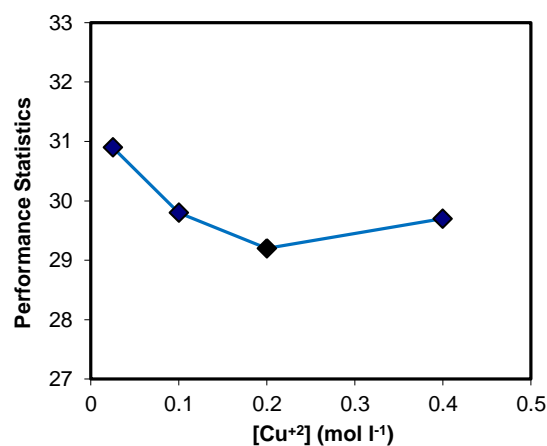
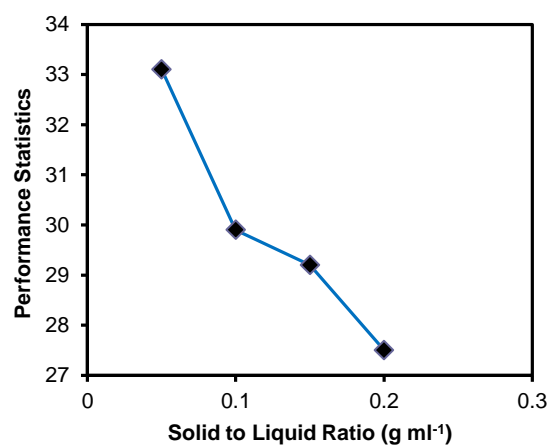
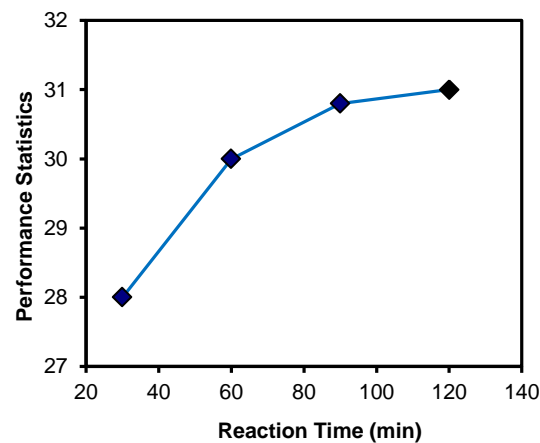
The data were evaluated according to Taguchi method.²³ Effective parameters and their levels on the leaching process were determined by analysis of variance. The results are shown in Table 3.

Likewise, the effects of the parameters on the performance characteristic are graphically shown in Figures 3-7. It had been determined that the temperature was 45°C in Figure 3, solid / liquid ratio, 0.05 g l⁻¹ in Figure 4, [Fe³⁺], 0.2 mmol l⁻¹ in Figure 5, [Cu²⁺], 0.025 mol l⁻¹ in Figure 6 and the reaction time, 120 min in Figure 7 as optimum conditions for Cu²⁺ leaching. Any experiment corresponding to the optimum conditions is not available in the experimental plan in Table 2.

Using optimum conditions and Equations (3) and (4), the predicted result and the confidence interval are calculated.

Table 3. Results of the analysis of variance for the chlorination of chalcopyrite concentrate

Parameters	Degrees of freedom	Sum of squares	Mean of squares	F
A Reaction temperature (°C)	3	568.9250	189.641	17.17
B Solid-to-liquid ratio (g.mL ⁻¹)	3	1929.829	643.276	58.26
C [Fe ³⁺] (mol l ⁻¹)	3	653.2051	217.735	19.72
D [Cu ²⁺] (mol l ⁻¹)	3	181.0988	60.3663	5.470
E Reaction time (min)	3	657.5962	219.198	19.85
Error	16	176.6779	11.0424	

**Figure 5.** The effect of [Fe³⁺] on performance statistics.**Figure 3.** The effect of reaction temperature on performance statistics.**Figure 6.** The effect of [Cu²⁺] on performance statistics.**Figure 4.** The effect of solid-to-liquid ratio on performance statistics**Figure 7.** The effect of reaction time on performance statistics.

In addition, two validation tests were performed under optimal conditions to test this predictor. The results are given in Table 4. Confirmation of test results show that the experimental plan and the results obtained are appropriate.

Table 4. Optimum working conditions and alternative working conditions for two different experimental conditions, observed and predicted dissolved quantities of Cu

Parameters	Value	Level
A Reaction temperature (°C)	45	4
B Solid-to-liquid ratio (g ml ⁻¹)	0.05	1
C [Fe ³⁺] (mol l ⁻¹)	0.2	3
D [Cu ²⁺] (mol l ⁻¹)	0.025	1
E Reaction time (min)	120	4
Observed dissolved quantity for Cu (%)	67.86	
Predicted dissolved quantity for Cu (%)	65.19	
Confidence limits of prediction for Cu (%)	60.21-70.17	

4. CONCLUSIONS

The results obtained from the realized study are:

1. The most effective parameter in leaching of chalcopyrite with chlorine gas in aqueous medium are solid-to-liquid ratio.
2. Under optimal conditions given in Table 4, 68.44% Cu can be leached.
3. The additive model is suitable to define dependence of chalcopyrite leaching on studied parameters.
4. The obtained results may be used for industrial application due to characteristics of Taguchi method.

Conflict of interest

Authors declare that there is no a conflict of interest with any person, institute, and company, etc.




REFERENCES

1. Çolak, S.; Alkan, M.; Kocakerim, M.M. *Hydrometallurgy* **1987**, 18, 183-193.
2. Mukherjee, T.K.; Gupta, C.K. *Miner. Process. Technol. Rev.* **1**, **1983**, 111-153.
3. Bayrakçeken, S.; Yaşar, Y.; Çolak, C. *Hydrometallurgy* **1990**, 25, 27-36.
4. Groves, R.D.; Smith, P.B. *Reactions of copper sulphide minerals with chlorine in an aqueous system.*

Bureau of Mines, Report of Investigation, 7801, 1973.

5. Flett, D.S. *Chloride Hydrometallurgy for Complex Sulphides: a Review, Chloride Hydrometallurgy*, International Conference on the Practice and Theory of Chloride/Metal Interaction, Montreal, Quebec, Canada, October 19-23, 2002.
6. Lu, Z.Y.; Jeffrey, M.I.; Lawson, F. *Hydrometallurgy* **2000**, 56(2), 189-202.
7. Bonan, M.; Demarthe, J.M.; Renon, H.; Baratin, F. *Metall. Trans. B*, **1981**, 12B, 269-274.
8. Wilson, J.P.; Fisher, W.W. *J. Met.* **1981** 33(2), 52-57.
9. Scrobian, M.; Havlik, T.; Ukasik, M. *Hydrometallurgy* **2005**, 77, 109-114.
10. Lundström, M.; Aromaa, J.; Forsén, O.; Hyvarinen, O.; Barker, M.H. *Hydrometallurgy* **2005**, 77, 89-95.
11. Havlik, T.; Skrobian, M.; Balaz, P.; Kammel, R. *Int. J. Miner. Process* **1995**, 43, 61-72.
12. Dutrizac, J.E. *Hydrometallurgy* **1990**, 23, 153-176.
13. Habashi, F.; Toor, T. *Metall. Trans. B.* **1979**, 10B, 49-56.
14. Puvvada, G.V.K.; Murthy, D.S.R. *Hydrometallurgy* **2000**, 58, 185-191.
15. Maurice, D.; Hawk, J.A. *Hydrometallurgy* **1999**, 51, 371-377.
16. Saraç, H.; Kocakerim, M.M.; Çolak, S. *Chim. Acta Turcica* **1994**, 22 (3), 259-370.
17. Padilla, R.; Zambrano, P.; Ruiz, M.C., *Metall. Mater. Trans. B*, **2002**, 34B, 153-159.
18. Abalı, Y.; Çolak, S.; Yapici, S. *Hydrometallurgy* **1997**, 46, 27.
19. Ata, O.N.; Çolak, S.; Çopur, M.; Çelik, C. *Ind. Eng. Chem. Res.* **2000**, 39, 488-493.
20. Ata, O. N.; Çolak, S.; Ekin, Z.; Çopur, M. *Chem. Eng. Technol.* **2001**, 24, 409.
21. Beşe, A.V.; Ata, O.N.; Çelik, C.; Çolak, S. *Chem. Eng. Process.* **2003**, 42, 291-298.
22. Çopur, M.; Pekdemir, T.; Çelik, C.; Çolak, S. *Ind. Eng. Chem. Res.* **1997**, 36, 682.
23. Çopur, M. *Chem. Biochem. Eng. Q.* **2002**, 15(4), 191-197.

24. Dönmez, B.; Çelik, Ç.; Çolak, S.; Yartaşı, A. *Ind. Eng. Chem. Res.* **1998**, 37, 3382-3387.
25. Dönmez, B.; Ekinci, Z.; Çelik, C.; Çolak, S. *Hydrometallurgy* **1999**, 52, 81-90.
26. Antonijevic, M.M.; Bogdanovic, G.D. *Hydrometallurgy* **2004**, 73, 245-256.
27. Aydoğan, S.; Uçar, G.; Cambazoğlu, G., *Hydrometallurgy* **2006**, 81, 45-51.
28. Cordoba, E.M., Munoz, J.A., Blazquez, M.L., Gonzales, F., Ballester, A., *Miner. Eng.* **2009**, 22, 229-235.
29. Li, Y., Qian, G., Li, J., Gerson, A.R., *Geochim. Cosmochim. Ac.* **2015**, 161, 188-202.
30. Moyo, T., Petersen, J., *J. S. Afri. I. Min. Metall.* **2016**, 116, 509-516.
31. Gülensoy, H. *Kompleksometrinin Esasları ve Kompleksometrik Titrasyonlar*, Fatih Yayınevi Matbaası, 259, İstanbul, Turkey, 1984 (in Turkish).
32. Phadke, M. S. *Quality Engineering using Robust Design*, Prentice Hall: New Jersey, USA, 1989; pp. 61-292.

ORCID 0000-0001-6356-7061 (H. Temur) 0000-0003-0469-4575 (A. Yartaşı) 0000-0003-3276-6097 (M. M. Kocakerim)



Electrochemical pesticide sensor based on anthraquinone substituted copper phthalocyanine

Yeliz İPEK^{1,*}, M. Kasım ŞENER², Atıf KOCA³

¹Department of Chemical Engineering, Faculty of Engineering, Munzur University, Merkez, 62000, Tunceli, Turkey

²Department of Chemistry, Faculty of Arts and Sciences, Yıldız Technical University, Esenler, 34220, Istanbul, Turkey

³Department of Chemical Engineering, Faculty of Engineering, Marmara University, Göztepe, 34722, Istanbul, Turkey

Received: 19 October 2017, Revised: 26 December 2017; Accepted: 26 December 2017

*Corresponding author's e-mail address: yelizipek@munzur.edu.tr (Y. İpek)

ABSTRACT

In this study, a biomimetic selective pesticide electrochemical sensor based on copper phthalocyanine-anthraquinone hybrid (CuPc-AQ) was studied. Electrochemical activities based on Pc ring and anthraquinone substituent of the CuPc-AQ make it valuable material for electrochemical sensor studies in detecting of pesticides. Thin film of CuPc-AQ on ITO electrode (ITO/CuPc-AQ) was exposed to water samples containing eserine and carbofuran pesticides, separately. Then in order to observe the sensor behavior of the modified electrode, square wave voltammetry (SWV), electrochemical impedance spectroscopy (EIS), and double potential step chronocoulometry (DPSCC) techniques were used. When the ITO/CuPc-AQ electrode was doped with nano-platinum (nPt) or nano-gold (nAu) particles, the sensitivity of ITO/CuPc-AQ electrode increased. The lowest detection limit (DL) (1.23×10^{-9} mol dm⁻³) was obtained with ITO/CuPc-AQ-nAu electrode using electrochemical impedance spectroscopy technique.

Keywords: Electrochemistry, Phthalocyanine, Pesticide sensor Langmuir-Blodgett

Antrakininon Substite Bakır Ftalosiyanınin Temelli Elektrokimyasal Pestisit Sensörü

ÖZ

Bu çalışmada antrakininon hibrit bakır ftalosiyanınin (CuPc-AQ) temelli, seçici bir elektrokimyasal pestisit sensörü üzerinde çalışılmıştır. CuPc-AQ'un, ftalosiyanınin halkası ve antrakininon substituenti kaynaklı elektrokimyasal aktiviteleri, bu malzemeyi pestisitlerin saptanmasında kullanılacak olan elektrokimyasal sensor çalışmaları için değerli kılmaktadır. ITO elektrot üzerinde bulunan CuPc-AQ ince filmi (ITO/CuPc-AQ) eserin ve carbofuran pestisitleri içeren su numunelerine ayrı ayrı maruz bırakılmış ve daha sonra kare dalga voltametri (SWV), elektrokimyasal empedans spektroskopisi (EIS) ve çift potansiyel basamaklı kronokulometri (DPSCC) teknikleri kullanılarak modifiye elektrodun sensor davranışları incelenmiştir. ITO/CuPc-AQ elektrodu, nano-Platin (nPt) ya da nano-Altın (nAu) parçacıkları ile yüklendiğinde ITO/CuPc-AQ elektrodunun hassasiyeti artmıştır. En düşük saptama limiti değeri (DL) (1.23×10^{-9} mol dm⁻³) ITO/CuPc-AQ-nAu elektrodu ile elektrokimyasal empedans spektroskopisi tekniği kullanıldığında elde edilmiştir.

Anahtar Kelimeler: Elektrokimya, Ftalosiyanınin, Pestisit sensörü, Langmuir-Blodgett,

1. INTRODUCTION

Farmers use numerous types of pesticides (herbicides, fungicides, insecticides), to protect crops and seeds and to increase the harvesting yield. However, the pesticide residues may enter into the ecosystem and food chain by means of air, water and soil.¹⁻⁴ Their increasing use in agriculture makes them the most important environmental pollutants since they are carcinogenic and cytotoxic for animals and human. Their toxicity is based on the inhibition effect on acetylcholinesterase (AChE) enzyme which has an important mission in neurologic system of animals and human.²⁻⁴ Acetylcholine (ACh) is

one of the numerous neurotransmitters in the nervous system and it has important roles in both peripheral nervous system and central nervous system. ACh carries the synaptic pulses between two neurons and when binds to the target synapse AChE which exists in the synaptic space, hydrolyzes ACh into acetate and choline rapidly. Thus, as an AChE inhibitor, pesticides cause accumulation of ACh at cholinergic synapses. As a result of this accumulation, bone marrow disorders, nerve disorders such as Alzheimer, infertility, and immunological and respiratory diseases may occur.⁵⁻⁶ Detection of pesticides at the levels established by the (EPA) remains a challenge.⁷ For this purpose.⁸ there are

some traditional detection methods such as gas chromatography (GC), high performance liquid chromatography (HPLC) combined with mass spectrometry (MS).⁹⁻¹⁰ Although these detection methods are time-consuming and require expensive equipment and highly trained technicians, they have been used traditionally because of their sensitivity and reliability. The developing science and technology is leading new alternative detection methods for pesticides like electrochemical sensors or biosensors.¹¹⁻¹⁴ For designing pesticide biosensors, AChE enzyme has been used frequently because of the inhibitory effect of pesticides on this enzyme. However, low stability of the biological species, difficulties of immobilization on the substrates, leakage from the substrate surface, high cost, and low chemical and thermal stabilities are some disadvantages of enzyme biosensors.¹⁵

Metallophthalocyanines (MPcs) have been studied extensively as electrochemical catalysts and sensor recognition materials because of their properties such as excellent redox behavior, thermal and chemical stability, ability of easy modification with different metal ions and substituents, and ability of easy coating on different substrate with various techniques.¹⁶⁻¹⁹ MPcs which are artificially derivate of natural protein, porphyrin, have been deeply used as mimetic enzyme receptors for the sensing of many harmful biological target species, such as insecticides and pesticides. Recently, there is a tendency towards finding new materials which can be used as recognition element of sensor instead of enzymes.²⁰⁻²³ Harbeck and co-workers have modified chemically the core of phthalocyanine to increase sensor sensitivity for organophosphorus and organonitrogen pesticides such as fenthion and methiocarb and they have obtained a detection limit down to 0.03 mg dm⁻³.²⁴ Pu-Hong Wang and co-workers have designed and synthesized a new phthalocyanine 2,9,16,23-tetrakis [4-(hexafluoroisopropanol)-anilinomethyl] phthalocyaninato zinc for electrochemical sarin gas sensor and obtained the detection limit as as 205.8 Hz/mg/m³.²⁵ İpek and co-workers have used a terminal-alkyl substituted cobalt phthalocyanine and constructed a biomimetic electrochemical biosensor with a new electrode modification technique, "click electrochemistry" (CEC) based on a functional cobalt phthalocyanine and they detected eserine pesticide with a sensitivity of 1.15 A dm³ mol⁻³ and DL of 1.75 × 10⁻⁷ mol dm⁻³.²⁶

The AChE enzyme is not selective for different type of pesticides, because all kind of pesticides have the same inhibitory effect on the enzyme. When there is a mixture of pesticides the enzymatic sensor detects them as the same kind. New artificial biomimetic sensors are especially advantageous for selective pesticide detection with high sensitivity. For this purpose, we prepared an electrochemical pesticide sensor based on a copper phthalocyanine–anthraquinone hybrid complex (CuPc-AQ).²⁷ Copper phthalocyanine–anthraquinone hybrid complex has two different redox active sides consisting

of phthalocyanine ring and anthraquinone substituents for catalytic and/or sensor applications. Phthalocyanine ring can give two reduction (at -1.22 V and -1.46 V) reactions and two oxidation reactions (at 1.40 V and 0.82 V), while four anthraquinone substituents of CuPc-AQ generally give one reduction reaction (at -0.91 V).²⁷ These redox activities of CuPc-AQ probably provide the electrochemical applications of the complex as especially cathode active electrocatalyst and/or electrochemical sensor.

In this study, Langmuir-Blodgett monolayer coating technique was used to prepare the modified electrode with CuPc-AQ (ITO/ CuPc-AQ). The Langmuir-Blodgett film of CuPc-AQ was constructed on ITO electrode and these sensors were tested for the detection of carbofuran and eserine pesticides.

2. MATERIALS AND METHOTDS

2.1. Materials

Dichloromethane (DCM), chloroform (CHCl₃), LiClO₄, CdCl₂.H₂O, stearic acid (SA), KCl, H₂PtCl₆, sodium dodecyl sulfate (SDS), eserine, carbofuran, and tetrabutylammonium perchlorate (TBAP) were purchased from Sigma Aldrich. Ultra-pure water having a resistance of 18.2 MΩ was used to prepare analyte solution. The stearic acid solution was used as a supporting agent for the modification of the electrodes via Langmuir-Blodgett coating technique. KCl and H₂PtCl₆ materials were dissolved in ultra-pure water for Pt coating solution and sodium dodecyl sulfate (SDS) was added to this solution for nano Pt coating of ITO electrode. On the other hand, a gold solution (Sigma, 1000941718) was used for nano gold coating process. Herein, CuPc-AQ (Figure 1) which is the recognition material used as the functional material of the biosensor was synthesized and spectroscopic studies were performed by our research group.²⁷ Eserine (Sigma, E8375) and carbofuran (Aldrich, 426008) pesticides were the analytes of modified biosensor.

2.2. Electrochemical measurements

Gamry Reference 600 potentiostat/galvanostat with a three-electrode cell was used for electrode modification and sensor measurements. All the experimental studies were applied at room temperature. The working electrode was ITO electrode or modified ITO electrode (ITO/CuPc-AQ). A Pt wire electrode was used as the counter electrode, and a saturated calomel electrode (SCE) was the reference electrode. A double bridge was employed to separate the reference electrode from the solution. TBAP solution was used as the supporting electrolyte. The solution was prepared with a concentration of 0.10 mol dm⁻³ in dichloromethane (DCM) solvent. During the electrochemical studies, the absorbed O₂ from the air effects the measurements. Thus,

the dissolved O₂ in the electrolytic solution was purged with high purity N₂ gas (%99.99) to obtain a nitrogen blanket and prevent O₂ absorption. Electrochemical impedance spectroscopy (EIS) measurements were performed under 10 mV AC voltage versus open circuit potential (open circuit voltage is 0.50 V) in the AC frequency range 300 kHz - 10 Hz with a 10 mV excitation AC voltage.

2.3. Electrode preparation

2.3.1. LB Coating of CuPc-AQ

Langmuir-Blodgett technique was applied for coating CuPc-AQ on ITO electrode using KSV NIMA Langmuir-Blodgett monolayer coating device. A subphase solution filled in the trough was obtained with aqueous CdCl₂.H₂O solution at a concentration of 1 mg ml⁻¹. The coating material CuPc-AQ solution was prepared at concentration of 1 mg ml⁻¹ with chloroform solvent and mixed with SA solution at concentration of 1 mg ml⁻¹ with a volumetric ratio of 1:1. The coating mixture was dropped on the subphase solution gradually until the surface pressure reached to 0.5mN/m. To detect the ideal surface pressure for monolayer film formation on the subphase, the surface pressure (SP)-Mean molecular area (Mma) isotherm was obtained, and the ideal surface pressure was detected as 35mN/m. 20 layers of CuPc-AQ:SA were coated on ITO electrodes with 5 mm s⁻¹ up and down stroke rates and the electrode was waited for 5 minutes at up position to dry the coated thin film.

2.3.2. Modification of ITO/CuPc-AQ

ITO/CuPc-AQ electrodes were modified with nano platinum and nano gold to increase the sensitivity. ITO/CuPc-AQ-nPt modified electrode was prepared with coating n-Pt on ITO/CuPc-AQ. A solution of 0.1 mol dm⁻³ KCl and 1 mmol dm⁻³ H₂PtCl₆ in 10 ml ultra-pure water which supported with 0.8 mg (1% of total weight of solution) sodium dodecyl sulfate (SDS) surfactant to prevent agglomeration of nano-Pt particles was prepared. SDS was added into this electrolyte before the addition of 1 mmol dm⁻³ H₂PtCl₆. 5 cycles of CV were applied between the potentials of 0.30 V and -0.70 V at 0.100 Vs⁻¹ scan rate for the deposition of nano-Pt on the ITO/CuPc-AQ electrode.

ITO/CuPc-AQ-nAu electrode was prepared by dropping 10 µl of nano-gold solution (Sigma, 1000941718) on the 0.64 cm² area of ITO/CuPc-AQ electrode and drying in a vacuum oven at room temperature.

2.4. Sensor measurements

Pesticide sensor measurements of ITO/CuPc-AQ, ITO/CuPc-AQ-nPt, and ITO/CuPc-AQ-nAu electrodes as electrochemical pesticide sensors were performed with cyclic voltammetry (CV), square wave voltammetry (SWV), electrochemical impedance spectroscopy (EIS) and double potential step chrono coulometry (DPSCC) analyses with two different pesticides. The three-electrode cell and the electrolyte solution of 0.1 mol dm⁻³ lithium perchlorate (LiClO₄) dissolved in 0.1 mol dm⁻³ PBS were used for sensor measurements. Before sensing measurements, the stable blank measurements were obtained. Then the pesticide solution was added drop by drop, and the electrochemical measurements of CV, SWV, DPSCC, and EIS techniques were performed sequentially. The detection linear range and detection limit parameters of the electrodes were calculated.

3. RESULTS AND DISCUSSION

CuPc-AQ complex shown in Figure 1 was synthesized by our research group.

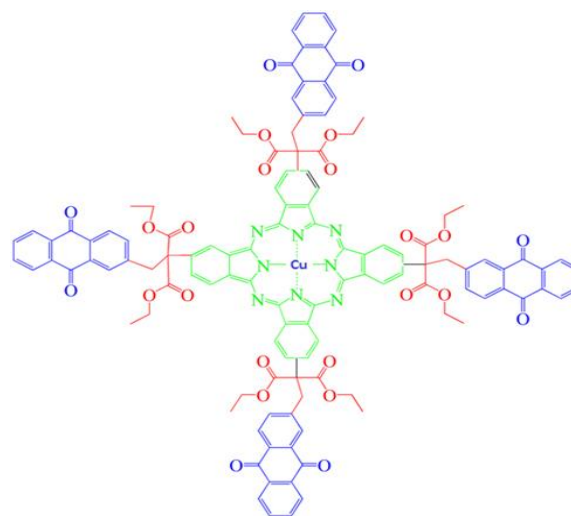


Figure 1. Molecular structure of CuPc-AQ phthalocyanine.

To see the usability in the electrochemical applications, its electrochemical characterizations were investigated.²⁷ The electro-chemical responses of CuPc-AQ in DCM solution are shown in Figure 2. When an electrical potential at cathodic region was applied to the system, three reduction reactions were recorded at -1.22 V and -1.46 V which is belong to phthalocyanine ring and at -0.91 V originated from AQ substituent of the CuPc-AQ. At anodic region two Pc ring reaction peaks were observed. CuPc-AQ has five reversible and diffusion controlled redox reactions.

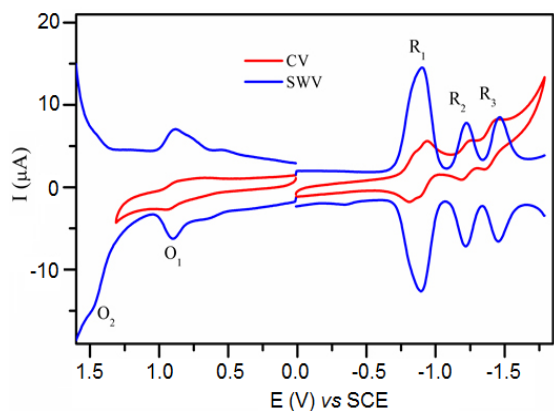


Figure 2. SWV and CV measurements of CuPc-AQ.

3.1. Langmuir-Blodgett film of CuPc-AQ

CuPc-AQ complex which was synthesized and electrochemically characterized by our research group was immobilized on ITO electrode with Langmuir Blodgett (LB) technique (ITO/CuPc-AQ) to determine possible practical usage of it. On the other hand, the ITO/CuPc-AQ electrode was modified with nano-platinum (ITO/CuPc-AQ-nPt) and nano gold (ITO/CuPc-AQ-nAu) as shown in Figure 3.

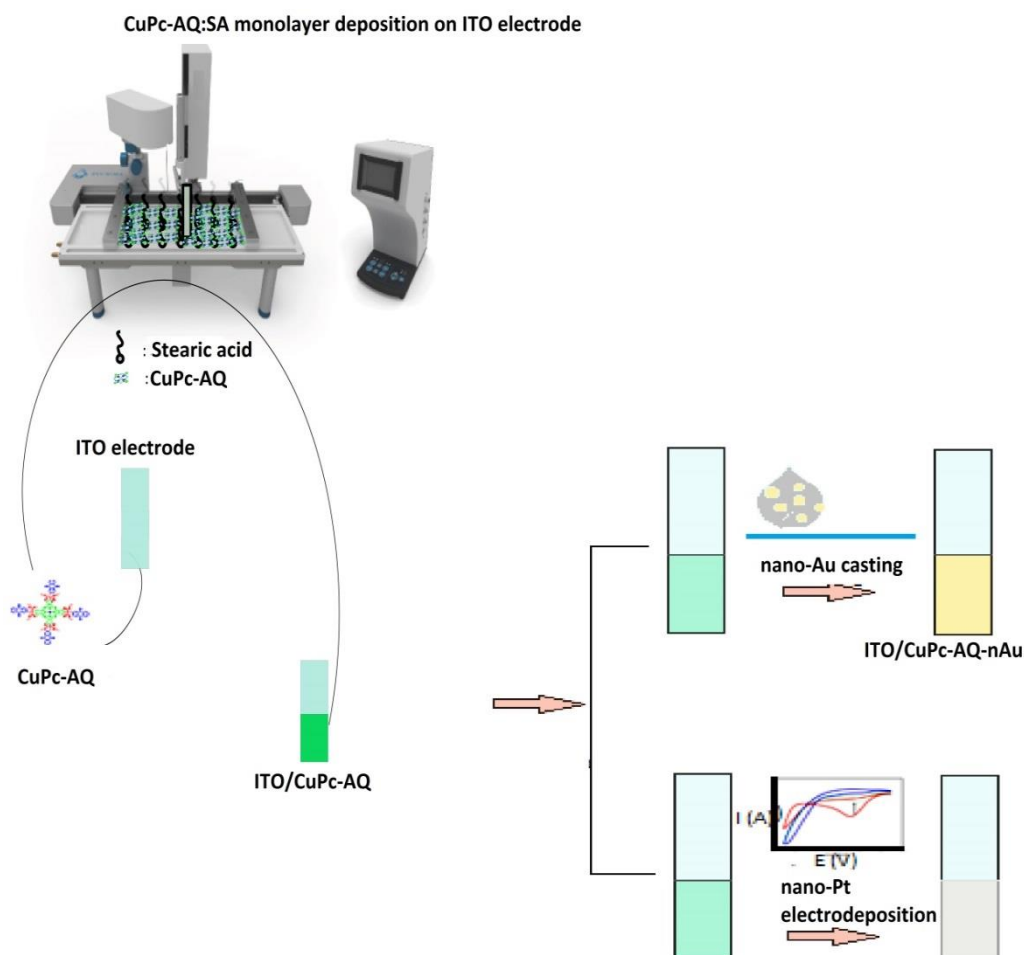


Figure 3. Preparation and modification techniques of ITO/CuPc-AQ pesticide biosensor.

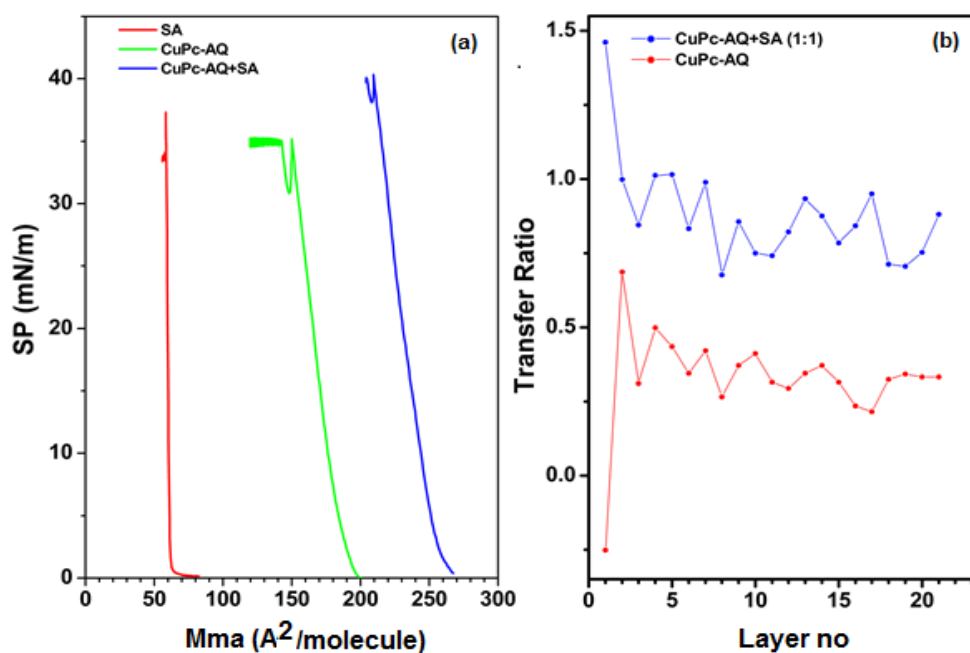


Figure 4. Langmuir-Blodgett coating results of CuPc-AQ-SA on ITO substrate: a) LB isotherms of SA, CuPc-AQ and CuPc-AQ-SA coating materials, b) LB transfer ratios of CuPc-AQ and CuPc-AQ-SA.

Figure 4 shows the Surface Pressure-Mean molecular area isotherm of CuPc-AQ and CuPc-AQ:SA mixture and transfer ratios. In Figure 4a, it seems that CuPc-AQ monolayer formed on the subphase of the LB trough, but it could not be coated on the ITO electrodes with a transfer ratio of 1.0. In Figure 4b, the transfer ratios of CuPc-AQ monolayer were about 0.4. To enhance the coating and obtain monolayers with 1.0 transfer ratio, stearic acid solution was used. A solution formed with a mixture of stearic acid solution and CuPc-AQ solution (1:1 by vol.) is employed to obtain 20 monolayers with a transfer ratio of 1.0 ± 0.1 . 21 μl of mixed solution was sufficient for a Y type 20 monolayers coating.

When the numbers of coated monolayers were more than 20 layers, the electrochemical measurements were not very successful because of the thick film which obstructs ion exchange during the measurements. The molecular area of CuPc-AQ was calculated from the slope of the isotherm curve as 184 \AA^2 which was in agreement with those of similar phthalocyanine in the literature.²⁸⁻²⁹ The exact molecular area of the complex indicates that it is orientated horizontally face-on on the subphase. Presence of SA in CuPc-AQ just increases the limiting area to 255 \AA^2 , that does not affect the electrochemical measurements.

3.2. Sensor measurements

The electrochemical reactions of ITO/CuPc-AQ, ITO/CuPc-AQ-nPt and ITO/CuPc-AQ-nAu the

electrodes were studied with carbofuran and eserine pesticides. For this purpose, SWV, EIS and DPSCC techniques were applied. ITO/CuPc-AQ electrode behaved as a selective sensor for these pesticides. The SWV responses of ITO/CuPc-AQ are shown in Figure 5 for the titration of eserine and carbofuran. The electrochemical responses of the CuPc-AQ LB thin film were different than the responses of the material in the dichloromethane solution. The potentials over 1.2 V burns the ITO electrode. Thus, for sensor measurements the applied potentials were kept between -1.0V and 1.0V. In this potential range, a broad cathodic peak was observed about -0.40V which was attributed to an overlapped peak of Pc ring reduction and AQ substituent reduction peaks.

The red colored curves that show the SWV responses of ITO/CuPc-AQ electrode without pesticide addition give a reduction couple, R_1 at about -0.40 V. Figure 5a illustrates the SWV responses of ITO/CuPc-AQ during gradual addition of carbofuran. Because of the titration with carbofuran pesticide, the current intensity of R_1^c (represents potential scan direction from -1.2 V to 1.2 V, cathodic scan) process at -0.40 V decreased and a new peak was formed at -0.08 V while the R_1^a (represents potential scan direction from 1.2 V to -1.2V, anodic scan) at -0.39 V potential gradually decreased in current intensity. Carbofuran pesticide has benzofuran active groups which may interact with Cu central metal. Thus this interaction may be resulted with a new peak about -0.08 V. According to these changes in SWV responses during the titration process of carbofuran, this electrode has a sensor activity for carbofuran.

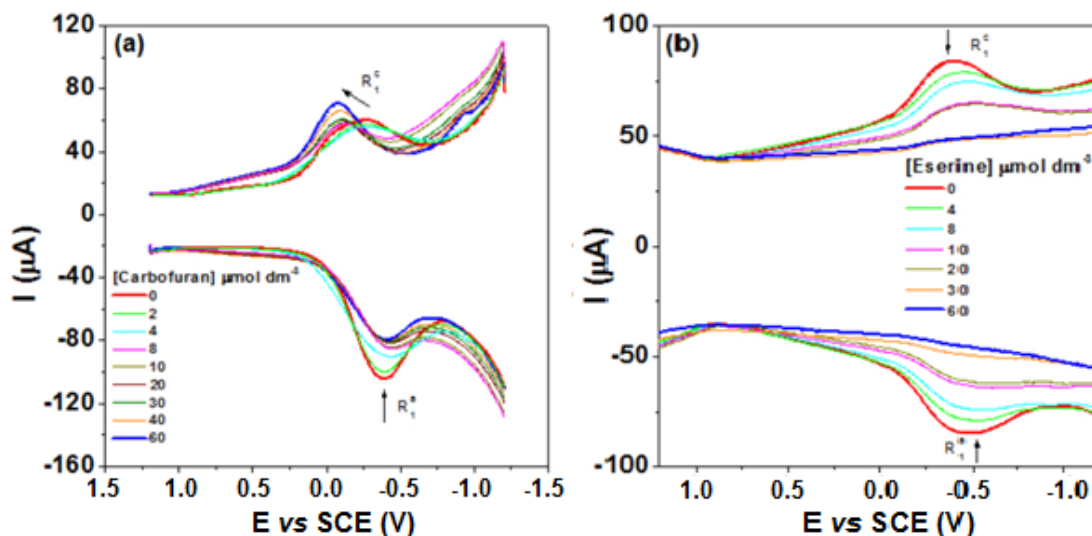


Figure 5. SWV responses of ITO/CuPc-AQ electrodes in PBS (pH= 7.0): a) During carbofuran titration, b) During eserine titration.

In Figure 5b, voltammetric responses of CuPc-AQ recorded during gradual addition of eserine are considerably different than carbofuran titration results. During the addition of eserine, voltammetric changes of R_1^c and R_1^a reduction current intensities continuously decreased with the increasing concentration of eserine. Eserine has functional group of indoline and has dispelled electrochemical activities of Pc ring and AQ moieties. Indoline may be interacted with both central metal and AQ substituent. These voltammetric analysis illustrates that ITO/CuPc-AQ electrode can be used as a selective sensor electrode for carbofuran and eserine while it behaves in a different manner for each pesticide. The current intensity decrease of the reduction peaks during the sensing measurements indicates that CuPc-AQ behaves as artificial sensing material instead of enzymes which were used for pesticide biosensors as organic sensing material. However, CuPc-AQ is preferable to enzymes because of its superior properties such as more stable and low cost.

The detection limits and linear ranges of the ITO/CuPc-AQ electrode were calculated from SWV measurements of carbofuran and eserine titration processes and the results are exhibited in Table 1.

The limit of detection (DL) of the ITO/CuPc-AQ electrode was calculated from Eq. (1):

$$DL = \frac{3S_B}{b} \quad (1)$$

where S_B is the standard deviation of the blank solution, and b is the slope of the analytical curve.³⁰ Standard deviation was calculated using four blank measurement results and the analytical curve that was obtained with pesticide concentration, and electrochemical signal data was used to calculate the slope.

To support the SWV responses, and to determine the sensor results of the other electrochemical techniques, the sensing responses of ITO/CuPc-AQ were also measured with EIS and DPSCC analysis methods. The EIS sensing measurement of ITO/CuPc-AQ with carbofuran and the calibration line derived from EIS data were illustrated in Figure 6.

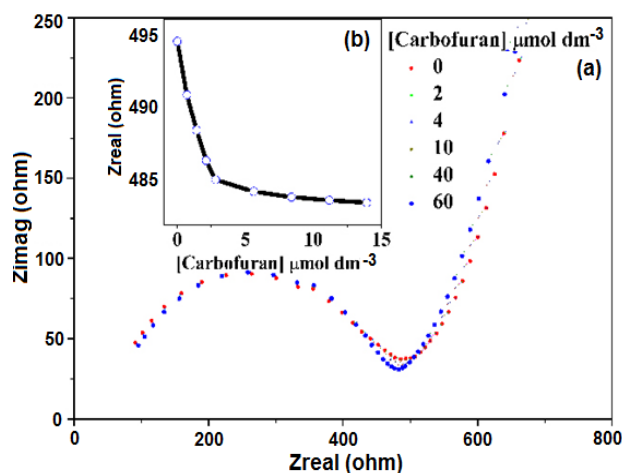


Figure 6. EIS responses and calibration line of ITO/CuPc-AQ electrode during the gradual addition of carbofuran.

The diameter of the Nyquist diagram semicircles gradually decreases as a function of the increasing carbofuran concentration in the electrochemical cell solution (Figure 6a). The interaction between ITO/CuPc-AQ and carbofuran increases the conductivity of the modified working electrode. The calibration line is given in Figure 6b and the detection linear range and detection limit values of this modified electrode obtained from this calibration line are tabulated in Table 1.

Table 1. Sensor parameters of modified ITO/CuPc-AQ electrodes for pesticide detection

Modified electrode	Sensing techniques	Pesticides				Reference
		Eserine		Carbofuran		
		Linear range (mol dm ⁻³) x 10 ⁶	Detection Limit (mol dm ⁻³)	Linear range (mol dm ⁻³) x 10 ⁶	Detection Limit (mol dm ⁻³)	
ITO/CuPc-AQ	SWV (Amperometric)	0.014 - 2.811	6.97 x 10 ⁻⁸	2.100- 16.681	2.08 x 10 ⁻⁷	This work
	SWV (Potentiometric)	0.014 - 1.332	3.03 x 10 ⁻⁷	0.003 - 1.276	9.04 x 10 ⁻⁸	This work
	EIS	0.736 - 5.395	5.93 x 10 ⁻⁸	0.010 - 1.962	8.44 x 10 ⁻⁹	This work
	DPSCC	0.002 - 2.822	6.58 x 10 ⁻⁸	0.024 - 1.266	2.95 x 10 ⁻⁷	This work
ITO/CuPc-AQ-nPt	SWV (Amperometric)	0.030 - 1.346	4.38 x 10 ⁻⁸	0.160 - 1.963	4.66 x 10 ⁻⁸	This work
	SWV (Potentiometric)	0.044 - 2.613	6.97 x 10 ⁻⁸	0.257 - 2.108	7.53 x 10 ⁻⁸	This work
	EIS	0.165 - 2.758	4.11 x 10 ⁻⁸	0.633 - 10.86	5.83 x 10 ⁻⁹	This work
	DPSCC	0.022 - 2.671	4.63 x 10 ⁻⁸	0.039 -1.351	1.63 x 10 ⁻⁷	This work
ITO/CuPc-AQ-nAu	SWV (Amperometric)	0.061 - 1.241	3.87 x 10 ⁻⁸	0.022 - 1.880	3.71 x 10 ⁻⁸	This work
	SWV (Potentiometric)	0.149 - 2.969	2.89 x 10 ⁻⁸	0.033 - 2.842	1.62 x 10 ⁻⁸	This work
	EIS	0.039 - 2.371	1.23 x 10 ⁻⁹	0.012 - 2.855	3.99 x 10 ⁻⁹	This work
	DPSCC	0.065 - 14.53	2.41 x 10 ⁻⁸	0.005 - 10.85	1.82 x 10 ⁻⁸	This work
CoO/rGO/GCE	CA (Amperometric)			1.9 x 10 ⁻⁸	32	
AChE–AuNPs–SF/Pt	CA (Amperometric)			1.0 x 10 ⁻⁹	33	
BSA/Ab/[DpAu/DMDPSE]2/Au	CA (Amperometric)			2.7 x 10 ⁻⁷	34	
AChE / TTF–TCNQ–EMIMTCB/CP	CA (Amperometric)		2.6 x 10 ⁻⁸		35	
AChE–ChO	CA (Amperometric)		1.0 x 10 ⁻⁸		36	
AChE/PAMAM dendrimers			0.03 ppb		37	

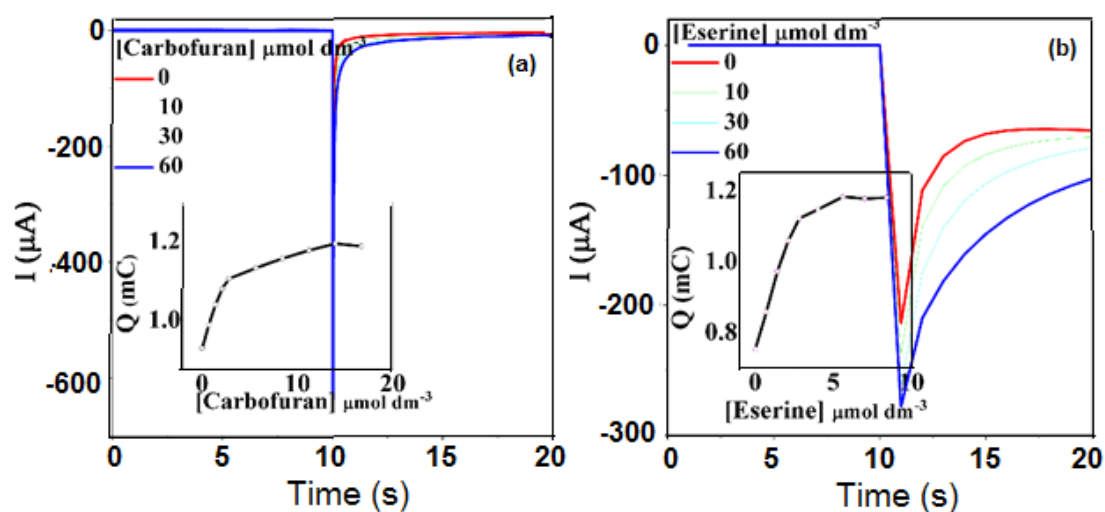


Figure 7. DPSCC responses and calibration lines of ITO/CuPc-AQ electrodes during the gradual addition of a) Carbofuran, b) Eserine.

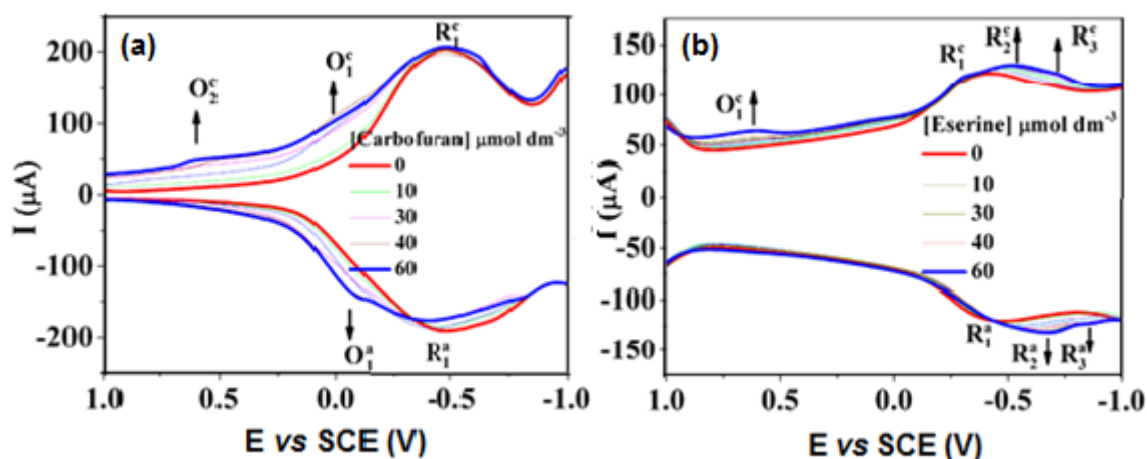


Figure 8. SWV responses of ITO/CuPc-AQ-nPt electrodes in PBS (pH= 7.0): a) During eserine titration, b) During carbofuran titration.

When compared with SWV analysis, the detection limit of the electrode decreases up to 5.44×10^{-9} mol dm^{-3} . DPSCC analyses for eserine and carbofuran were also performed between 0.0 V and -1.0 V constant potentials consecutively (Figure 7). There is an increase in the charge density during gradual addition of eserine and carbofuran during DPSCC measurements. When these three techniques are compared, the smallest DL is recorded with EIS technique.

To improve the sensing activity of CuPc-AQ, the ITO/CuPc-AQ electrodes were electrochemically coated with nano-Pt (ITO/CuPc-AQ-nPt), and sensing measurements were repeated on this electrode with the same conditions and methods. The SWV measurement results of ITO/CuPc-AQ-nPt during gradual addition of carbofuran and eserine into the phosphate buffer

electrolyte are illustrated in Figure 8. Without pesticide addition, ITO/CuPc-AQ-nPt electrode gives similar voltammetric responses with ITO/CuPc-AQ. ITO/CuPc-AQ-nPt electrode gives AQ reduction peak at -0.42 V during the forward SWV scan and at the reverse SWV scan, the couples of AQ reduction peak is seen at -0.40 V. In Figure 8a, the SWV response of ITO/CuPc-AQ-nPt seems to be differing with the gradual addition of carbofuran pesticide. After gradually addition of carbofuran, a new reversible peak forms at oxidation region for ITO/CuPc-AQ-nPt, although ITO/CuPc-AQ electrode gives different response. In Figure 8b, during titration with eserine, the interaction of pesticide with ITO/CuPc-AQ-nPt affects the SWV responses and two new reduction peaks are observed at -0.67 V and -0.85 V while the reduction peaks of ITO/CuPc-AQ electrode

decreases and no new peaks form. The presence of nPt particles in the recognizer film leads to formation of new electroactive structures by acting as a catalyst. This situation makes more evident the selectivity of the electrode. These voltammetric responses illustrate that CuPc-AQ is a selective sensor material against carbofuran and eserine. The sensor parameters derived from SWV analyses are exhibited in Table 1. Detection limit (DL) of ITO/CuPc-AQ-nPt is smaller than that of ITO/CuPc-AQ, which indicates that nano Pt coated on CuPc-AQ improves the sensor activity of the ITO/CuPc-AQ electrode. Figure 9 exhibits the EIS responses of ITO/CuPc-AQ-nPt during gradual addition of eserine into the phosphate buffer electrolyte.

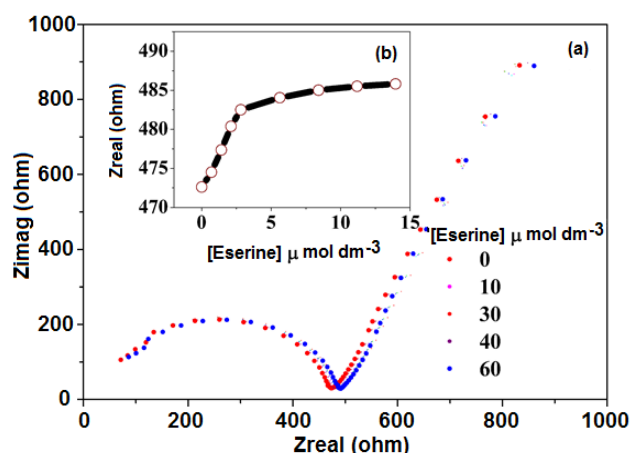


Figure 9. EIS responses of ITO/CuPc-AQ-nPt electrodes during the gradual addition of eserine and calibration line of the eserine sensing measurements derived from EIS responses of ITO/CuPc-AQ-nPt electrodes.

During gradual addition of eserine, the radius of the Nyquist diagram semicircles increases with increasing eserine concentration, which also supports the interaction of eserine with the sensor electrode. On the other hand, Figure 9 illustrates that the electrical conductivity of the ITO/CuPc-AQ-nPt electrode has improved since the semicircle radius of the electrode is shorter than those of ITO/CuPc-AQ electrode. On the other side, DL of the electrode derived from EIS analysis is also lower than that of ITO/CuPc-AQ electrode.

DPSCC sensor measurement results of ITO/CuPc-AQ-nPt electrode are shown in Figure 10. The potentials $E_o = 0.0$ V and $E_f = -1.00$ V were applied consecutively after each pesticide addition and considerable DPSCC response changes were recorded during the forward step of the technique as a function of pesticide concentration. As shown in Figure 10a, ITO/CuPc-AQ-nPt electrode gives a linear range between 3.87×10^{-8} and -1.460×10^{-6} mol dm⁻³ and DL of 1.63×10^{-7} mol dm⁻³ for carbofuran. However, in Figure 10b, after $8 \mu\text{mol dm}^{-3}$ eserine concentration in the phosphate buffer electrolyte solution, the electrical charge of the working electrode remained almost constant that determined the linear range of the ITO/CuPc-AQ-nPt electrode as 0.0219×10^{-6} and -2.87×10^{-6} mol dm⁻³ and DL of 4.63×10^{-8} mol dm⁻³ for DPSCC technique. These DPSCC responses are in agreement with SWV responses of the electrode that two new reduction peaks are observed at -0.67 V and -0.85 V, leading the charge increase of the working electrodes between 0.0 V and -1.0 V.

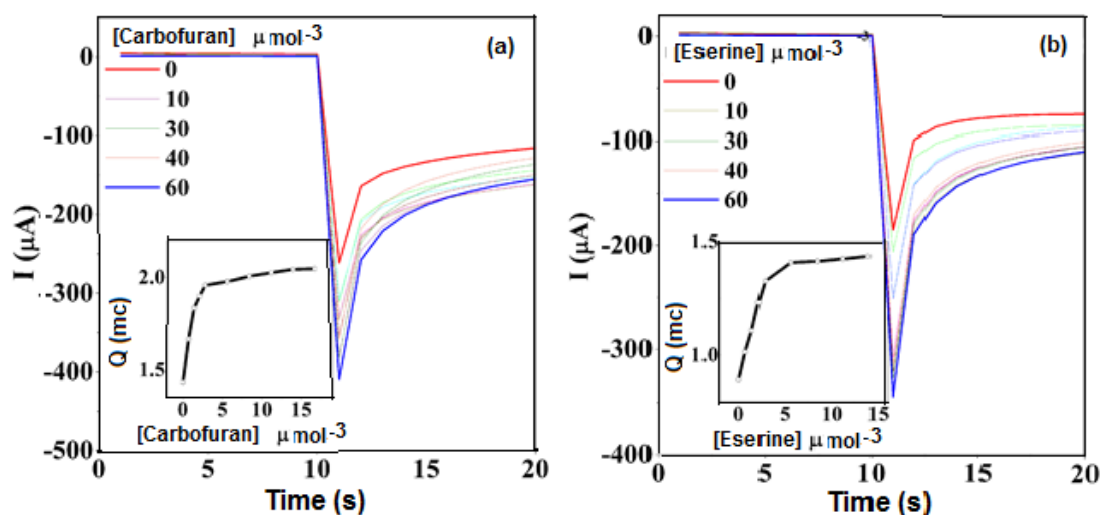


Figure 10. DPSCC responses and calibration line derived from DPSCC responses of ITO/CuPc-AQ-nPt electrodes: a) Gradual addition of carbofuran, b) Gradual addition of eserine.

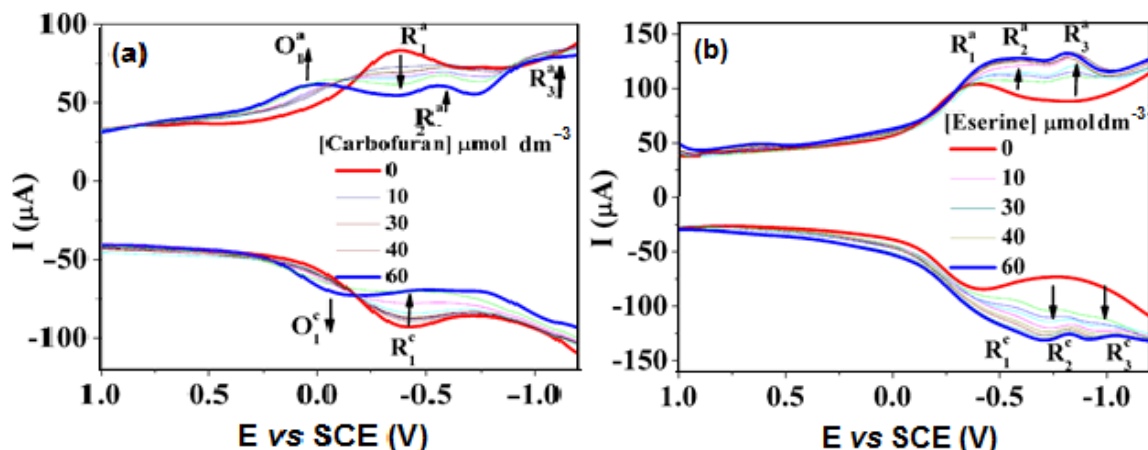


Figure 11. SWV responses of ITO/CuPc-AQ-nAu electrode during the gradual addition of **a)** Carbofuran, **b)** Eserine.

Similarly, the ITO/CuPc-AQ electrode was modified with Au to improve the sensor parameters and sensing measurements were carried out with SWV, EIS and DPSCC techniques. As shown in Figure 11, SWV diagrams of ITO/CuPc-AQ-nAu electrode without any pesticide addition illustrates that ITO/CuPc-AQ-nAu electrode gives similar SWV responses with those of ITO/CuPc-AQ-nPt and ITO/CuPc-AQ electrodes. A reduction couple R_1^a/R_1^c at -0.39 V and -0.43 V attributed to overlapped peaks of AQ and Pc are observed (Figure 11a). However, during gradual addition of carbofuran, the peaks of R_1^a/R_1^c couple decreases in current intensity, a cathodic peak at -0.56 V, a cathodic couple at -1.0 V, and an anodic couple at 0.04 V and -0.10 V were observed and peak current of these new waves gradually increased as a function of increasing carbofuran concentration. Two new cathodic couples are formed with the increasing concentration of eserine at about -0.60 V and -0.83 V (Figure 11b). EIS and DPSCC analyses of the electrode for carbofuran and eserine sensing were also carried out under the same conditions and basic sensor parameters were derived from the responses of these different techniques separately. The results obtained are given in Table 1. Modifying the electrode with nAu particles increased the sensitivity of the sensor against both eserine and carbofuran. The lowest detection limit was obtained with ITO/CuPc-AQ-nAu electrode as $1.23 \times 10^{-9} \text{ mol dm}^{-3}$ for eserine and $3.99 \times 10^{-9} \text{ mol dm}^{-3}$ for carbofuran.

4. CONCLUSIONS

The strong redox activity of CuPc-AQ exhibits potential usage of the complex for electrochemical technologies. In our previous study the CoPc-AQ complex was used as recognition material for eserine and

carbofuran detection which was supported with nano-Au and nano-Pt in the reference 31. As a result of this study, ITO/CoPc-AQ behaved as a selective electrochemical sensor for eserine and carbofuran. Immobilization of nano-Pt and nano-Au on the ITO/CoPc-AQ electrode increased the sensitivity. The lowest detection limit of $2.30 \times 10^{-9} \text{ mol dm}^{-3}$ was obtained for eserine with EIS method using ITO/CoPc-AQ-nPt electrode while the detection limit for eserine with EIS method using ITO/CuPc-AQ-nPt was $4.11 \times 10^{-8} \text{ mol dm}^{-3}$. Collaboration of Co as central metal of the Pc with nPt exhibited better results than that of Cu to increase the sensitivity of the sensor.

In this study, modified ITO electrode based on copper phthalocyanine-anthraquinone hybrid (CuPc-AQ) was constructed with Langmuir-Blodgett (LB) monolayer film coating technique. The modified electrode was tested as pesticide electrochemical sensor. Sensing measurements with three different electrochemical techniques denoted that ITO/CuPc-AQ electrode could be used as a selective and sensitive pesticide electrochemical sensor for eserine and carbofuran pesticides. While ITO/CuPc-AQ electrode sensed carbofuran at anodic potentials, the interaction of the electrode with eserine was detected with cathodic electrochemical signals. This situation provided the selectivity of the biomimetic sensor against carbofuran and eserine. Doping the CuPc-AQ thin film with nano-platinum and nano-gold particles increased the sensitivity of ITO/CuPc-AQ electrode.

The central metal of the anthraquinone substituted phthalocyanine did not affect the selectivity of the sensor material but affected the sensitivity. Also the presence of nPt and nAu particles as agents with catalytic effect made more evident the selectivity of the CuPc-AQ against carbofuran and eserine besides increasing the sensitivity.

New artificial biomimetic sensors instead of enzyme sensors were developed, which were more advantageous for being durable at room conditions and selective for pesticide detection with high sensitivity. The lowest detection limit was found as 1.23×10^{-9} mol dm⁻³ for eserine using ITO/CuPc-AQ-nAu electrode by EIS technique.

ACKNOWLEDGEMENTS

This work is supported by research fund of Marmara University (Project Nos. FEN-C-DRP-070211-0011 and FEN-A-150513-0166).




Conflict of interest

Authors declare that there is no a conflict of interest with any person, institute, and company, etc.

REFERENCES

- Samanta, S. *Aquat. Ecosyst. Health Manag.* **2013**, 16 (4), 454-464.
- Hami, H.A., Azzaoui, F.Z.; Idrissi, M.; Ouammi, L.; Mokhtari, A.; Soulaymani-Bencheikh, R.; Soulaymani, A.. *Am. J. Epidemiol.* **2012**, 175 (11 Supl):S1-S145.
- Hoai, P.M.; Sebesvari, Z.; Minh, T.B.; Viet, P.H.; Renaud, F.G. *Environ. Pollut.* **2011**, 159 (2), 3344-3350.
- Rodriguez-Liebana, J.A.; Mingorance, M.D.; Pena, A. *Colloid Surface. A* **2013**, 435, 71-77.
- Singh, N.K.; Chhillar, N.; Banerjee, B.D.; Bala, K.; Basu, M.; Mustafa, M. *Hum. Exp. Toxicol.* **2013**, 32 (1), 24-30.
- Sapbamrer, R.; Nata, S. *Environ. Health Prev.* **2014**, 19 (1), 12-20.
- Lee, K.G.; Jo, E.K. *Food Chem.* **2012**, 134 (4), 2497-2503.
- Gaffney, S.H.; Curriero, F.C.; Strickland, P.T.; Glass, G.E.; Helzlsouer, K.J.; Breysse, P.N. *Environ. Health Perspect.* **2005**, 113 (12), 1712-1716.
- Xu, M.L.; Liu, J.B.; Lu, J. *Appl. Spectrosc. Rev.* **2014**, 49 (2), 97-120.
- Fatoki, O.S.; Awofolu, R.O. *J. Chromatogr A* **2003**, 983 (1-2), 225-236.
- Luo, F.F.; Liao, S.Z.; Zhang, R.L.; Wu, Z.Y.; Yu, R.Q.; Shen, G.L. *Chinese J. Anal. Chem.* **2013**, 41 (10), 1549-1554.
- Tran, H.V.; Reisberg, S.; Piro, B.; Nguyen, T.D.; Pham, M.C. *Electroanal.* **2013**, 25 (3), 664-670.
- Chen, H.D.; Zuo, X.L.; Su, S.; Tang, Z.Z.; Wu, A.B.; Song, S.P.; Zhang, D.B.; Fan, C.H. *Analyst* **2008**, 133 (9), 1182-1186.
- Svorc, L.; Rievaj, M.; Bustin, D. *Sens. Actuators B: Chem.* **2013**, 181, 294-300.
- Eggins, B.R. *Chem. Sens. Biosens.* UK, 2002.
- Wong, A.; Sotomayor, M.D.T. *Sens. Actuators B: Chem.* **2013**, 181, 332-339.
- Boni, A.C.; Wong, A.; Dutra, R.A.F.; Sotomayor, M.D.P.T. *Talanta* **2011**, 85 (4), 2067-2073.
- Shahrokhian, S.; Amini, M.K.; Mohammadpoor-Baltork, I.; Tangestaninejad, S. *Electroanal.* **2000**, 12 (11), 863-867.
- Rahim, A.; Barros, S.B.A.; Kubota, L.T.; Gushikem, Y. *Electrochim. Acta* **2011**, 56 (27), 10116-10121.
- Wujcik, E.K.; Londono, N.J.; Duirk, S.E.; Monty, C.N.; Masel, R.I. *Chemosphere* **2013**, 91 (8), 1176-1182.
- Lin, T.; Lin, J.; Huang, X.; Liu, J. *Comm. Comp. Interface Sci.* **2011**, 214, 257-262.
- Vial, L.; Dumy, P. *New J. Chem.* **2009**, 33 (5), 939-946.
- Bhattachayay, D.; Pal, P.; Banerjee, S.; Sanyal, S.K.; Turner, A.P.F.; Sarkar, P. *Anal. Lett.* **2008**, 41 (8), 1387-1397.
- Erbahar, D.D.; Gurol, I.; Gumus, G.; Musluoglu, E.; Ozturk, Z.Z.; Ahsen, V.; Harbeck, M. *Sens. Actuators B: Chem.* **2012**, 173, 562-568.
- Wang, P.H.; Yu, J.H.; Li, Z.J.; Ding, Z.J.; Guo, L.; Du, B. *Sens. Actuators B: Chem.* **2013**, 188, 1306-1311.
- Ipek, Y.; Dincer, H.; Koca, A. *Sens. Actuators B: Chem.* **2014**, 193, 830-837.
- Sezer, B.; Sener, M.K.; Koca, A.; Erdogmus, A.; Avciata, U. *Synth. Met.* **2010**, 160 (19-20), 2155-2166.
- Wiederkehr, N.A. *Phys. Chem. Glasses: B* **2008**, 49 (6), 326-333.

29. Valli, L. *Adv. Colloid Interface*. **2005**, 116 (1-3), 13-44.
30. Mahmoudian, M.R.; Alias, Y.; Basirun, W.J.; MengWoi, P.; Jamali-Sheini, F.; Sookhakian, M.; Silakhori, M. *J. Electroanal. Chem.* **2015**, 751, 30-36.
31. İpek, Y.; Şener, M.K.; Koca, A.. *J. Porphyrins Phthalocyanines* **2015**, 19, 708-718.
32. Wang, M.; Huang, J.; Wang, M.; Zhang, D. Chen, J. *Food Chem.* **2014**, 151, 191-197.
33. Yin, H.; Ai., S.; Xu, J.; Shi, W.; Zhu, L. *J. Electroanal. Chem.* **2009**, 637(1-2), 21-27.
34. Sun, X.; Zhu, Y.; Wang, X. *Food Control* **2012**, 28, 184-191.
35. Zamfir, L.G.; Rotariu, L.; Bala, C. *Biosens. Bioelectron.* **2013**, 46, 61-67.
36. Snejdarkova, M.; Svobodova, L.; Evtugyn, G.; Budnikov, H.; Karyakin, A.; Nikolelis, D.P.; Hianik, T. *Anal. Chim. Acta* **2004**, 514, 79-88.
37. Snejdarkova, M.; Svobodova, L.; Nikolelis, D.P.; Wang, J.; Hianik, T. *Electroanalysis* **2003**, 15(14), 1185-1191.

ORCID 0000-0002-9390-9875 (Y. İpek) 0000-0003-3560-2995 (M. Kasım Şener) 0000-0003-0141-5817 (A. Koca)